CONJUGATED POLYMER BRUSHES AS MOLECULAR WIRES IN ELECTRONIC DEVICES: SYNTHESIS, DEVICE DESIGN, AND CHARACTERIZATION

Travis William LaJoie

A dissertation submitted to the faculty at the University of North Carolina at Chapel Hill in partial fulfillment of the requirements for the degree of Doctor of Philosophy in the Department of Chemistry.

Chapel Hill
2015

Approved by:

Wei You

Sergei Sheiko

Royce Murray

Andrew Moran

James Cahoon

ABSTRACT

Travis William LaJoie: Polymer Molecular Wires in Electronic Devices: Synthesis, Design, and Characterization
(Under the direction of Wei You)

Lack of efficient charge transport is a major factor holding back performance of organic electronic devices. For polymer semiconductors, some of the best performing devices have significant contributions from intramolecular transport mechanism on the process of charge transport as a whole. This is because charge transport along conjugated polymer backbones is much faster than transport between polymers, but measurements of intramolecular charge transport have only ever been done using technique that measure local properties, not device properties. Few devices have measured properties like charge carrier mobility as a function of polymer chain orientation, but in every case charges are required to hop between chains to transport through the film.

This work endeavors to make charge transport devices from monolayers of poly(3-methylthiophene) (P3MT) in brush conformation grown from an ITO surface via Palladium catalyzed surface initiated Kumada catalyst-transfer polycondensation and to characterize the charge transport through the polymer brush films. Though the polymer synthesis is not new, it was thoroughly characterized in order to grow films with the maximum level of control possible. The

polymer growth was found to be linear with respect to time and concentration of monomer, suggesting that the polymerization follows first order kinetics.

The P3MT films were characterized to determine film morphology. As grown, films exhibited some degree of vertical orientation, which could be increased with thermal annealing. Besides increasing orientation, annealing also increased film thickness and chain rigidity making structures ideal for measuring intramolecular charge transport.

In order to make devices, a new transfer printing method was adapted for called kinetically controlled transfer printing (KTP). Gold electrodes were deposited on the P3MT brush surface by KTP, and devices were measured by conducting atomic force microscopy. The data were modelled with a cubic fit to compare transport between films. Before annealing, P3MT films were found to be quite conductive as evidenced by their charge transport decay coefficient (ß), and SCLC charge carrier (hole) mobilities were measured to be similar to other poly(3-alkylthiophene) materials. After annealing, the SCLC charge carrier mobility increased in every film measured. The enhancement of charge transport properties is likely due to the change in the structure of the film.

ACKNOWLEDGEMENTS

I would like to first and foremost extend my heartfelt gratitude to my advisor Prof. Wei You. I will always remember the way you pushed me to become a better leader and scientist. I will miss our talks, meetings, and of course, barbecues.

I also thank my committee members Prof. Sheiko, Prof. Murray, Prof. Cahoon, and Prof. Moran, who have each given me advice and assistance. I also thank Prof. Tsui and his student Mark Moog for their tireless efforts in collaboration to do this work, and Prof. Jason Locklin and his SI-KCTP group.

I never thought I would be so close to such a great group of people as I am with the You group. More than anything else from graduate school, I am going to take my memories of day-to-day life with all of you.

I also acknowledge and give my greatest appreciation to all of my teachers and professors who worked so selflessly to not only educate me and countless others but also to inspire us to become thinkers and doers.

Also, my family, who more than anyone else has shaped the young man I am today. I definitely could not have done any of this without their support.

Finally, I thank Lindsay. During our time in graduate school, we have grown together and built a life together. I hope that after this chapter closes for us the next one we open will be just as wonderful. I love you!

TABLE OF CONTENTS

LIST OF FIGURES

Figure

LIST OF TABLES

Table

LIST OF EQUATIONS

Equation

LIST OF ABBREVIATIONS AND SYMBOLS

Å	Angstrom, $1x10^{-10}$ m
A	Area
AFM	Atomic Force Microscopy
cAFM	Conducting Atomic Force Microscopy
BHJ	Bulk Heterojunction
COM	Center of Mass
CP	Conducting Polymer
CV	Cyclic Voltammetry
Fc	Ferrocene
Fc^+	Ferrocenium
FET	Field Effect Transistor
G	Conductance
HOMO	Highest Occupied Molecular Orbital
I	Current
ITO	Indium Tin Oxide, or Tin-Doped Indium Oxide
IV	Current-Voltage
k	Extinction Coefficient
KCTP	Kumada Catalyst-Transfer Polycondensation
KTP	Kinetically Controlled Transfer Printing
LED	Light Emitting Diode
LUMO	Lowest Unoccupied Molecular Orbital

μ	Charge Carrier Mobility
M_n	Number Average Molecular Weight
M_w	Weight Average Molecular Weight
MMM	Metal-Molecule-Metal
MOSFET	Metal Oxide Semiconductor Field Effect Transistor
MSE	Mean Squared Error
n	Index of Refraction
NEXAFS	Near Edge X-Ray Absorption Fine Structure Spectroscopy
nTP	nanoTransfer Printing
OFET	Organic Field Effect Transistor
OLED	Organic Light Emitting Diode
OPV	Organic Photovoltaic
PA	poly(acetylene)
P3AT	poly(3-alkylthiophene)
P3BT	poly(3-butylthiophene)
P3HT	poly(3-hexylthiophene)
P3MT	poly(3-methylthiophene)
PDI	Polydispersity Index
PEDOT:PSS	Poly(3,4-ethylenedioxy)thiophene poly(sulfonate)
PSC	Polymer Solar Cell
PV	Photovoltaic
q	Charge

ρ	Resistivity
R	Resistance
RMS	Root Mean Square
SAM	Self-Assembled Monolayer
SEM	Scanning Electron Microscopy
SI-KCTP	Surface Initiated Kumada Catalyst-Transfer Polycondensation
STM	Scanning Tunneling Microscopy
UPS	Ultraviolet Photoelectron Spectroscopy
UV	Ultraviolet
V	Voltage
XPS	X-Ray Photoelectron Spectroscopy

CHAPTER 1 INTRODUCTION TO ORGANIC ELECTRONICS AND MOLECULAR ELECTRONICS

1.1 Background

With the advent of the 21st century and the demand for cheap, ubiquitous personal electronic devices, research interest in new electronic materials and design motifs has skyrocketed. Between 2012 and 2015, the percentage of the world population that uses smart phones has increased from 16.0% to 28.0% with 33.8% of the world population projected to be using smartphones by 2017.[1] The need for cheap, energy-efficient, flexible electronics has driven researchers to find alternatives to traditional wafer-based technologies. High performance components and devices have typically been made using inorganic wafers, but in order to meet the demands of next generation electronics, new materials and technologies must be developed and integrated into devices.

One burgeoning alternative class of materials is organic electronic materials. In 2000, the Nobel Prize in Chemistry was awarded to Alan Heeger, Alan McDiarmid, and Hideki Shirakawa "*for the discovery and development of conductive polymers,*" and the field has been growing steadily since the modern discovery of conducting polymers in the 1970s.[2,3] Consisting of either small molecules or polymeric materials, organic electronics have proven to be possible candidates to replace and/or supplement silicon in applications such as photovoltaics (OPVs),[4] light emitting diodes (OLEDs),[5] and logic devices (OFETs)[6]

due to factors such as lower cost than inorganic counterparts, flexibility, and ease of processability[7]. In fact, many cellular telephones and televisions already use OLED displays because of their low power consumption, high field of view, brightness, and flexibility. Revenue from OLED displays alone is projected to increase from $2

Figure 1-1: Prototype Flexible Display

Mobile displays based on this Samsung prototype are projected to release in 2016. Image copyright to its respectful owner.

billion annually in 2015 to nearly $20 billion over the next five years, with over half of increased revenue going towards flexible displays.[8] This projection implies that next generation mobile devices will take advantage of the unique properties of OLEDs and contain flexible displays (Figure 1-1)[9] marking a new age in display technology. Though organic materials show promise, only OLEDs are used in widespread commercial applications. This is because, despite their low cost, organic materials are still outperformed by their silicon counterparts in many applications.

There are many difficult hurdles organic materials must overcome in order to compete with wafer materials. Wafer technology has matured organically with modern electronics, so current industry efforts are already focused on the manufacture and integration of wafers into functional devices. Organic materials

must compete against the head start afforded to inorganic materials including 60 years of maturation and billions of invested dollars per year. Practical concerns facing organic materials such as reliability, lifetime, and processability must be addressed and solved.

Though these are all paramount issues, this work will not focus on problems of this kind and instead focus on the more fundamental question of measuring charge transport through the backbone of polymer semiconductors. Because of their chainlike nature, polymers are geometrically anisotropic and therefore should also have electron transport properties of interest that depend on the one dimensional nature of a polymer chain (Figure 1-2). Charges can transport along the backbone of the chain, between adjacent polymer chains, or a combination of the two.[10] Though this may seem to be a trivial problem, device level measurements of this behavior has never been reported. As will be outlined below, the nature of charge transport through polymer semiconductors is of prime importance to their function in devices.

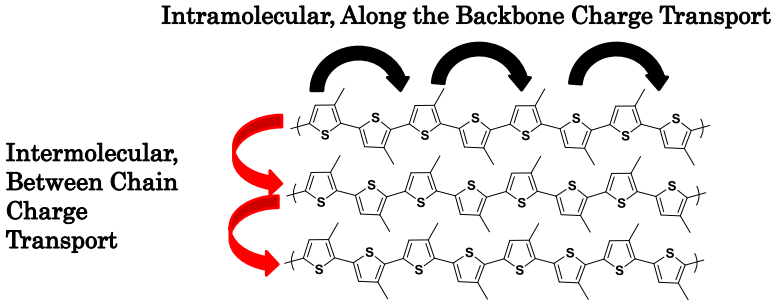

Figure 1-2: Inter- vs. Intra Molecular Charge Transport

Charge carriers can transport two ways through polymer thin films: either by intramolecular charge transport (black arrows) or intermolecular charge transport (red arrows). In polymer thin films, intermolecular charge transport dominates the overall transport properties due to its slow nature with respect to intramolecular charge transport.

In order for polymers to be viable materials for widespread use in devices, the one dimensional nature of charge transport through them must be understood so functional materials can be designed and synthesized to take full advantage of polymer properties.

1.2 Organic Electronics

1.2.1 History of Organic Electronics

The discovery of the first organic conducting material is attributed to Henry Letheby in 1862.[11] His self-described "Blue Substance" was later identified as poly(aniline). To put this discovery into historical perspective, it would not be until 60 years later that Hermann Staudinger would first publish on the macromolecule concept for which he won the Nobel Prize in 1953.[12]

The first report of an organic electronic device was a small molecule OPV in 1958[13] with an active layer consisting of magnesium pthalocyanine and tetramethyl *p*-phenylenediamine. The meteoric rise of conjugated polymers in organic electronics can be traced back to the work of Nobel laureates Alan Heeger, Alan McDiarmid, and Hideki Shirakawa in the 1970s. Throughout the 1970s, in several papers published separately and together,[2-3] Heeger, McDiarmid, and Shirakawa laid the fundamental groundwork for understanding the mode of charge transport in doped conjugated polymers by studying the effects of oxidative doping on the conductivity of poly(acetylene).

It was not until 1987 that the first OFET[14] and OLED[15] were fabricated by the Mitsubishi Electric Corporation and Eastman Kodak, respectively. The first OFET used poly(thiophene), a conjugated polymer, as the active material while the

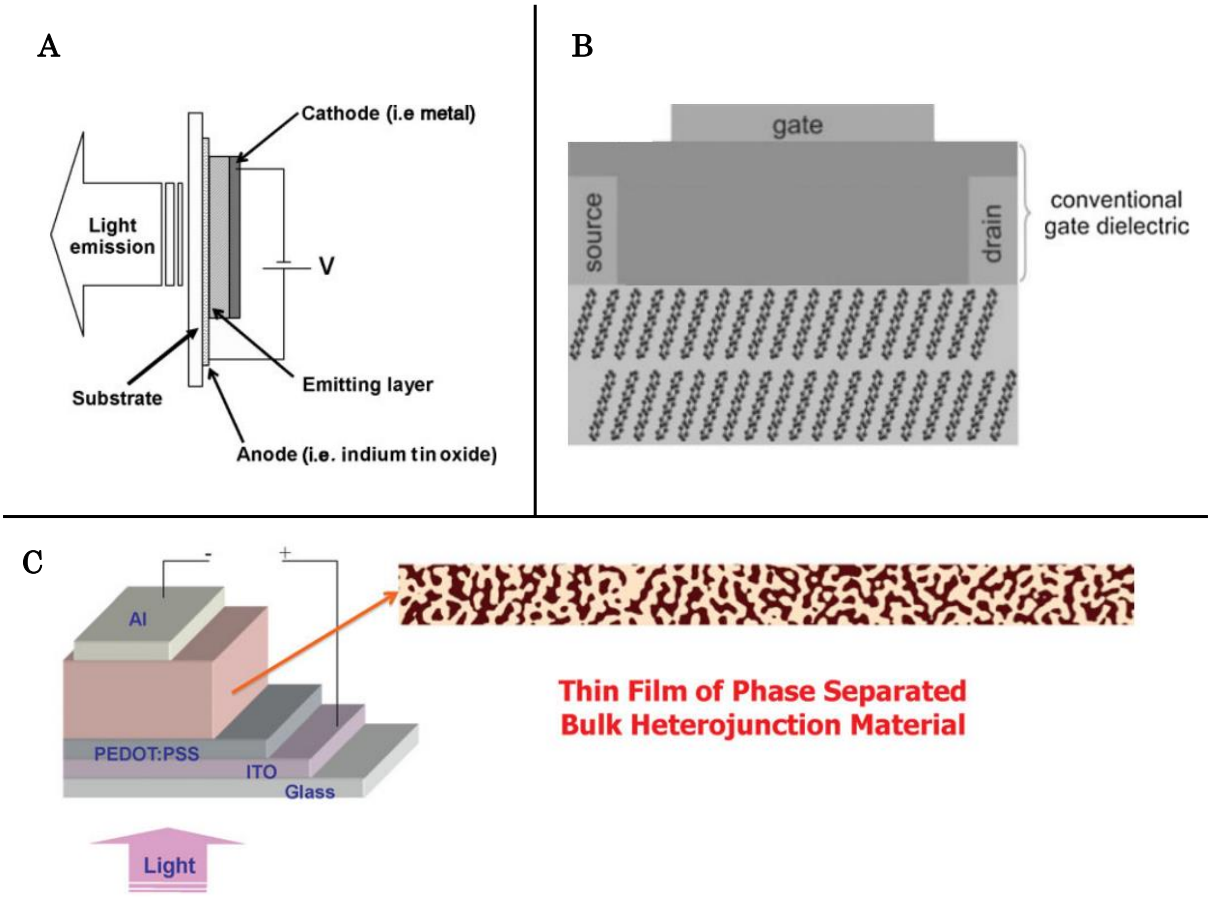

Figure 1-3: Basic OLED, OFET, and OPV Device Geometries and Function

(A) Simple OLED devices consist of an active layer sandwiched between a transparent anode, usually ITO and a metallic cathode. An applied voltage causes electrons and holes to inject into the active layer and recombine to form excitons, which relax and emit photons.
(B) OFET devices function similar to other FETs. Charge carriers are generated along a conduction channel adjacent to a dielectric layer by applying a bias to a gate electrode. The generated charge carriers allow current to flow between source and drain electrodes.
(C) The most dominant OPV device motif is the BHJ. In a BHJ, a polymer semiconductor is blended with a modified fullerene and spuncast on a surface to form an interpenetrating network of an electron donating material (polymer) and electron accepting material (PCBM). The light absorbing polymer semiconductor absorbs incoming light to excite an electron from the ground state to form an electron hole pair, or exciton. The exciton is split at the interface between polymer and PCBM with electrons travelling through the PCBM network and holes travelling through the polymer network. Charges are collected at electrodes to generate electricity.

original OLED used 8-hydroxyquinilone aluminum (Alq_3) as the light emitter. As already discussed, OLEDs matured into a commercially viable technology over the next 20 years, while OFETs are still a subject of intense academic research. Examples of OLED and OFET devices are illustrated in Figure 1-3.

The modern era of OPV research began in 1995 with the report of the first bulk heterojunction (BHJ)[16,17] devices by Heeger and the synthesis of soluble carbon fullerene derivatives by Fred Wudl.[18] These devices were fabricated by dissolving light absorbing conjugated polymers and $PC_{61}BM$ in solution and casting a film to create a solution processed active layer (Figure 1-3).[5-6, 19] Over the course of the next twenty years, significant work in device fabrication and polymer synthesis has pushed OPV power conversion efficiencies to over 11%.[19,20]

Nearly 50 years after the foundational work of Shirakawa, McDiarmid, and Heeger, researchers are still pushing the limits of conjugated polymers to create new materials and better understand their function in electronic devices. This dissertation seeks to build on the foundation laid over the course of the last half century and expand the fundamental knowledge of charge transport through polymer semiconductors.

1.2.2 The Molecular Origin of Conductivity in Conjugated Polymers

The origin of conductivity in conjugated polymers is due to the regular, alternating structure of single and double bonds which delocalize electrons along the polymer backbone (Figure 1-4).[2] Due to defects and torsional angles in the polymer backbone, an entire polymer chain is not conjugated, but can be thought of as a series of conjugated segments which delocalized electrons along a conjugation length. Though the electrons are spread over a large area, this property alone will not make a conjugated polymer a conductor, there must be free charge carriers in the material.

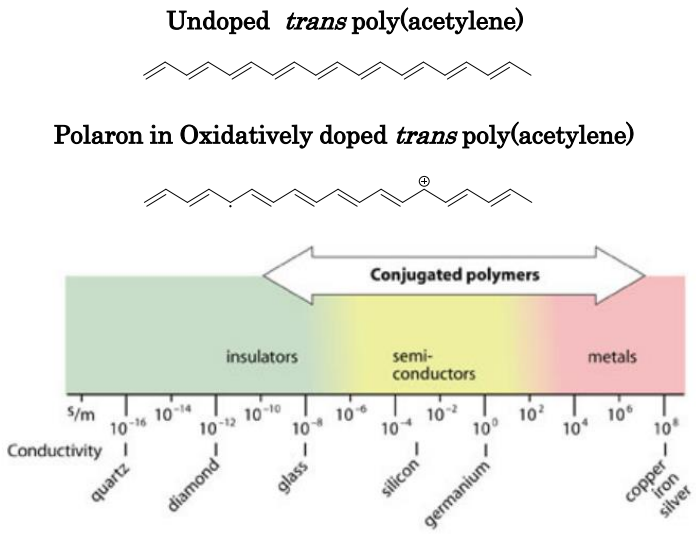

Figure 1-4: Molecular Origin of Conductivity in CPs and Classes of Conductive Materials

(Top) In undoped poly(acetylene) there are few to no free charge carriers on the polymer chain so the polymer does not allow current to flow through it. When poly(acetylene) is oxidatively doped, it loses an electron to form a positive polaron, a free charge carrier.

(Bottom) Materials can be classified based on their conductivity. Conjugated polymers can be insulators, semiconductors, or metals (conductors).

Materials can be classified grouping them based upon their conductivities. Materials with high conductivities are classified as conductors or metals while materials with low conductivities are considered insulators, and between these two regimes lay semiconductors (Figure 1-4). Typical organic materials do not conduct electricity very well, so are classified as insulators, but doped conducting polymers have conductivities similar to metals (Table 1-1).[21]

Material	Conductivity (S/cm)
Doped Polyacetylene	10^3-1.7×10^5
Undoped Polyacetylene	10^{-10}
Doped Polyaniline	10^2-10^3
Undoped Polyaniline	10^{-10}
Teflon	10^{-18}
Platinum	$9.43\text{x}10^6$
Gold	$4.1\text{x}10^7$

Table 1-1: Conductivities of Various Materials

The conductivity of a material is given by

$$\boldsymbol{\sigma = nq\mu} \tag{1}$$

In order for a polymer to be a conductor, it must be doped to generate free charge carriers (Figure 1-4). Charges can move along the polymer backbone, hopping between conjugated segments via intramolecular charge transport or they can hop between adjacent chains via intermolecular charge transport. If a conjugated polymer is not doped, it can still transport charges, but due to having few charge carriers it will not be a conductor. Undoped conjugated polymers typically only have thermally generated charge carriers, so the component of

conductivity determined by the number of charge carries is quite low. The doping level is something that can be controlled on the device level, for instance in OFETs,[6] where a polymer's conductivity can be increased by applying a gate bias to control device function, and conductivity can also be controlled chemically by chemically oxidizing or reducing the material.[22] The doping level is important when making a material a conductor, but it is something that is independently controlled and not an intrinsic property of the material. In devices such as OPVs, OFETs, and OLEDs, the active material must be a semiconductor, so doping is not useful to increase conductivity. For functional polymer devices, the charge carrier mobility μ is a much more useful parameter to increase to improve device performance.

1.2.3 Mobility in Conjugated Polymers

1.2.3.1 Theory Behind Charge Mobility in Conjugated Polymers

Mobility is the speed at which charges travel through a material. Currently, the highest mobility published for an organic material is a hole mobility of 45 cm^2/Vs measured in a single crystal of rubrene.[23] Though single crystals perform well in devices, they are difficult and expensive to make. Single crystal devices are usually made painstakingly by hand and cannot be mass produced. Thus, polymer materials which can be printed and processed out of solution are a much more realistic alternative. Recently, two record breaking polymer mobilities in OFETs were published with hole mobilities is 43 cm^2/Vs and 23.7 cm^2/Vs achieved by aligning polymer chains to enhance effects of intrachain charge transfer.[24,25] As organized in Table 1-2,[24-26] the mobilities of the best polymers are still lower than in

commonly used inorganic materials. In order to create new materials and devices with better mobilities with a rational approach, the mechanics of charge transport in polymer thin films must be understood. By their nature, polymers are one-dimensional materials and polymer thin films which are used in devices transport

Material	Mobility ($cm^2V^{-1}s^{-1}$)
C8-BTBT	25 (43 high)
PCDTPT	23.7
P3HT	0.1
Amorphous Silicon	~1
Strained Silicon	170,000 (at 4K) 1000 (RT)

Table 1-2: Device Mobilities of Organic and Inorganic Materials

charges along backbones of polymers and between polymer chains. The canonical dogma of the field is that charges transport better along the backbone of a polymer (intramolecular) with mobilities several orders of magnitude higher than charges that transport between polymer chains (intermolecular transport), and devices with high charge carrier mobilities are usually attributed to having higher degrees of intramolecular transport. Microwave conductivity can be used to measure local intrachain charge carrier mobilities, and hole mobilities up to 600 cm^2/Vs are measured on rigid polymer chains.[27] Despite this incredibly high mobility measured for intrachain transport, there are no reports of devices measuring single chain length intramolecular mobilities. The current theories of charge transport through organic materials and attempts at measuring intramolecular transport must be taken into account to understand why this is so and how to design devices and materials to make such a measurement.

In 2006, Kline and McGeehee, published a theory on the morphology and charge transport in polymers.[28] Their theory, briefly stated, is that a film with high degree of crystallinity (usually consisting of polymers with low molecular weight) will not have high mobility due to electrical discontinuity between highly conductive, crystalline domains. Additionally, films with disorder (usually films consisting of polymers with high molecular weight) will have high mobilities due to the ability for long chains to bridge connections between semicrystalline domains (Figure 1-5).[28] This theory implies that the bridging connections both enable and limit high charge carrier mobility in polymer thin films. This theory is also used to explain why high molecular weight materials seemingly have better charge mobilities than low molecular weight materials.

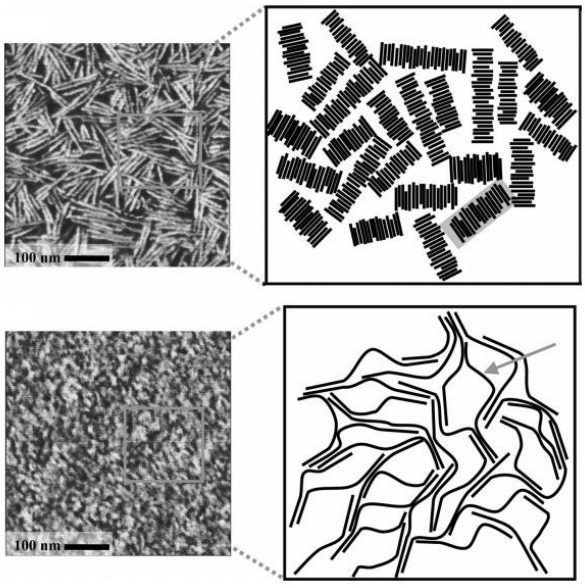

Figure 1-5: Model of Charge Transport in Spuncast Polymer Films

(Top) Low molecular weight (3.2kDa) P3HT forms semicrystalline nanorods (gray) which trap charge carriers and prohibit movement, causing low charge carrier mobilities in the film. (Bottom) High molecular weight P3HT (31.1kDa) form more amorphous films with long polymers (gray arrows) interconnecting semicrystalline domains in the film for higher charge carrier mobilities. Images copyright their respective owners.

In 2014, Heeney and Salleo published an updated model after investigating the role of polydispersity (PDI) of P3HT on the mobility in OFETs.[29] Their model demonstrates that charge carriers do not discriminate between high and low molecular weight chains, and thus crystalline and noncrystalline regions, and that charge transport and mobility in polymer thin films are limited by interchain hopping.

Further work by Salleo and Spakowitz models the charge mobility in individual polymer chains at different length scales.[30] They calculate high mobilities with fast transport for short intrachain charge transport processes and low mobilities with slow transport for long interchain charge transport processes. This behavior is easily explained by the strong coupling electron coupling along the chemically bound backbone of the polymer as compared to the weaker coupling between π-stacked chains. Using the macromolecular nature of polymers and the inherent order/disorder in polymer chains they are able to provide a better insight into the behavior of charges at short intramolecular and long intermolecular charge transport distances (Figure 1-6).[30] In a typical polymer thin film, both of these processes occur, and the slowest transport (lowest mobility) will limit device performance.

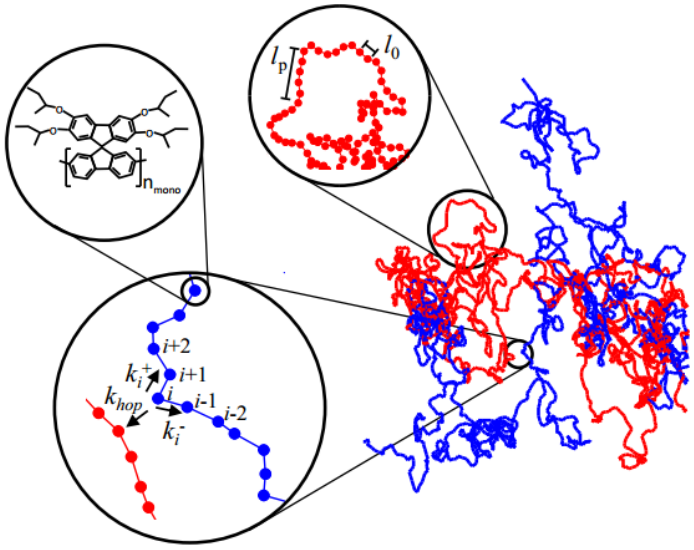

Figure 1-6: Theoretical Model of Mobility in Single and adjacent Polymer Chains

Different energies and times are calculated for charge transport phenomena between polymer chains and along single polymer chains. Due to strong coupling between monomer units on a polymer backbone and close proximity of monomers, transport along the chain is faster than transport between chains. Image copyright to its respective owner.

Current literature on intramolecular transport in devices is sparse. In OFETs, several examples were already given of oriented films having high mobilities.[10, 24-25] In vertical device architectures, traditional P3ATs are induced to have vertical structure through both surface treatment and end group modification to see a 10-40 times enhancement in mobility.[31,32]

1.2.3.2 Outlook on High Mobility Materials

High mobilities and conductivities due to enhanced intrachain transport are reported in several polymers and devices,[10, 24-25, 31-32] and current theories describing charge transport through polymer films suggest that this is due to increasing the contribution of intrachain charge transport.[5, 10, 15] These devices do not measure

intrinsic along the backbone charge transport of due to having multiple polymer layers in the active device, meaning that carriers must hop between multiple polymers in order to transport between electrodes. Using the principles of the above theories, and correcting shortcomings of current organic films, a better approach would be to make a device with one conjugated polymer layer where each end of the polymer is attached to an electrode. This approach is already common using small molecules where single molecules and monolayers are integrated into devices. This field of study is called molecular electronics.

1.3 Molecular Electronics

1.3.1 History and Conception of Molecular Electronics

In 1974, Mark Ratner and Arieh Aviram theorized that a functional rectifying device can be made using a single molecule to imbue functionality between two electrodes.[33] This idea revolutionized the way people thought about electronics considering it was only three years earlier, in 1971, that a group of researchers investigated electron tunneling across monolayers of fatty acid molecules as a way to experimentally verify aspects of the length dependence of quantum tunneling.[34] Only three years after researchers were able to reliable measure and model electric currents across layers of single molecules, the idea that a molecule can be integrated into a functional device caused a paradigm shift in the way people thought about molecules and electronics with the promise that future components for applications in memory storage, integrated circuits, and digital logic could have a device size on the scale of one or few molecules. Though integrating

single molecule components in functional electronics devices remains on a distant horizon, the field of molecular electronics presses on studying the electronic properties of electronic materials on a molecular level.[35] Charge transport in molecular devices is dominated by transport across or through a single molecule—or a single layer of molecules—which is different than the previously discussed examples where charges transport through thin films several layers thick, and the limiting processes in charge transport or transporting between polymer or molecular units.

For the past 40 years, advances in the field of molecular electronics have been in two directions: the first is advancing fundamental knowledge about how charges transport through molecules, including functional molecules, and the second is engineering devices to form molecular junctions and measure new properties. These advances are often not always mutually exclusive. A brief survey of the kinds of devices and their use are discussed below.

1.3.2 Molecular Electronic Device Fabrication

A common motif in molecular electronics is to sandwich one or more molecules between two electrodes to form a metal-molecule-metal junction (Figure 1-7). A MMM junction has five components: two electrodes, two contacts which link the molecule and electrodes, and the molecule. Each of these components can be changed to tune the properties of a molecular junction and impart functionality to a device.

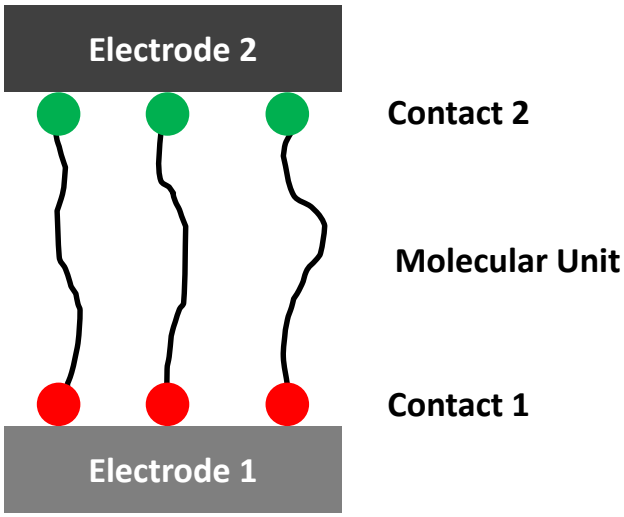

Figure 1-7: Schematic of Metal Molecule Metal Junction

A metal molecule junction has five distinct components. There are two metallic electrodes, a molecular unit, and two contacts or linkers to attach the molecule to the electrodes. Junctions can have or many molecules sandwiched between two electrodes. The chemical species of metal electrodes and spacers may be identical or different.

When Ratner and Avirem first theorized a single molecule rectifier there was no way to make and test a single molecule device, but with the invention of the STM in 1981, a useful tool to make and test conductances of single molecule devices presented itself.[35] Single molecule devices measured by STM are analytic in nature, forming briefly and only long enough to be measured.[36] Another single molecule device configuration is a break junction, which forms a device by breaking a gold wire in the presence of organic molecules and measuring the current through the junction that forms when a molecule or molecules bridges the gap.[37] In single molecule devices the conformation of a molecule is difficult to control when in contact with electrodes. Analyzing these devices is necessarily highly statistical. A single molecule with only 15 atoms can have as many as 10^{60} conformations, each with a different conductance.[35] Thus, several thousand measurements of single

molecules must be made, and histograms of conductances are analyzed to glean a statistical understanding of the conductance and charge transport through a molecule (Figure 1-8).[36, 38]

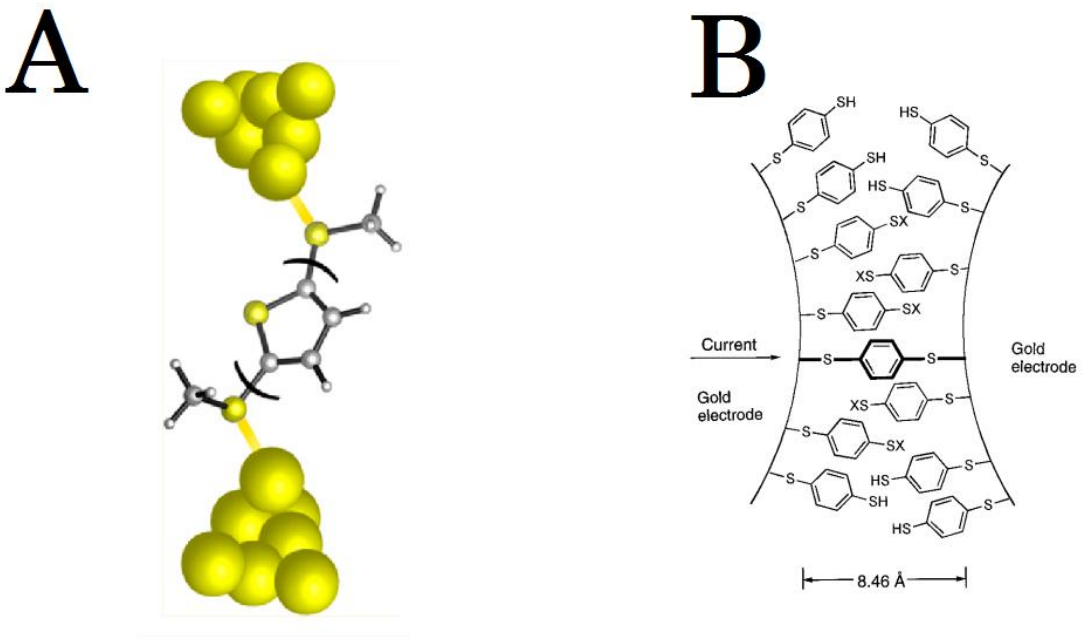

Figure 1-8: Single Molecule Electronic Devices

Measuring conductance through single molecules is a highly statistical endeavor. Molecules can adopt many conformations which affect charge transport and conductance through the molecule.
(A) Schematic of STM junction of a single oligothiophene molecule. The attachment between molecule and STM tip is temporary, and the conformation of the molecule during attachment, and the atom of Au the molecule attaches to significantly influence conductance
(B) Schematic of break junction formed by breaking a thin Au wire in the presence of analyte molecule. The MMM junction forms with one or few molecules and is broken when the distance between Au wire segments is too large. Images copyright their respective owners.

Another approach is to use an ensemble of molecules or SAM to measure hundreds to thousands of molecules at a time. One such approach is to use a conductive AFM tip to contact molecules analogous to the STM type measurement, but instead of measuring the current through a single molecule as with the STM the

AFM measures many molecules at once.[39,40,41,42,43,44,39] Devices formed this way measure conductance over several molecules at once, averaging over many molecular conformations. Though there is less variance in conductance than seen in single molecule measurements, there is still significant variation in the measurement due to molecular conformations and imperfect contact with the cAFM probe.

Though using a cAFM probe to form a top electrode in a molecular junction is a reliable way to test molecules, it is a temporary junction that is formed and broken to make a measurement. Making permanent contact with single molecule and single molecule layers is much more difficult due to the destructive nature of traditional metal deposition.[45] Evaporation and sputtering penetrate thin organic layers causing devices to short, so a more reliable must be used to form a top contact. One way to mitigate this is to protect the single molecule layer with an organic conductor either transferred or spuncast on top of the molecules.[46,47,48] This is a reliable method to form devices, but it adds an extra organic layer between metal electrodes, which can complicate measurements that require coherence between electrodes and molecules.

Another motif that has seen recent research interest is transfer printing a metal electrode on top of a layer of molecules. In this approach, a metallic layer is deposited on a donor material, and a polymeric stamp is used to bring the metal into contact with a molecular layer, so that the molecular layer is never subjected to the harsh conditions of metal evaporation.[49,50] For example, in nanoTranfer printing

(nTP), metal is evaporated directly on a patterned PFPE stamp, which is brought into contact with SAM. The deposited metal has a greater affinity for the SAM than the PFPE, due to a covalent bond that forms between the metal and the SAM and the low surface energy of the polymer, so that when the stamp is removed, the patterned electrode is left behind.

Device schematics of the ensemble devices are summarized in (Figure 1-9).[46-47, 49-51] When measuring molecular electronic transport of a polymer system, an

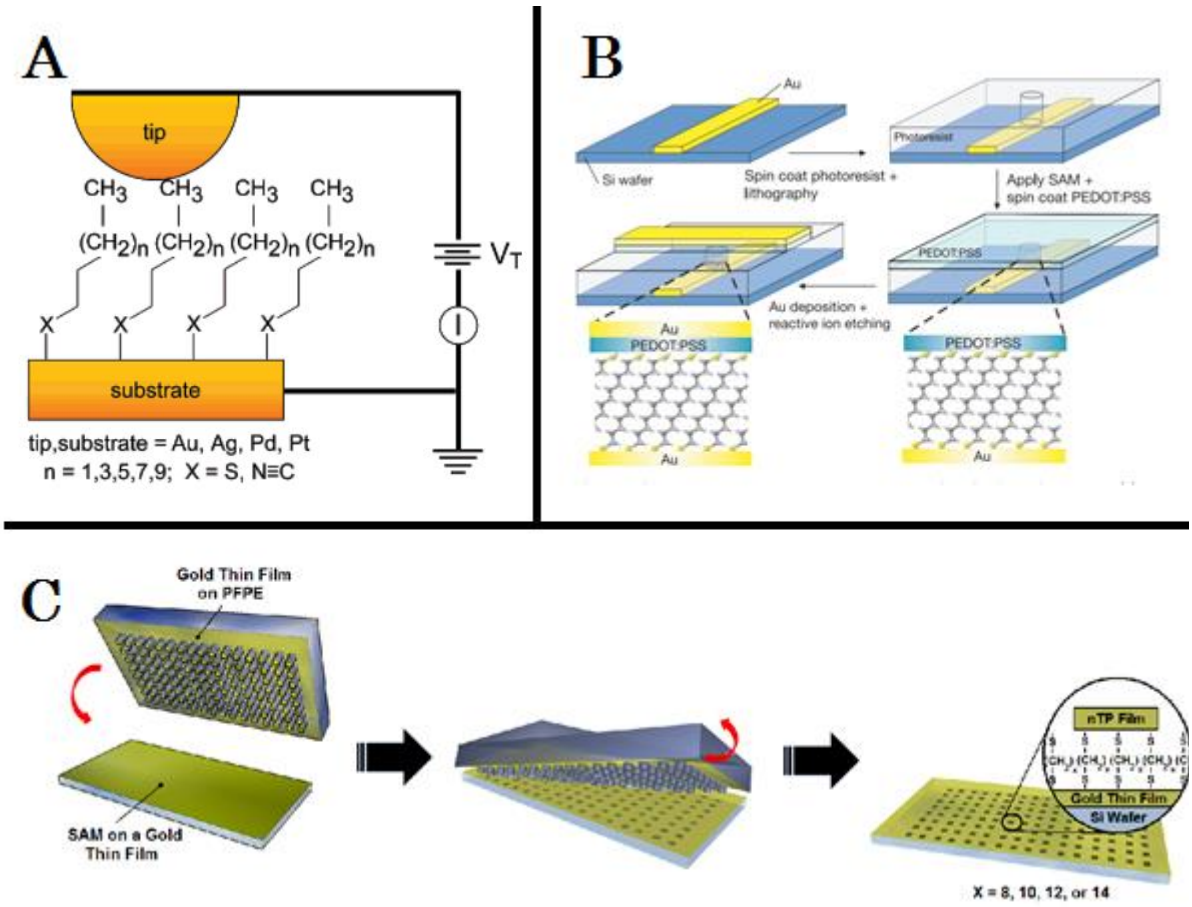

Figure 1-9: Large-Area Molecular Electronics Device Schematics
(A) Device made with a temporary cAFM electrode formed by bringing a cAFM tip in contact with a SAM
(B) Device made by evaporating metal contact on top of PEDOT:PSS buffer layer.
(C) Device made by nTP top contact directly on top of SAM
Images copyright their respective owners.

ensemble device is the best option due to extremely low currents measured in devices. Many single molecule oligomer devices push the practical limits of measurement, and in the case of oligothiophenes, thiophene chains up to only six units can be measured.[36]

1.3.3 Measuring Resistance of Molecules

One of the most basic properties of molecular electronic devices is the device conductance or resistance. Typically, a homologous series of molecules such as alkanes, oligo *p*-phenyls, or other oligo arylenes are put into devices as listed above and their conductance as a function of molecular length are measured. In short molecules, tunneling is usually the dominate charge transport mechanism, and the current through the molecules can be modelled via the Simmons model:[52]

$$\boldsymbol{I = \left(\frac{qA}{4\pi^2\hbar d_0^2}\right)\left\{\left(\Phi - \frac{qV}{2}\right)exp\left[-\frac{2(2m)^{\frac{1}{2}}}{\hbar}\alpha\left(\Phi - \frac{qV}{2}\right)^{\frac{1}{2}}d_0\right]\right.} \quad (2)$$
$$\boldsymbol{\left. - \left(\Phi + \frac{qV}{2}\right)exp\left[-\frac{2(2m)^{\frac{1}{2}}}{\hbar}\alpha\left(\Phi + \frac{qV}{2}\right)^{\frac{1}{2}}d_0\right]\right\}}$$

where I is the current, q the electron charge, A is the area of the junction, $\hbar$ is the reduced Heisenberg constant, d_0 is the tunneling distance, Φ is the tunneling barrier, V is the applied bias, and m is the carrier mass. The positive exponential term corresponds to tunneling in the forward bias direction, and the negative term

corresponds to tunneling in the reverse direction which can be neglected when there is an applied bias.

At low applied biases, the current scales linearly with voltage, so the resistance of a molecular device can be calculated using Ohm's law:

$$\boldsymbol{V = IR} \tag{3}$$

and a simplified version of equation (2):

$$\boldsymbol{I = I_0 V e^{-\beta l}} \tag{4}$$

where I_0 is a prefactor, l is the molecular length, and β is the tunneling decay coefficient which describes the efficiency charges tunnel through a material. High β-values correspond to large values of $\boldsymbol{\Phi}$ in equation (2) and can be interpreted as being more difficult to tunnel through than materials with lower β-values. Inserting equation (4) into equation (3) and solving for resistance gives:

$$\boldsymbol{R = R_0 e^{\beta l}} \tag{5}$$

For a homologous series of molecules, the β-value is a figure of merit which describes how charges through a molecular repeat unit (such as a methylene unit or a phenyl ring) and is calculated from a semilog plot of resistance vs. molecular length (Figure 1-10).[40,44] The numerical β value can range from greater than 10 nm^{-1} in alkanethiols to as low as 0.1nm^{-1} in conjugated molecules.[53] Changing the molecule between electrodes will change the β-value, and therefore the conductance of the junction.

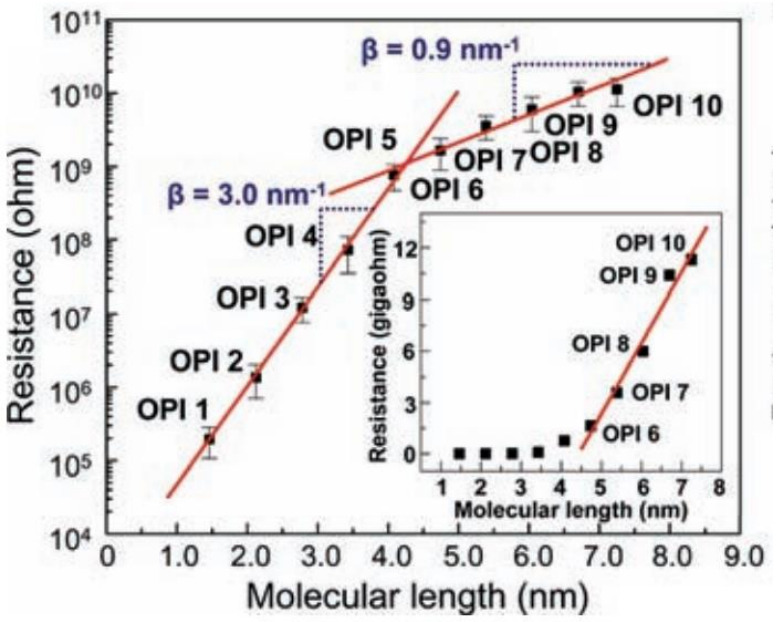

Figure 1-10: Plotting Beta Values

The ß value for long molecular wires is determined from linear portions of a semilog plot of resistance and molecular length. As the molecular length increases, the ß value decreases. This is most likely due to a change in the charge transport method at greater molecular lengths. Image is copyright its respective owner.

1.3.4 Outlook for Molecular Electronic Devices

Molecular electronics shows great promise in testing new effects and properties in organic molecules. In this work, device fabrication, testing, and function in molecular electronics will be applied to the polymer semiconductors traditionally measured in organic electronics. Though there are superficial similarities between traditional polymer semiconductors and molecular electronics (both use organic materials as active materials), the two fields differ fundamentally in the scope at which these materials are studied. Molecular electronics, by definition, focuses on molecular interpretations of charge transport properties in devices of molecular dimension.

For polymer semiconductors, molecular interpretations are also important, but the bulk properties that dominate behavior are due to transport between polymer chains despite careful engineering at synthetic and device levels. By taking a molecular approach to traditional polymer semiconductors, properties at the molecular level can be fully realized at a device level without being inhibited by intermolecular transport in polymer thin films.

1.4 Polymer Brushes

1.4.1 Definitions and Examples of Polymer Brushes

A polymer brush is an architecture consisting of polymer chains packed densely together where each polymer is immobilized at one end. Chains can be

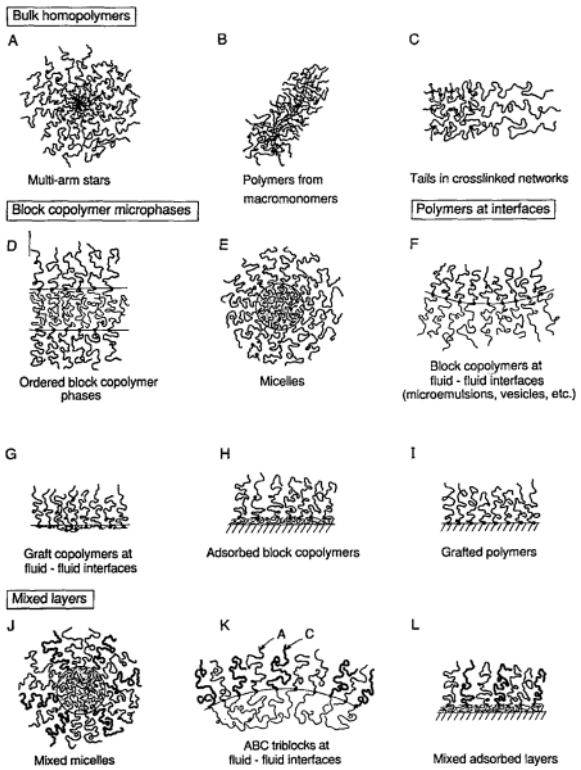

Figure 1-11: Examples of Tethered Polymer microstructures

bound covalently on a surface or polymer backbone, aggregated physically at an interface, or in a micelle (Figure 1-11).[54] There are many kinds of polymer brush frameworks, and the previous list is not exhaustive, but in any case, the fact that the polymer is immobilized at one end imbues it with many interesting properties. Of interest in this work is the ability for a polymer to stretch into a non-ideal conformation. Ideal polymers coil in a random walk with no long range order, and the polymer radius is given by the equation:[55]

$$\boldsymbol{R = N^{\frac{1}{2}} b} \tag{6}$$

However, when a polymer is immobilized on a surface, the conformation can change due to interactions between neighboring chains. The polymer conformation becomes stretched and the new chain length is described by the equation:[54]

$$\boldsymbol{\frac{L}{b} = N(\frac{b}{d})^{\frac{2}{3}}} \tag{7}$$

where L is the length of the polymer layer, b is the monomer length, N is the degree

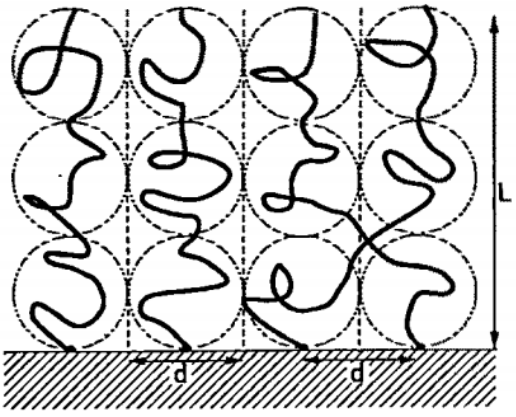

Figure 1-12: Brushlike Conformation of Tethered Polymer Chains

of polymerization, and d is the distance between chains (Figure 1-12).[54]

To construct a molecular junction based on an ensemble of polymer semiconductors, a polymer brush framework must be assembled such that a monolayer of well-ordered polymers can be electrically addressed. Many synthetic efforts have driven towards growing conjugated polymer brushes from surfaces, and in order to make devices, careful consideration of synthetic methods must be used to create the ideal architecture.

There are three general strategies to attach polymers to a surface (Figure 1-13).[56] The *grafting to* method is not useful to this work due to the low grafting density of polymers on the surface and in general is not used to make films of polymer semiconductors. The *grafting through* suffers from similar shortcomings.

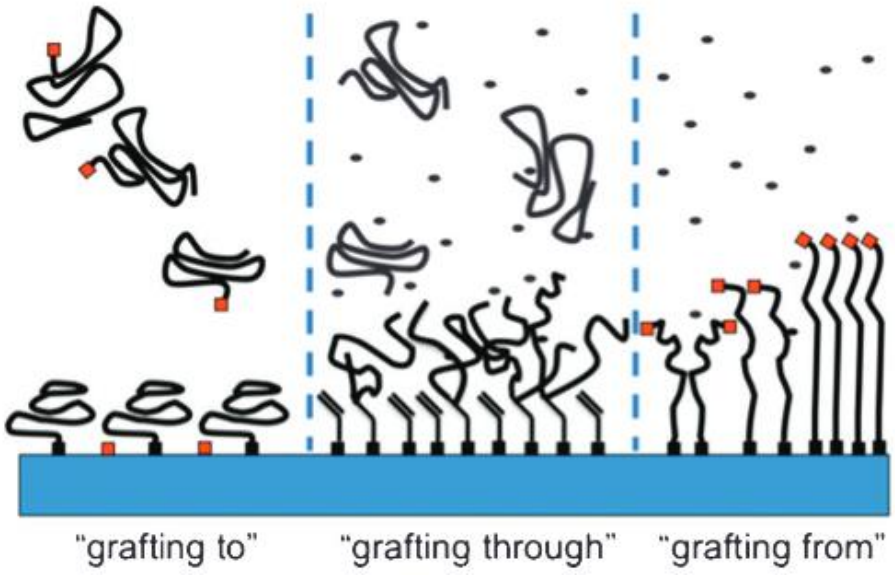

Figure 1-13: Grafting Methods for Polymer Brush Formation

Only the grafting from method allows for dense brushlike microstructures to form. This is because the grafting density is the highest in this regime. In the grafting to and through regimes, the grafting density is limited by the size of the macromolecular species being attached to the surface rather than by the small initiating species. Image copyright its respective owner

In order to achieve a brushlike conformation, the "grafting from" approach will be employed in this work. As will be discussed later, "grafting from" allows high surface density of polymers so they can stand normal from the surface.[57]

1.5 Research Overview

There is already a large body of research exploring charge transport, carrier mobility, thermal transport, and spin transport through conjugated polymers thin films. Despite the tireless efforts of researchers across the world, solid device-level measurements of intramolecular carrier transport along the backbone of conjugate polymers is still absent from the literature.

This work strives to take measured steps toward measuring intramolecular, along-the-backbone charge transport in polymer semiconductors. To this end, large area molecular devices are fabricated by growing poly(3-methylthiophene) wires in a brushlike conformation from conducting substrates and depositing electrodes on top of the resulting by soft lithographic transfer. In order to ensure high quality devices are made, film microstructure is characterized by optical and X-ray spectroscopy as well as atomic force microscopy (AFM) and scanning electron microscopy (SEM). Charge transport in devices is measured by using a cAFM tip and a metal wire as probes to make electrical connection to the device. Measured IV curves are modelled to gain an understanding of charge transport in these novel devices.

CHAPTER 2 POLYMER BRUSH SYNTHESIS

2.1 Introduction and Overview of Synthetic procedures

With the relatively recent discovery and rise in popularity of metal catalyzed cross coupling reactions to form bonds between aromatic rings, new polymers and polymerization methods have expanded the scope and applications of conjugated polymers.[58] The synthesis of polymers in solution is well studied and understood. There are two main polymer growth mechanisms in solution: chain growth and step growth.[59] In a chain growth polymerization, monomers are added to the propagating

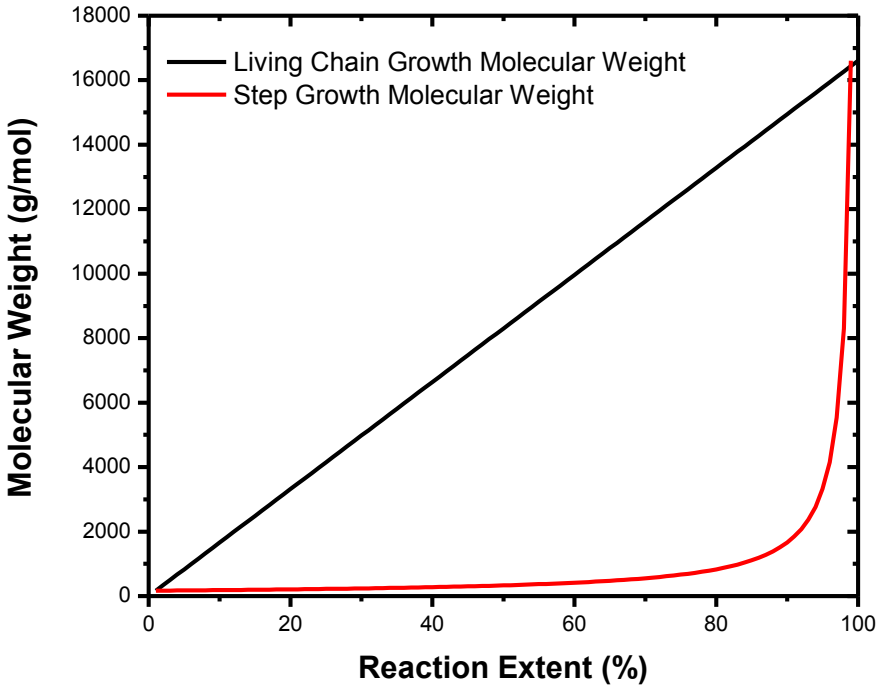

Figure 2-1: Polymer Chain Growth Mechanisms

In Step growth polymers, high molecular weights are only achieved at as the percent conversion approaches 100%, but for living chain growth polymerizations, molecular weight increases linearly throughout the polymerization. These two behaviors are consequences of the growth mechanism of the different polymerization types.

chain end sequentially to form a polymer. This is in contrast to a step growth polymerization where bifunctional monomers are put together two functional groups at a time to form dimers, then larger oligomers, and finally polymers (Figure 2-1).[60] In order to grow a polymer thin film as described in chapter 1, the reactive chain end must be immobilized to a surface so monomers are added to a propagating chain one at a time. The recent discovery of the living cross coupling polymerization called Kumada catalyst-transfer polycondensation (KCTP) or Grignard metathesis (GRIM) has marshalled several methods to grow and study surface bound conjugated polymers.[61,62] The fundamental difference between KCTP and typical cross coupling mechanism is the ability for a catalyst to stay associated with one chain during the entire course of polymerization by "chain walking" to the polymer chain end and inserting oxidatively into the same polymer chain every time (Figure 2-2).[63] Of particular interest it palladium catalyzed surface initiated KCTP (SI-KCTP), which has been demonstrated to produce P3MT films oriented with some degree vertically from a conductive substrate.

The proposed growth mechanism for KCTP and SI-KCTP (Figure 2-2) follows living, chain growth kinetics.[64] Thus, the polymerization kinetics should be sensitive to parameters such as monomer concentration and temperature, and the growth of polymer films should be linear as a function of reaction extent. In order to make brushlike thin films, all of these parameters must be controllable to create films with high grafting density, controllable length, and controllable morphology. The synthetic methods to achieve these goals are discussed below.

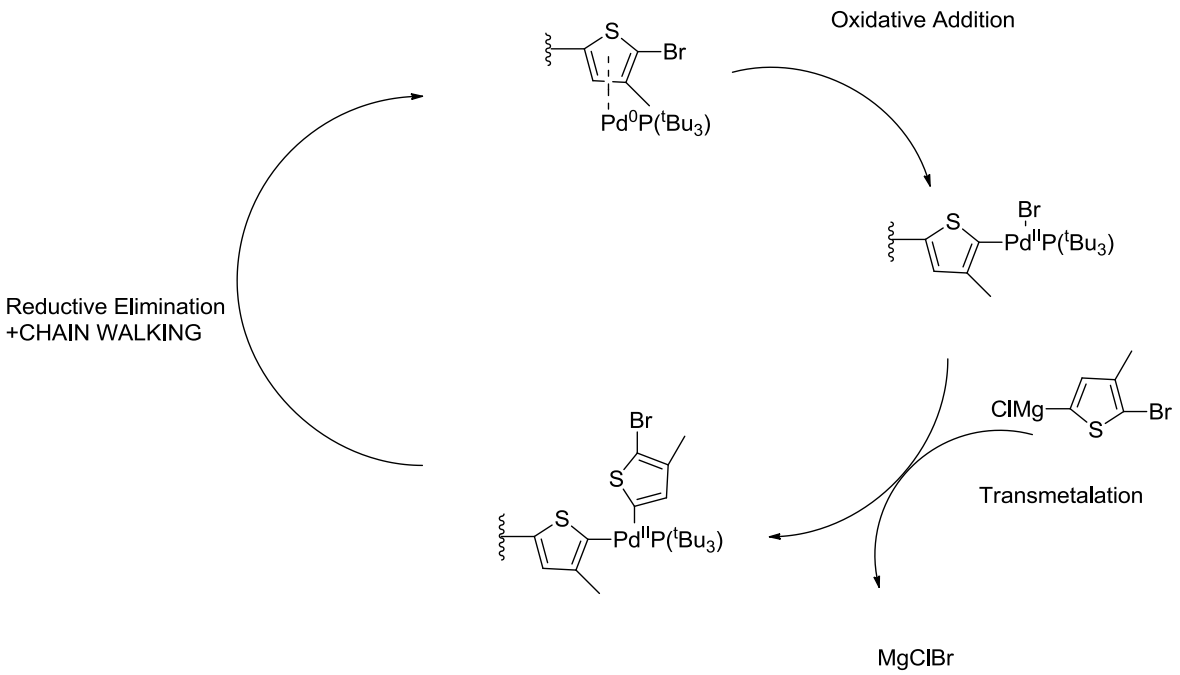

Figure 2-2: Proposed(SI-)KCTP Mechanism

Polymer chains grown by SI-KCTP and KCTP grow by living chain growth kinetics, unlike other cross coupling polymerization mechanisms that grow by step growth kinetics. The above mechanism is nearly identical to similar cross coupling mechanisms such as Stille and Suzuki coupling, but with one fundamental difference. After reductive elimination, the catalyst, in this case $Pd^0P(^tBu_3)$ does not dissociate form the growing chain but remains associated with the π system of the polymer backbone. The catalyst is either trapped at the growing chain end or walks between chain ends to oxidatively insert into an Ar-Br bond to continue propagation.

2.2 General Polymerization Protocols

The general procedure for Pd catalyzed SI-KCTP has been published elsewhere,[57] but each step of the synthesis is integral to forming high quality polymer brush thin films. The parameter space of each step can be tuned to produce high quality polymer films.

In Figure 2-3, the SI-KCTP steps are summarized. A cleaned ITO substrate is functionalized with a monolayer with free aryl bromine. The functionalized ITO slide is soaked in a solution of bis(tri-*tert*-butylphosphine)palladium(0), which is inserted oxidatively into the free aryl bromine bond to form a reactive species on the surface. The reactive substrate is then soaked in a solution of monomer to grow the

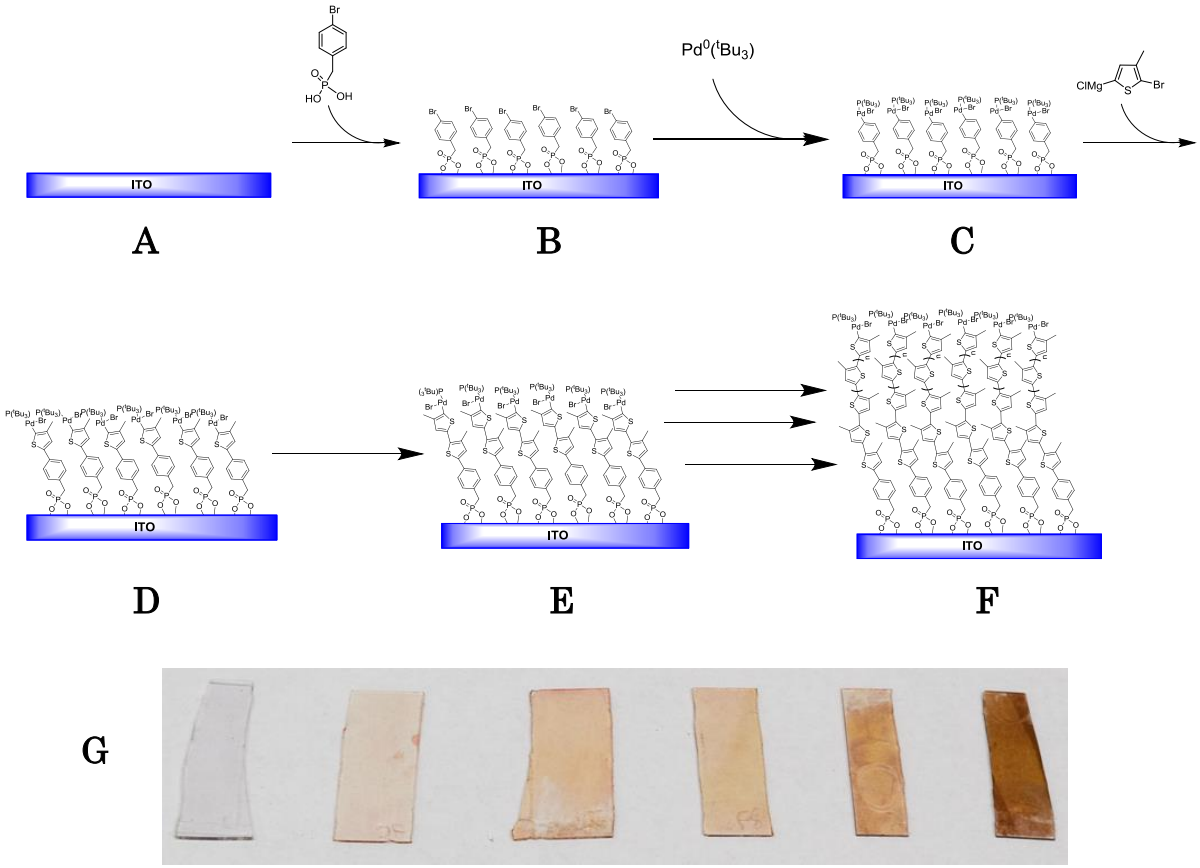

Figure 2-3: SI-KCTP Protocol

For and in depth description of the procedure, see section 2.8.
(A) ITO Slides are first thoroughly cleaned and prepared for monolayer deposition.
(B) A monolayer is deposited on the ITO slide and annealed to improve film formation.
(C) A catalyst is inserted into the monolayer to form the initiating species. This is analogous to forming an external initiator in a solution polymerization
(D) The initiated ITO slides are put into a solution containing an active monomer to propagate the polymer chain.
(E-F) Polymer chains are extended by letting the slides sit in solution for a period of time.
(G) ITO Slides with grown P3MT brushes
Steps C-F are conducted in a nitrogen glovebox with <1ppm water and oxygen.

polymer from the surface by the *grafting from* method. The polymer chain length is controlled by varying the reaction time, and the rate of polymerization can be controlled by varying the monomer concentration. During the polymerization, some reactive species become detached from growth substrate to initiate solution grown polymer and contributing to surface roughness and inhomogeneity. In this chapter, the parameter space for each step is explored to determine controllable reaction conditions to grow P3MT brushes.

2.3 Initiator Attachment Chemistry

The initiating species for SI-KCTP is a Pd(II) catalyst immobilized on an ITO surface which propagates with growing chain end. The catalyst complexes are initially fixed to the surface by inserting into an aryl-bromine bond on an SAM. Several attachment chemistries have been used to attach molecules to ITO surfaces, and such two attachment chemistries are explored here: –COOH and –POOHOH (carboxylic and phosphonic acid) functional groups. Phosphonic acids form robust linkages that do not strongly couple electronically with metal oxides. Carboxylic acids, however, do not form robust linkages to metal oxides but have strong

Figure 2-4: Target Initiator Molecules

The two target molecules for forming surface initiators for SI-KCTP. (4-bromobenzyl)phosphonic acid (left) has been used in several literature reports while 5-bromo-4-methylthiophene-2-carboxylic acid has not been reported for use in SI-KCTP.

electronic coupling. Monolayers of 5-bromo-4-methylthiophene-2-carboxylic acid and (4-bromobenzyl)phosphonic acid are used here as comparative molecules.

Previous reports of SI-KCTP from ITO use phosphonic acid functional groups.[56,65,66,57,67] In an effort to control the interface through which charge carriers inject into the polymer brush, and thus the charge transport properties, two anchoring molecules (Figure 2-4) are investigated using different attachment chemistries. Several figure of merit are used to evaluate the utility of each molecule for use in polymer brush devices. First, the molecule must form a good monolayer on an ITO surface. The grafting density of the polymer brush is limited by this factor. Second, the monolayer must be reactive to the Pd catalyst used in polymerization. Finally, the monolayer must support the growth of P3MT polymer brushes.

The monolayer quality is investigated by measuring advancing contact angle of water on modified ITO surfaces to measure the hydrophobicity of the surface and by atomic concentration via XPS. These measurements provide a zeroth order estimation of monolayer quality, with high contact angles correlating with good monolayer qualities. The XPS measurements provide information about the relative concentrations of atomic species on the ITO surface, but do not give a quantitative figure for the number of molecules on the surface. In order to determine the number of molecules on the surface, a ferrocene unit is added to the monolayer via surface initiated Kumada coupling. The number of ferrocene units on the surface is measured via cyclic voltammetry and provides a quantitative assessment of the grafting density of polymer on the surface. This may not be equal to the total

number of molecules on the surface,[66] but it provides a figure for the grafting density for the surface grown polymer. Finally, the most important figure of merit when determining if a monolayer is suitable for SI-KCTP is measured by determining whether or not polymer brushes can be reliably grown from the substrate.

2.3.1 Investigating Monolayer Quality through Contact Angle and XPS

Monolayers of 5-bromo-4-methylthiophene-2-carboxylic acid and (4-bromobenzyl)phosphonic acid are prepared and annealed similar to literature reports. For contact angle analysis, advancing contact angles are compared to a monolayer of octadecylphosphonic acid on ITO. Contact angles are listed in Table 2-1. For these monolayers on ITO, high contact anglers are not seen until after the monolayers are annealed at 150°C under N_2, possibly because the heat drives the dehydration reaction that anchors the molecules on the surface to completion to

Molecule	Contact Angle Before Annealing	Contact Angle After Annealing
Octadecylphosphonic acid	--	89°
4-bromobenzyl phosphonic acid	72°	86°
5-bromo-4-methylthiophene-2-carboxylic acid	62°	73°

Table 2-1: Contact Angles for Initiator Anchoring Groups

ITO soaked in 5mM solutions of octadecylphosphonic acid, 4-bromobenzyl phosphonic acid, and 5-bromothiophene-2-carboxylic acid , respectively. Contact angles are averaged over 5 samples.

form well-ordered monolayers. Based on the contact angle measurements, the phosphonic acid monolayer is more hydrophobic than the carboxylic acid monolayer, implying that the monolayer quality is better for the phosphonic acid than for the carboxylic acid linker. Annealed phosphonic acid monolayers are nearly as hydrophobic as the octadecylphosphonic acid monolayer, implying that the quality of these monolayers is quite good. The data suggest that in the case of both 5-bromo-4-methylthiophene-2-carboxylic acid and (4-bromobenzyl) phosphonic acid a monolayer forms on the ITO surface.

The XPS data provide a complementary picture to the monolayer. From XPS measurements, atomic ratios and relative atomic abundances for the 5-bromo-4-methylthiophene-2-carboxylic acid and (4-bromobenzyl) phosphonic acid monolayers are determined for ITO substrates functionalized with each respective molecule. Atomic ratios are used to determine if the proper chemical species is observed on the ITO surface, while the relative atomic abundances can provide a comparative assessment of the surface coverage of the molecules.

Molecule	Ratio P:Br	Ratio S:Br	Relative Atomic Abundance Br
(4-bromobenzyl) phosphonic acid	0.93:1	0:1	2.42%
5-bromo-4-methylthiophene-2-carboxylic acid	0:1	1.3:1	0.84%
Bare ITO	0:0	0:0	0%

Table 2-2 : XPS Analysis of Monolayers

XPS measurements verify the atomic ratios of elements of interest on ITO surfaces. The relative

Based on the 5-bromo-4-methylthiophene-2-carboxylic acid monolayer, the ratio between sulfur and bromine should be 1:1 if the correct chemical species is on the surface. Likewise, for (4-bromobenzyl) phosphonic acid, the ratio between P:Br should also be 1:1. The XPS data are tabulated below in Table 2-2. The ratio for each molecule matches the prediction based on the chemical structure. Furthermore, bare ITO substrates do not express any of the atomic species of interest, so each atomic species present on the surface is attributed to a monolayer molecule of interest. Based on the relative atomic abundance of bromine on the surface for monolayers of each molecule, the (4-bromobenzyl) phosphonic acid monolayer is approximately three times as dense as the 5-bromo-4-methylthiophene-2-carboxylic acid monolayer. These data corroborate what was observed with the contact angle measurements, that the phosphonic acid linker molecules form better monolayers than the carboxylic acid linker.

2.3.2 Determining Initiator Grafting Density with Cyclic Voltammetry

The grafting density of initiators on ITO surface for monolayers of 5-bromo-4-methylthiophene-2-carboxylic acid and (4-bromobenzyl)phosphonic acid monolayers is quantitatively determined by using a surface initiated Kumada coupling reaction to add a ferrocene molecule to the surface that can be probed by cyclic voltammetry (Figure 2-5). The grafting density of initiators on (4-bromobenzyl)phosphonic acid monolayers is in close agreement with literature reports, with values measured here approximately 20% greater than literature at $(1.3\pm0.2)\text{x}10^{14}$ molecules/cm^2.[57] Initiators formed on carboxylate monolayers are one

third as dense with at $(4.1\pm1.3)\times10^{13}$ molecules/cm^2. This ratio is in close agreement with the difference in surface coverage determined by XPS, and the trend in contact angle. The carboxylic acid monolayer is not as dense as the phosphonic acid monolayer.

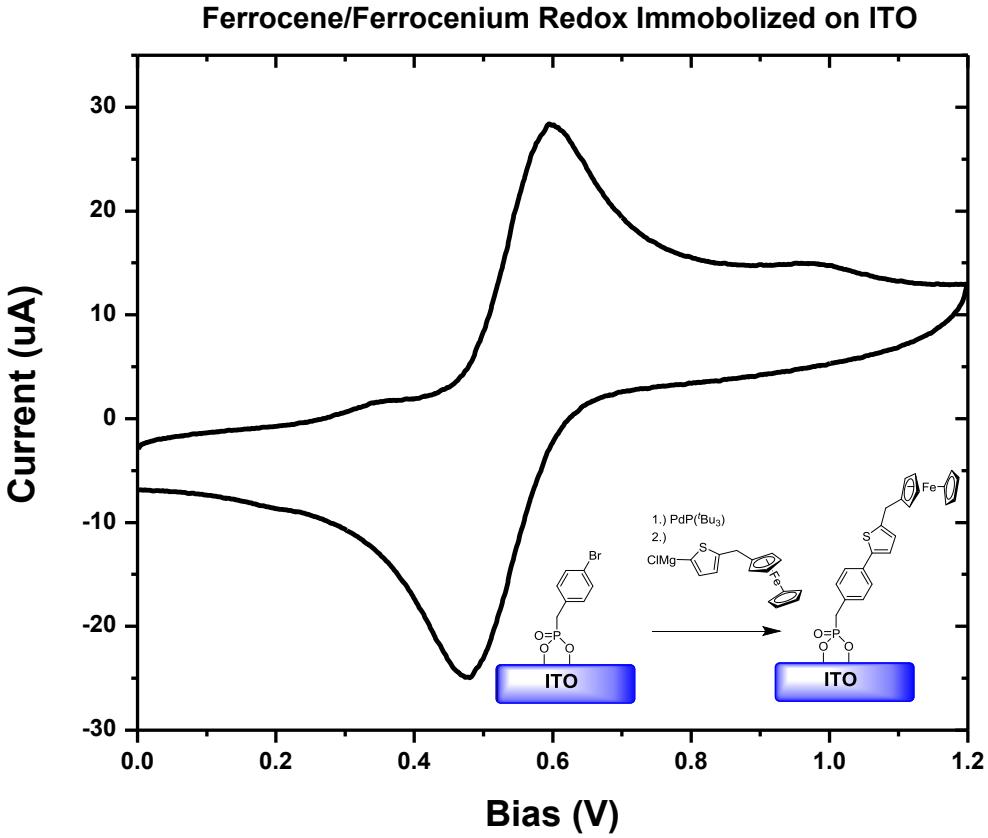

Figure 2-5: Electrochemically Determining Initiator Grafting Density
A ferrocene labeled thiopehene unit is attached to both monolayers (Inset) and the oxidation peak area for the Fc/Fc$^+$ redox cycle is used to determine the amount of charge, and thus the number of electrons for the reaction. Each Fc/Fc$^+$ redox reaction is a one electron process, so the number of electrons making up the charge in the peak is equal to the number of initiators.

2.3.3 Growing Poly(3-methylthiophene) Brushes from Carboxylic and Phosphonic Acid Based Monolayers

Despite the relatively poor surface coverage of 5-bromo-4-methylthiophene-2-carboxylic acid compared to (4-bromobenzyl)phosphonic acid based on the above metrics, polymers are attempted to be grown from 5-bromo-4-methylthiophene-2-carboxylic acid initiators. This is the ultimate test to the utility of a monolayer for use in SI-KCTP is how well polymers can be grown from the surface. The efficacy of the carboxylic acid monolayer is tested by subjecting ITO slides with Pd loaded into the thiophene-Br bond, to SI-KCTP conditions as reported in literature. The resulting polymer film is compared to a substrate prepared at the same time with a (4-bromobenzyl)phosphonic acid monolayer instead of the carboxylic acid based

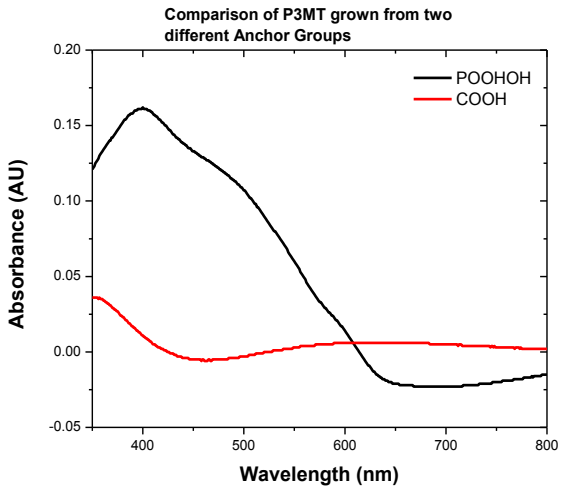

Figure 2-6: P3MT Films Grown from Different Monolayers

Polymer films grown from phosphonic acid monolayers (black) grow to appreciable lengths (approx. 15nm) and demonstrate evidence of densely packed polymer chains. Polymers grown from carboxylic acid monolayers grow unreliably to thin film lengths and do not exhibit optical properties typical to P3MT films.

monolayer. The UV/Vis spectra of the resulting organic thin films are compared in Figure 2-6.

Though there is some residue that grows on the film after subjecting the carboxylic acid modified slides to SI-KCTP conditions, the resulting film is significantly different from that grown from the phosphonic acid monolayer. Thin films of P3MT normally absorb strongest between 400-650nm, and in this range there is little to no absorption for films from carboxylic acids. Vials that films are grown in show significant signs of solution polymerization. This is most likely due to carboxylic acid molecules falling off the surface during polymerization. The poor initiator coverage relative to the amount of molecules on the surface combined with the poor polymerization results suggest that carboxylic acid monolayer is not a good candidate to support an initiating species for SI-KCTP.

2.4 Polymer Film Quality and Thickness Dependence on Reaction Temperature

In many polymerizations, the temperature can be a factor that is used to control reaction rate. Literature reports of Pd catalyzed SI-KCTP are only conducted at 40 °C,[57] so the effects of temperature on the reaction rate are not documented. Here, the polymerization temperature is varied over 20 °C between 30 °C-50 °C, and the polymer thickness and absorption spectra after 16 h reaction time are compared. The polymer thickness film thickness and the shape of the absorption spectra provide insight to the polymerization kinetics as well as the quality of the grown film (Figure 2-7).

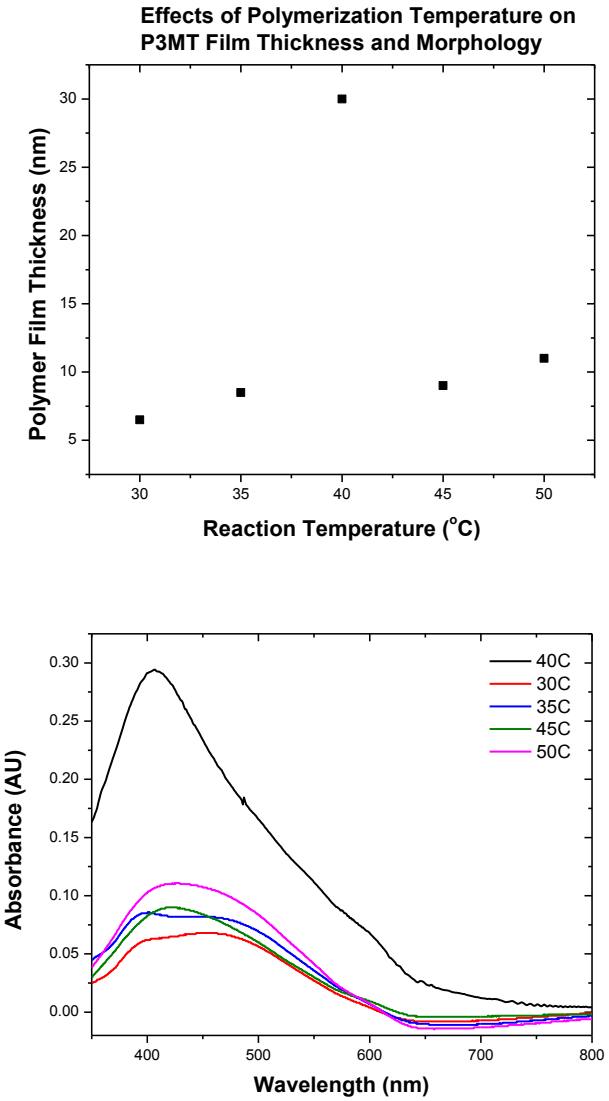

Figure 2-7: Temperature Dependence of SI-KCTP
[Top] The P3MT film thicknesses after 16 h reaction time are compared here. For reaction temperatures below 40 °C, polymer films are thin, but little solution polymerization is observed. At reaction temperatures above 40 °C, the thin films are also observed, but after only three hours, the monomer stock which feeds the surface polymerization is an opaque red, implying many initiators fall off the surface. There is a small window at 40 °C where thick films can be grown.
[Bottom] The film quality can be assessed by the absorption spectrum. For polymerization temperatures at and below 40 °C peaks at 400 nm combined with the absorption onset at 650 nm give evidence of P3MT films with H-aggregation, meaning that the films are densely packed. For films grown at temperatures above 40 °C, there are no such peaks, which combined with the experimental observation of increased solution polymerization and literature interpretation of broad absorption spectra similar to these imply these films lack high grafting density.

As reported in literature, 40 °C is the ideal temperature for polymerization with Pd catalyzed SI-KCTP. For polymerizations conducted at 40°C, some solution polymerization is observed after six or more hours reaction time, but final film thickness after 16 h reaction time under these conditions are consistently thicker than other temperatures, reaching thicknesses up to 30 nm under these reaction conditions. For reaction temperatures below 40 °C, there is less solution polymerization than observed at 40 °C—that is the monomer solution does not turn opaque red during the polymerization—but some solid polymer is observed in solution. The polymer thickness is determined from the absorption maximum, and at either temperature below 40 °C, the thickness is much thinner than the polymer grown at 40 °C reaching less than 10 nm. At temperatures above 40 °C, solution polymerization is observed after only three hours of reaction time and the reaction solution turns opaque red. The polymer film thickness for reaction temperatures at 45 °C and 50 °C are nearly identical to those at 30 °C and 35 °C. At temperatures below 40 °C, the system has enough energy to polymerize, but the rate of reaction is quite slow. Though some catalysts fall off the surface during the polymerization, most of the reactive species stay on the surface yielding a densely packed, high quality, short film as evidenced by the UV/Vis absorption spectra in Figure 2-7.

This is in contrast to reactions above 40 °C. The rate of reaction is most likely faster—direct experimental evidence of this is difficult to acquire—but there is sufficient energy to overcome the intramolecular oxidative addition during the polymerization process. This excess energy causes reactive species to fall off the

surface, thereby lowering the grafting density of the polymer on the surface. These films have longer chains, but because the grafting density is lower, the film thickness is lower, too. This is evidenced by the broad absorption peak in the absorption spectra signifying a lack of H-aggregation for films grown with polymerization temperatures above 40 °C in Figure 2-7. The H-aggregate peak at 400 nm is observed in P3MT films with high grafting densities due to the confinement of chains in close proximity. Films with low grafting densities do not exhibit the same behavior because the chains do not form aggregates on the ITO surface in the same way films with higher grafting densities can. For the films grown at low temperatures, this peak is observed as one of two local maxima in the absorption spectrum.

Films grown at 40 °C occupy an intermediate regime where there is sufficient energy for polymerization to occur at a reasonable rate, but there is not excess thermal energy for a large number of reactive species to leave the ITO surface and polymerize in solution. Thus, these films grow thickest and exhibit evidence of H-aggregation, implying strong interchain interactions due to close confinement of polymer chains on the surface.

2.5 Polymer Film Thickness on Reaction Time

Possibly the most facile way to systematically control polymer chain length is by varying the polymerization's is the reaction time. In solution polymerizations, as the extent of reaction for a living or pseudo living polymerization tends towards 100%, the molecular weight of the polymers increase linearly. By taking aliquots of

a single living polymerization throughout the reaction, several different molecular weight polymer samples can be easily acquired. When polymerizing from a surface, where the monomer in solution is typically not used up completely, the molecular weight of the surface bound chains increases linearly with time because the concentration of the monomer does not change appreciably. In literature reports for

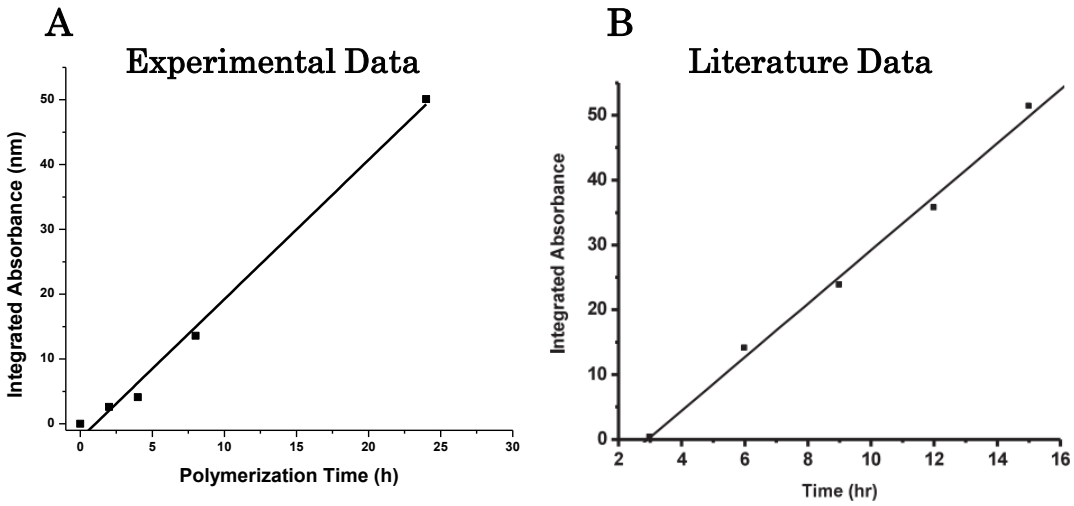

Figure 2-8: Integrated Absorbance from Experiment and Literature

Integrated absorbance increases linearly with time in experiment and literature reports. Integrated absorbance is often used to compare the total amount of material on a surface rather than using the absorption maximum. This is especially good when the maximum absorption wavelength shifts between samples. Image copyright its respective owner.

SI-KCTP catalyzed by of bis(tri-*tert*-butylphosphine)palladium(0), increase in absorbance of grown polymer brush films is recorded with respect to polymerization time (Figure 2-8),[57] but no correlation of polymer thickness with absorbance is reported.

The experiment to test the polymer film thickness with respect to time is simple: ITO substrates with surface bound initiators are placed into a solution of

monomer and are taken out at regular intervals and cleaned. The UV/Vis absorption spectrum of each film is taken (Figure 2-8). As observed in literature, the polymer integrated absorbance grows linearly with respect to time. In order to confirm that the film thickness increases with respect to time, the thickness of each film was characterized by AFM profilometry (described in detail in Chapter 3). The calibration plot between absorbance maximum and P3MT film thickness (Figure 2-9) shows a linear relationship between the two, and when the measured thicknesses are plotted against time the linear growth of the polymer thin films is verified, something not before reported in the literature.

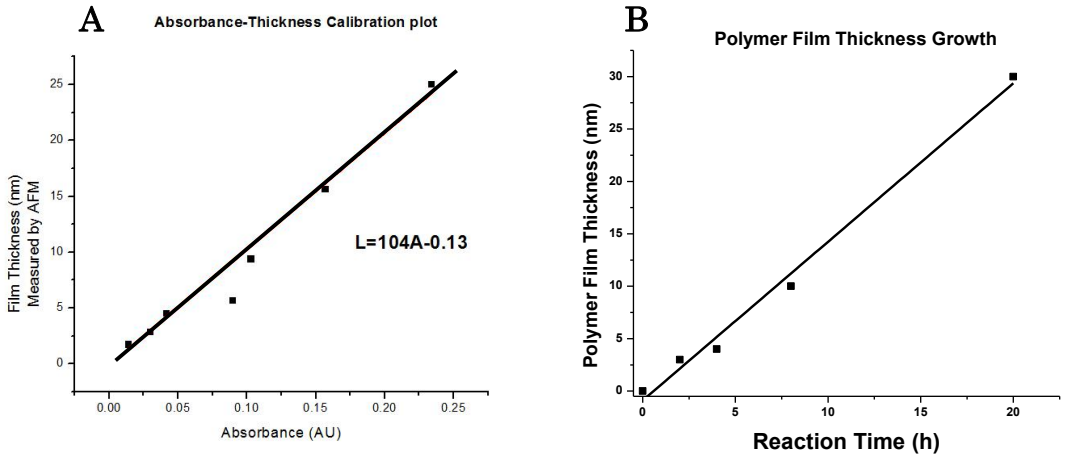

Figure 2-9: Polymer Thickness Calibration plot and Film Thickness Growth

(A) Polymer film thickness measured by AFM is plotted against the maximum absorbance of similar H-aggregated P3MT films. A linear relationship between the length of the polymer thin film (L) and Absorbance (A) relates the two parameters.
(B) The polymer film thickness with respect to time increases linearly based on this method of measuring film thickness. This relationship has not been reported before for films made by SI-KCTP.

The linear growth of the polymer thin film with respect to time is not a hallmark of a living polymerization because the film thickness is not necessarily correlated with the molecular weight of the polymer.

2.6 Concentration Dependence on Polymer Film Thickness

Another useful parameter for controlling a polymerization is the monomer concentration. In solution based living polymerizations, the rate of propagation and kinetic chain length are determined by the concentration of monomer. For classic ionic polymerizations, the rate of propagation is given by:[59]

$$\boldsymbol{rate = k_p[I][M]} \tag{8}$$

In a typical solution polymerization, the concentration of monomer decreases as it is used up in the polymerization, but in the surface initiated case, the amount of monomer used up is small relative to the total amount of monomer, so the monomer concentration (minus parasitic solution polymerization) is constant. Also, since the number of initiators is fixed on the surface, the concentration of initiators is not able to be changed. Using these assumptions, the rate of the polymerization should be constant throughout the polymerization (which is observed in the linear growth with respect to time discussed in the previous section) and the rate should depend linearly on the initial concentration of monomer.

Several monomer concentrations are surveyed and the rate of polymerization for each is calculated. The polymerization rate increases linearly with respect to concentration for concentrations below 0.1M, but for concentrations higher than 0.1M, the polymerization rate levels out (Figure 2-10). This is most likely due to high concentrations of Grignard monomer etching the initiators off the surface. For 0.2M monomer concentrations, the solution turns red and opaque indicating that for these surface initiated polymerizations solution polymerization is occurring similar to what is observed for polymerizations at elevated temperature. For surface initiated polymerizations with lower monomer concentrations the solution only has a small amount of red solids, indicating that solution polymerization does still

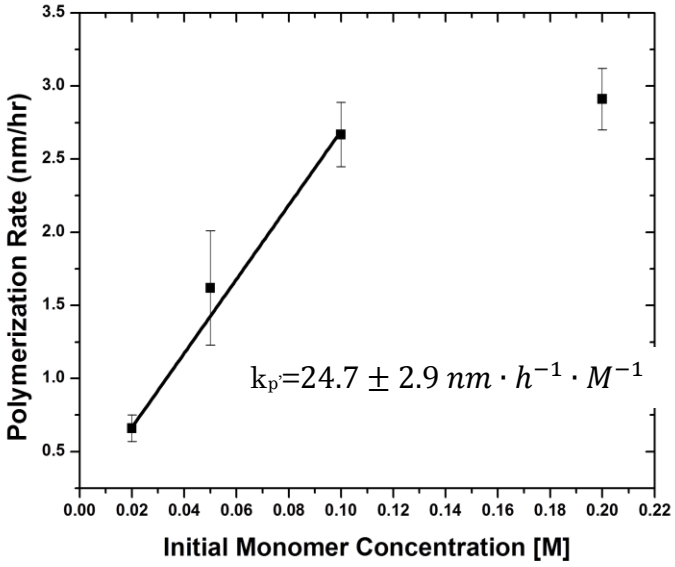

Figure 2-10: Determining Polymerization Rate Constant

There is a linear increase in polymerization rate with an increase monomer concentration up to a point of at least 0.1 M. Above 0.1 M, the polymerization rate decreases, most likely due to the harsh polymerization conditions etching the ITO substrate. This behavior further suggests that SI-KCTP polymerizations follow first order kinetics.

occur, but not as much as in higher concentration solutions. The slope of the linear portion of the graph in Figure 2-10 gives a parameter similar to k_p in equation (8). Modifying equation (8), to make physical sense to for SI-KCTP simply gives:

$$\boldsymbol{rate = k_{p'}[M]_0} \tag{9}$$

In the new equation, the rate of polymerization depends only on the initial concentration of monomer, and the concentration of initiators on the surface is a constant absorbed into $k_{p'}$. The rate constant $\boldsymbol{24.7 \pm 2.9\ nm \cdot h^{-1} \cdot M^{-1}}$ is the only one of its kind, but can be used to compare different catalyst and monomer systems investigated in the future. The existence of the linear region of the graph in Figure 2-10 gives more evidence that the polymerization is controlled under ideal conditions.

2.7 Discussion

The growth of P3MT polymer brushes via Pd catalyzed SI-KCTP can be controlled under narrow conditions of temperature, and concentration. The polymerization is remarkably sensitive to temperature. Polymerization will only occur at a reasonable rate under very narrow temperature range. The film thickness increases linearly with respect to time demonstrating linear growth under all tested conditions. The rate of polymerization also increases linearly with respect to film thickness, more evidence that that the reaction kinetics are first order and controlled. Though the polymerization may be called controlled given the evidence established by control over film thickness, the molecular weight of the polymers on the surface cannot be accurately estimated even with knowledge the film

morphology. For these reasons, it would not be accurate to call these polymerizations living. Film characterization will be discussed more extensively in Chapter 3, but grown films are not completely uniform and the polymer chains are not oriented completely vertically, so SI-KCTP cannot be accurately depicted as controlled as solution based KCTP. Two of the key components of living polymerizations, low PDI and chain ends that do not terminate, have not been adequately demonstrated in SI-KCTP.

Despite the control exercised over the polymerization, the chemical attaching species for the monolayer used to generate the initiating species was not able to be changed. The conditions in SI-KCTP are too harsh for carboxylic acid linking groups. Though different attachment groups have been used on other surfaces for SI-KCTP such as thiols on gold and siloxanes on silicon,[56, 65-66] still only phosphonic acid linkers have been shown to be useful for SI-KCTP from ITO substrates.[57, 66-67]

Though sufficient control can be exercised over films in ideal cases, there is significant batch to batch variation between films most likely due to polymer chains initiating over a long period of time (up to 3 hours), initiators falling off the surface due to etching, and catalysts disassociating with growing chain ends. Even under optimized conditions, these factors contribute to irregularities in the film.

2.8 Experimental Procedures

All chemicals and reagents are purchased from commercial sources unless otherwise noted (Acros, Strem, Aldrich, etc.) and used without further purification. Solvents were purified by distillation (THF) and solvent system (toluene) when necessary. Air free reactions are done on a Schlenk line using standard techniques and in an MBraun UNILab glovebox. UV/Vis absorption spectra were taken with a Shimadzu UV-2600 Spectrophotometer. AFM Measurements were taken on an Asylum MFP3D Atomic Force Microscope. Cyclic voltammetry measurements were taken with a BASI Epsilon potentiostat.

(1) Synthesis of 2-bromo-3-methyl-5-iodothiophene

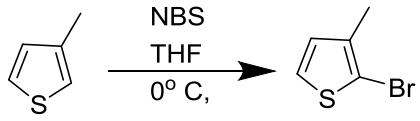

To a 250 mL round bottom flask, 21.0555g (214 mmol) 3-methylthiophene and 23.8168 g (214 mmol) NBS are dissolved in 120 mL THF at 0C. The reaction is stirred overnight, poured over water, extracted with diethyl ether, dried over $MgSO_4$, filtered, and concentrated to yield 32.2 g (85%) pure 2-bromo-3-methylthiophene

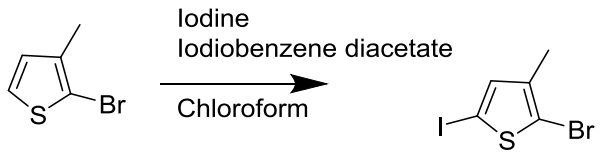

To a 250 mL round bottom flask with 70mL $CHCl_3$ are added 6.7797 g (38.3 mmol) 2-bromo-3-methylthiophene, 4.8641 g (19.15 mmol) iodine, 6.1663 g (19.15 mmol) iodobenzene diacetate. This is let stir overnight. The reaction is dumped into a solution of $NaSO_3$, washed with above solution twice, washed with brine, dried over $MgSO_4$, filtered, concentrated, and distilled. In the second fraction, 9.2839 g (80%) 2-bromo-3-methyl-5-iodothiophene is collected as a faint yellow oil. ^1H NMR ($CDCl_3$, 40 MHz) δ (ppm): 6.900 (s, 1H) , 2.191 (s, 3H)

(2) Synthesis of 2-ferrocenyl-5-bromothiophene

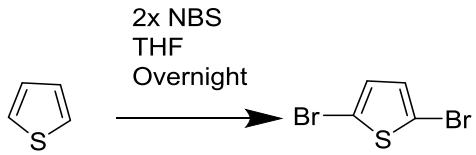

To a 100mL round bottom flask, 40 mL THF, 3.45 g (41.33 mmol) thiophene and 15.45 g (86.8 mmol) NBS are added and let stir overnight. The reaction mixture is dumped into cold water and extracted three times with diethyl ether and dried over $MgSO_4$. The solvent is removed, the oil is redissolved in hexanes and flashed through a plug of hexanes to yield 7.0099 g of Pure 2,5-dibromothiophene. ^1H NMR ($CDCl_3$, 40 MHz) δ (ppm): 7.176 (d, 1H J=5.6Hz), 6.909 (d, 1H J=4.8Hz) , 2.200 (s, 3H).

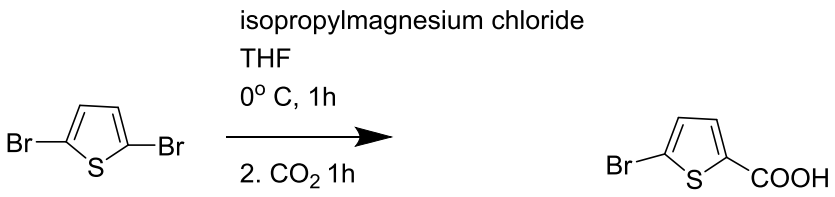

To a 250 mL two neck round bottom flask in an ice bath, 5.0 g (20.66 mmol) 2,5-dibromothiophene and 60 mL dry THF are added at 0C. To this solution, 10.33 mL (20.66 mmol) isopropyl magnesium chloride is added dropwise and let stir for one hour. Carbon dioxide is then bubbled through the reaction mixture for one hour, then the reaction is stirred for 1.5 hours. The solvent is removed and the residue was dissolved in 10% KOH and reacidified with conc. HCl to form white crystals. The crystals are filetered yielding 2.9812g 5-bromothiophene-2-carboxylic acid as white crystals (70%) ^{1}H NMR ($CDCl_3$, 40 MHz) δ (ppm): 7.644 (d, 1H J=4Hz), 7.122 (d, 1H J=4Hz).

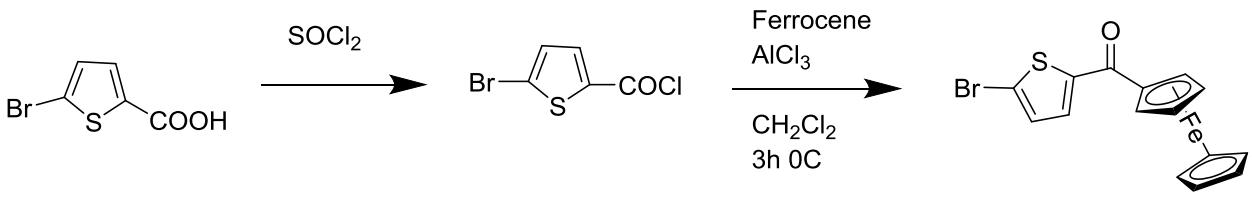

To a dry 250 mL 2 neck flask, 6.4735 g (31 mmol) and 27 mL (375 mmol) are added and refluxed overnight. A condenser is added to the flask and excess $SOCl_2$ is distilled off leaving a faint yellow liquid. This is dissolved in 10mL DCM, then transferred into a dry 250 mL flask containing 100 mL DCM 8.6490 g (46.5 mmol) ferrocene and 4.1230 g (31 mmol) $AlCl_3$ and let stir for 3h at 0C. The solution is warmed up to room temperature, neutralized with water, extracted with DCM,

dried over $MgSO_4$, concentrated, and flashed through a column of 1:4 Hex:EtOAc to yield 4.0362 g ferrocene-2-yl-(5-bromothiophen-2-yl)methanone as dark red powdery crystals (35%).^{1}H NMR ($CDCl_3$, 40 MHz) δ (ppm):7.660 (d, 1H, J=4 Hz), 7.115 (d, 1H, J=4 Hz), 4.982 (t, 2H, J=1.8 Hz), 4.606 (t, 2H, J=1.8 Hz), 4.225 (s, 5H)

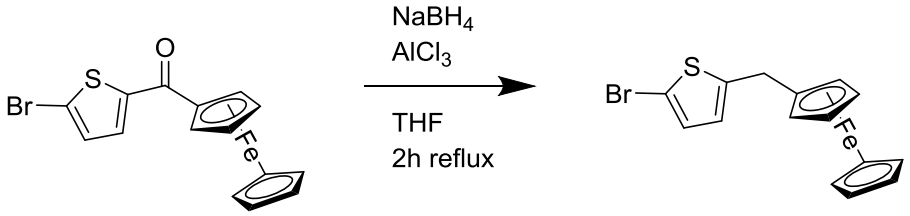

To a 100 mL 2 neck flask with a reflux condenser, 1.2550 g (3.1 mmol) ferrocene-2-yl-(5-bromothiophen-2-yl)methanone, 0.47 g (12 mmol) $NaBH_4$, 0.6 g (45 mmol) $AlCl_3$, and 40 mL dry THF are added. The solution is refluxed for 2h then turns orange. The solution is cooled, neutralized with water, extracted with DCM, dried with $MgSO_4$, concentrated, then flashed through a hexane column to yield 0.5002 g (43%) 2-ferrocenyl-5-bromothiophene. ^{1}H NMR ($CDCl_3$, 40 MHz) δ (ppm): 6.758 (d, 1H, J=3.7 Hz), 6.451 (d, 1H, J=3.7 Hz), 4.063 (s, 5H), 4.041 (s, 2H), 3.734 (s, 2H).

(3) Synthesis of 5-bromo-4-methylthiophene-2-carboxylic acid

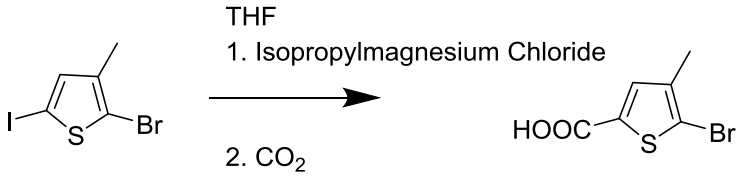

To a 100mL 2 neck flask at 0C are added 50mL dry THF and 5.0603 g (16.7 mmol) 2-bromo-3-methyl-5-iodothiophene, and 7.5 mL (15 mmol) isopropylmagnesium chloride is added dropwise and let stir for 1h. After 1h stirring, carbon dioxide is

bubbled through the reaction for 1.5h. The solvent is removed, residue dissolved in 10% KOH, then reacidified in conc. HCl, and filtered to yield 2.0301 g 5-bromo-4-methylthiophene-2-carboxylic acid as white powder (55%). ^{1}H NMR ($CDCl_3$, 40 MHz) δ (ppm): 7.556 (s, 1H), 2.224 (s, 3H).

(4) Synthesis of (4-bromobenzyl)phosphonic acid

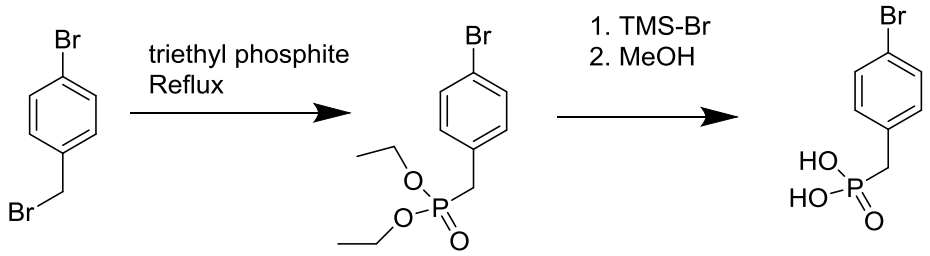

To a 100 mL round bottom flask with a condenser are added 11.98 g (46 mmol) and 50 mL (300 mmol) triethyl phosphite. This is refluxed overnight. The triethyl phosphite is distilled off, and TMS-Br 19mL (150 mmol) is added and let stir overnight. TMS-Br is distilled off, 50mL MeOH is added under Ar and refluxed for 4h. The solvent was removed to yield whitish powder that was dissolved in 10% KOH and reacidified with conc. HCl. to yield 8.79 g (76%) (4-bromobenzyl) phosphonic acid. ^{1}H NMR (MeOD, 40 MHz) δ (ppm): 7.440 (d, 2H, J=8 Hz), 7.233 (d, 2H, J=8 Hz), 3.099 (d, 2H, J=17.6).

Preparation of SI-KCTP initiators of (4) and (6) on ITO

ITO slides are cut and sonicated for 15 min in water, acetone, and IPA. Slides are then dried and soaked for 1h in 5:1:1: water: hydrogen peroxide: ammonium hydroxide, washed with water and EtOH, dried under N_2, and cleaned with ozone for 15 mins. Slides are then soaked in a solution of either (4) or (6) (1-5 mM) for 24h,

dried under Nitrogen, and annealed on a hotplate overnight at 150C. Slides are washed with chloroform and ethanol.

Inserting palladium catalysts into initiator monolayers

In a glovebox, functionalized ITO Slides are placed in a solution of 10mL Toluene 50mg $PdP(t\text{-}Bu_3)_2$ and heated at 70C for 3h. The Slides are taken and washed with toluene and THF.

SI-KCTP Reaction protocol

For a typical reaction, 0.1M solutions of monomer are made by dissolving 0.673 (2.2 mmol) g 2-bromo-3-methyl-5-iodothiophene in 20mL dry THF at 0C. To this solution, 1 mL (2 mmol) isopropylmagnesium chloride is added and the solution is stirred for 2h and let warm to RT. In a glovebox, the monomer solution is poured over prepared slides and the reaction is left without stirringfor the desired amount of time.

Measuring initiator coverage by cyclic voltammetry

For a typical reaction, 0.01M solutions of monomer are made by dissolving 0.08400 (2.3 mmol) g 2-ferrocenyl-5-bromothiophene in 20mL dry THF at 0C. To this solution, 0.09 mL (0.2 mmol) isopropylmagnesium chloride is added and the solution

is stirred for 2h and let warm to RT. In a glovebox, the solution is poured over prepared slides and the reaction is left to react overnight without stirring.

Cyclic voltammograms are measured using a BASI Epsilon potentiostat. Supporting electrolyte of 0.1 M tetrabutylammonium hexaflouorophospate in DCM is used. The working electrode is the ITO substrate, counter electrode platinum wire, and a silver pseudoreference is used with a 100 mV/s scan rate.

2.9 Supporting Spectra

2.9.1 NMR Spectra

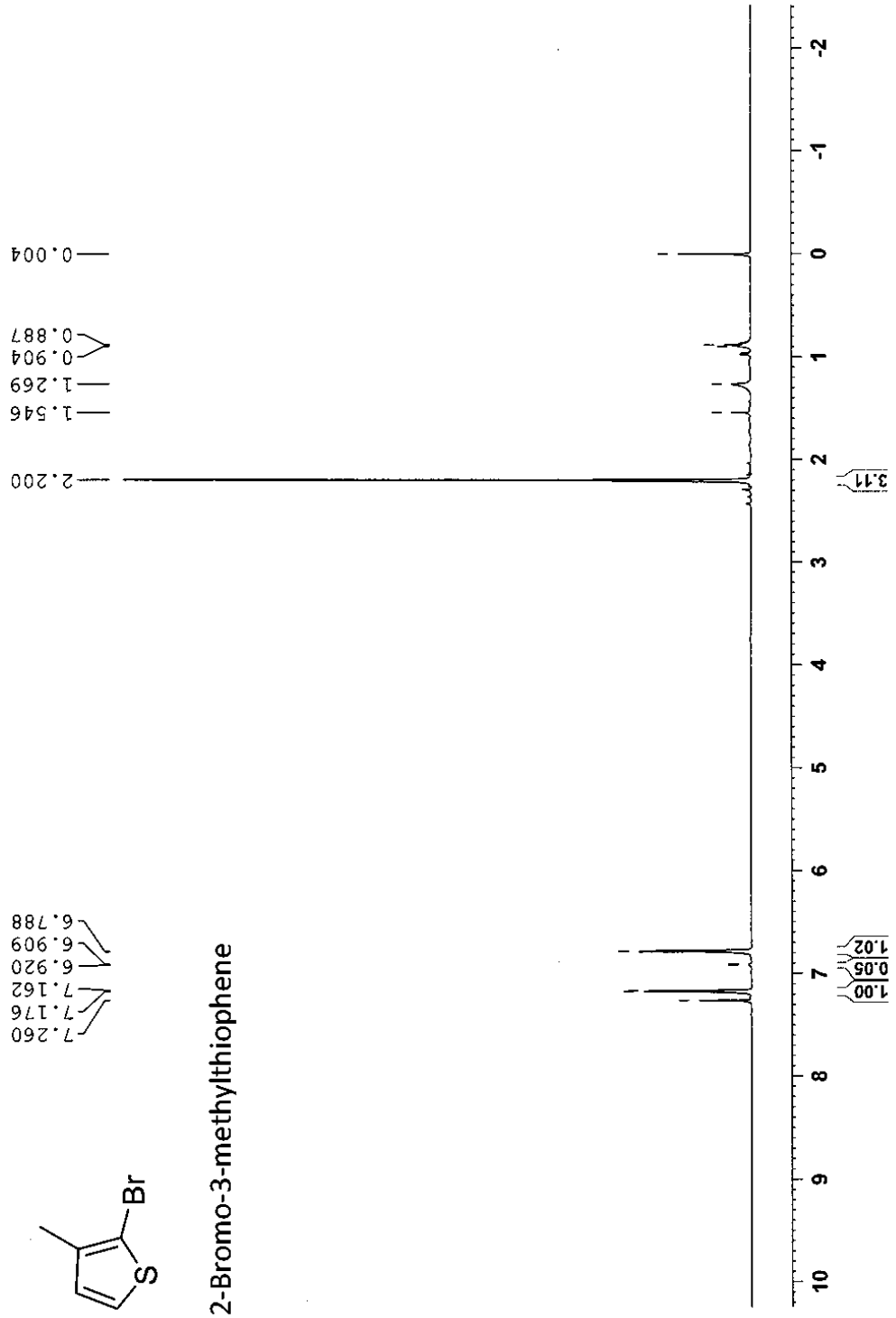

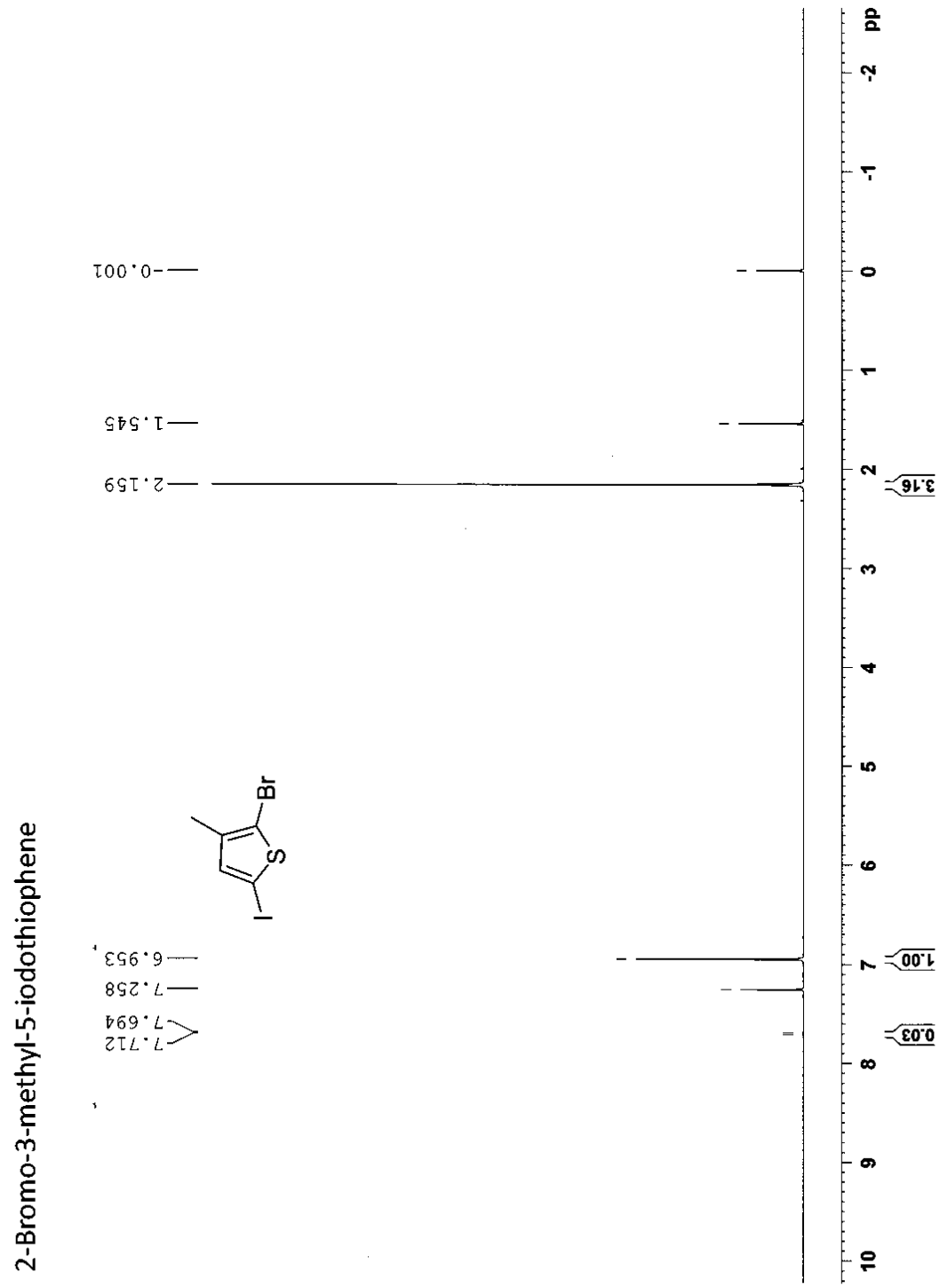
2-Bromo-3-methyl-5-iodothiophene
Br
S
I
7.712
7.694
7.258
6.953
2.159
1.545
-0.001
3.16
1.00
0.03
ppm

5-bromothiophene-2-carboxylic acid

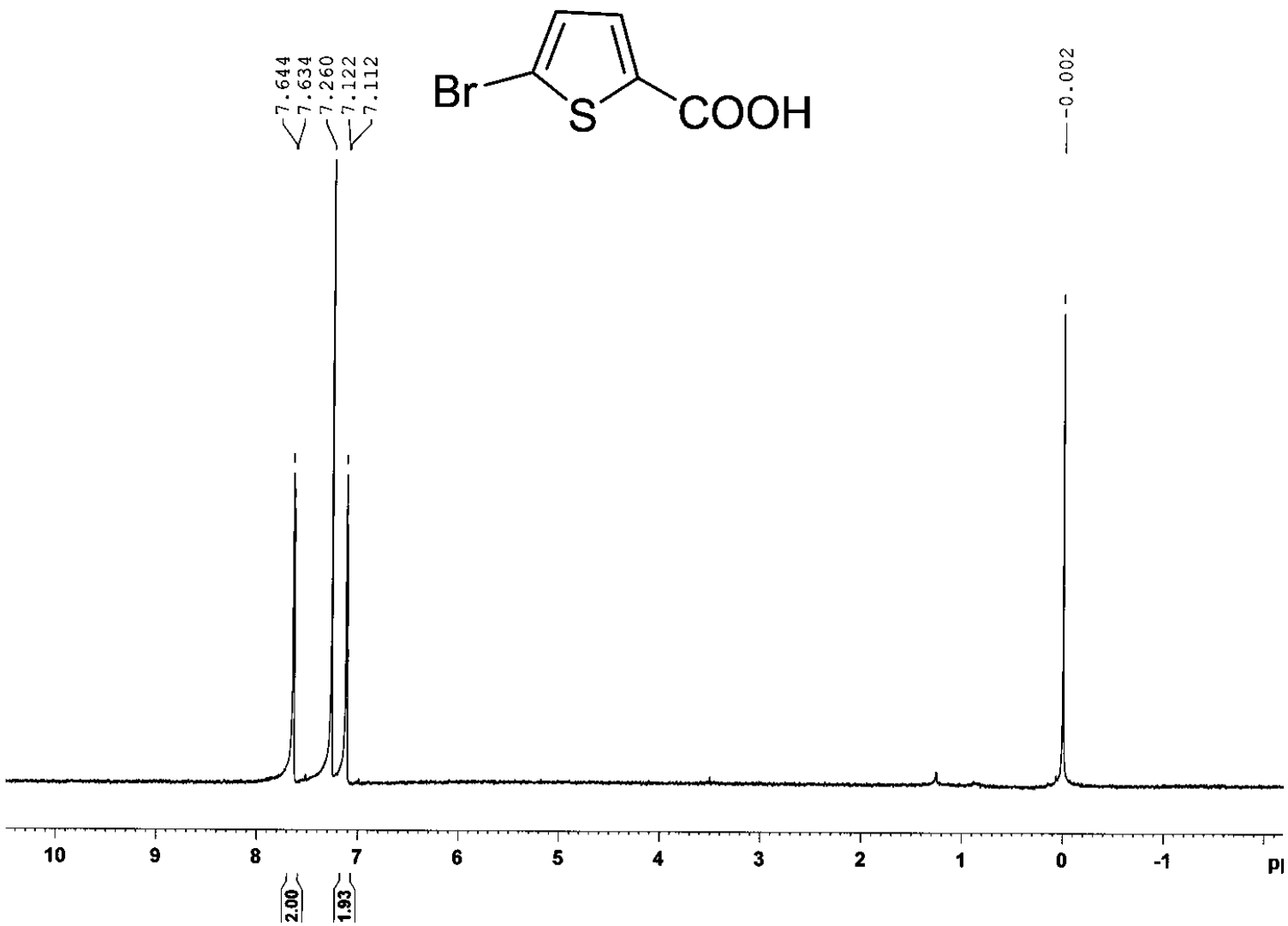

2-ferrocenyl-5-bromothiophene

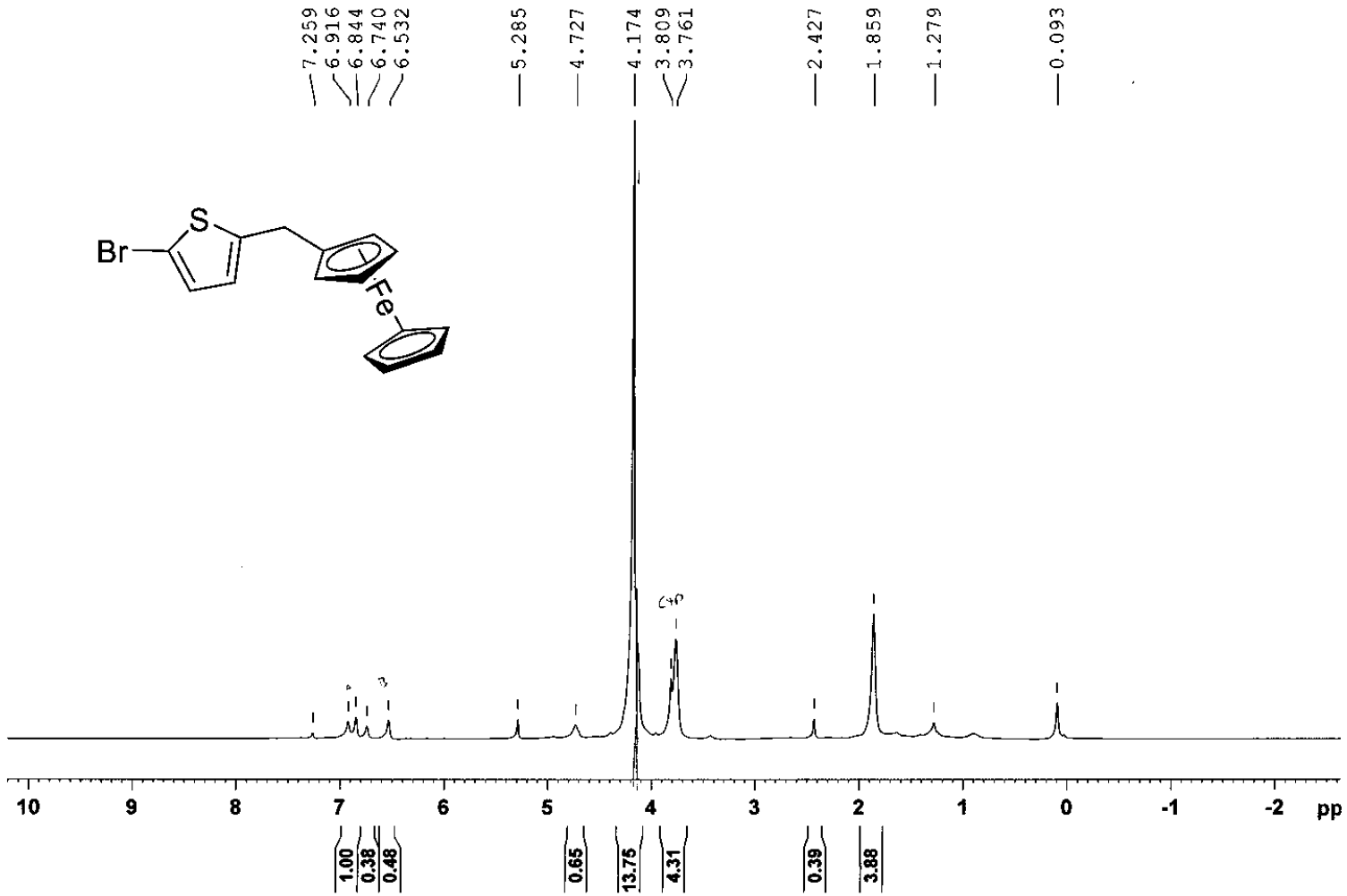

5-bromo-4-methlythiophene-2-carboxylic acid

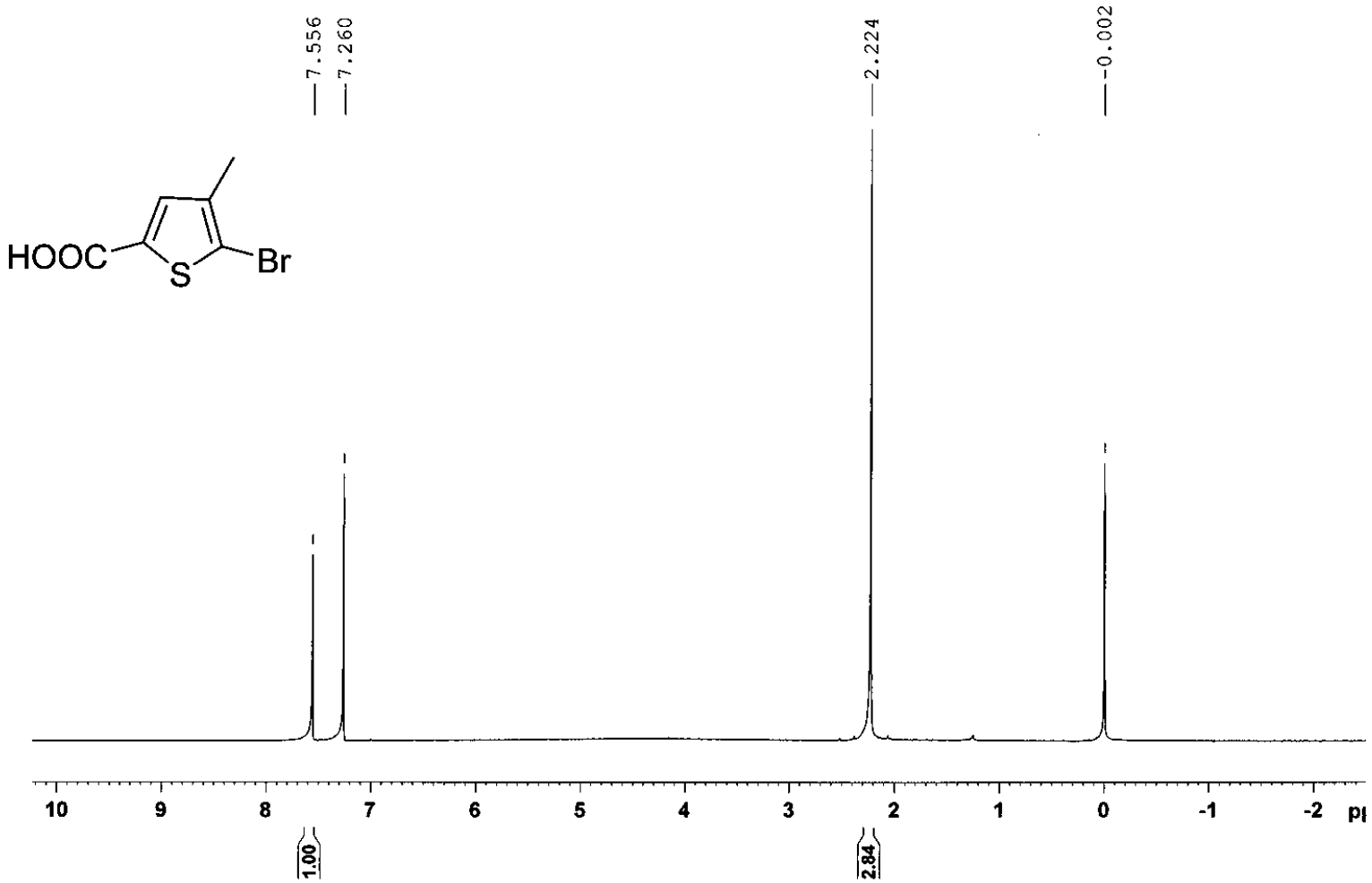

(4-bromobenzyl)phosphonic acid

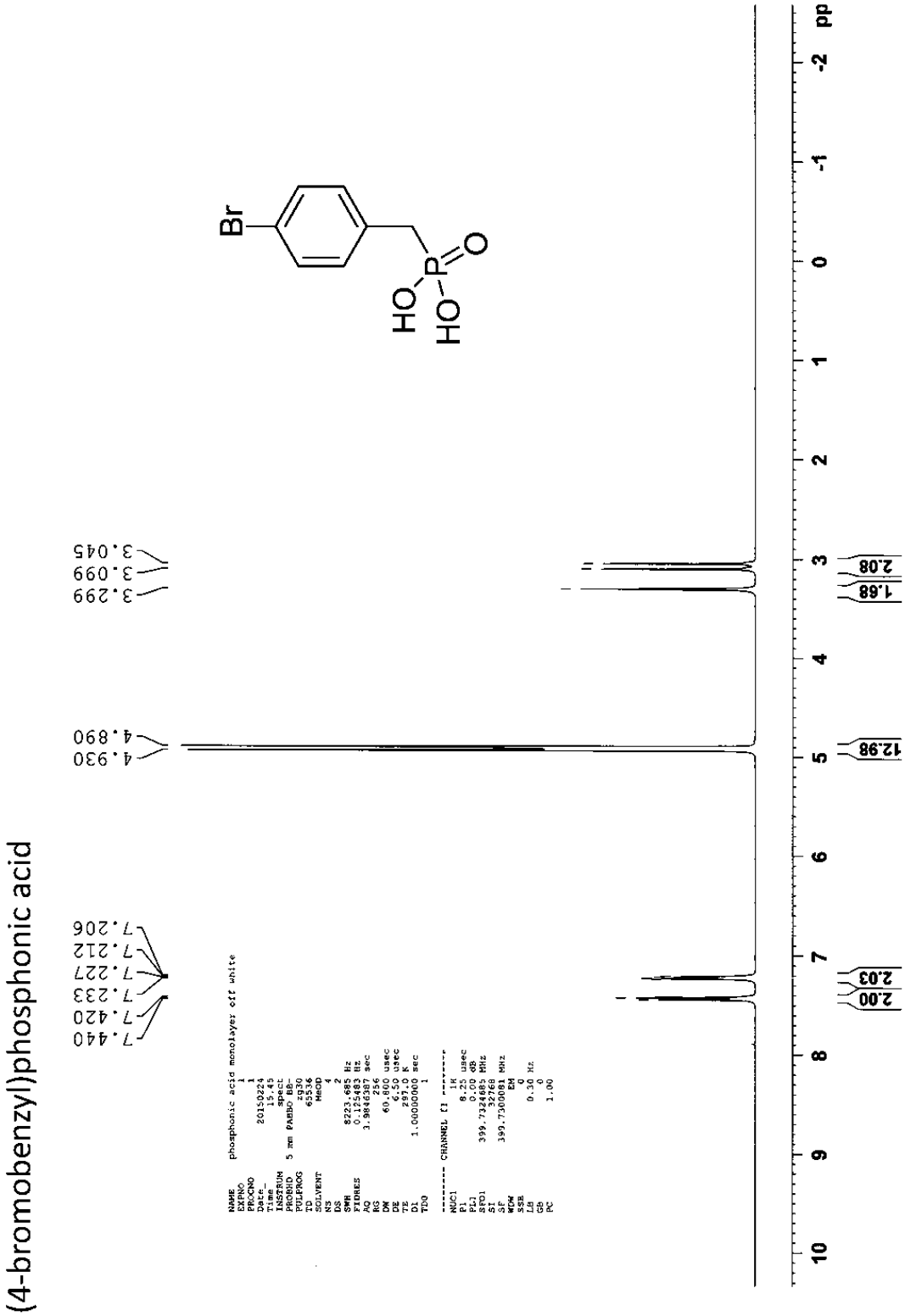

2.9.2 XPS Spectra

Blank ITO

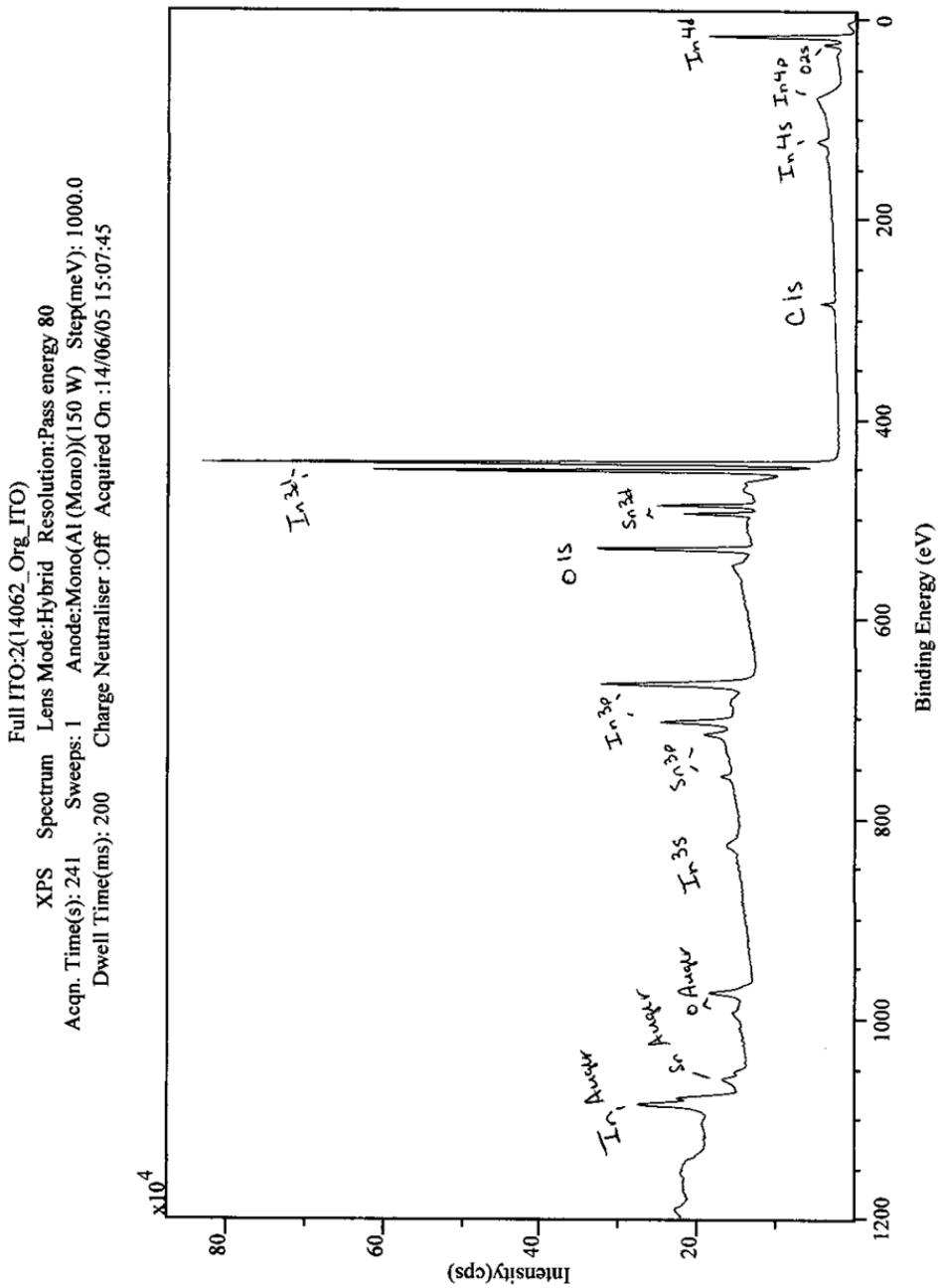

Blank ITO

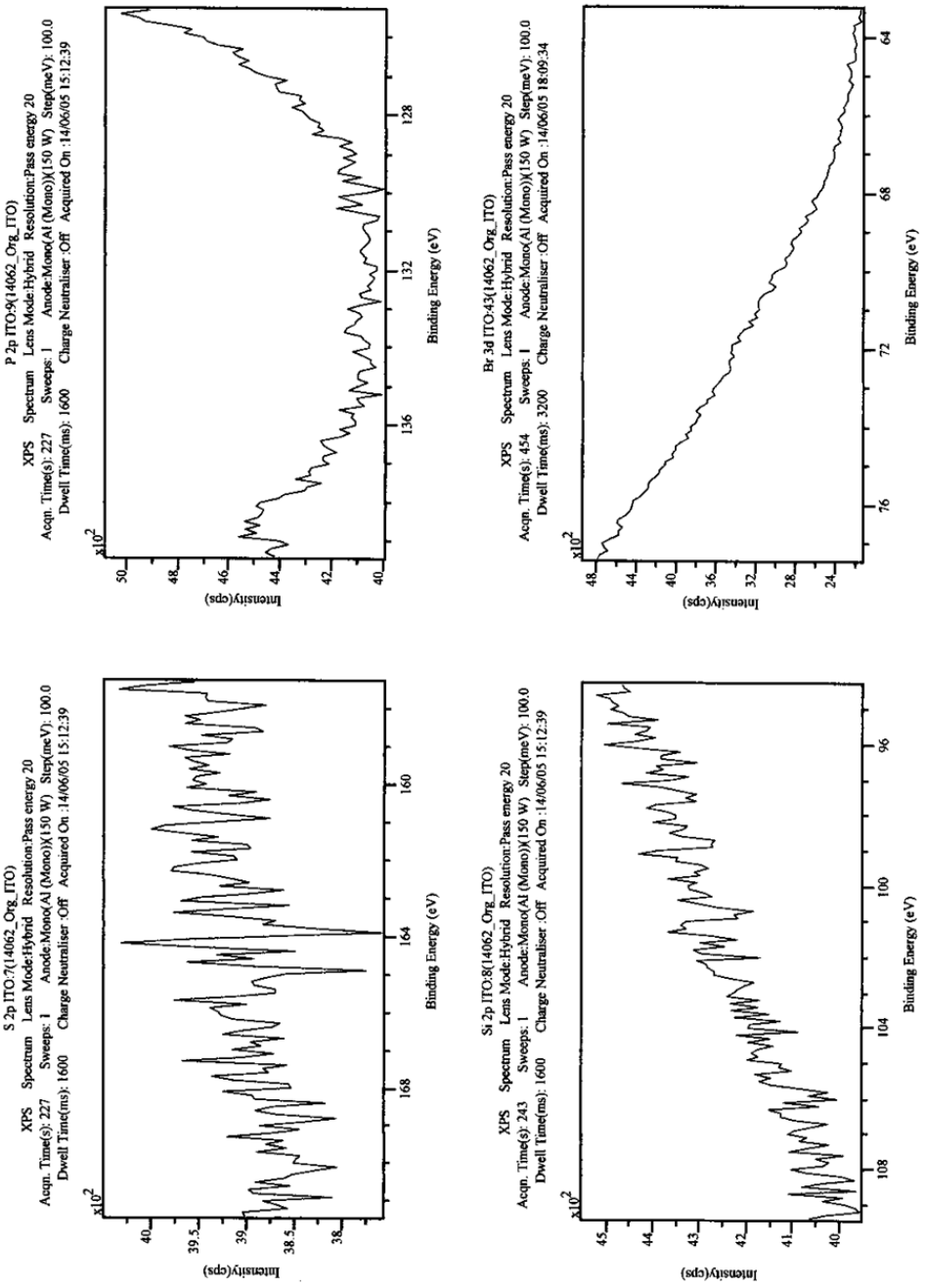
P 2p ITO:9(14062_Org_ITO)
XPS Spectrum Lens Mode:Hybrid Resolution:Pass energy 20
Acqn. Time(s): 227 Sweeps: 1 Anode:Mono(Al (Mono))(150 W) Step(meV): 100.0
Dwell Time(ms): 1600 Charge Neutraliser :Off Acquired On :14/06/05 15:12:39
Intensity(cps)
Binding Energy (eV)
Br 3d ITO:43(14062_Org_ITO)
XPS Spectrum Lens Mode:Hybrid Resolution:Pass energy 20
Acqn. Time(s): 454 Sweeps: 1 Anode:Mono(Al (Mono))(150 W) Step(meV): 100.0
Dwell Time(ms): 3200 Charge Neutraliser :Off Acquired On :14/06/05 18:09:34
Intensity(cps)
Binding Energy (eV)
S 2p ITO:7(14062_Org_ITO)
XPS Spectrum Lens Mode:Hybrid Resolution:Pass energy 20
Acqn. Time(s): 227 Sweeps: 1 Anode:Mono(Al (Mono))(150 W) Step(meV): 100.0
Dwell Time(ms): 1600 Charge Neutraliser :Off Acquired On :14/06/05 15:12:39
Intensity(cps)
Binding Energy (eV)
Si 2p ITO:8(14062_Org_ITO)
XPS Spectrum Lens Mode:Hybrid Resolution:Pass energy 20
Acqn. Time(s): 243 Sweeps: 1 Anode:Mono(Al (Mono))(150 W) Step(meV): 100.0
Dwell Time(ms): 1600 Charge Neutraliser :Off Acquired On :14/06/05 15:12:39
Intensity(cps)
Binding Energy (eV)

Blank ITO

ITO

Quantification Report

/C=/data/You/Travis/-DATA-/14062_Org_ITO.dset Fri Jun 6 09:12:41 2014

State #0 : Etch Time 0.00 seconds

Peak	Type	Position BE (eV)	FWHM (eV)	Raw Area (cps eV)	RSF	Atomic Mass	Atomic Conc %	Mass Conc %
In 3d	Reg	444.232	1.414	478781.6	7.265	114.820	33.08	71.66
Sn 3d	Reg	486.232	1.631	73606.1	7.875	118.744	4.62	10.35
O 1s	Reg	529.882	1.503	82076.2	0.780	15.999	51.30	15.48
C 1s	Reg	284.532	1.458	5779.2	0.278	12.011	10.97	2.49
S 2p	Reg	158.432	0.000	3.9	0.668	32.065	0.00	0.00
Si 2p	Reg	95.432	0.000	10.5	0.328	28.086	0.02	0.01
P 2p	Reg	127.932	0.000	3.2	0.486	30.974	0.00	0.00
Br 3d	Reg	74.432	0.000	0.0	1.055	79.905	0.00	0.00

5-bromo-4-methylthiophene-2-carboxylic acid on ITO

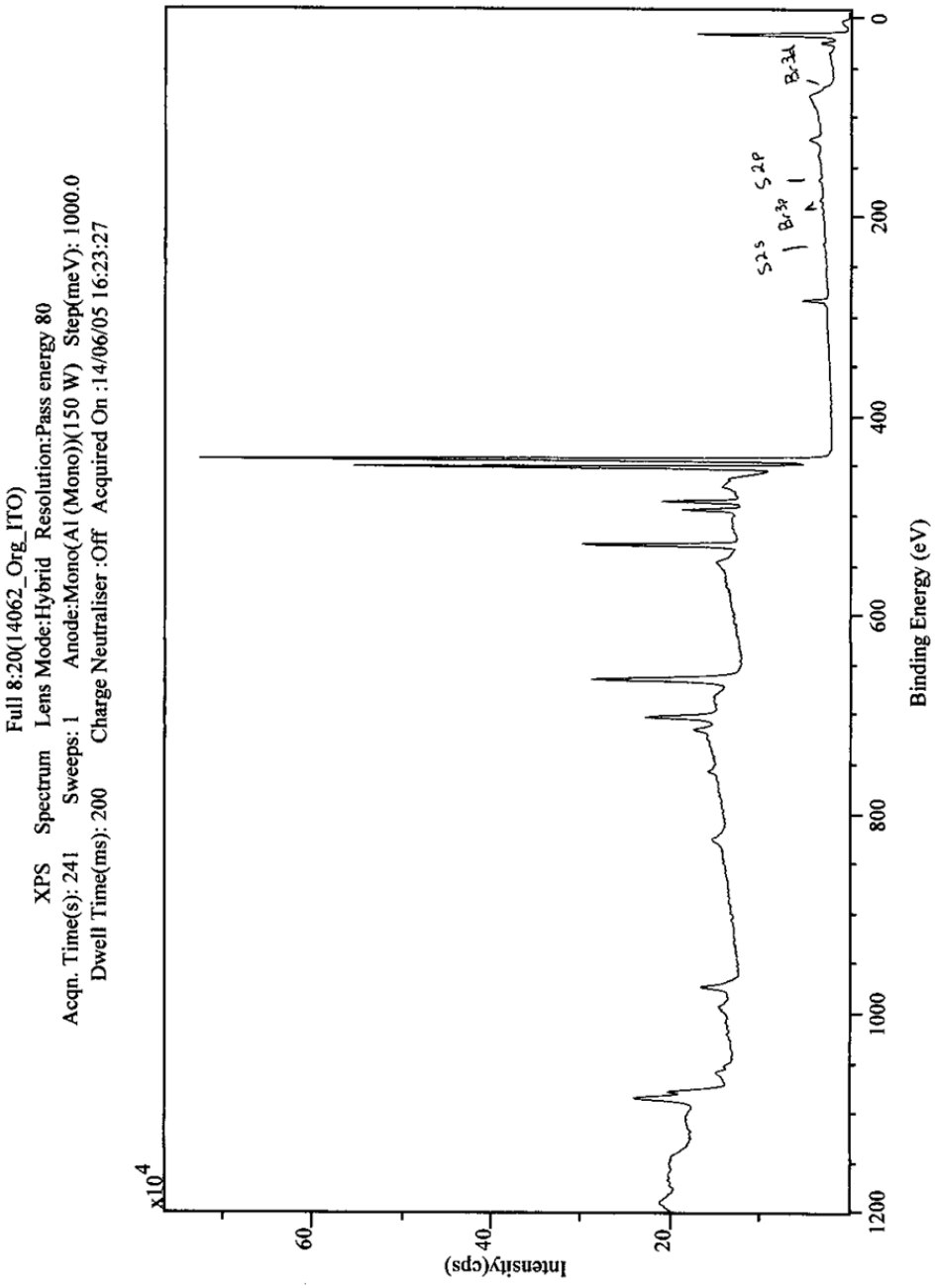

5-bromo-4-methylthiophene-2-carboxylic acid on ITO

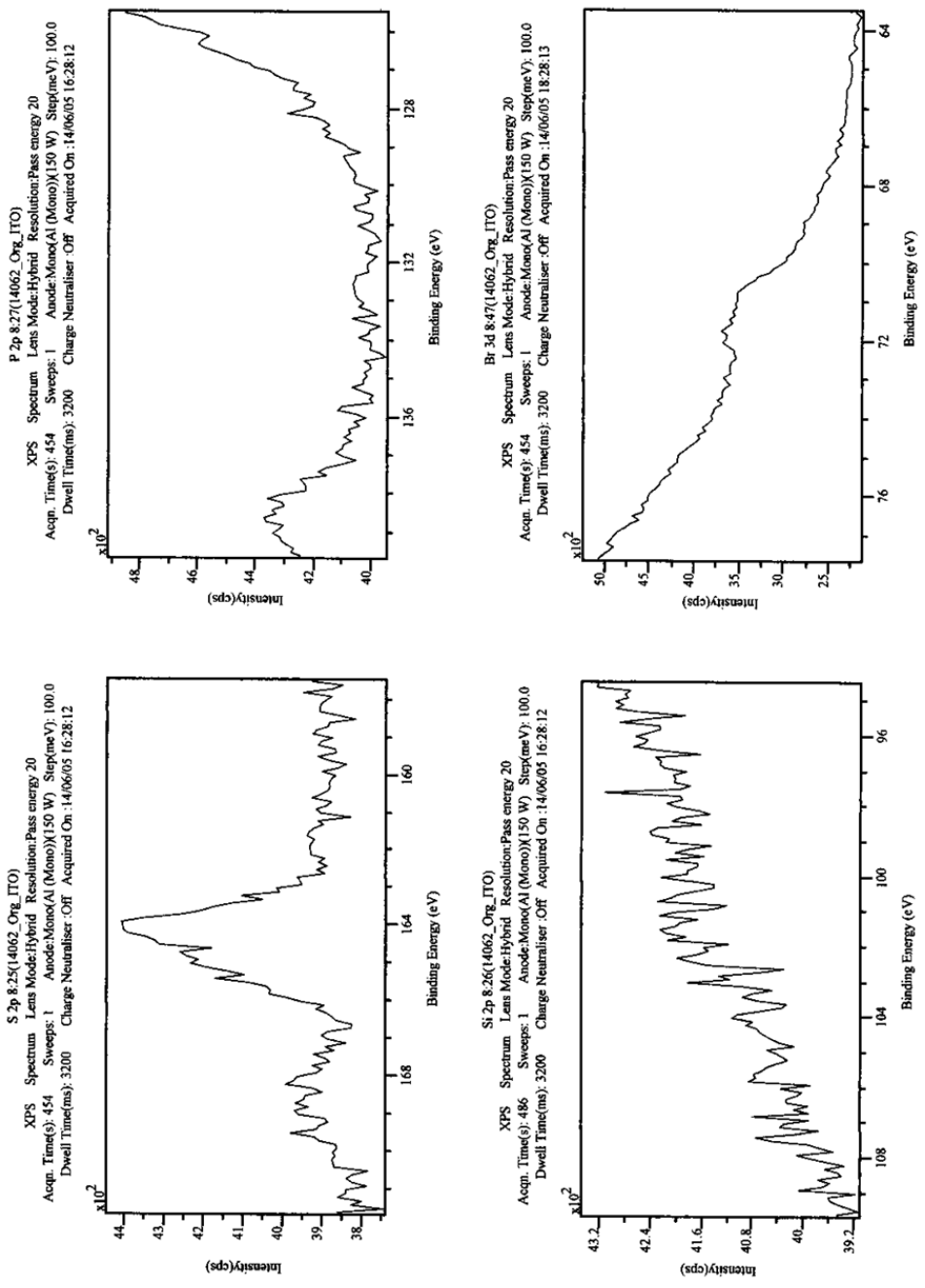

5-bromo-4-methylthiophene-2-carboxylic acid on ITO

Quantification Report

/C=/data/You/Travis/-DATA-/14062_Org_ITO.dset Fri Jun 6 09:11:46 2014

State #0 : Etch Time 0.00 seconds

Peak	Type	Position BE (eV)	FWHM (eV)	Raw Area (cps eV)	RSF	Atomic Mass	Atomic Conc %	Mass Conc %
In 3d	Reg	444.366	1.349	423152.5	7.265	114.820	29.97	70.20
Sn 3d	Reg	486.466	1.554	52427.6	7.875	118.744	3.37	8.17
O 1s	Reg	530.116	1.626	70491.8	0.780	15.999	45.16	14.74
C 1s	Reg	284.666	1.431	10045.2	0.278	12.011	19.54	4.79
S 2p	Reg	163.966	1.801	1325.1	0.668	32.065	1.11	0.73
Si 2p	Reg	95.666	0.000	3.8	0.328	28.086	0.01	0.00
P 2p	Reg	128.466	0.000	1.7	0.486	30.974	0.00	0.00
Br 3d	Reg	70.766	2.119	1541.4	1.055	79.905	0.84	1.37

(4-bromobenzyl)phosphonic acid on ITO

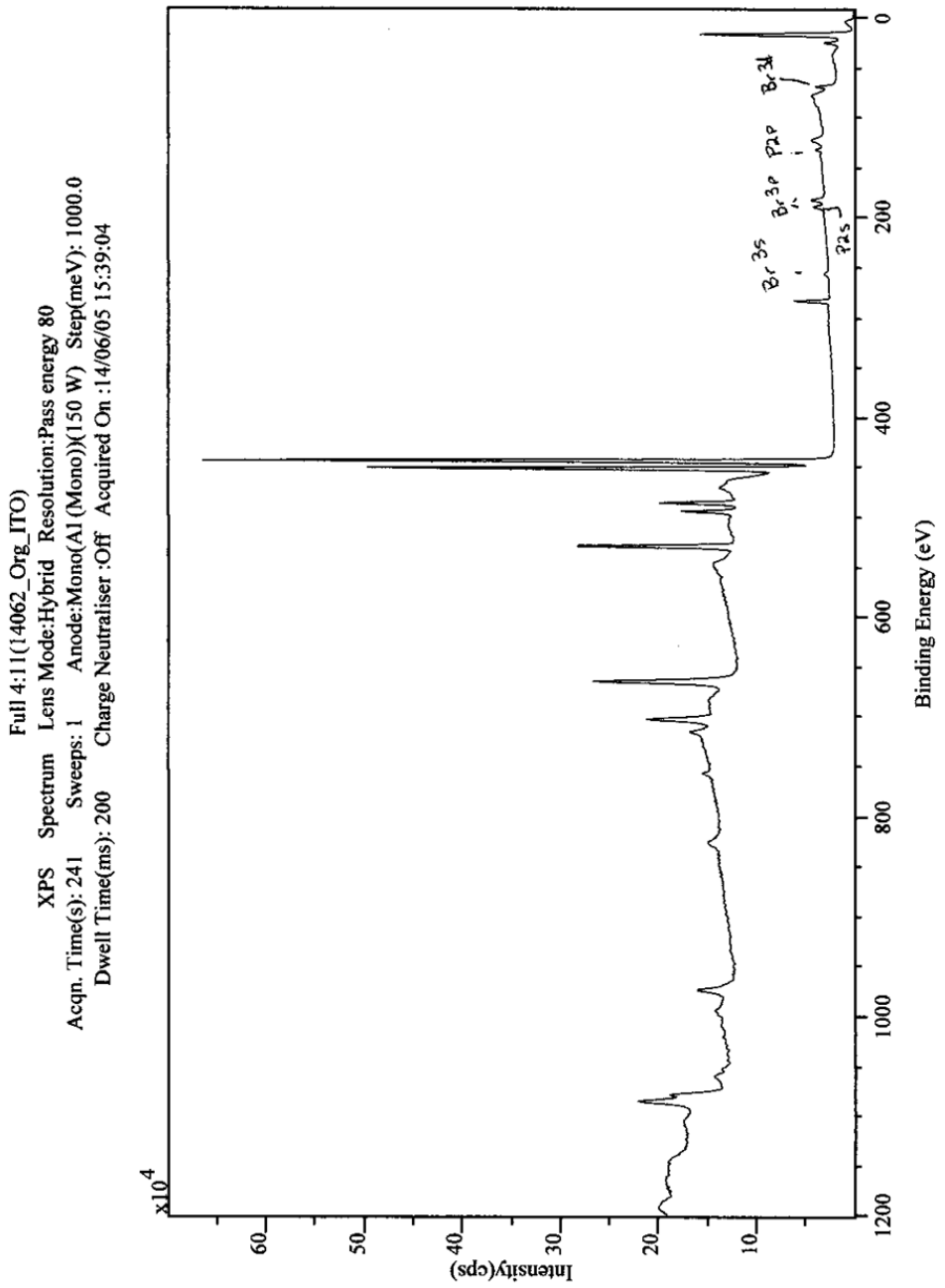

(4-bromobenzyl)phosphonic acid on ITO

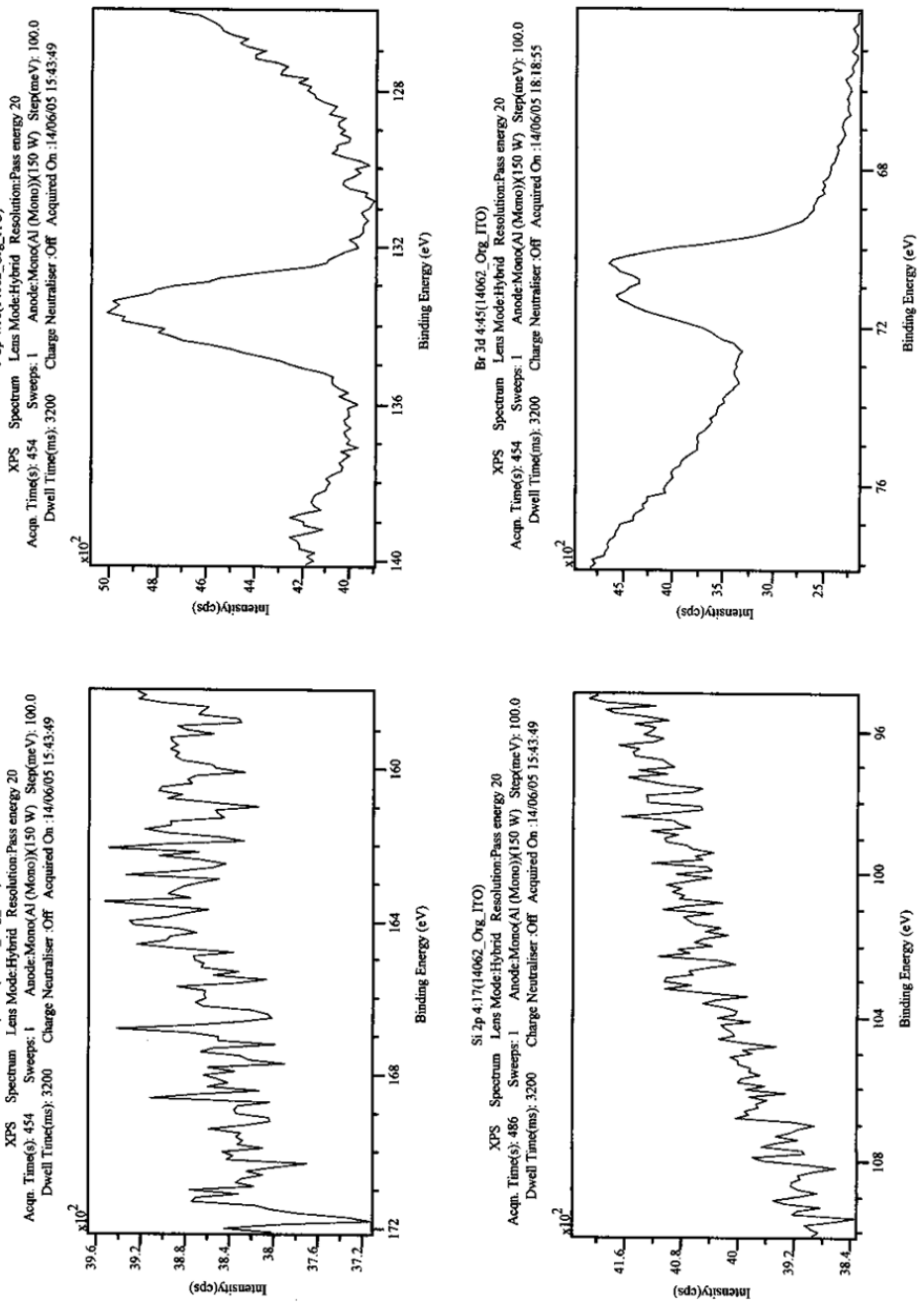

4

Quantification Report

/C=/data/You/Travis/-DATA-/14062_Org_ITO.dset Fri Jun 6 09:12:20 2014

State #0 : Etch Time 0.00 seconds

Peak	Type	Position BE (eV)	FWHM (eV)	Raw Area (cps eV)	RSF	Atomic Mass	Atomic Conc %	Mass Conc %
In 3d	Reg	444.831	1.373	385676.2	7.265	114.820	27.17	66.50
Sn 3d	Reg	486.931	1.625	46729.8	7.875	118.744	2.99	7.57
O 1s	Reg	530.581	1.720	67149.6	0.780	15.999	42.80	14.59
C 1s	Reg	284.631	1.328	11559.7	0.278	12.011	22.38	5.73
S 2p	Reg	171.131	0.000	0.0	0.668	32.065	0.00	0.00
Si 2p	Reg	96.131	0.000	0.0	0.328	28.086	0.00	0.00
P 2p	Reg	133.731	1.846	1937.0	0.486	30.974	2.24	1.48
Br 3d	Reg	70.431	1.959	4456.4	1.055	79.905	2.42	4.12

2.9.3 Cyclic Voltammograms

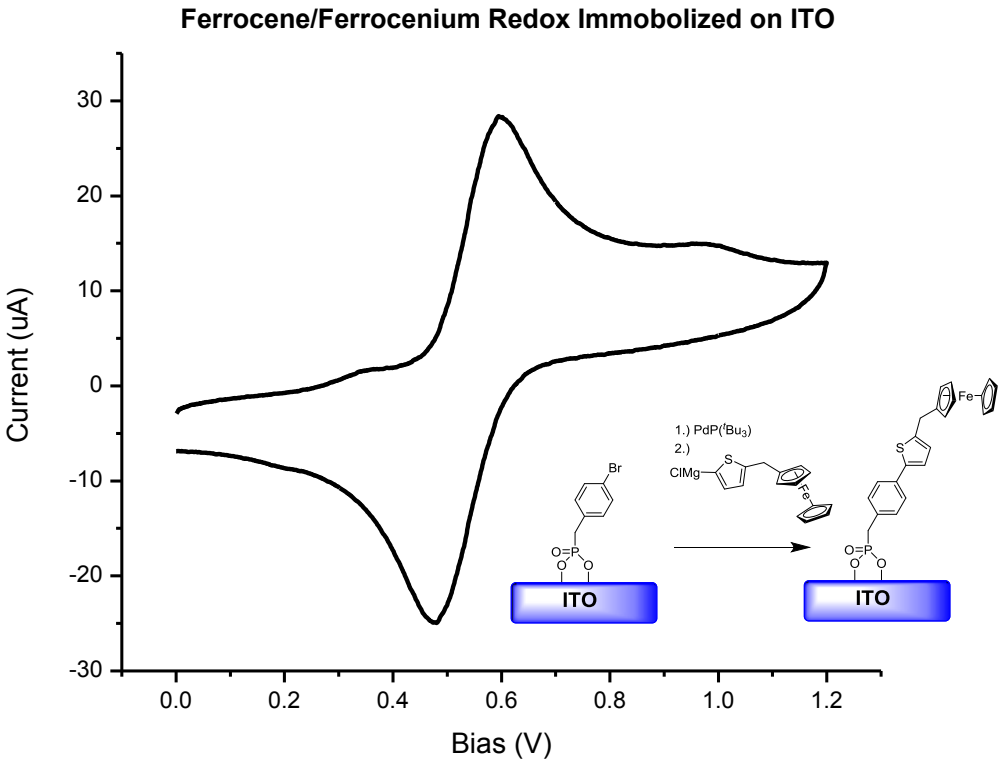

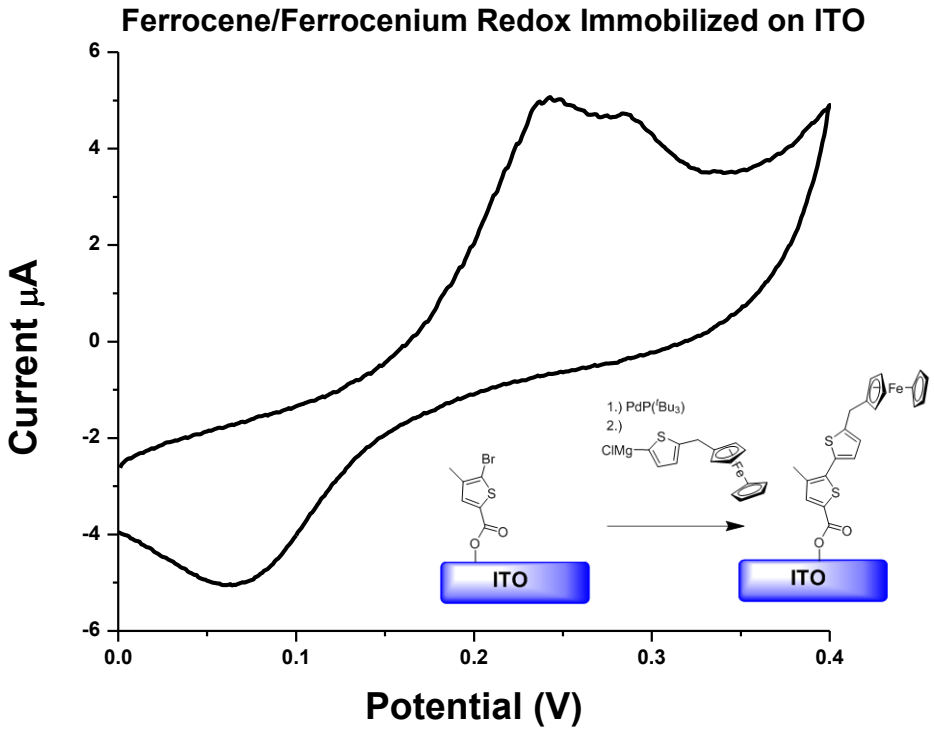

CHAPTER 3 CHARACTERIZATION OF POLYMER BRUSH THIN FILMS

3.1 Introduction to Characterization techniques

Though SI-KCTP was thoroughly characterized in Chapter 2, the synthesis of P3MT brushes in a controlled manner does not necessarily guarantee controlled film morphology. For SAMs used in a molecular electronic device described in Chapter 1, film morphologies are homogeneous and smooth due to all molecules being the same chemical species and anchored to the substrate at the same time. In the case of grown P3MT brushes, the morphology is not as straightforward. The dispersity of polymer chain lengths on the surface makes surfaces rough, and though the density of initiators on the surface is known, the regularity of the placement of reactive species is not. It is not expected that polymer chains will be ordered on a surface as regularly as alkane thiols on (111) Au surfaces. The key components of the film morphology for this work are the density of polymer chains on the surface, their orientation to the surface, and the surface roughness. Ideally, polymer chains would be densely packed, placed at regular intervals, oriented vertically from the substrate, and form a smooth surface in a well ordered film. Films such as these would ensure intramolecular charge transport pathways exist in a vertical device.

A number of techniques were employed to characterize these films. UV/Vis spectroscopy is used to measure film absorbance. Film thickness can be estimated

from absorbance using the calibration plot constructed in section 2.5. The optical HOMO-LUMO bandgap can be calculated from the absorption spectrum. Film absorption also contains signatures from film aggregation characterize the local environment around chains. Polarized, variable angle UV/Vis absorption is used to probe aggregation orientation to measure components of film order in and out of the plane of the substrate giving evidence of film orientation in the vertical plane. Besides polarized UV/Vis, NEXAFS is used to measure the ensemble average orientation of polymer chains on the surface to give the most quantitative picture of film orientation. Cyclic voltammetry is used to measure the HOMO level of polymer brush thin films which is combined with the optical bandgap to estimate the LUMO of the polymer film. Atomic force microscopy (AFM) is used to measure surface roughness and film thickness. Ellipsometry is used as a noninvasive method for measuring film thickness, and its ability to provide accurate measurements of film thickness are compared with estimation by UV/Vis spectroscopy and AFM profilometry.

In an effort to enhance the film morphology to create films with the desired microstructure, polymer films are annealed at high temperature and are characterized after annealing to measure the effects of annealing on conjugated polymer brushes.

3.2 UV/Vis Absorption Spectroscopy

The most versatile tool used to characterize the polymer brushes is UV/Vis spectroscopy. This technique is used to estimate the HOMO-LUMO bandgap, probe

the aggregation and vibronic structure between polymer chains, and measure the orientation of polymer chains in the films. Poly(3-alkylthiophene) and conjugated polymers UV/Vis absorption spectra are extensively studied in the literature.[32,68,69,70] The properties listed above can be easily extracted from UV/Vis absorption spectra to characterize the morphology and quality of grown polymer films.

3.2.1 Measuring the Optical Bandgap

The bandgap of a conjugated polymer is defined by the HOMO-LUMO bandgap. A material's bandgap corresponds to the lowest energy transition in a material. For materials with bandgaps corresponding to energies in the visible and ultraviolet spectra, the onset of absorption in the UV/Vis spectra corresponds to the HOMO-LUMO bandgap (Figure 3-1). For P3MT polymer brushes, the onset of absorption at 640nm corresponds to an optical bandgap of 1.94 eV. This is similar to the measured optical bandgap for P3HT of 1.88 eV. For conjugated polymers, the relationship between bandgap and conjugation is well understood. Due to orbital mixing between conjugated monomers and the delocalization of energy levels over many repeat units, as the conjugation length of a polymer increases, the bandgap decreases to a minimum. The similar optical bandgaps in P3MT and P3HT indicate that the conjugation length is also similar, with P3HT having a longer conjugation length than P3MT due to the lower bandgap.

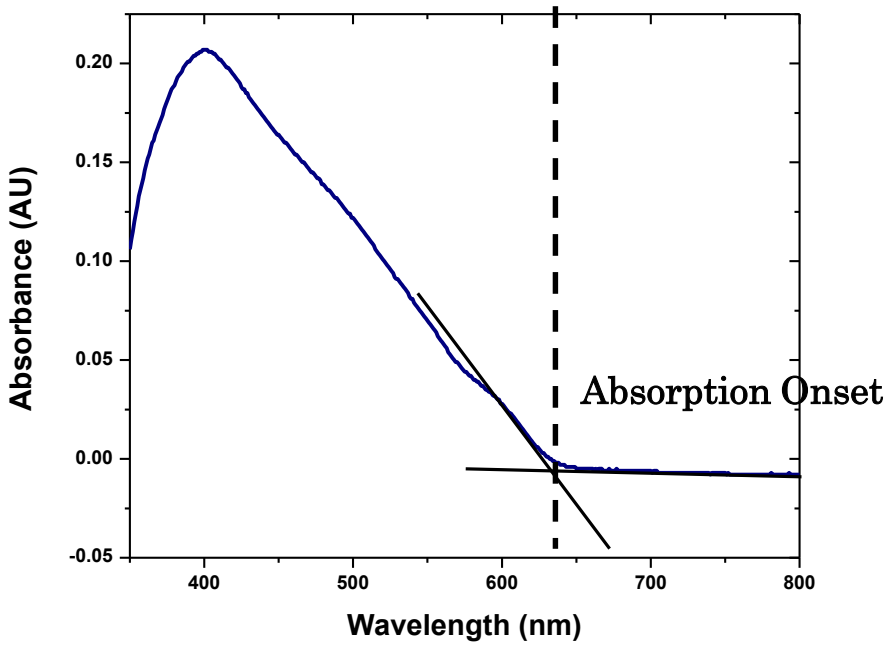

Figure 3-1: Optical Bandgap of P3MT from UV/Vis Absorption Spectra

The onset of absorption is the point used to calculate the optical bandgap. This point corresponds to the lowest energy optical excitation in the material. It is calculated by linearly extrapolating the baseline and polymer absorption spectrum. The intersection of these two lines is the onset of absorption. This value in nm is converted to eV to calculate the optical bandgap. For P3MT brushes, the optical bandgap is 1.94 eV, which is very similar to spuncast P3HT which has an onset of absorption of 660nm and an optical bandgap of 1.88 eV.

The optical bandgap is relatively consistent with respect to polymer film thickness. For example, the onset of absorption for polymer brush films with thickness 1.7nm is similar to that of 80nm polymer brushes, suggesting that the conjugation length is reached at low film thicknesses. An oligothiophene with a contour length of 1.7nm corresponds to a short chain of only 4 to 5 repeat units long, which would correspond to an onset of absorption of 2.8 eV (440 nm).[71] This obvious paradox suggests that the polymer chains cannot be standing perfectly vertically from the surface, and a significant portion of the polymers chain is in the plane of

the substrate. If brushes ideally oriented, the absorption onset would systematically red shift to the maximum conjugation length of the polymer brush.

3.2.2 Aggregation in P3MT Brush Films

Aggregation occurs when molecules or polymers come together in solution or solid state due to intermolecular interactions. In conjugated organic molecules, these interactions are divided based on how transition dipole moments in neighboring molecules interact and the subsequent change in photophysical properties into two types of aggregates: H-aggregation (hypsochromatic, blue shifting interactions) and J-aggregation (bathochromic, red shifting

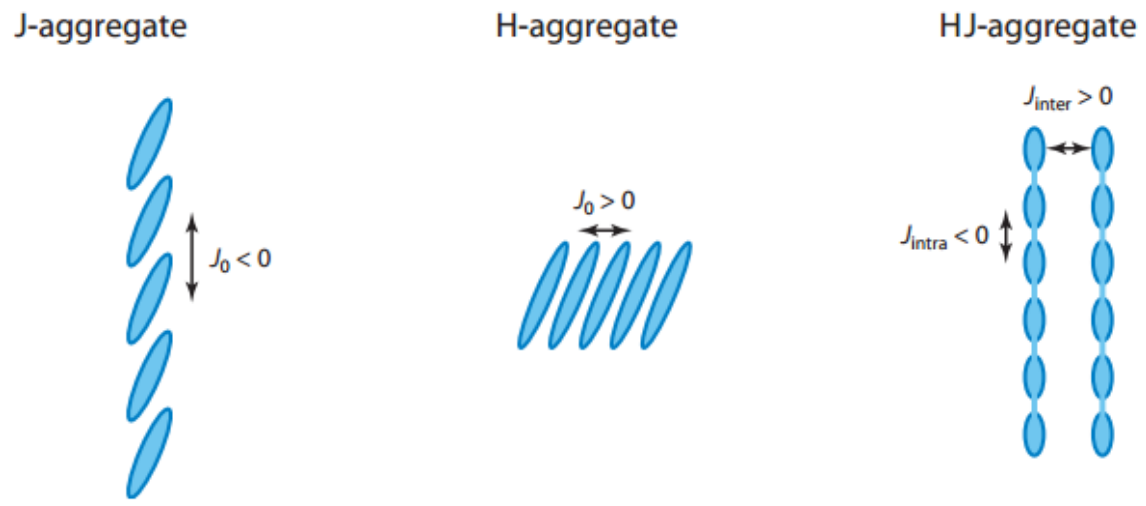

Figure 3-2: H and J Aggregates

(Left) In J-aggregates, head-to-tail interactions lead to negative coupling between nearest neighbors (J_0 not to be confused with current density) which causes a red shift in absorbance.
(Middle) In H-aggregates, side-to-side interactions cause positive nearest neighbor coupling interactions which leads to a blue shift in absorbance.
(Right) In polymeric HJ-Aggregates, coupling between monomers is negative as in J-aggregates due to through bond interactions, and coupling between chains is positive, as in H-aggregates. Polymer semiconductors such as P3HT have been shown to have both J and H like properties. Image copyright its respective owner.

interactions).[69,72] In small molecules, the angle between monomer units is what determines the interaction (Figure 3-2).[69] For "head-to-tail" type interactions, J aggregation occurs, and for "side-to-side" type interactions, H aggregation occurs.[69] The strength of the interaction between molecules determines the magnitude of the effect observed in the photophysical properties of the aggregates. Polymer semiconductors often express both H and J like properties, and have been said to form HJ-aggregates. These aggregates have properties of both H and J aggregates, but only the H-aggregation will be discussed.

For polymer samples, H-aggregation manifests itself in a blue shift of the absorption maximum in the spectrum of an aggregated sample compared to that of a sample with no aggregation, and has been reported in P3MT brushes grown with

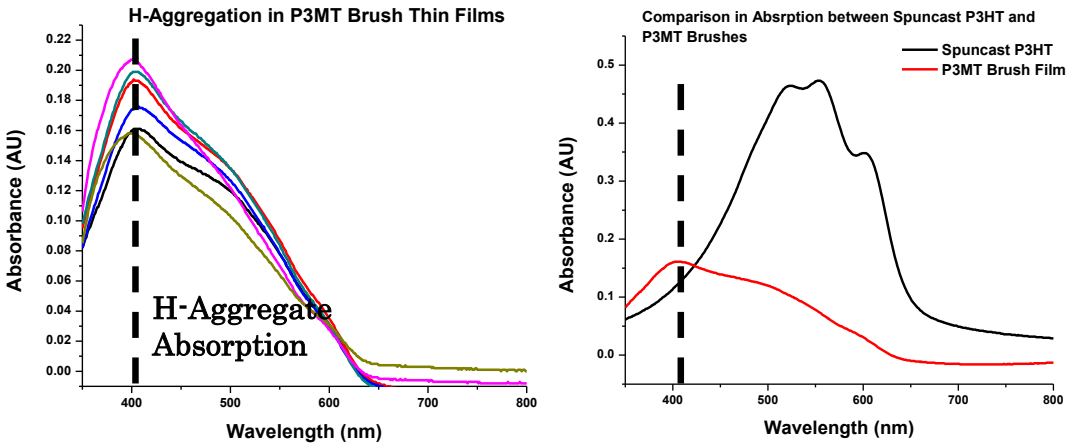

Figure 3-3: Comparing H-Aggregation in P3AT films

(Left) P3MT films grown here have a strong signature of H-aggregation as evidenced by the blue shifted maximum absorbance. Regardless of the film thickness, the maximum is at approximately 400 nm.
(Right) Spuncast P3HT films have a similar absorption band to P3MT brush films, but the spectra are shaped completely differently. This is due to the much higher strength of H-aggregation in P3MT films.

Pd catalyzed SI-KCTP in literature.[57,73]

Films grown here often exhibit the signatures of H-aggregation (Figure 3-3). There are many physical interpretations as to why there are H-aggregates in these films. From literature reports, the spectra of P3MT films grown by SI-KCTP using Pd and Ni as catalysts show different signs of aggregation. For Pd catalyzed reactions, there is a signature of strong H-aggregation, but there is no such sign for films made with Ni catalysts.[57, 66] The authors attribute this to the increased grafting density measured in films grown with Pd catalysts. Confined chains may have stronger interchain interactions, and thus larger signatures of H-aggregation. Many polymer properties affect the strength of H-aggregates besides distance between chains including molecular weight, conjugation length, and the strength of the physical interaction between molecules.[69,73] Here, as in literature, the presence of H-aggregation in P3MT films is used to qualitatively affirm that the films have high grafting density. Unpolarized, normal-incident UV/Vis absorption spectroscopy measures the film characteristics in the plane of the substrate, so the H-aggregates here have a significant component in the plane of the substrate.

3.2.3 Measuring Orientation with Polarized Variable Angle UV/Vis Absorption

Polarized variable angle UV/Vis spectroscopy has been used to measure the orientation of small molecule and polymer films.[32,74] The incident polarized light will have a projection on the transition dipole moments of the chromophores (molecules) depending on the angle of incidence of the light and the orientation of the molecule on the surface. If molecules are highly oriented, the optical response of

the film will be different depending on the angle of incident light. Polarized variable angle UV/Vis can be used to measure orientation in polymer films that exhibit H-aggregation. If the polymer chains are oriented then the aggregates will exist primarily in one plane of the film and the signature of the aggregation will be dependent on the polarization and incidence of the light (Figure 3-4).

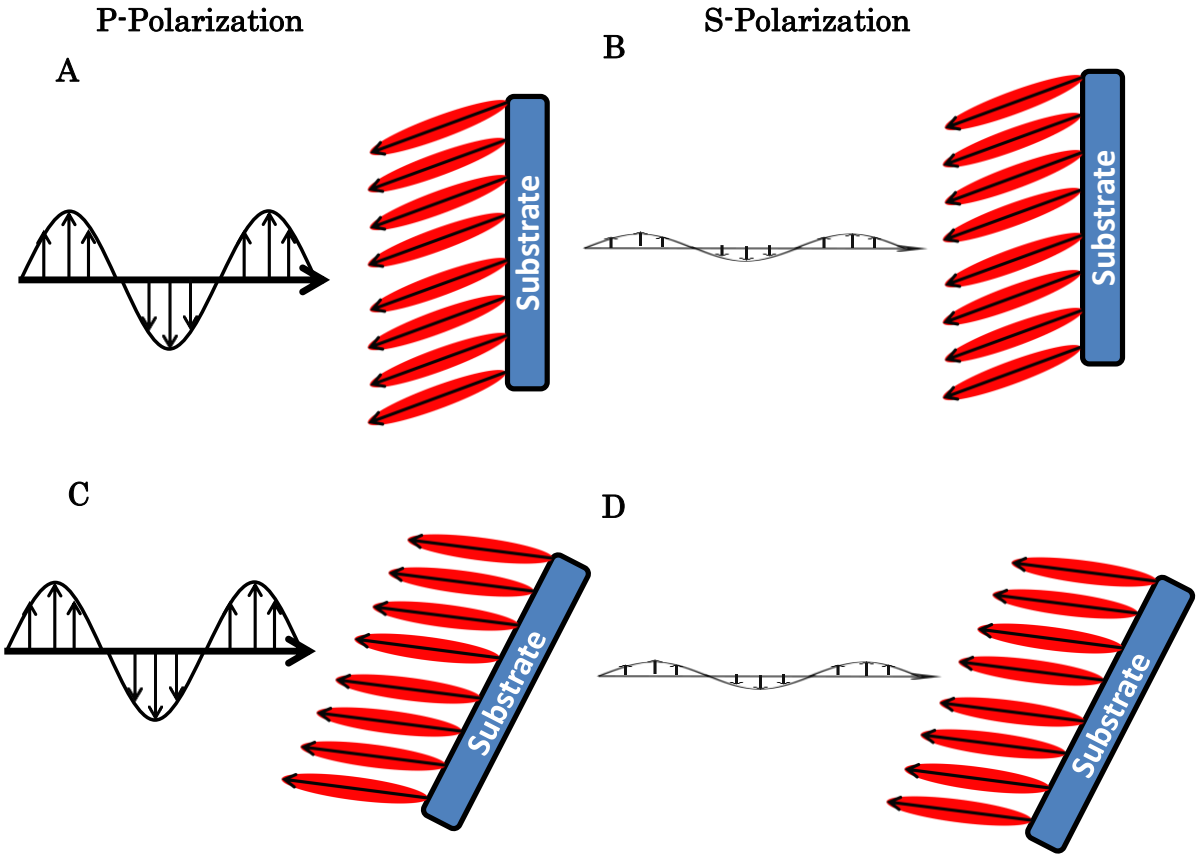

Figure 3-4: Measuring Orientation with Polarized Variable Angle UV/Vis Absorption

(A,B) Both S and P polarized light at normal incidence should have identical absorption spectra based on the overlap of the electric field of incident light (black arrows) and transition dipole in oriented molecules (red ellipse with black arrow).
(C) In the P polarization, at angles away from normal, the overlap between transition dipoles and electric field of incoming light is greater, and if present, the light can excite H-aggregates.
(D) In the S polarization, there is no appreciable change in the overlap between transition dipoles and electric field of incident light, so spectra should not change significantly.

In the example from literature, absorption spectra of unoriented P3BT films do not have any dependence on either angle of incidence or polarization of light. For films with oriented chains, there is a distinct shift in the p-polarization spectrum at angles away from normal, characteristic of the presence of H-aggregates oriented vertical to the substrate (Figure 3-5). There should only be a change in the p-polarized spectrum for oriented films due to the change in projection of the electric field of the incident light on the transition dipole moment of the polymer chain. The

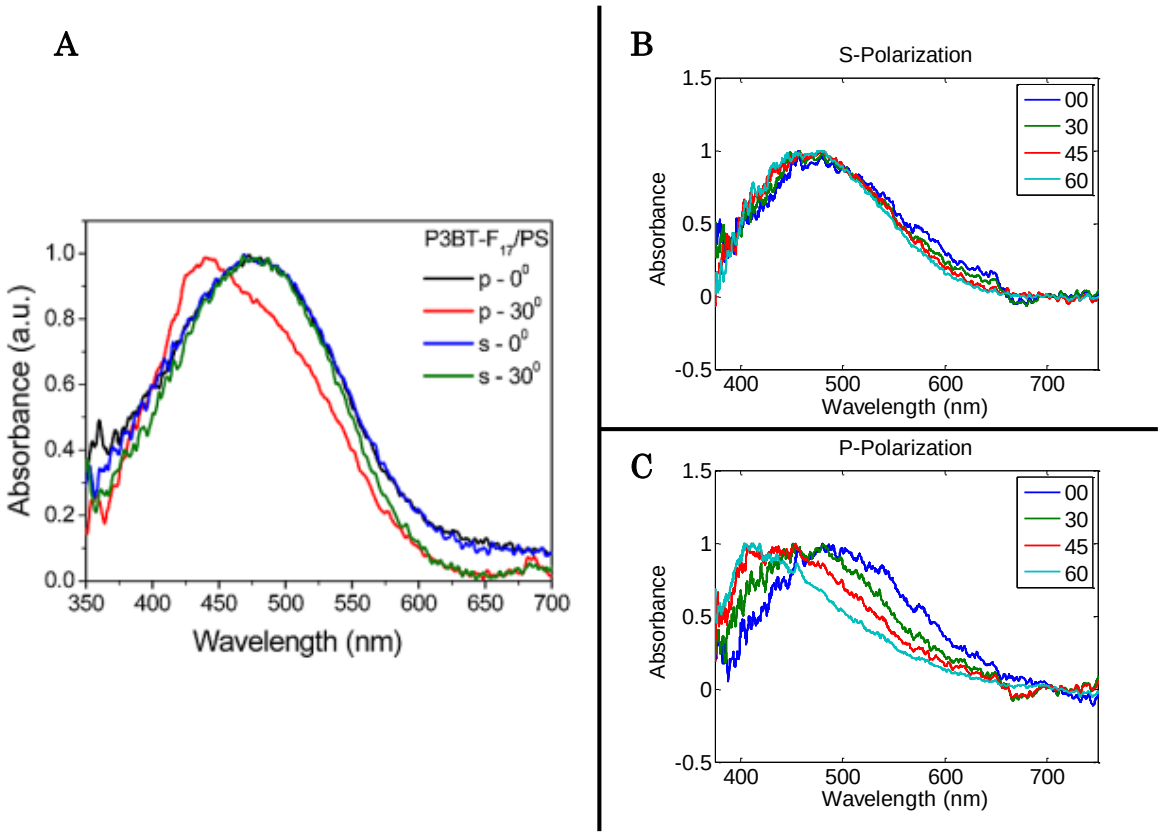

Figure 3-5: Vertical Orientation in Short P3MT Brushes

(A) Variable angle polarized UV/Vis spectrum of P3BT films with aligned chains from literature. There is a signature from H-aggregation in the p-polarization spectrum only, indicating that chains are aligned vertically. (Image copyright its respective owner)
(B) In a thin (<10 nm) film, S polarized light does not show signs of H-aggregation at any angle of incidence.
(C) P-polarized light shows signatures of H-aggregation in a thin (<10 nm) film only at angles away from normal, indicating chains in this film are highly oriented.

projection of s-polarized light on transition dipole moments does not change with angle of incidence, so the signature of vertical orientation only exists in the p-polarized spectrum.

Some films exhibit significant vertical orientation as grown, particularly shorter films (Figure 3-5 B and C). The lack of spectral signature of H-aggregation in the normal incident absorption spectrum may suggest that there is no order in shorter films, but normal incident absorbance only measures H-aggregation in the plane of the film. The polarized angle dependent spectra provide evidence that there is significant order out of the plane of the substrate. This order cannot be observed with normal incident light, demonstrating the importance for angle dependent measurements.

For P3MT brush films that exhibit H-aggregation in normal incident unpolarized UV/Vis spectra, the characteristic shift is not readily apparent (Figure 3-6), and visually inspecting spectra is not a quantitative method for characterizing the orientation of polymer chains in a film. Thus, a different method of analysis is employed besides visually comparing spectra. The centers of mass (COM) of absorption spectra are calculated as a function of angle of incident light and polarization of light to determine subtle shifts in the spectra. The center of mass is given by:

$$\boldsymbol{Center\ of\ Mass} = \frac{\int_a^b \boldsymbol{A(\lambda)\lambda d\lambda}}{\int_a^b \boldsymbol{A(\lambda)d\lambda}} \tag{10}$$

where “a” and “b” are the lower and upper limits of the absorption band.

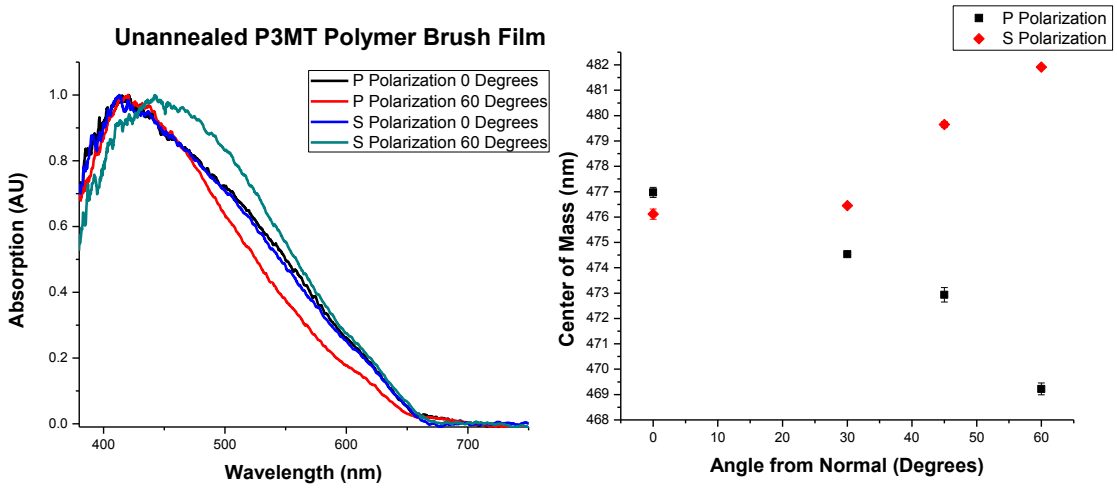

Figure 3-6: Measuring Orientation in Films with in plane H-Aggregates

(Left) S and P polarization at normal incident (0 degrees) are identical, but the spectrum exhibits a large signature of H-aggregation. At angles 60 degrees from normal, Both P and S polarizations appear different, but the peak foes not shift in the same characteristic was as in Figure 3-5. (Right) By plotting the center of mass of the absorption spectrum, a systematic blue shift is made clear in the P-polarized spectrum, indicating the presence of H-aggregates in the vertical plane. The presence of H-aggregates in the horizontal plane, as indicated by the spectra (left) signifies that the film has significant order in the horizontal plane, as well, implying films are not perfectly oriented vertically.

Applying equation (10) to polarized angle dependent absorption spectra reveals a trend that otherwise may be missed. There is a clear, systematic blue shift in the p-polarized absorption spectra as the incident light deviates from normal (Figure 3-6). This indicates that there is some degree of orientation out of the plane of the film, but there is still significant H-aggregation in the plane of the film for longer samples.

Applying this technique to films reveals that there is significant variation in the orientation in films as grown. Nearly identical unpolarized normal incident UV/Vis absorption spectra exhibit significant differences in the change in center of

mass as a function of incident angle. This is likely from the inconsistencies and variation in the growth of the films, where catalysts disassociate from growing chain ends and anchoring groups are etched from ITO surfaces.

3.3 Cyclic Voltammetry

Poly(3-methylthiophene) brush films are electrochemically probed by cyclic voltammetry. The ITO substrate the films are grown from is used as the working electrode with a platinum counter electrode and silver pseudoreference electrode used as supporting electrodes in dichloromethane tetra(*n*-butylammonium hexaflouorophospate) as the electrolyte. Cyclic voltammograms are taken by positively biasing the working electrode to reversibly oxidize the P3MT film. The onset of the oxidation wave corresponds to removing electrons from the film and is associated with the HOMO of the polymer brush thin film. The HOMO level is calculated by using a ferrocene standard, and the HOMO for the P3MT Brush is calculated to be -5.02 eV, corresponding closely to the HOMO level of dropcast films of P3HT at -5.1 eV. There were no observable peaks when applying a negative bias to the film, so the LUMO cannot be measured in this way. This is not uncommon for polymer films, where often only the electrochemical HOMO is reported.

3.4 Near Edge X-Ray Absorption Fine Structure Spectroscopy (NEXAFS)

Though there are many x-ray techniques to characterize thin films, NEXAFS is the one measurement that directly measures the orientation of molecules on a surface. The principles underlying the measurement are simple: at different

incident angles, x-rays are used to excite an analyte molecule in the solid state, and emitted, soft x-ray photons are detected. Depending on the transition excited, and the orientation of that transitions dipole, different behavior with respect to incident angle should be observed. This behavior is known for oligothiophenes oriented vertically to the substrate (Figure 3-7).[75] The core→σ* transition for an oligothiophene is in the plane of conjugation of the molecule, and the core→π* transition is out of the plane of the molecule, so the two transitions should trace each other out of phase by 90 degrees for a perfectly vertically oriented poly or

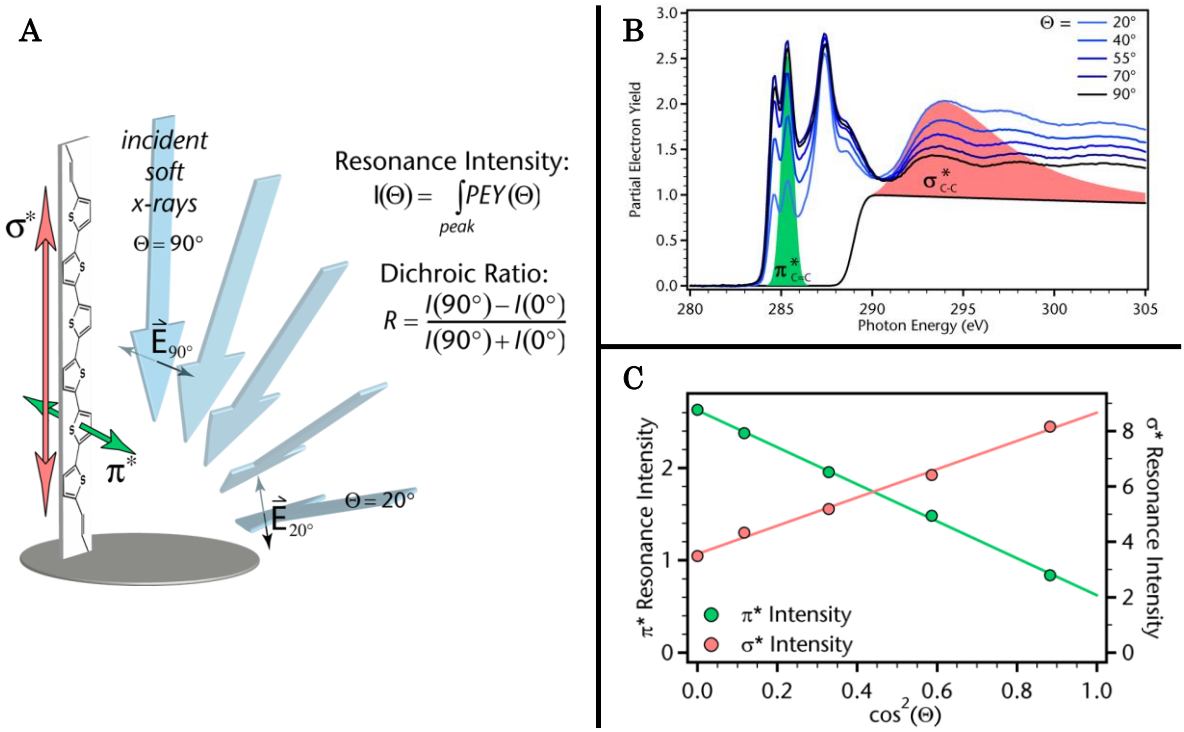

Figure 3-7: NEXAFS in Oriented Oligothiophenes
(A) Schematic depicting overlap between polarized x-rays and core→excited state transitions. The ratios of the intensities of the transitions are used to determine the orientation of molecules in a film.
(B) Plot of data from literature illustrating change in resonance between core→σ* transition and core→σ* transition as a function of angle of incident x-rays.
(C) Graphical depiction of the change represented in (B). This trend is consistent with molecules that are both "edge-on" and "standing"

oligothiophene film, that is the σ* transition should be greatest at low incident angles (grazing angles) and the π* should be greatest near normal incidence.

Due to measurement restrictions, only two samples could be tested using the NEXAFS technique, one sample of physisorbed P3MT and one sample of a short P3MT brush (Figure 3-8). The spectra of the two samples demonstrate opposite trends. For the physisorbed polymer, the core→σ* transition signal is greatest at

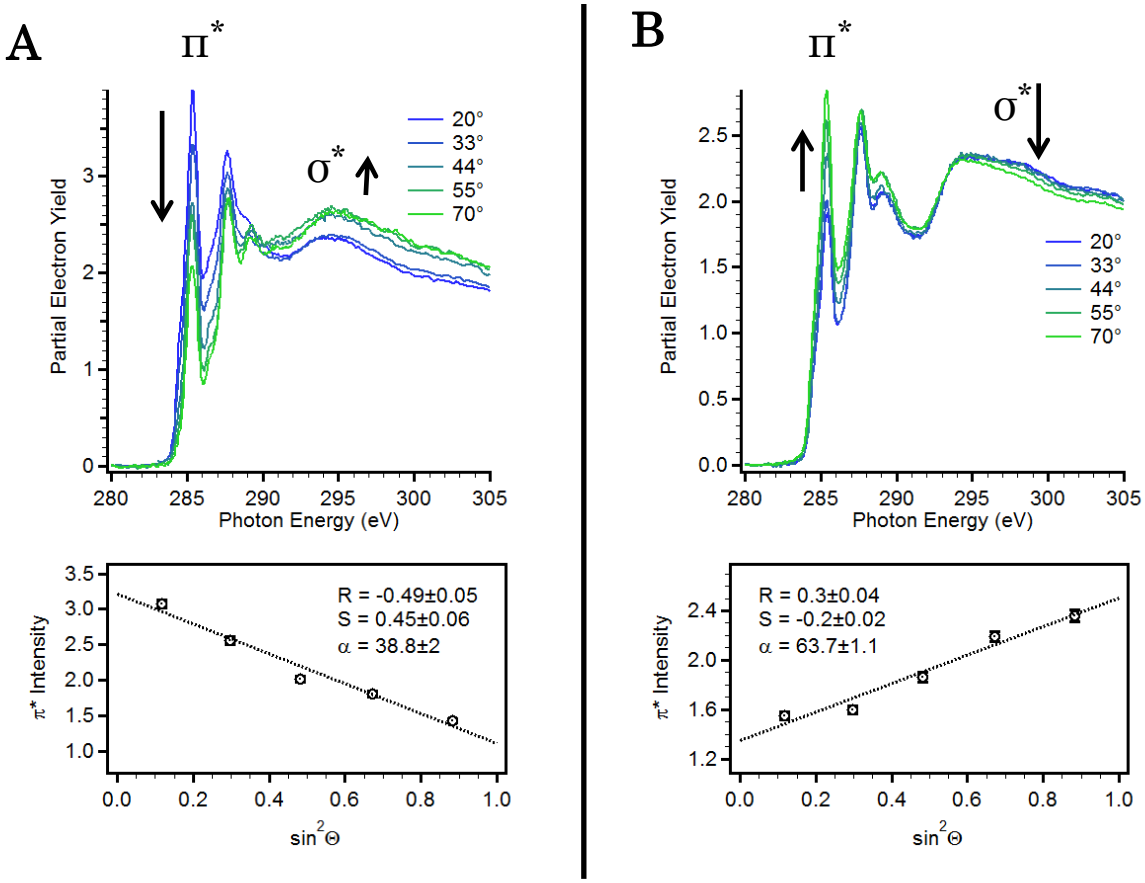

Figure 3-8: NEXAFS Orientation in P3MT Brushes

(A) (Top) NEXAFS spectra of physisorbed P3MT traces the opposite trend of edge on standing oligothiophenes. This spectrum is consistent with thiophene lying flat on a surface. (Bottom) the π* intensity trace gives clear evidence that chains are not standing in the physisorbed case. (B) (Top) The NEXAFS Spectra of P3MT Brushes have followed the same trend as that of vertically oriented oligothiophenes. (Bottom) The π* intensity trace is consistent with oligothiophenes standing up.

angles closest to normal and monotonically decreases as the angle approaches grazing incidence while the core→π* transition signal follows an opposite trend. This is consistent with molecules laying face on to the ITO surface with little vertical orientation. For the polymer brush film, the core→σ* transition signal is greatest at angles away from normal and decreases monotonically as the angle of incident x-rays approaches normal. The core→π* transition signal in the polymer brush film increases as the angle of incident x-rays approaches normal. These data suggest that the brush polymer is significantly oriented vertically from the surface. Comparing the trends observed in the physisorbed and brush films demonstrates that P3MT on a surface can have multiple orientations, but only in the grafted polymer brush case do the NEXAFS data suggest that the polymer chains are oriented normal to the surface. The "α parameter" can be interpreted as an ensemble average orientation angle from the substrate. For the physisorbed film, the α parameter suggests that the average dipole orientation is 38±2, while the orientation for the polymer brush film is 63.7±1.1. The NEXAFS data demonstrate that the short polymer brush thin films are somewhat vertically oriented as grown.

3.5 Ellipsometry

Ellipsometry measures the change in the polarization of polarized that is reflected from a surface. The phase and amplitude differences of the light after it is reflected can be modelled to calculate film thickness and optical constants *n* and *k*. Here, ellipsometry is used to calculate film thickness. All fitting and modelling is done as directed in the J.A. Woollam ellipsometry handbook.[76] For multilayered

sampled like those analyzed here, each layer must be modelled and fit to obtain the thickness. Here a three layer model is used to calculate film thickness with glass being the bottom layer, ITO as the middle layer, and the polymer brush layer being the top. The modelling of each layer is important, because changes in one layer will affect the modelled thickness of the other layers.

Glass is the substrate layer and was modelled from experimental data using a Cauchy fit. The Cauchy fit is primarily used for materials that do not absorb light in the visible region, and are not conductive. ITO is the next layer, and is modelled using the graded Lorentz model. The graded Lorentz model is used for ITO because ITO is vertically inhomogeneous, and the graded Lorentz model allows for fit variables to change. The polymer layer uses a Cauchy model, which is typically used

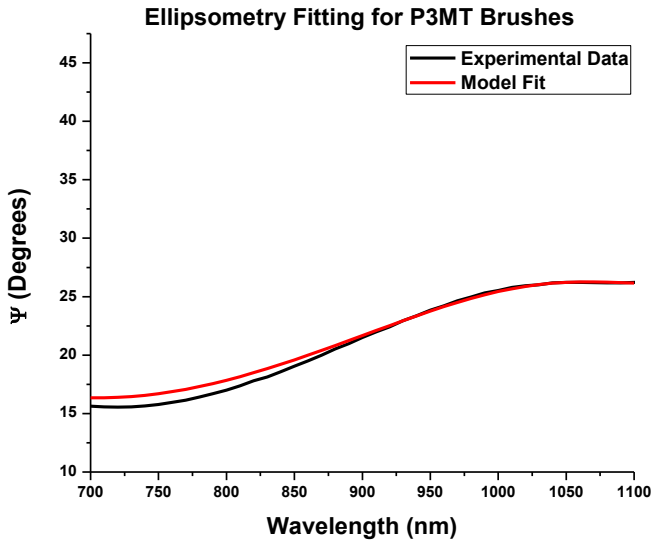

Figure 3-9: Model of P3MT Brush for determining Polymer Film Thickness

The raw data from ellipsometry measurements of P3MT brushes is modelled using three layers, a glass substrate, an ITO film , and a polymer film. The model can be fit to the experimental data (shown above) to determine the polymer film thickness.

for organic semiconductors. The whole spectrum was measured, but only wavelengths after 700 nm are used because the Cauchy model works best when the material does not absorb light. Each sample is modelled using these three layers to build up the complete film (Figure 3-9). Film thicknesses determined by ellipsometry are in close agreement with AFM profilometry, and will be discussed at the end of the chapter.

3.6 Atomic Force Microscopy

Atomic force microscopy (AFM) is a useful tool to characterize surface grafted P3MT films as it is the only tool used to directly measure the thickness of conjugated polymer brush films in literature. It can also be used to measure the surface roughness of the film, which can be used to estimate the local surface coverage and as a stand-in for the polydispersity of the film.

Film thickness is directly measured by scratching the P3MT brush film with a needle and using the AFM tip to measure the step height between the exposed ITO surface and the surface of the polymer brush film (Figure 3-10). Though this is a good measure of absolute film thickness, it is a destructive method. After the film has been scratched, the quality of the film is compromised, and measurements requiring pristine films can no longer be made. Also, scratching the film so that only polymer is removed and trenches are not dug into the ITO substrate is difficult to control. In order to verify that only polymer is removed, the roughness of the exposed ITO is compared to the roughness of pristine ITO, and the phase of the AFM tip between the scratched and unscratched regions are compared. When the

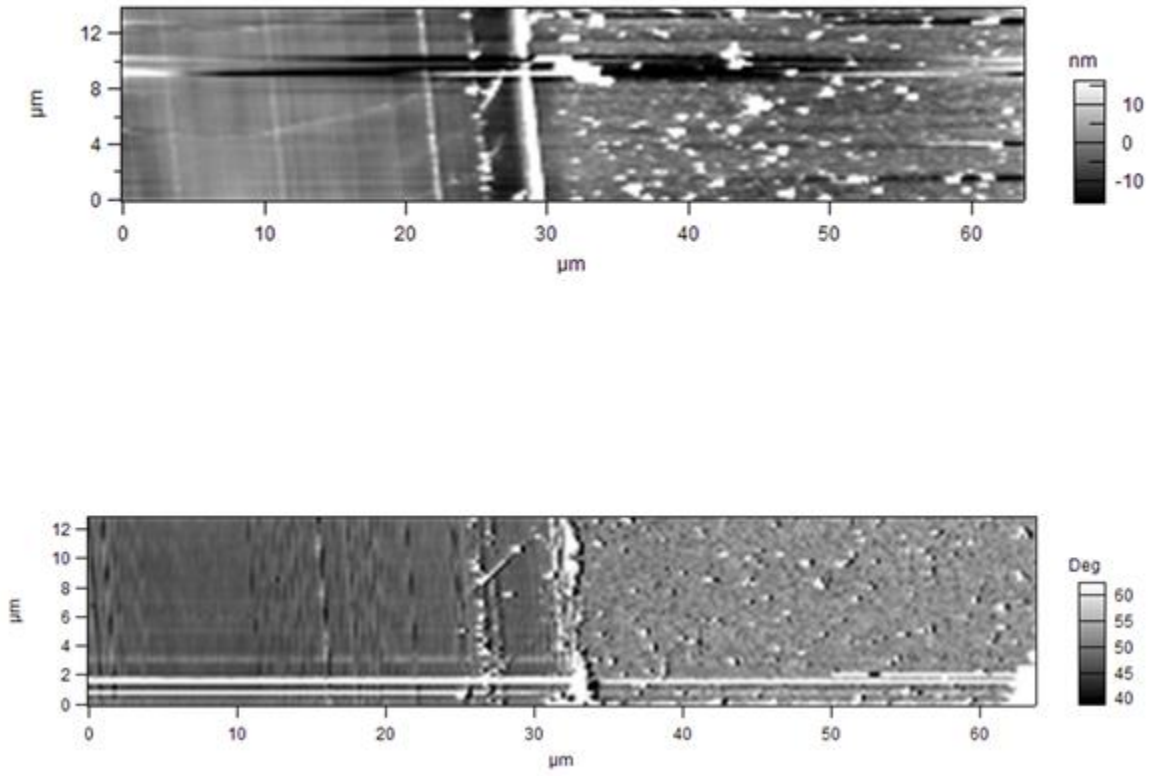

Figure 3-10: Measuring film thickness with AFM Profilometry

(Top) Scratching P3MT brushes introduces defects onto the surface, but a step height can be measured between the ITO surface (left) and polymer film (right). The relatively pristine ITO (left) indicates that polymer was completely removed by scratching, and the smoothness indicates that the needle does not dig a trench into the ITO. (Bottom) The change in phase between ITO (left) and P3MT (right) gives further evidence that all polymer is removed by scratching.

AFM tip is over the softer polymer material, the phase of the AFM tip is different than when it is over the hard ITO material. Choosing the step height accordingly gives an accurate depiction of the film thickness.

As described in Chapter 2, the film thickness can be plotted against film absorption to make a calibration plot (Figure 2-9) to estimate film thickness from absorbance. Though the trend is generally good, differences in absorption spectra

between films makes this useful only as a gross estimation of film thickness, because the absorption maxima correspond to different features in the spectrum.

The RMS surface roughness of films grown in this work is generally quite low compared to those reported in literature.[57] Physically interpreting RMS film roughness is difficult without knowing the chemical identity of the surface—that is whether the surface of the polymer brush film is composed of end groups or repeating units on the polymer chains (Figure 3-11). If the chains are terminated at the surface, and the chain ends are exposed, that would mean the RMS roughness

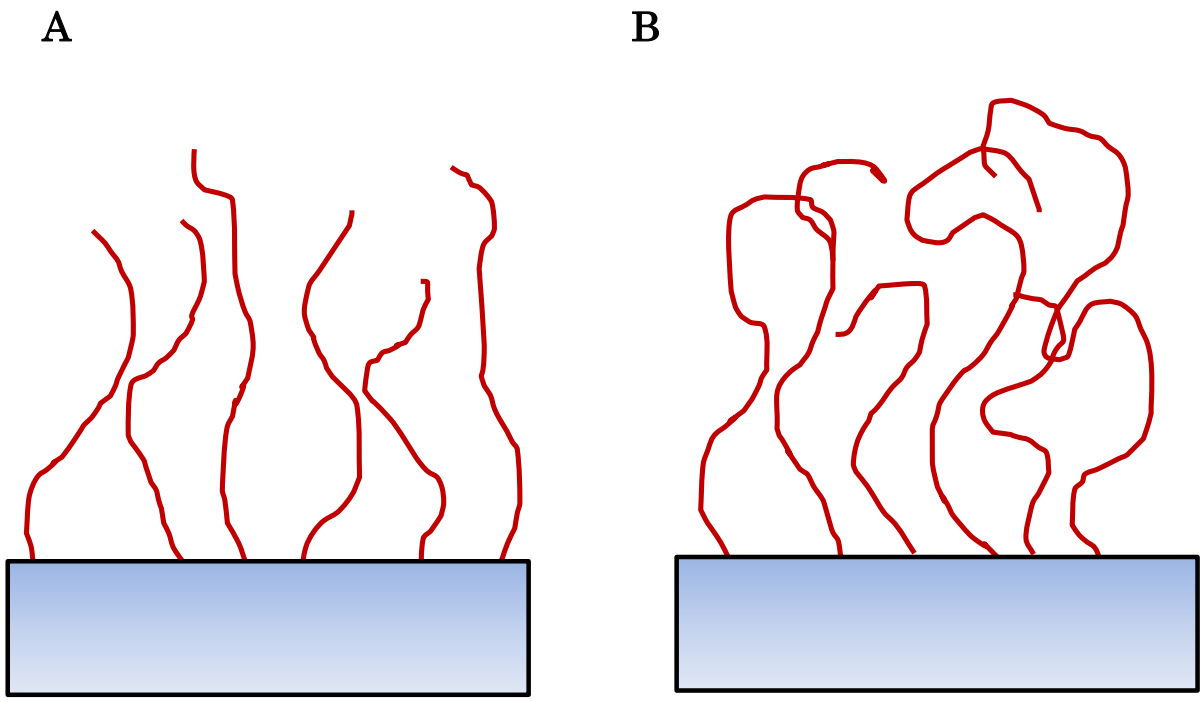

Figure 3-11: Possible Surface Configurations of P3MT Chains

(A) In this case, the surface polymer brush film consists entirely of end groups. If the assumption is made that films will generally have the same amount of coiling, the dispersity of end groups can be used as a stand-in for PDI that is typically used in solution polymerizations. (B) In this case, the surface is composed entirely of monomers internal to the chain. In this case, roughness is still important to know, as in (A), because significantly rough films are not good for devices due to large differences in distances charges must transport through films.

could be used as a gross stand in for the PDI of the polymer, despite evidence that the chains are not oriented vertically and somewhat coiled. The RMS roughness is also an indicator for inhomogeneity of the distances charges must transport through films in a device. If the surface is not composed of chain ends, but internal fragments of the polymer and the chain end is buried beneath the film surface, the surface roughness would not represent the dispersity of polymer chains, but it still gives an indication to the inhomogeneity between the path lengths for charges to transport through the film.

Two typical AFM micrographs for thin and thick P3MT brush (Figure 3-12) show that the surface is covered uniformly and is relatively smooth for thick (30 nm) and thin (10 nm) films with RMS roughness of 8.3 nm and 4.2 nm, respectively. The roughness does significantly increase with respect to length, but adjusting the roughness for the thickness of the films shows that the relative roughness of the films decreases as the length of the film increases. If the film surface represents chain ends, that would mean that the polymer chains vary by less as thickness increases. Though this cannot be converted directly to PDI, and it may not be a good indicator of polydispersity the RMS roughness corresponds to a difference of 8-16 3-methylthiophene repeat units. This number does not necessarily make physical sense, but as a quick comparison to polydispersity in solution polymerizations, that represents a quite monodisperse sample.[77] Even if the surface does not represent chain ends, typical alkanedithiol monolayers measured have RMS roughnesses on the order of 0.5-1nm RMS,[50] or approximately 50% of the

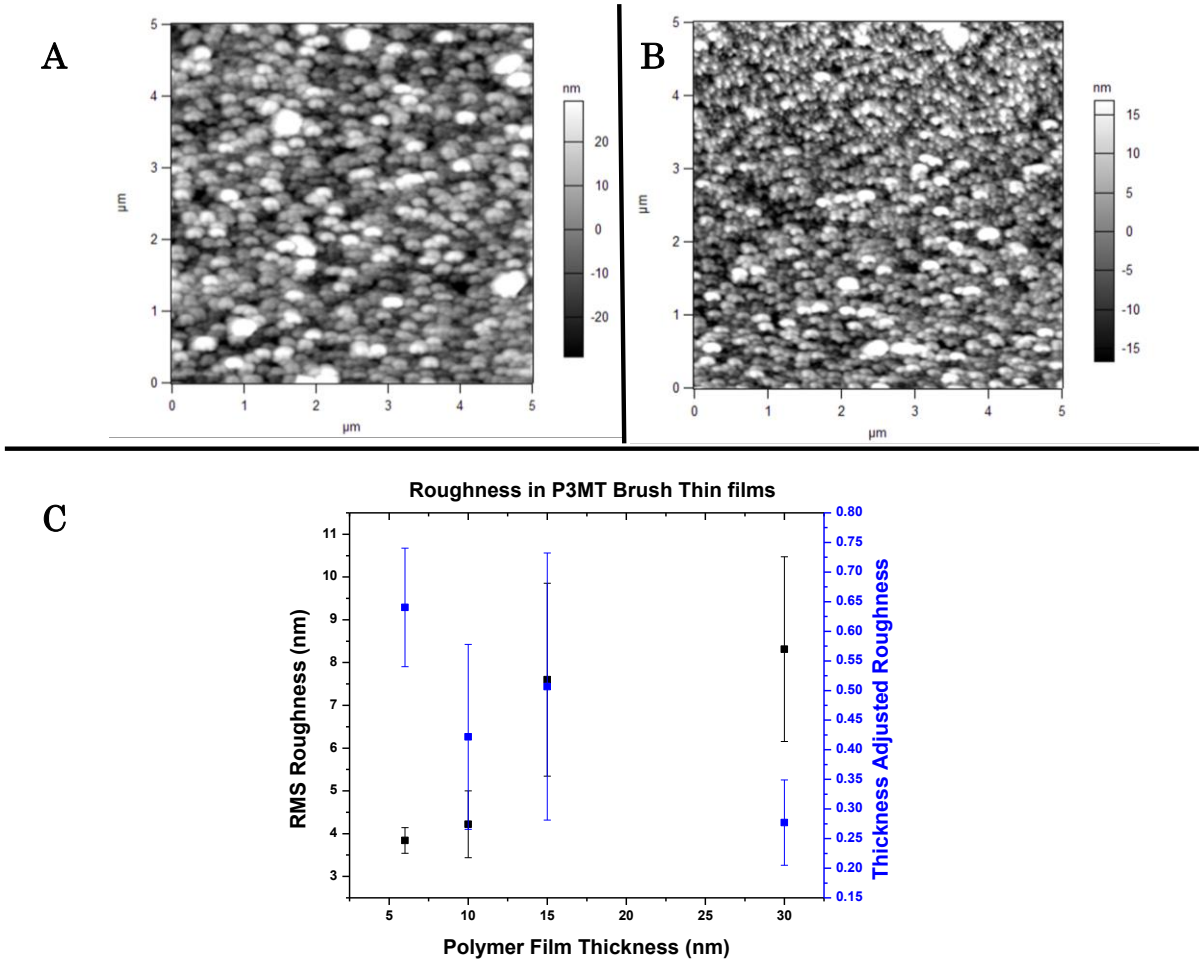

Figure 3-12: AFM Surface Roughness

(A) Short (10 nm) P3MT brush films present a surface free of large defects, with some small features.
(B) Long (30 nm) P3MT Brushes present a relatively smooth film with fewer defects. Although the absolute RMS roughness is greater than in the thin film in (A), its relative roughness is lower.
(C) This plot of roughness vs. length shows that roughness does increase as films get longer, but the relative roughness decreases. This makes sense for films that have a long induction period to being reacting. If shorter films and longer films have the same absolute difference in chain length, then the relative roughness will decrease as chains become longer.

molecular length, so these brushes do not present a surface that is significantly rougher, comparatively. Thus, consideration of surface roughness should be taken only in the cases of extreme roughness, but in general the corrected roughnesses are

comparable to molecular electronic devices. Smooth films should be selected when choosing films for charge transport measurements.

3.7 Characterizing Annealed Films

3.7.1 Annealing Polymer Brush Thin Films

As grown, P3MT brushes are good candidates for accomplishing the goals of this work of measuring charge transport across a single layer of polymer chains. In an effort to create films with more ideal morphology, several methods are used to alter the morphology of films after they are grown to enhance vertical orientation, especially in thicker films. To do this, films are annealed under several conditions and differences in the absorption spectrum of each film are tracked before and after annealing. Films that show significant changes in absorbance are further characterized by variable angle polarized UV/Vis, ellipsometry, and AFM to track changes in thickness and surface morphology.

Two approaches are chosen to anneal films: annealing with solvent and with heat. Solvent annealing could break up interactions between polymer chains to allow chains to relax from semioriented, semicoiled morphologies to brushlike morphologies, which should have lower global energy. Annealing with heat should do the same thing, but instead of solvent causing chains to swell and relax, heat is used to overcome the interactions locking the grafted polymer chains in place to erase the thermal history of the film.

Films are solvent annealed in chlorobenzene at room temperature and at elevated temperature (85 °C), and thermally annealed at 150 °C, 200 °C, and

250 °C. Solvent annealing normally refers to annealing spuncast films in the solvent they are spun in, but in this case solvent annealing refers to soaking in a bath of chlorobenzene. Solvent annealing at room temperature and thermally annealing at and below 200°C did not significantly change the absorption spectrum of the film. Only solvent annealing at 85°C and above and thermally annealing at 250°C caused changes in the absorption spectra of P3MT bush films. Films solvent

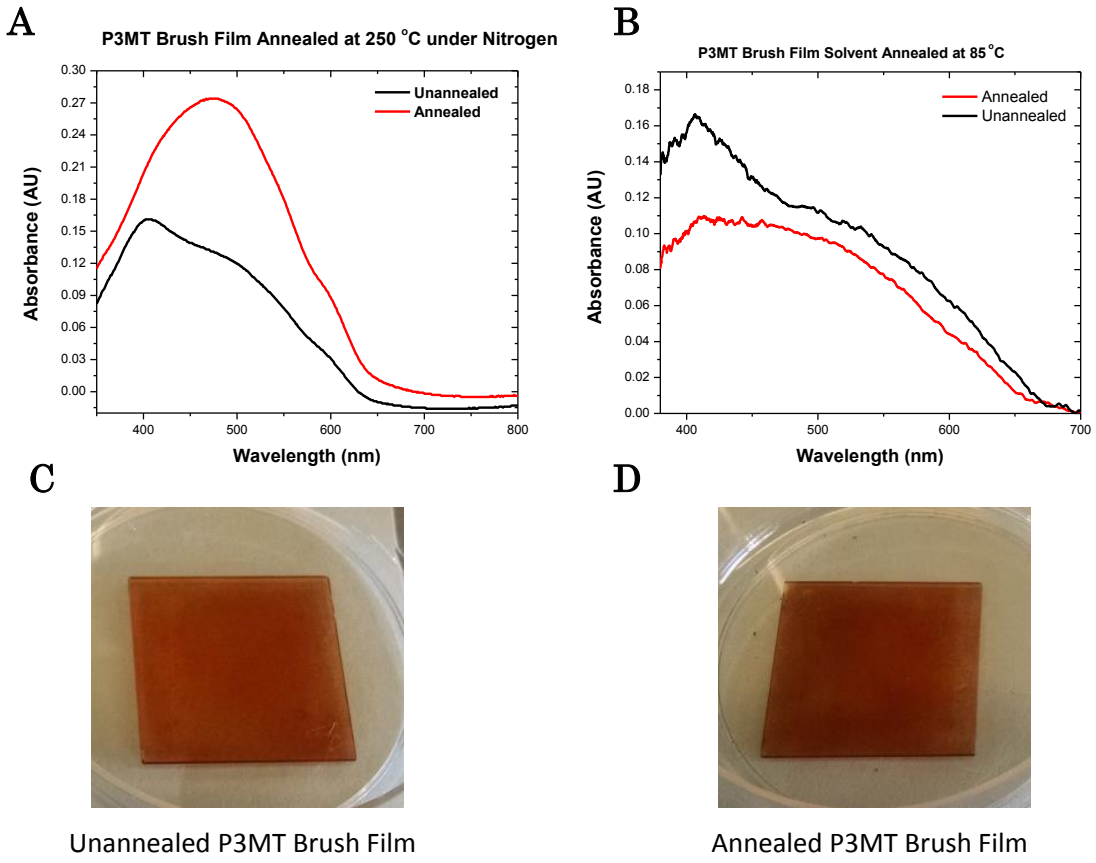

Figure 3-13: Thermally Annealing P3MT Brushes

(A) Films annealed at 250 °C show the most drastic change in absorption. The absorption increases by a factor of 1.7 and the maximum shifts by 80 nm The integrated absorbance increases by a factor of 2.3.
(B) Films annealed at 85 °C in chlorobenzene do not have as significant a change. After annealing, the absorption maximum does not change and the total absorbance decreases (C and D) The color of P3MT Films changes before and after annealing at 250 °C. Annealed films appear purple, similar to spuncast P3HT.

annealed at 85 °C do not change in shape, but the absorption max decreases slightly. The most drastic change observed was in films annealed at 250°C, with the absorption maximum shifting by 80 nm (from 40 nm and 80 nm) and losing the strong signature of H-aggregation. There is some difference in the film annealed at 85°C, but the absorption maximum does not change. There is still significant evidence of H-aggregation in the plane of the film evidenced by the strong absorbance near 400nm. This is unlike the film annealed at 250°C. Films annealed at 250°C are further characterized with closer analysis of UV/Vis absorption spectra, polarized UV/Vis, AFM, and ellipsometry to determine the effects annealing has on film morphology.

3.7.2 UV/Vis Absorption of Annealed Films

The changes in the UV/Vis absorption spectrum of films annealed at 250°C indicate that there are significant differences in the morphology of the film after annealing (Figure 3-13). The onset of absorption does not change, meaning that the lowest energy excitation does not change either. This means that the conjugation length does not change significantly before and after annealing. The overall absorption increases after annealing, corresponding to an increase in the maximum absorbance by a factor of 1.7 and a 2.3 times increase in the integrated absorption of the entire spectrum. This is anecdotally attributed to stronger interaction between polymer chains, and is often observed after annealing.[70] The spacing between local maxima in the absorbance spectra is similar, suggesting that similar transitions are being observed in the spectrum before and after annealing, but the difference in the

shape of the spectrum as evidenced by the relative intensities of absorption peaks is consistent with a shift in the strength of the H-aggregation of the chromophores being excited by incident light.[73] This shift is consistent with the strength of H-aggregates decreasing significantly or the amount of H-aggregated material that can be observed in the plane of the film decreasing. Normal incident light cannot excite H-aggregates vertical to the plane of the film, so ordered segments in that plane are not observable by this technique. This means that the polymer chains being excited after annealing are in a different environment and have different morphologies than before annealing.

3.7.3 Polarized UV/Vis of Annealed Films

Polarized UV/Vis is used as it was previously: to measure the aggregation in the plane vertical to the growth substrate. The disappearance of the signature of H-

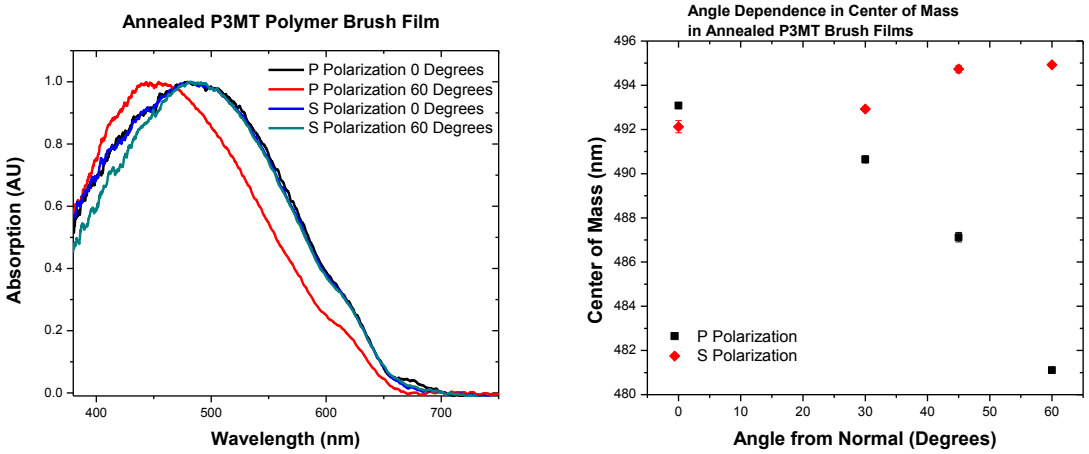

Figure 3-14: Variable Angle Polarized UV/Vis of Annealed P3MT Films

Annealed films have the same photophysical properties of oriented films reported in literature (Figure 3-5). There is a clear signature of H-aggregation in only the p-polarized spectra at angles away from normal, and the COM systematically decrease (blue shifts) indicating that the films are highly oriented. the COM shift is 2-3 times large for annealed films than it is to identical unannealed films.

aggregation in films in the plane of the substrate signifies a lack of interchain interaction in the plane of the film, and this technique can be used to probe the existence of H-aggregates vertical to the plane of the substrate that cannot be observed with normal incident, unpolarized light.

When long (20-30nm), annealed P3MT brush films are measured using this polarized UV/Vis technique, they exhibit a clear signature of H-aggregation in the vertical plane with a lack of H-aggregation in the plane parallel to the substrate, indicating that films have a high degree of vertical orientation after annealing (

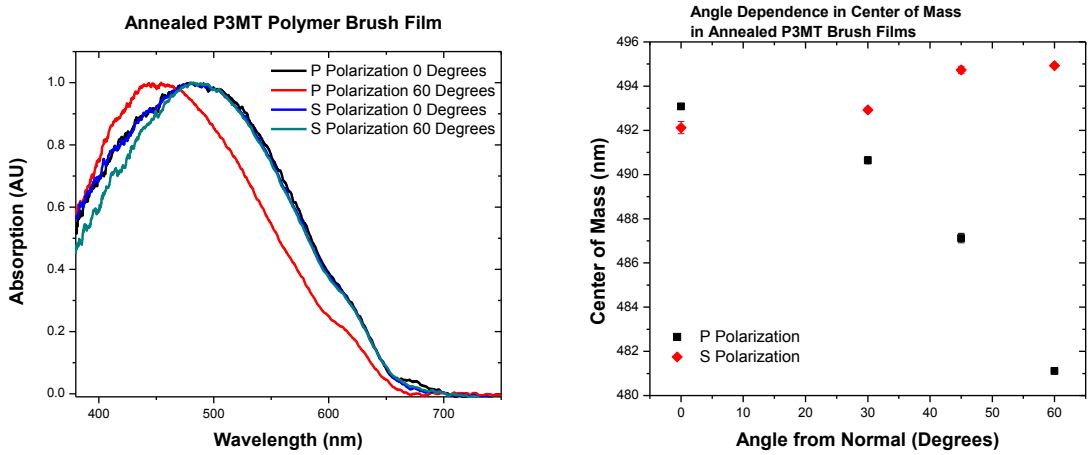

Figure 3-14). This signature does not appear as dramatic as that observed in the thinner films, but the change in the COM of the absorption spectra of polymer brush films are significantly greater in films after they are annealed.

3.7.4 Ellipsometry of Annealed Films

Several films were analyzed by ellipsometry before and after annealing to track the change in film thickness due to thermally annealing samples. Films are modelled using the same fits, though the parameters obtained are slightly different.

In every sample measured, film thickness increases after annealing. Since the amount of material is not changing on the surface, the change in thickness must be due to a change in the film morphology and chain conformation. This change is interpreted as chains becoming uncoiled and becoming more linear and brushlike. This is consistent with the interpretations of polarized UV/Vis. The ramifications this may have on film morphology are discussed at the end of this chapter, and the changes in film thickness are tabulated in Table 3-1.

The ratio for the change in polymer thickness decreases as a function of the initial length of the polymer brush. This may be because short brushes do not have

Polymer Film Thickness Before Annealing (nm)	Polymer Film Thickness After Annealing (nm)	Change in Film Thickness (nm)	Ratio Change
3.5±0.9	13.7±0.7	10.2±1.1	3.9±1.0
7.1±0.5	22.1±0.9	15.0±1.0	3.1±0.3
9.39±0.05	21.3±2.3	11.9±2.3	2.3±0.2
10.2±0.5	17.5±2.9	7.3±2.9	1.7±0.3

Table 3-1: Polymer Film Thicknesses Before and After Annealing

the ability to induce standing behavior below 5-7 nm (Figure 3-15).

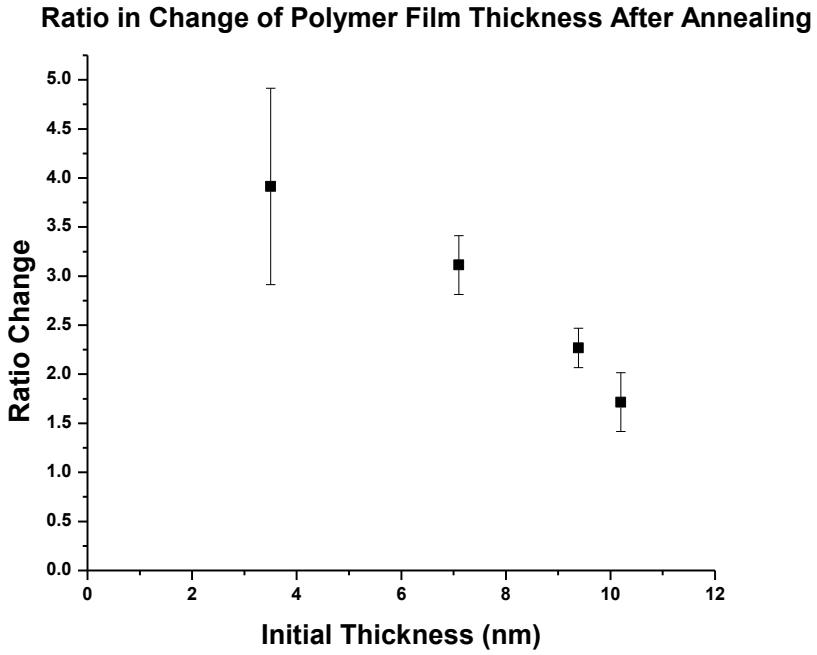

Figure 3-15: Ratio of P3MT Chain Extension After Annealing

Thicker initial polymer thicknesses have smaller increases in length after annealing. This is likely due to chains growing first as mushrooms before chains are able to repel each other and induce vertical orientation. The initial blob near the ITO surface, if it exists, will untie after annealing.

3.7.5 AFM of Annealed Films

Surface roughness scans after annealing films indicate that the RMS roughness of films may slightly increase, however the roughness relative to the thickness of the polymer decreases. For a short film (7.1 nm), the RMS roughness was measured to be 3.1 nm before annealing. After annealing, the film was measured to be 22.1 nm, but the RMS roughness only increased to 4.5 nm. The relative roughness decreases from 0.43 before annealing to 0.20 after annealing. If the surface is comprised of chain ends, this decrease in roughness gives further evidence that the polymerization is controlled if the relative RMS is taken as a stand in for PDI. If the P3MT brush film surface is comprised of chain ends or not,

the relative roughness of the surface is much lower, meaning that annealed films have a more ideal surface for measuring charge transport through polymer chains.

3.8 Discussion

Before film morphology is discussed, the merits of the three techniques to determine film thickness must be compared. Two films were characterized side by side using AFM profilometry, the UV/Vis absorbance calibration plot, and ellipsometry. The lengths determined by each of these measurements for these films are tabulated in Table 3-2. The three methods are in generally good agreement. The calibration plot is just an estimate based on the maximum absorbance peak, which can shift up to 80 nm, so it is not the ideal method for determining thickness. Nonetheless, all three methods agree within error. Depending on the purpose of the film, one technique may be more useful than another. If the film needs to be pristine, ellipsometry is the best choice for measuring film thickness. If the film has no more use or does not need to be pristine for any reason, the destructive AFM profilometry may prove the better method.

Film	AFM Profilometry Thickness (nm)	Calibration Plot Thickness from UV/Vis (Estimate) (nm)	Ellipsometry Thickness (nm)
Film 1 (Not Annealed)	29.0±3.0	30.1	31.5±1.5
Film 2 (Annealed)	22.0±1.0	25.0	23.9±2.3

Table 3-2: Comparing Methods for Calculating Film Thickness

Interpreting the results from the characterization techniques as a whole may provide a depiction of polymer film morphology and what happens to the polymer film when it is annealed. The most quantitative and conclusive piece of evidence to characterize film morphology comes from NEXAFS measurements on unannealed films, which suggest that X-ray chromophores in polymer brush films have an average orientation of 60 degrees from normal. This average orientation is consistent with literature reports.[57] This is in contrast to films that are not chemically grafted and only physisorbed to the surface, which do not show signs of vertical orientation. Though only two films were measured with NEXAFS, these results can be used as a baseline for interpreting the rest of the measurements.

The rest of the characterization techniques can be interpreted together to provide a picture of P3MT brush film morphology. AFM data suggest that films are locally dense and defect free, as well as relatively smooth compared to films reported in literature.[57, 66-67] After annealing, film roughness does not change significantly, though the roughness of the film relative to the thickness does. Polarized and unpolarized UV/Vis absorption spectra indicate that the optical bandgap does not significantly change from film to film regardless if it is annealed, and that H-aggregation in the plane of the film mostly disappears after annealing. Also, the signature of H-aggregation in polarized spectra as a function of angle of incidence increases after annealing as evidenced in the COM, suggesting that annealing polymer brush thin films increases the degree of vertical orientation and order of polymer chains. Roughness measured by AFM suggests film surfaces do not

appreciably change. Finally, ellipsometry, UV/Vis absorption, and AFM profilometry all suggest that film thickness increases after annealing polymer films. Taking these changes into account with respect to each other, several conditions can be made that models of P3MT brush morphology must follow. These are described below.

Analyzing the changes in the P3MT brush due to annealing may be the best way to construct a model of film morphology and chain conformation. The discussion of film morphology begins with the increase in thickness of films after annealing. Put in context of the polarized UV/Vis result indicating that chains become more vertically oriented after annealing, the increase in thickness is most likely due to polymer chains becoming more ordered in the vertical direction. In Figure 3-16, the effect of having polymers with significant intermolecular interaction in the horizontal direction reorienting towards vertical to both increase length and increase the chain order in the vertical direction. Chains do not uncoil or become rigid in this model. This cartoon satisfies these two conditions are met, but does not add any more assumptions. This will be called **condition one**.

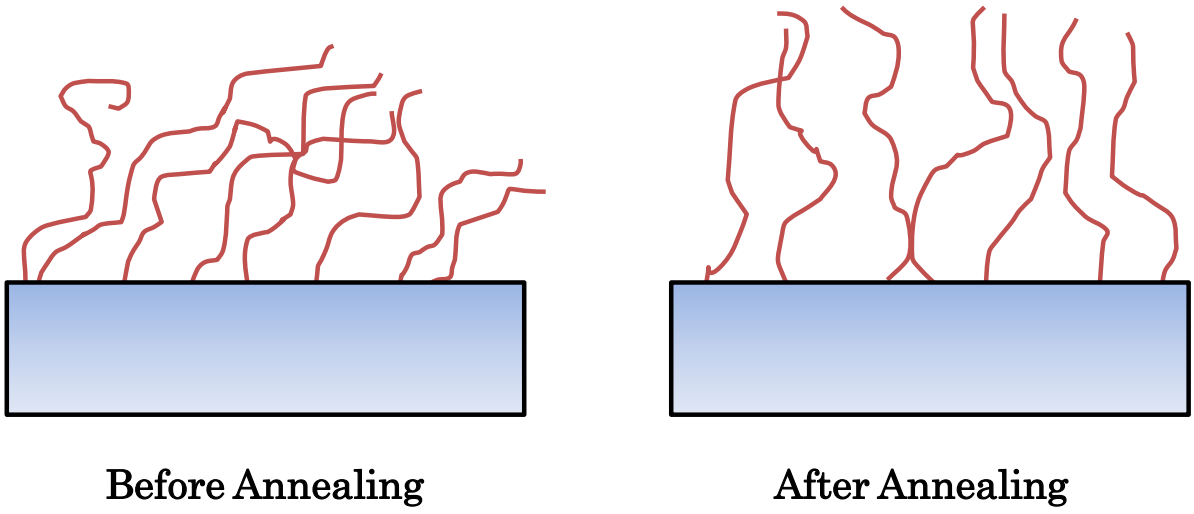

Figure 3-16: Shift in H-Aggregation from Horizontal to Vertical Plane Causing Film Thickness Increase

This sketch of the polymer film accomplishes two things: it demonstrates a film with intermolecular order (depicted by chains aligning with each other) in the horizontal direction changing as it is annealed to a film with chains with vertical order (chains aligning in the vertical direction). In this case, the film thickness increases only because chains are changing their average angle of orientation. There is no uncoiling or straightening.

The change in film thickness can be more thoroughly explained by reverse engineering an ideal film using three parameters at boundary conditions: the angle between the substrate and polymer chain, the polymer chain rigidity, and the distance between monomers on adjacent chains. A perfect film would have all three parameters at their upper limits which would correspond to the upper bound for film thickness. A change in each of these parameters will necessarily affect the others. The upper bound for film thickness is equal to the contour length of the polymer chains in the film and occurs when the angle between the growth substrate and polymer chains of exactly 90° and polymers are perfectly rigid and spaced. Any deviation in the angle between polymer chains and substrate would cause the film thickness to decrease. Likewise, if the end to end distance of the polymer is any less

than the contour length, then the film thickness would decrease accordingly at a given angle of orientation. This is similar to the cartoon sketched in Figure 3-16. Decreases in the end to end distance are due to deviations from planarity and imperfect torsional order between 3-methylthiophene monomers making the polymer less rigid. This would cause polymer chains to have kinks and bends which would necessarily cause monomer units on adjacent chains to become closer. The upper bound for average distance between monomer units is the grafting density of polymer chains on the surface. The polymer end to end distance and average distance between monomer units on adjacent chains are necessarily related as described above. The evidence of increased vertical orientation of chains from UV/Vis suggests that annealing does increase the angle between chains and substrate towards the optimum angle, as described by **condition one**. The change in thickness after annealing indicates that the initial state of the polymer is not in the ideal conformation. An increase in thickness could be due to changing the angle between polymer chains and the growth substrate, increasing the planarity of polymer chains, increasing the distance between polymer chains, or some combination of the all three. However, using the NEXAFS result that films are oriented at an average angle of 60°, the large increases in thicknesses as reported in Table 3-1 Annealing cannot be accounted for by only increasing the orientation angle by 30°, which would only increase film thickness by a factor of about 15%. This means that chains must be uncoiling as well as becoming more vertically oriented. This will be called **condition two**. Combining condition one and two gives a new

depiction of polymer film morphology after annealing (Figure 3-17). Since films are uncoiling and becoming vertically oriented, all three parameters are approaching their upper bounds as described above, but it cannot be conclusively determined to what extent with the given information.

Another explanation of the increase in film thickness that is consistent with the results but not dependent on the above model starting from an average orientation of 60° is that the volume of the polymer brush film necessarily increases after annealing because of the increase in film thickness while the cross sectional area remains constant. Thus, the density of polymer chains must decrease as well. Therefore, the average distance between monomer units must increase as well. Using the same three parameters (orientation angle, chain rigidity, and distance

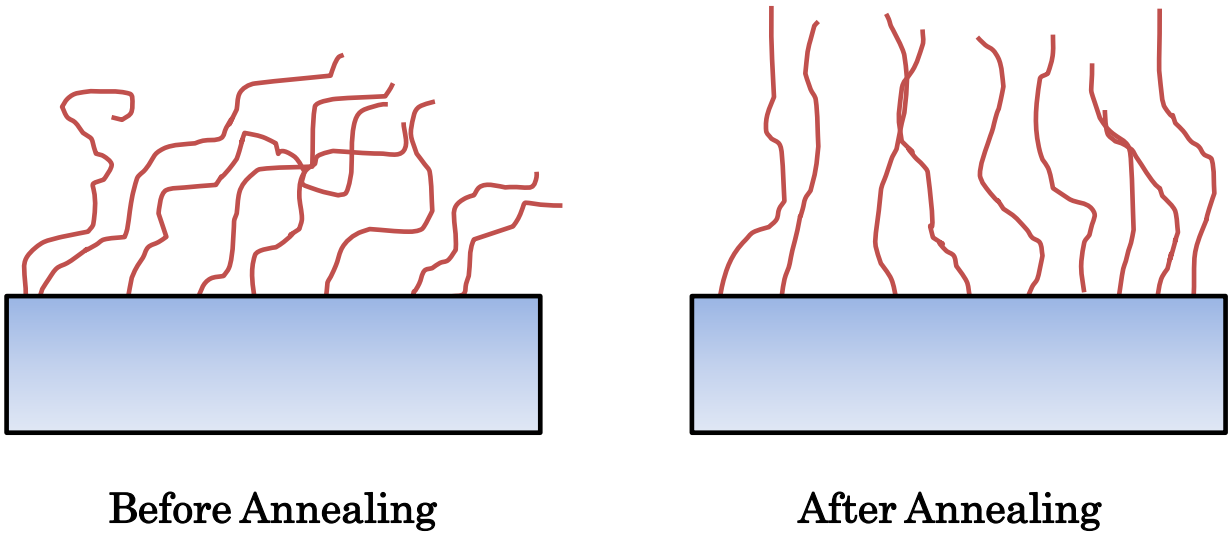

Figure 3-17: P3MT Chains Uncoil and Orient Vertically upon Annealing

In order to meet conditions one and two described above, polymer chains must uncoil and orient vertically when annealed. When polymer chains do this, they necessarily become, on average, more distant from each other.

between chains) and upper bounds as before, but different reasoning, the same conclusion can be drawn. The decrease in film density suggests the average distance between monomer units in the film is larger after annealing. Therefore, the distance between monomers on the same chain and adjacent chains is increasing. For both of these things to occur, polymer chains must adopt a strained, rodlike conformation. That is, for monomers on a single chain to become on average less dense in the film, the chain must uncoil. For monomers on adjacent chains to become more distant, adjacent chains must become more distant as well. The deviation between monomer units from a point immediately above the graft must decrease. In essence, the volume occupied by the chain must increase by increasing the rigidity of the chain with a larger repulsive volume. This will be called **condition three**. Conditions one and three necessitate condition two be met as well, so the exceptionally large increase in film thickness vs. the assumed oriented film is not necessary to determine that polymers are uncoiling. Nevertheless, a model of polymer film morphology with conditions one, two, and three is sketched in fFigure 3-18. When conditions one, two, and three are met, which they are after annealing, the polymer film becomes more ideal.

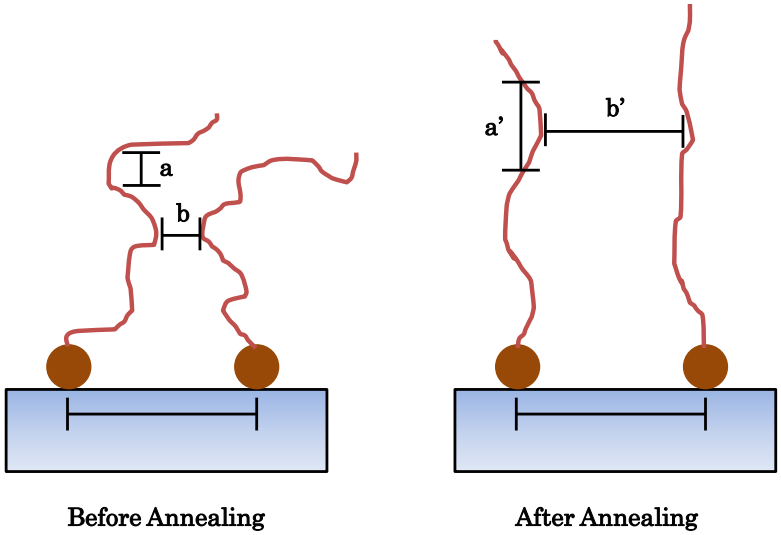

Figure 3-18: P3MT Chains Orienting Vertically, Uncoiling, and Becoming Less Dense

Polymer chains adopt conditions one through three. They are oriented vertically, uncoiled, and less dense. Parameters *a* and *b* are used to signify distance between monomer units on the same and adjacent chains, respectively. After annealing, new parameters *a'* and *b'* measure the same thing as *a* and *b*, but the magnitude of the parameters after annealing is increased.

Using either line of reasoning to explain the global change in film morphology and chain conformation toward the ideal case, fine changes in the chain can be added to the model using the observation that the conjugation length does not change after annealing to create a final condition. The onset of absorption in UV/Vis absorption spectra is used to estimate the optical bandgap P3MT brushes. For P3HT, the onset of absorption for a solution samples is blue shifted approximately 100nm from that of the solid state, implying that films planarize and extend conjugation in the solid state.[68a] In P3MT brushes, the onset of absorption is approximately equal to the extended conjugation onset for P3HT, and after annealing P3MT brushes, onset of absorbance, and therefore the conjugation length

does not significantly change. This suggests that chains as grown have achieved a maximum conjugation length.

Polymer chains are modelled as having rigid segments representing conjugation lengths that are free to rotate at kinked segments at points of connection between conjugated segments. Before annealing, segments are severely kinked consistent with coiled polymers attached to the surface, though the actual chain conformation and morphology is likely not initially so extreme. After annealing, the kinks still exist as evidenced by the unchanging conjugation length, but the angle between segments must decrease. The increase in thickness suggests

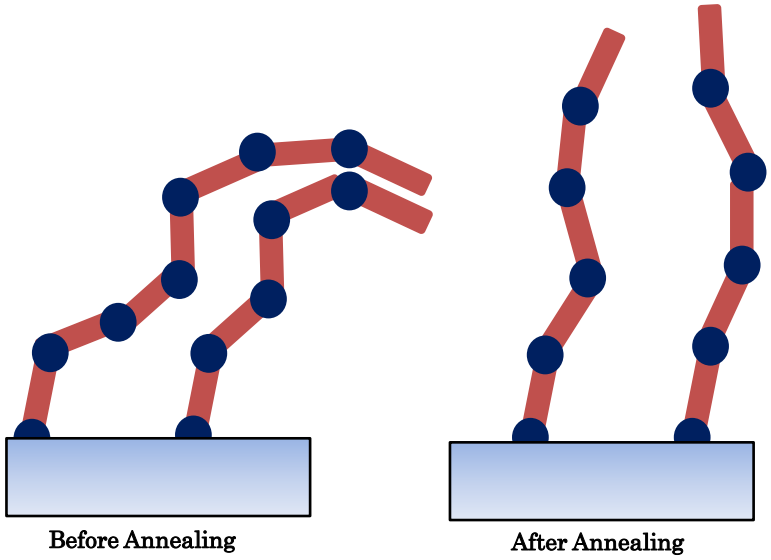

Figure 3-19: P3MT Chains Orienting Vertically, Uncoiling, Becoming Less Dense, and Maintaining Conjugation Length

The chain conformation and morphology is identical when all four conditions are met as it was when the first three were met. The difference achieved by adding the fourth condition is that the increased rodlike structure of the polymer chains after annealing are attributed to planar segments of the conjugated backbone separated by kinks. After annealing, the kinks decrease in severity, along with the changes outlined in the first 3 conditions.

that the polymer chain length is being expressed in the vertical direction to a greater degree after annealing between 60-90° from the surface as outlined by conditions one and two. At this extreme, the angle between conjugated segments approaches zero, but the conjugation length does not increase as evidence by the onset of absorbance. This could be due to the persistence length of the polymer already being reached (keeping the polymer from planarizing) or the kinks between conjugated segments never disappearing. Either way, the final condition of the model is the same: the conjugation length does not increase and the polymer chain does not completely planarize. This means that the ideal film is not made, though all conditions suggest the morphology is approaching that case. The final model of all conditions is sketched in Figure 3-19.

3.9 Experimental Procedures

AFM Profilometry

AFM scans are done with an Asylum MFP3d Atomic Force Microscope. AFM profilometry is accomplished by gently pulling a 20 gauge steel needle across the P3MT brush surface to scratch to the bottom of the ITO. Several scratches are made at different areas of the substrate. Step heights at each area are made and averaged to determine the thickness of the sample.

Polarized Variable Angle UV/Vis Spectroscopy

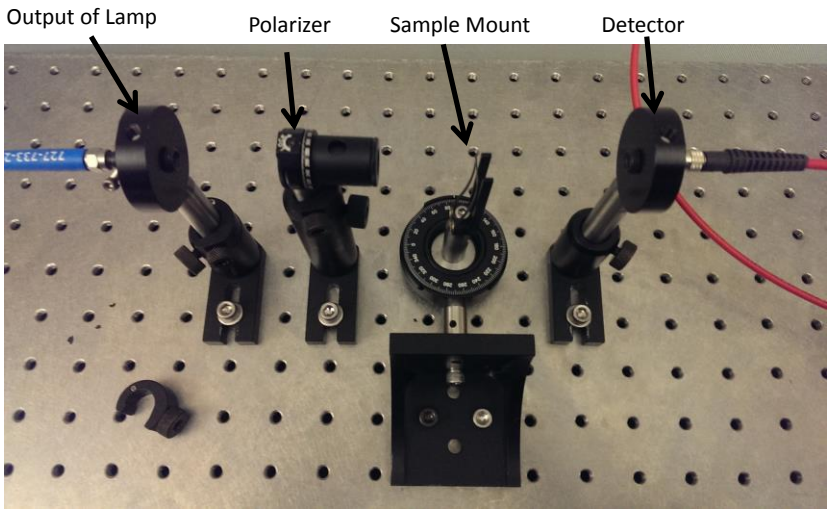

An Ocean Optics 2000 spectrophotometer is used to analyze spectra. A blank ITO slide is mounted in the sample mount, and reference spectra at 0, 30 ,45, and 60 degree angles from normal are taken at S and P polarizations. Each sample is measured in the same way. Four measurements of each polarization and angle are done for each sample so an average and standard deviation in center of mass can be calculated.

Ellipsometry

Ellipsometry measurements are taken with a J.A. Woollam Variable Angle Spectroscopic Ellipsometer. Spectra are measured from 400nm-1600nm at an angle of incidence 70 degrees. Spectra are analyzed and fit with J.A. Woollam WVASE software as described in the body of the text. Fitting for P3MT brushes is done between 700-100 nm so optical absorbance does not interfere with the measurement.

3.10 Supporting Spectra

3.10.1 Normal Incident UV/Vis Absorption

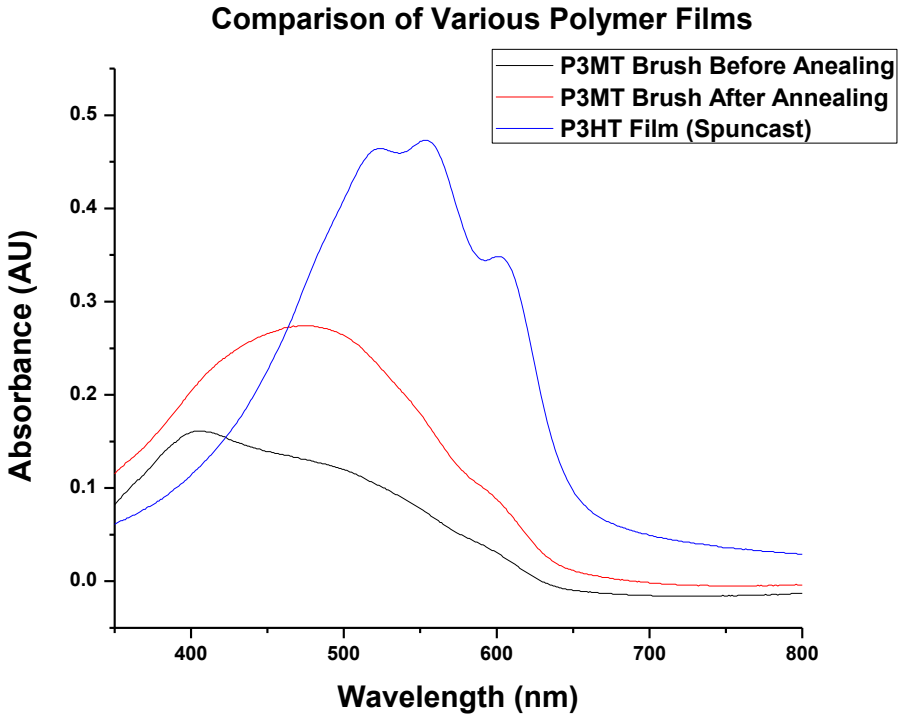

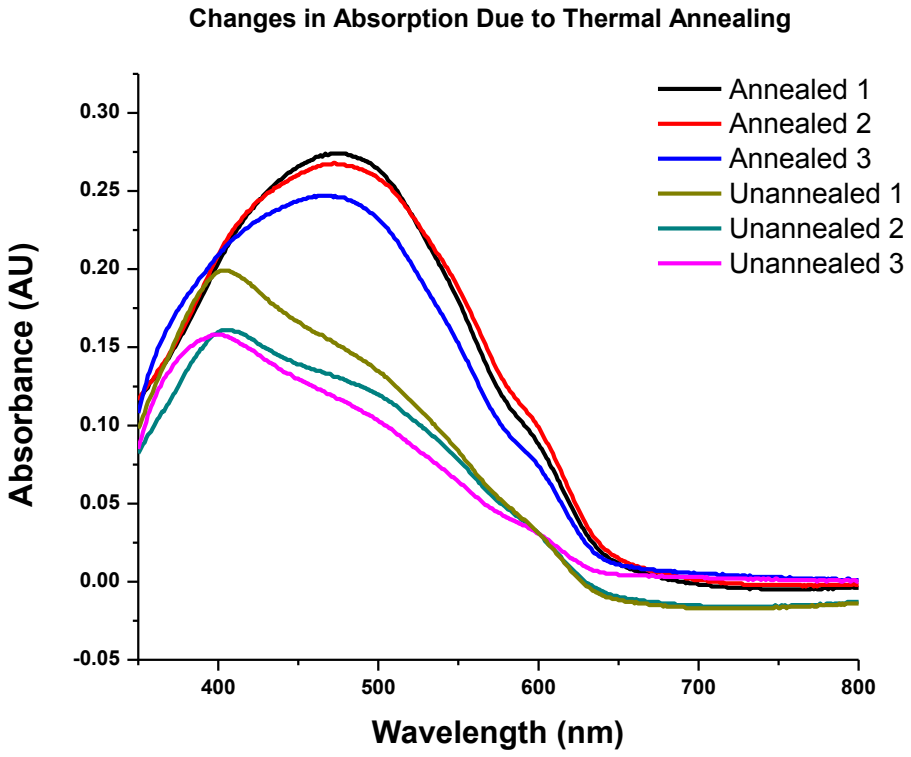

3.10.2 Cyclic Voltammograms

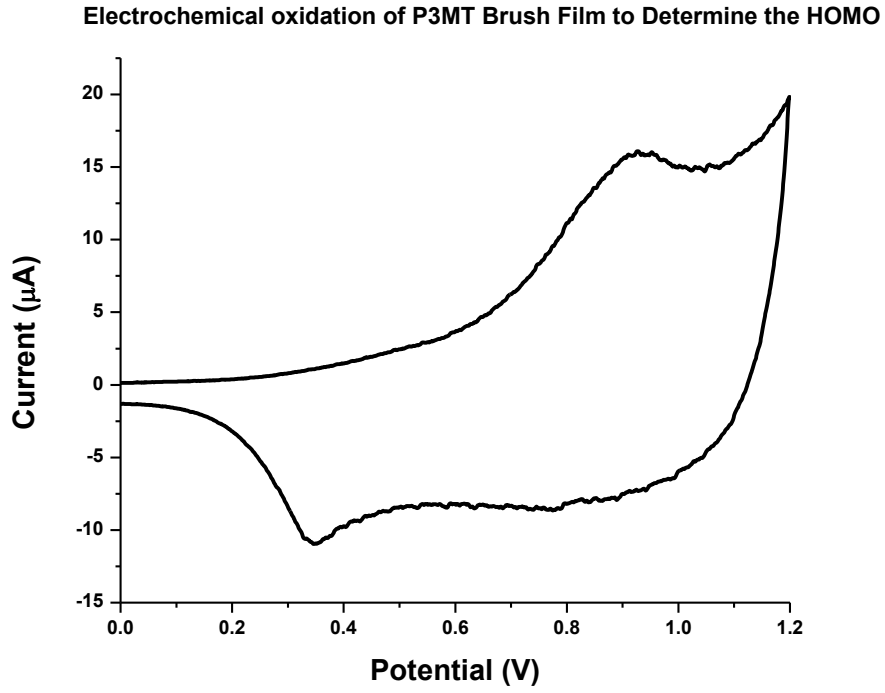

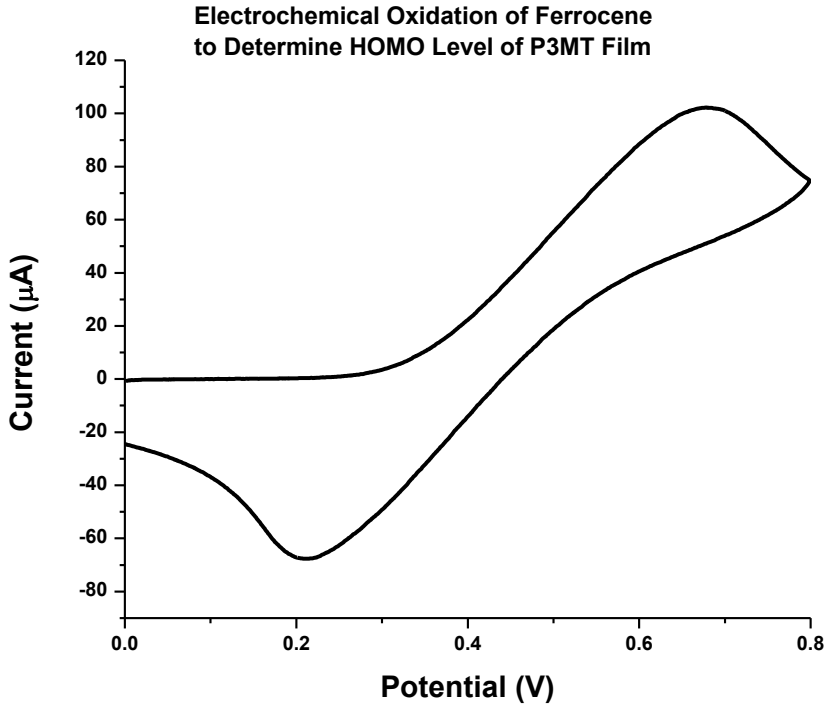

3.10.3 Ellipsometry Models

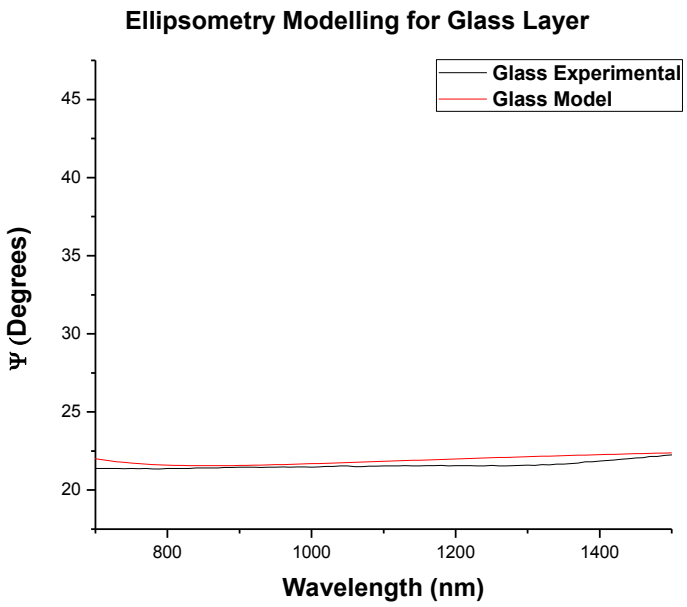

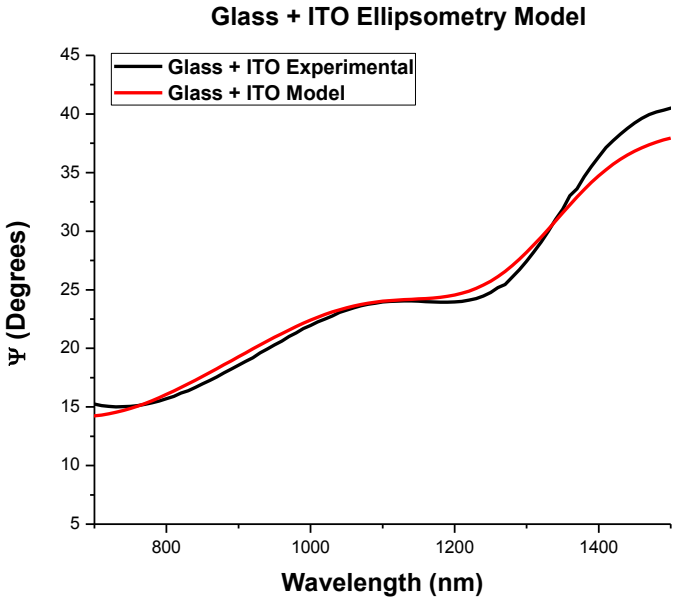

3.10.4 AFM Step Profilometry Measurements

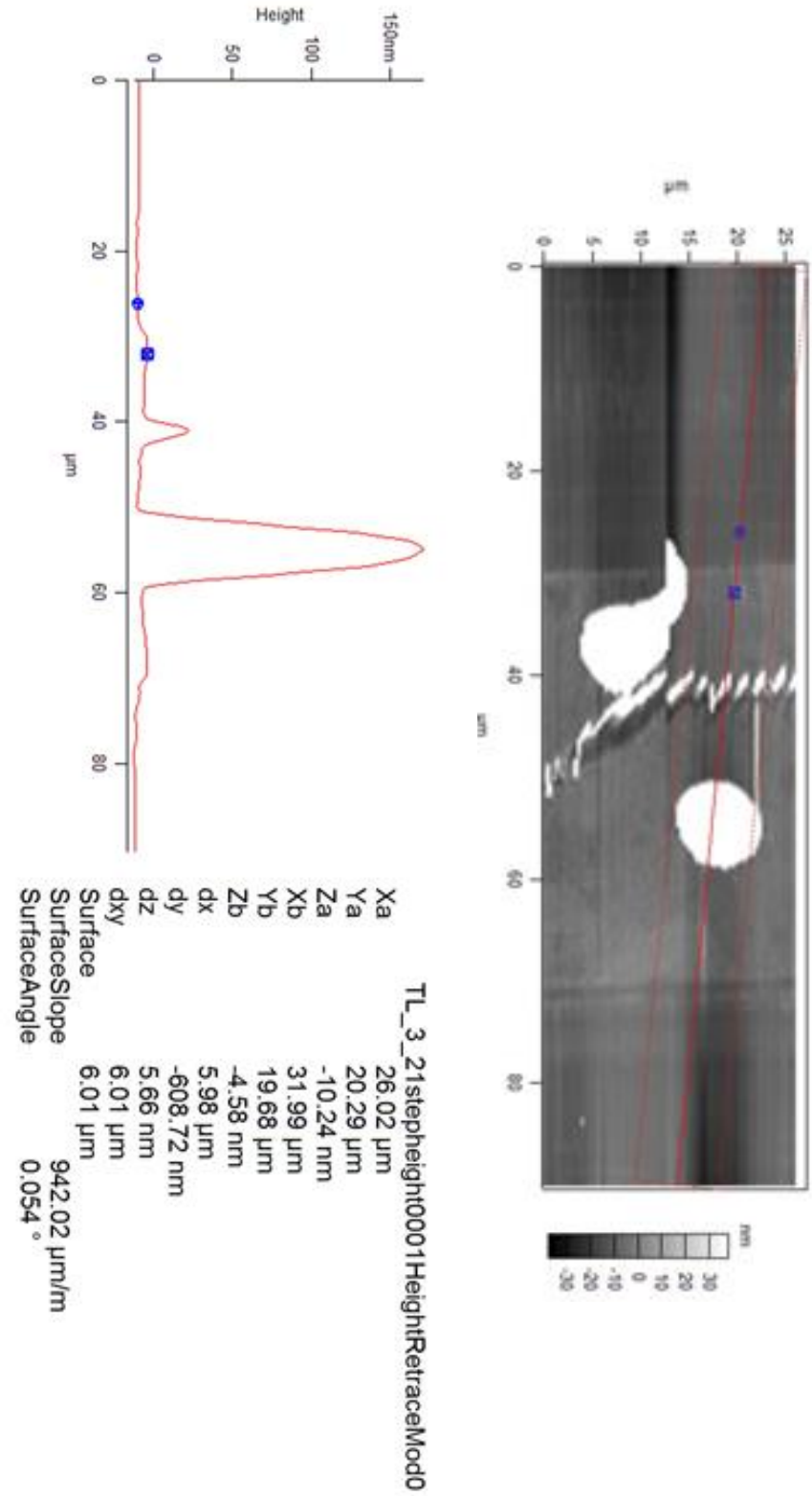

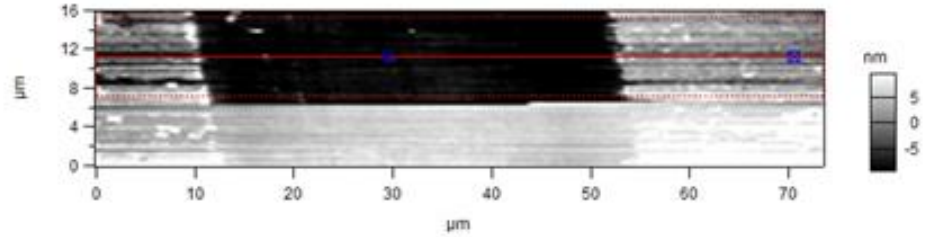

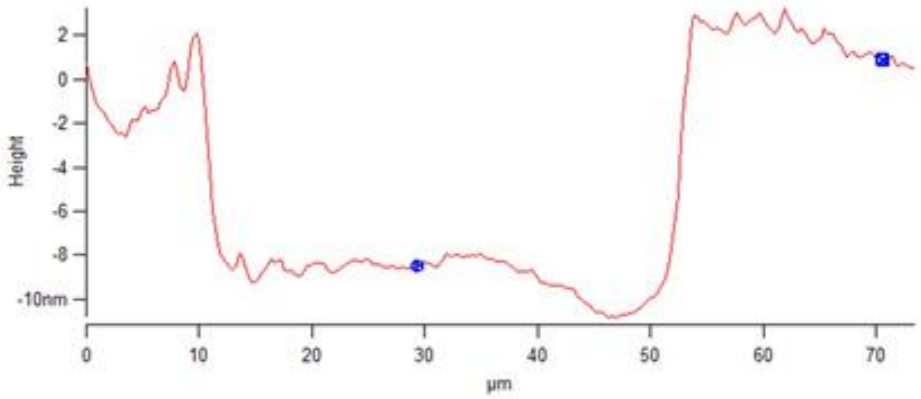

TL_3_33K2Step_Hei0000HeightRetraceMod0

Xa	29.39 µm
Ya	11.24 µm
Za	-8.48 nm
Xb	70.60 µm
Yb	11.24 µm
Zb	898.23 pm
dx	41.21 µm
dy	0.00 m
dz	9.38 nm
dxy	41.21 µm
Surface	41.21 µm
SurfaceSlope	227.67 µm/m
SurfaceAngle	0.013 °

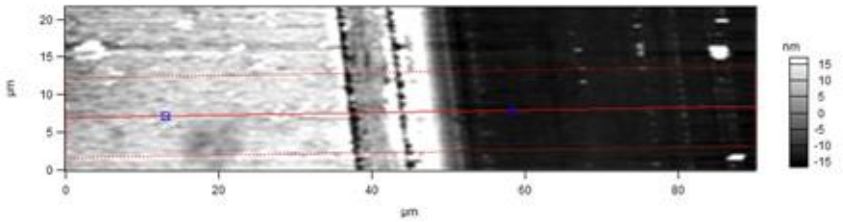

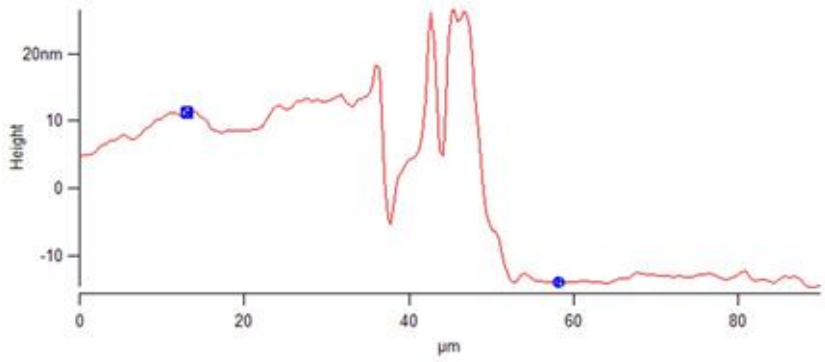

TL__3_56K3StepHei0000HeightRetraceMod0

Xa	58.24 µm
Ya	7.90 µm
Za	-14.04 nm
Xb	13.06 µm
Yb	7.13 µm
Zb	11.13 nm
dx	-45.18 µm
dy	-765.70 nm
dz	25.17 nm
dxy	-45.18 µm
Surface	45.18 µm
SurfaceSlope	-557.11 µm/m
SurfaceAngle	-0.032 °

3.11 SEM Micrograph of P3MT Surface

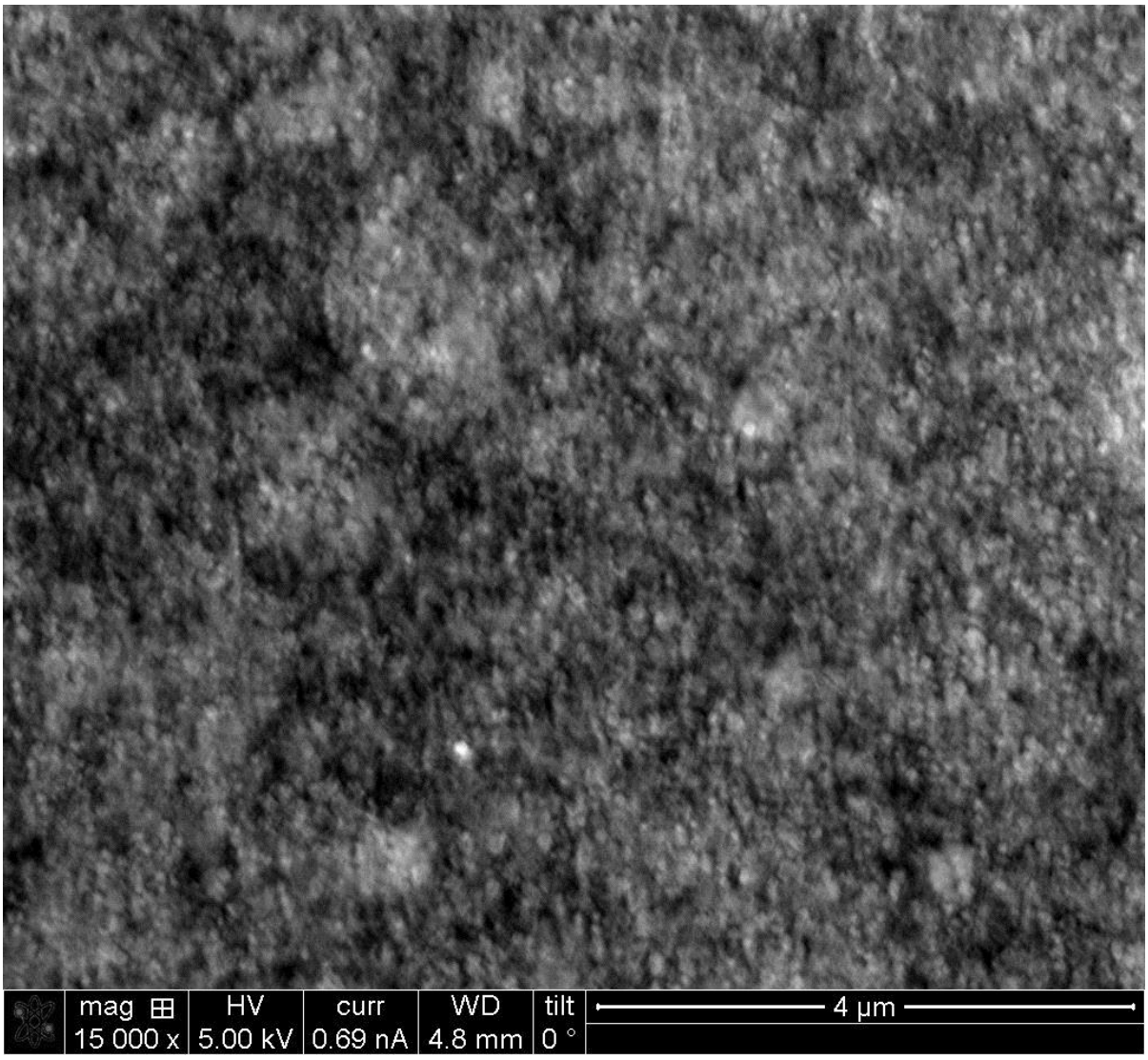

CHAPTER 4 DEVICE FABRICATION AND ELECTRICAL MEASUREMENTS OF POLYMER BRUSH THIN FILMS

4.1 Introduction to Device Design, Electronic Measurements, and Modelling

The goal of this work is to measure intramolecular charge transport along P3MT backbones. To accomplish this, P3MT brush films we synthesized in a controlled manner (Chapter 2) and characterized to understand the film morphology (Chapter 3). Polymers can be grown to a controlled height, and in general there is some vertical orientation and order observed in the films. Annealing the film enhances the vertical orientation to make a more ideal film to measure intramolecular transport. Other reports have made devices with vertically oriented polymers,[31-32] but in each case there were polymer buffer layers between electrodes and vertically oriented polymer, making intermolecular pathways a significant part of the total charge transport pathway. Nonetheless, recent record breaking reports of hole mobility in polymer films are attributed to enhanced intrachain transport.[24-25] In measuring charge transport through P3MT brush films, the goal is not to break an efficiency record but rather to observe an effect on charge transport that can be attributed to charges transporting through chains rather than between them.

4.1.1 Integrating Conjugated Polymer Brushes into Electronic Devices

As described in the introduction, a typical molecular electronic device is a metal-molecule-metal (MMM) junction that can be formed with permanent or temporary contacts. The goal in this work is to create in high yield that can be easily accessed to measure charge transport properties. Five approaches to fabricate devices are explored using three different methods of electrode deposition: nanoTranfer printing (nTP), kinetically controlled transfer printing (KTP), and direct evaporation.

Among these five device designs, there are two methods of testing devices. The first, cAFM, has been used to take measurements of MMM junctions by forming direct contact with molecules to form a device in situ (as described in chapter 1)[39-43] and to make contact to already formed MMM devices where the top contact is transferred on a surface.[49-50] The cAFM will be used in the latter mode, to probe devices made by transfer printing electrodes on to the P3MT brush film. The second method of testing devices involves using a probe station to make a four-terminal or four-point measurement. This method has a distinct advantage over measuring devices with cAFM because the four-point measurement removes the contact resistance and any resistance due to wires and leads. For practical purposes, the four-point measurement requires large, macroscopically addressable contacts that will not short through the P3MT brush film if a probe is pressed onto it. This makes device fabrication exceptionally difficult compared to transfer printing devices to test with cAFM.

4.1.2 Introduction to Measurements, Modelling, and Properties of Interest

All experimental electronic data in this work used to characterize charge transport is taken from measuring IV curves. The IV curves are modelled to determine the conductance and resistance of junctions as well as to compare the charge transport mechanism in films. In molecular electronics, which is the study of transport through single molecular layers, resistance or conductance is usually plotted against molecule length to determine the charge carrier transport efficiency through the film, which is a characteristic property of a material.[40-41, 43, 45-47, 49-50, 78]

Tunneling in molecular junctions is often modelled at low bias using the Simmons model (2),[52] but in this case Simmons may not be useful. Polymers tested here are quite long, out of the length regime typically associated with tunneling.[79] The shape of the IV curve is an odd function similar to a third order polynomial, so curves are modelled using a cubic fit to determine three fitting parameters:

$$\boldsymbol{I = a(V + bV^2 + cV^3) + d} \qquad (11)$$

The cubic fit is used in the *BDR* model, another model used to model tunneling in thin films.[80] For the same reasons the Simmons model is not useful, the BDR model is also not used, so the terms *a, b,* and c do not have the same physical meaning as they do in the case of BDR. If the charge transport mechanism is known, the fitting parameters *a, b,* and c can be given physical meaning, but if it is not, then the values of the fitting parameters can be used mathematically to track changes in the charge transport properties of the film, even if the particular mechanism is not known.

The first order or linear term corresponds to the slope of the IV-curve near zero and is directly related to the conductance of the junction regardless of the transport mechanism. The larger the slope of the first ordered term, the greater the conductance and the smaller the resistance. This is consistent both physically and mathematically for small voltages near zero. Mathematically, a cubic polynomial will be close to linear near zero, and when voltage and current have a linear relationship, the factor relating them is the resistance or conductance. No matter what the transport mechanism is, the region around zero bias will be linear.

The second order or quadratic term corresponds to the asymmetry of an IV curve. Mathematically, a large second order term corresponds to larger asymmetry in the fit, with positive fitting parameters corresponding to curves that have higher currents for positive voltages and negative fitting parameters corresponding to curves that have higher currents when biased negatively. A second order fitting parameter of zero corresponds to a symmetric IV curve. Physically, asymmetry in IV curves for a molecular device can be interpreted as the efficiency of transport through the interfaces. If an IV curve is symmetrical, then charges transport equally well across both of the interfaces.

The third order or cubic fit parameter is determined by the shape of the IV curve, which is dominated by the shape of the curve at high biases. The larger this fit parameter is, the more the curve deviates from linearity. The deviation from linearity of an IV curve for a device is determined by the charge transport

mechanism. At the very least, this term can be used to determine if one IV curve is representing one type of transport or another.

Besides modelling IV curves with a cubic function, the power law relationship between voltage and current can be used to resolve changes in transport as a function of voltage. This has been used in literature to identify different regimes of transport in a given junction using an IV curve,[40, 42] and in conjugated polymer thin films, the power law relationship of several transport mechanisms is known.[81] Using the Mott-Gurney law and the region of an IV curve where the power law is two, the SCLC mobility can be calculated using that region of the IV curve.[82]

4.2 Creating Polymer Brush Devices: Principles and Characterization

As stated in the introduction, five device types are discussed in more detail here. Devices are evaluated using working device yield after fabrication, consistency and reproducibility of fabrication, and throughput of device fabrication. Ideally, devices should be made in high volume with a consistent fabrication method that yields a high percentage of working devices.

4.2.1 Types of Transfer Printing

Transfer printing is a technique that has been used to efficiently deposit electrodes on to thin molecular layers using conditions more mild than evaporation or sputtering.[49-50] The main advantage of transfer printing is that receiving substrates, in this case organic thin films, are not subjected to the harsh conditions that films are normally subjected to during metal evaporation. Instead an

intermediate substrate is used to deposit metals on under harsh conditions so that it can be transferred to a more fragile layer.

Two transfer printing techniques are employed in this study: nTP and KTP. Previous work using nTP has proven it as an efficient technique to create MMM junctions using alkyne thiols, but KTP has not been used to create molecular junctions and has been adapted from transferring etched semiconductor films to transfer metallic electrodes.[83] The principles behind each technique are described below.

4.2.1.1 NanoTransfer Printing

NanoTransfer printing has been used to create small area molecular electronic devices, and the technique has been sufficiently described and characterized elsewhere. Metal films (Au, Ni, and Co have been reported) are deposited on a patterned elastomeric (PFPE) stamp, and the metallated stamp is brought into contact with a thiol terminated SAM (Figure 4-1).[49-50] The stamp is

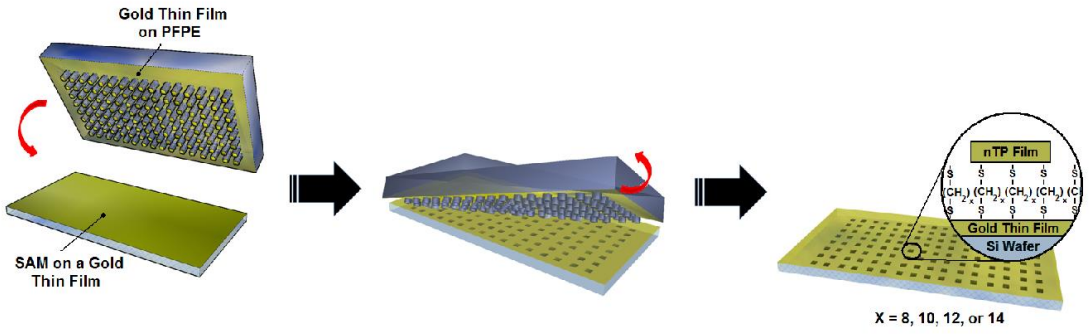

Figure 4-1: Making Electronic Devices by nTP
A patterned PFPE stamp is metallated and brought into contact with a SAM functionalized with a terminal thiol. The thiol bonds to the metal on the raised patterned portions of the stamp, and the stamp is removed, leaving behind a pattern of metallic electrodes. Image copyright its respective owner

removed and the patterned metal film is left behind. The terminal thiol group serves to bind the metal to the surface so the features on the stamp can be completely transferred. For this application, there are no thiol binding groups on the surface, so nTP may not be the optimal technique to use.

4.2.1.2 Kinetically Controlled Transfer Printing

This application of KTP is modified from a procedure reported in literature used to transfer etched inorganic semiconductors.[83] Kinetically controlled transfer

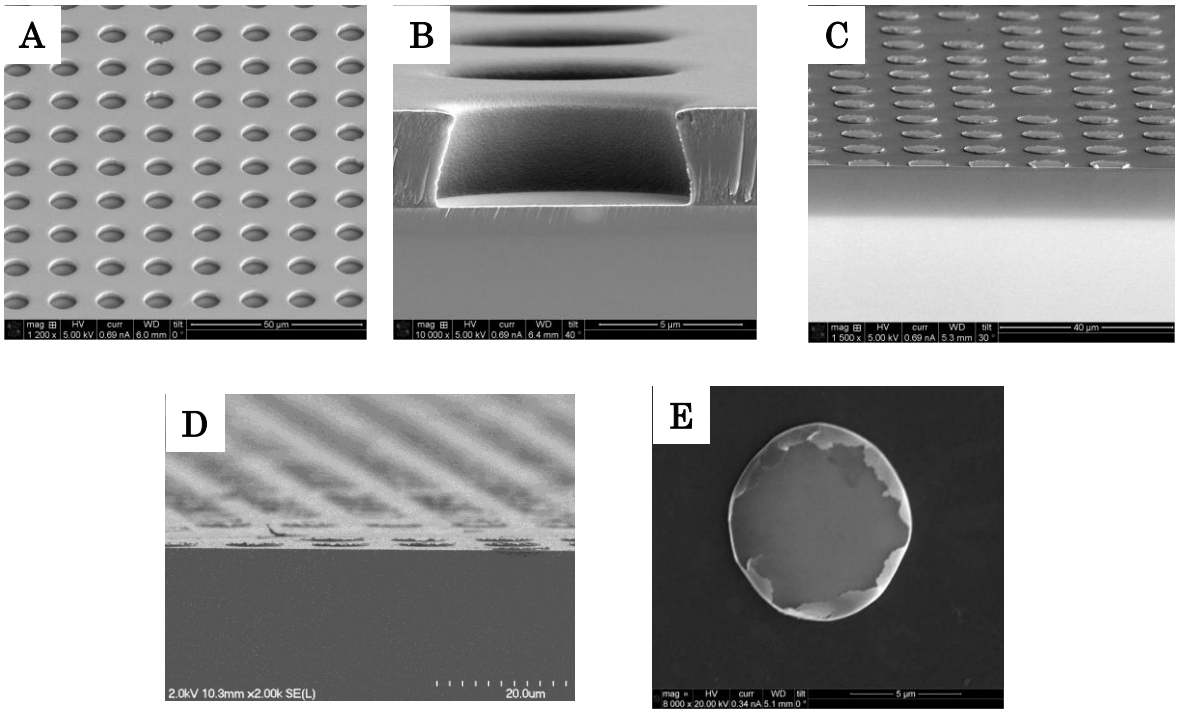

Figure 4-2: Patterning a Donor Substrate for KTP
(A) SiOx wafer patterned with photoresist with a thin (150 nm) layer of Au sputtered to define electrodes.
(B) Cross-section of (A). Despite the undercut in the photoresist, the Au coats the sides of the well.
(C) Tilted SEM of patterned SiOx wafer with removed photoresist. Some Au features fall off during this process.
(D) Tilted SEM of features transferred to a P3MT Brush thin film shows that features make good contact with surface after transfer
(E) SEM Micrograph of a single KTP transferred feature. There are small frills around the edge of the feature. This is an artifact from the Au coating the undercut of the well used to define the feature area.

printing uses the elastic properties of PDMS to induce the transfer of patterned metal thin films from a donor substrate (SiOx) to a receiving substrate (polymer brush surface). To create a donor substrate, a silicon oxide substrate is patterned with photoresist, and Au is evaporated onto the patterned substrate. The photoresist is removed with acetone in a sonication bath, and the wafer is briefly etched with hydrofluoric acid to help detach the gold film from the wafer (Figure 4-2).

The transfer printing process (Figure 4-3) occurs when a PDMS stamp is brought into contact with the etched Au and SiOx surface. The stamp is wetted to

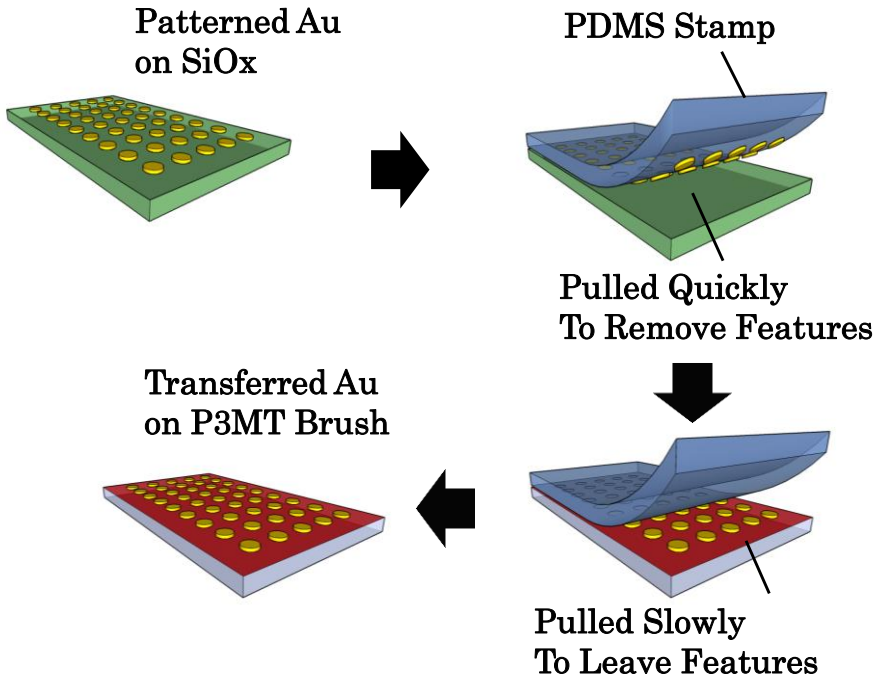

Figure 4-3: Schematic of KTP Transfer

The patterned Au film is lifted off by a flat PDMS stamp by peeling it off quickly to increase the adhesion between stamp and Au. The metallated stamp is brought into contact with the receiving substrate, and peeled slowly to lower the surface energy of the PDMS, leaving the patterned Au film on the receiving substrate.

the surface, and removed quickly. Removing the stamp quickly increases the surface energy of the stamp, inducing transfer of the Au features to the stamp. The metallated stamp is then brought into contact with the polymer brush thin film to wet the surface. The stamp is then removed slowly to reduce the surface energy of the PDMS stamp, to induce transfer from the stamp to the receiving surface. Because of the kinetic component of this transfer,[84] it is not necessary to have a thiolated surface to induce transfer. Also, the Au that is transferred from SiOx to polymer is templated from a SiOx wafer, so the transferred film is quite smooth compared to films transferred with nTP. In contrast, the surface transferred with nTP is defined by the growing surface of an evaporated thin film, so it is not as smooth as the surface used to transfer with KTP. This makes KTP an ideal candidate for transfer printing top electrodes on to fragile organic thin films.

4.2.2 Device Architectures

4.2.2.1 Devices Created by Transfer printing 200 nm Au electrodes via PFPE Assisted nTP

NanoTranfer printed electrodes like this have been used to create MMM junctions on top of alkanedithiol SAMs on Au.[49-50] Out of all of the transfer printing methods, this is the only one that has been proven to work to create devices in literature.[49-50] Unfortunately, no electrodes were able to be transferred using this technique. This is likely because there are no thiol acceptor groups on the polymer chain ends to induce transfer from the PFPE film and the polymer brush surface.

4.2.2.2 Devices Made with Large (50μm) Electrodes Transferred by KTP and Tested by cAFM

Large Area KTP electrodes do not suffer from the disadvantages exhibited by large are nTP electrodes, so are ideal candidates for devices. Electrodes are thick, cohesive units ten times thicker (150-200 nm) than nTP pads (between 15-20 nm), and do not show any signs of cracking, (Figure 4-3).

Electrical measurements are taken by bringing a gold plated cAFM tip into contact with the transfer printed electrode and biasing the tip to drive a current through the junction. Measurements made in this way are slow due to limitations with the AFM, only two to three devices can be measured with one scan. Despite the low throughput, the yield of working devices is high. Approximately 94% of tested devices yield measurable IV curves, with the other 6% being shorted. Shorting most likely occurs due to printed electrodes puckering and penetrating through the polymer film and touching the bottom ITO electrode.

4.2.2.3 Devices made with Large (50 μm) Electrodes Transferred by KTP and Macroscopically Addressed via Fabricated Permanent Contacts

The active junctions in these devices are identical to the previous devices, but instead of measuring the devices with AFM, macroscopic contacts are fabricated on the top of printed devices that can be measured in a probe station. Devices made in this way are even less numerically dense on a substrate. Only four to 6 devices can be made on a single substrate. Furthermore, the device yield is quite low, with less than 20% of devices working after seven continuous days of fabrication. In this case,

most devices are not shorted or working, but open, indicating that the fabricated top electrodes are not making good contact with the printed electrode.

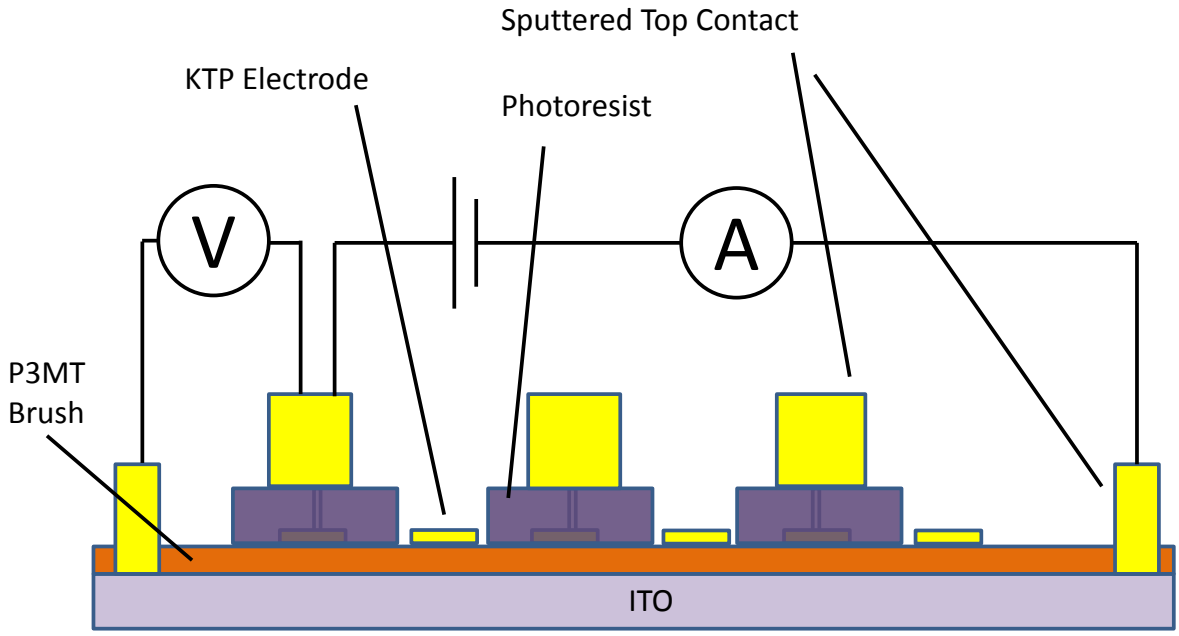

Figure 4-4: Schematic of Large area KTP device with Macroscopically Addressable Contacts
To make this device, photoresist is spuncast on top of a P3MT brush film, then wells are opened over printed electrodes. The photoresist is developed, and Au contacts are sputtered to make contacts for a four-terminal measurement.

4.2.2.4 Devices Made with Small (7μm) Electrodes Transferred by KTP and Tested by cAFM

Devices made in this way combine the advantages of high working device yields of large KTP transferred pads and the numerically dense device transfer of the small 200 nm PFPE devices that could not be transferred on to polymer brush thin films. More than 20 devices can be measured on a single AFM scan, and device yields of 90% working devices, 8% open devices, and 2% shorted devices.

4.2.2.5 Device Made by Directly Evaporating on Top of Polymer Brush Films

Large area devices (0.13 cm^2) are attempted by direct evaporation of metal films on top of polymer brush thin films. Polymer films up to 90 nm are grown, and various metals and oxides including Au, Al, Ag, and MoO_3 are thermally evaporated on top of the thin film. Various rates and powers are used to evaporate the metals, but in every case the top electrode deposition penetrates through the polymer film to the bottom ITO, yielding 0% working devices.

4.2.3 Moving Forward with Devices

Of all device types tested, the best performing, highest throughput motif is printing 7 µm circles via KTP as a top contact and testing by cAFM. Though the larger 50 µm squares have a higher percentage yield of working devices, the 7 µm devices are more numerous on a surface by an order of magnitude, and ten times as many 7 µm circle devices can be measured as 50 µm square devices in a given amount of time. Though the lithography techniques used to create permanent devices on top of 50 µm square devices cannot be used to create devices on 7 µm devices, the yield of devices using photolithography is so low that meaningful data sets would be difficult and time consuming to acquire. Therefore, out of the working device types, only 7 µm KTP printed electrode devices are used to characterize the charge transport in polymer brush thin films.

4.3 Charge Transport through P3MT Brushes

Measuring and analyzing IV curves of P3MT (Figure 4-5) brushes can identify several key charge transport properties and characteristics. The change in

cubic fitting parameters as a function of polymer brush film thickness determines properties of thin films such as the ß value, which describes how easily charges transport through a material, and identify changes in charge transport mechanism at different lengths. Furthermore, the power law dependence of current and voltage can also describe the transport of charges through films and is used to determine the charge carrier mobility.

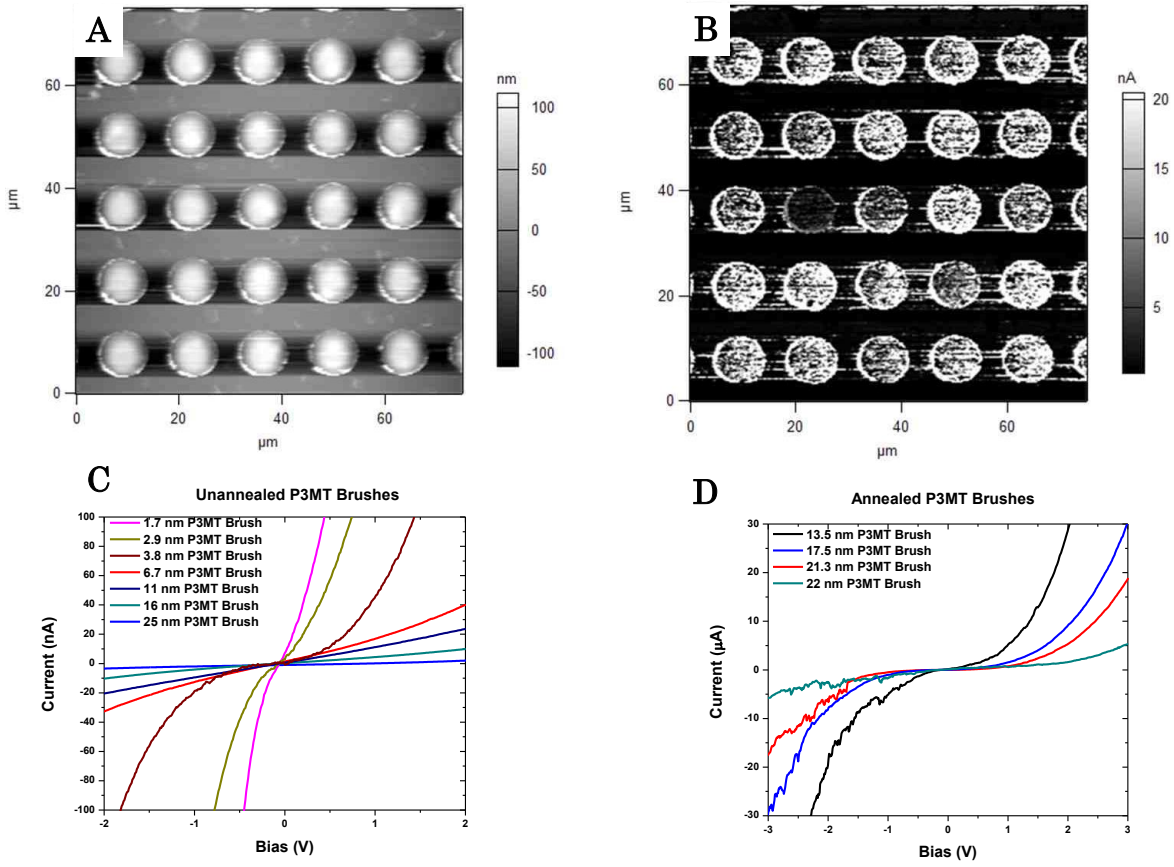

Figure 4-5: Measuring IV-Curves with KTP

(A) Transferred KTP electrodes imaged by AFM during data acquisition.
(B) Current map of KTP taken indicating that current is only measured through transferred electrodes.
(C) Representative IV-curves for good unannealed P3MT films.
(D) Representative IV-curves for annealed P3MT films.

4.3.1 Modelling IV Curves with Cubic Fits

Data are modelled (Figure 4-6) using WaveMetrics IGOR software. Curves are fit to a cubic function between -0.5 V and 0.5 V yielding three polynomial fit

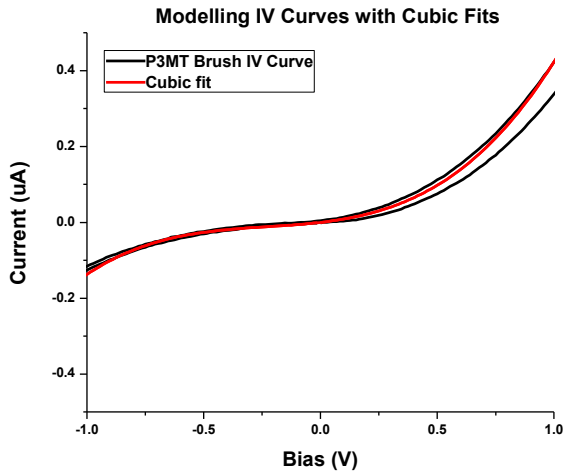

Figure 4-6: Modelling IV Curves with Cubic Fits
Curves are fit with a cubic polynomial between -0.5 V and 0.5 V. The fitted curve agrees with the experimental curve in this range. Typically, there is some deviation in the curves at higher bias.

parameters and a constant for each IV curve. The constant fit parameter is ignored, and the remaining fit parameters are averaged for each device substrate, yielding fit three parameters per P3MT brush length that are used to describe charge transport. Normalized quadratic and cubic terms are used for analysis by diving the raw terms by the linear term.

4.3.1.1 Linear Term: Resistance/Conductance

As discussed earlier, the linear term corresponds with the conductance of the device. The reciprocal of this term is the resistance, and is used in all further

analysis. The resistance is used in two separate pieces of analysis: calculating the relative effective area distribution and the transport decay parameter or ß value.

4.3.1.1.1 Effective Area Distribution of Printed Devices

All samples tested had a similar distribution in linear fitting parameter (Figure 4-7). From a histogram of the linear term for each device tested, the relative area is calculated by normalizing the average to one, and expressing the bins as a multiple of the average. A relative area of one on the graph in Figure 4-7 corresponds to the average area. If the maximum device area (100% effective area) is taken to be the extreme right of the curve, then that means that on average, approximately 33% of the electrode area is contributing to charge transport. This is the upper bound of effective area, because it is unlikely that the extreme right tail

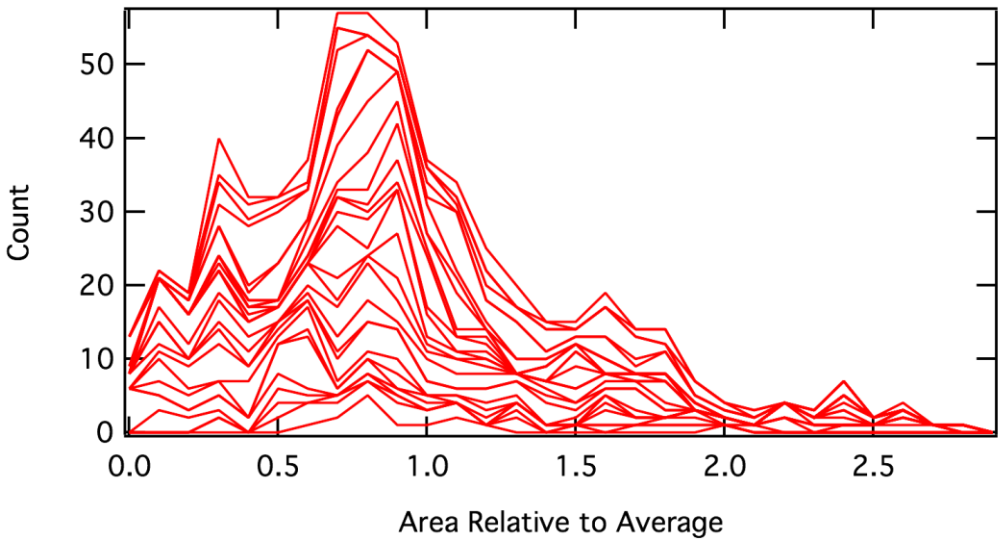

Figure 4-7: Effective Area Distribution of Printed Devices

This distribution is a superposition of relative areas calculations using the distribution of conductances in all samples. Across all samples, the data are similarly distributed, suggesting the quality of prints are similar in all of the samples.

corresponds to 100% effective area. Though this distribution is not ideal, it is very similar for every sample, so films should be equally affected. This is could be due to nanocracking on the underside of the electrode or incomplete contact of the bottom of KTP pads with polymer films. Either way, the distribution of identically shaped IV curves suggests that the other fitting parameters and properties will be affected accordingly.

4.3.1.1.2 Resistance-Length Dependence: Transport/Current Decay Parameter (ß Value)

The resistance is the most sensitive parameter in the fit. To gain an understanding of the relationship between resistance and P3MT brush thickness, only "high quality" devices and IV-curves are used and were chosen based on having smooth surfaces and UV/Vis absorption spectra that suggest films are vertically ordered. As thickness increases, there are two distinct trends in the resistance increase (Figure 4-8). The values calculated for ß are both incredibly low, indicating that charge transport does not decay quickly through the brushes. High ß values are associated with processes transport processes that have resistances that have large exponential dependences on length, like tunneling through large tunneling barriers. Processes that have little or no exponential dependence, like charge hopping, usually have low ß values. The magnitude of ß cannot be used to diagnose the charge transport mechanism, but taken with no physical context it can be used to describe transport as being conductive or resistive. To put these ß values in perspective, one of the lowest ß values reported, observed in highly conjugated,

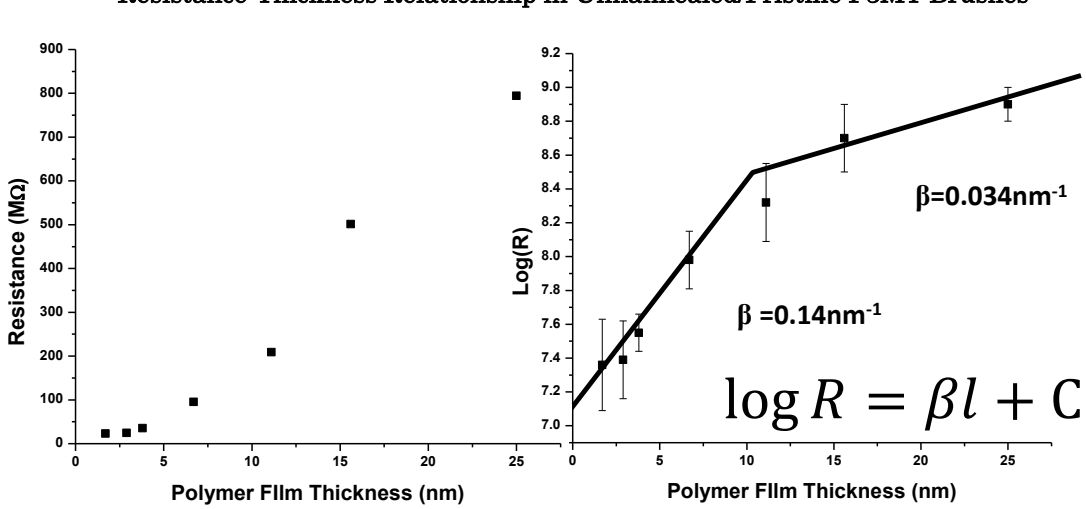

Figure 4-8: Resistance-Thickness Relationship in P3MT Brushes
(Left) Raw plot of resistance verse P3MT film shows what looks like geometric growth in the resistance as film thickness increases. This is possibly either an exponential growth followed by linear growth or two or more regimes of linear growth.
(Right) Semilog plot of resistance vs film thickness implies there are two separate regimes for increase in the logarithm of resistance. This behavior has been attributed to a change from a hopping regime to a tunneling regime, but can also represent a change in the number of hops to cross a junction.

conductive organometallic wires, ranges between 0.28-0.01 nm^{-1} depending on electrodes.[78c] These β values (Figure 4-8) are on par with the lowest reported.

4.3.1.2 Normalized Quadratic Term: Asymmetry

The quadratic term in the cubic fit is determined by the asymmetry of an IV-curve, with positive and negative terms corresponding to higher currents in positive and negative bias directions, respectively. A value of zero for this term indicates that the transport is perfectly symmetrical. Since the modelling is done close to zero bias, this term only captures the behavior within that range.

In nearly every device tested at every length, the quadratic term is a near zero and positive (Figure 4-9). In fact, nearly every normalized quadratic term is within one standard deviation from zero, indicating that the transport through

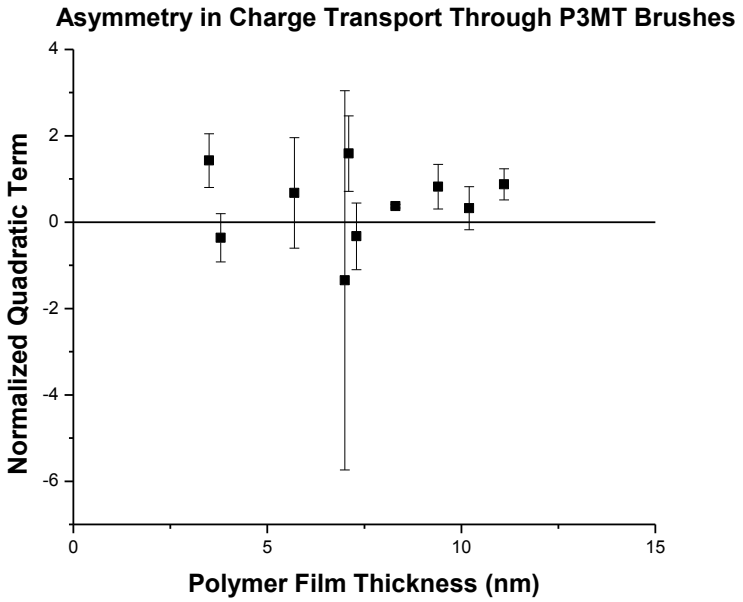

Figure 4-9: Asymmetry in Charge Transport Through P3MT Brushes

The normalized quadratic term is used as a measure of asymmetry of charge transport through devices. The values of the quadratic term are unchanging with length. Values are nearly all small, and positive, indicating currents are slightly higher in the positive bias. For the values that are less than zero, the standard deviations are quite large, overlapping with zero in each case. This term corresponds to "b" in equation 11.

these devices is quite symmetrical at low bias. This is neither trivial nor intuitive. The electrodes are two different materials, ITO and Au, and the contact between electrodes is different, covalently attached with phosphonic acid to ITO and physically adsorbed to Au. Measuring the work function of phosphonic acid monolayers on ITO by UPS show that the work function of this surface is 4.9 eV, which is quite close to the literature value of Au in vacuum of 5.1 eV.[85] A measured work function for Au near the P3MT surface could not be obtained due to the surface being obscured beneath 200 nm of Au. Nonetheless, this estimate can be used to propose that the difference in Fermi level of the two electrodes will not cause asymmetry in the IV curve. This also means that the phosphonic acid

monolayer used to graft polymers to the ITO surface is not preferentially transporting charges across the ITO-polymer interface compared to the physical polymer-Au interface. There is no length dependence on the normalized quadratic term, suggesting that this behavior is true for all lengths of polymer.

4.3.1.3 Cubic Term: Deviation from Linearity

The normalized cubic term would be expected to deviate significantly between samples if the mode of charge transport were to change. This is not observed, however, and the normalized cubic term of devices of all length is the same within error (Figure 4-10). This suggests that charges are transported by identical methods regardless of length. This is in contrast to the behavior observed with the linear fit parameter in the charge transport decay plot. Without knowing the charge transport method through the film, it is difficult to interpret this difference, but for similar organic molecules, temperature activated charge hopping has been proposed as the charge transport mechanism. If this is the case, increasing the number of discreet hops to get across the junction will cause a decrease in the ß value, but it will not change the charge transport mechanism. The deviation of the ß value at longer lengths coupled with the constant value of the normalized cubic fit suggests that this could be occurring. It is also important to note, that as in the case with the quadratic term, the cubic term is modelled only around zero bias, so this does not take into account deviations at larger voltages.

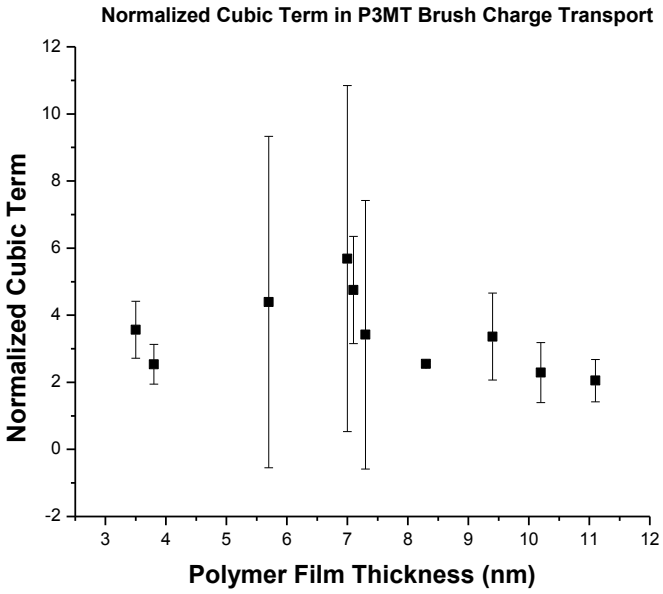

Figure 4-10: Cubic Fit Parameter in P3MT Brush Charge Transport

Cubic fit parameters (term c in equation 11), are nearly identical within error in all P3MT thicknesses. This is most likely due to charges transporting by identical mechanism regardless of film thickness.

4.3.2 Power Laws of Charge Transport in P3MT Brush Films

Rather than using polynomial fits to determine characteristic parameters of IV curves, log-log plots can be used to determine the power law relationship between current and voltage. This relationship between current and voltage can be used to determine changes in the charge transport mechanism in a single device at different applied biases. This analysis has been done in several literature reports to determine transitions between charge transport types in molecular junctions.[40, 42,]

Transport in polymer brush junctions as grown follow very similar power law progressions regardless of film thickness (Figure 4-11). The similar power law progression for all film thicknesses is in agreement with the trend observed in the

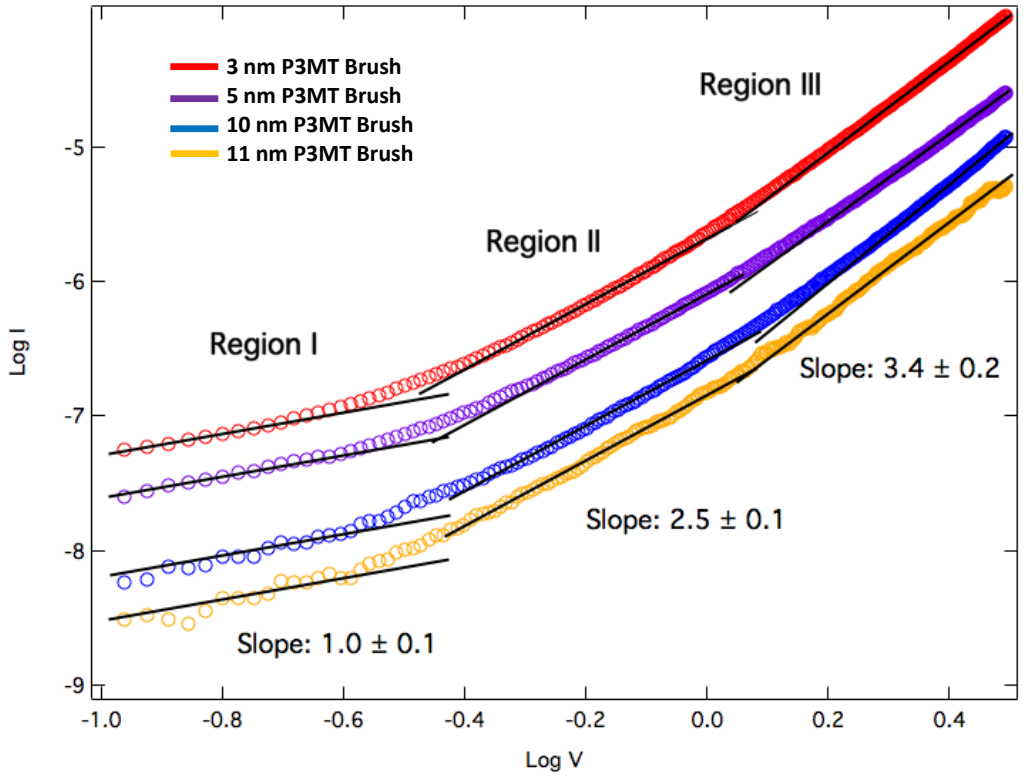

Figure 4-11: Log-Log IV Curves

Regardless of polymer thickness, the slopes of the log-log plots are the same at the same points on the IV-curve. This suggests that transport in the brushes is similar.

normalized cubic fitting parameter that the charge transport mechanism is the same in films regardless of the thickness. The cubic fitting parameter comes from only a small region near zero bias, so the log-log plot provides better evidence that charge transport is similar between samples. Though these two pieces of evidence come from the same source, the IV curve, it is significant because the analyses are sensitive to different behaviors. The IV curve best approximates a cubic function near zero, so changes in that cubic behavior due to differences in the charge transport mechanism would show up in the fitting parameters. Changes in the behavior at higher behavior, when the IV curve is not as well represented by a cubic fit, is well represented by the log-log plot.

4.3.2.1 SCLC Mobility from Mott-Gurney Law

The Mott-Gurney law is used to calculate the mobility in P3MT thin films. The Mott-Gurney Law:

$$J = \frac{9\epsilon\mu V_a^2}{8L^3} \tag{12}$$

The region of the IV curve with a power law equal to two can be extracted from the log-log plot by finding the portion of the graph with slope of two. This region is known to correspond to space charge limited transport in polymer thin films, and the SCLC mobility is calculated from this portion of the IV curve.[81] Dividing the current by the area to obtain current density and plotting against the square of voltage should yield a linear plot of which the slope can be used to calculate mobility μ. Nonetheless, the average mobility observed in unannealed P3MT brush films is

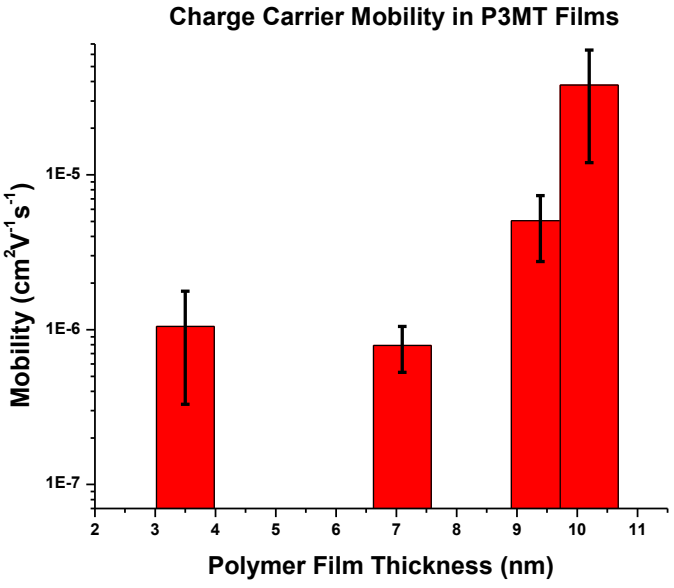

Figure 4-12: SCLC Mobility in Unannealed P3MT Brushes

SCLC Mobilities in unannealed P3MT Brushes are similar to those reported in literature. There may be a thickness dependence on mobility.

on the same order of magnitude as other films of P3MT, indicating that this is most likely a good measure of SCLC (Figure 4-12).

4.3.3 Charge Transport through annealed P3MT Brushes

Annealed P3MT brushes are characterized in electronic devices using the same methods as unannealed brushes.

4.3.3.1 Film Thickness-Resistance Relationship for Annealed Brushes

In films measured previously, the logarithm of resistance increased linearly with device thickness in two regimes representing a clear relationship between the resistance and film thickness. However, in this set of films, no such relationship is observed. This is due to careful selection of films used in the previous study. Only high quality films were used in the previous study. In this study, however, four

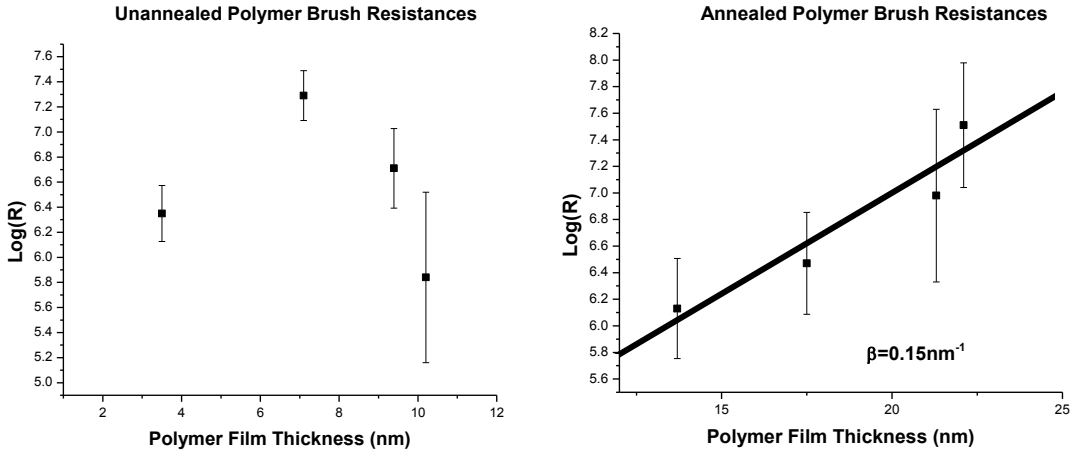

Figure 4-13: P3MT Thickness-Resistance Plots for Annealed Films

Before annealing, the polymer brushes have no trend in resistance with regards to length. After annealing, however, a clear trend emerges and the ß value from the carefully selected P3MT films is recovered. This implies that annealing films may recover "good" charge transport behavior in films with poor morphology.

films were chosen regardless of quality and electrodes were printed on top. IV curves were measured and the films were annealed (Figure 4-13). New electrodes were put on top of the films after annealing to achieve the known distribution in active device areas. After annealing, the film may make better contact with printed electrodes, causing artificially high currents through devices. After the new electrodes were printed, IV curves were measured for the newly annealed films. After annealing, a linear increase in the resistance with respect to film thickness is observed. The ß value is approximately the same as that observed in the first portion of the slope in the previous graph, suggesting that annealing is able to recover electronic properties of films of poor quality. The ß value of 0.15 nm^{-1} in the annealed films is observed for much longer brushes than in the pristine films.

4.3.3.2 Normalized Quadratic and Cubic Fitting Parameters in Annealed P3MT Brush Devices

In addition to the linear fitting terms of annealed films being in agreement with trends observed in unannealed films, the normalized quadratic and cubic terms fit into the distribution of normalized higher order terms for unannealed films (Figure 4-14). These terms suggest that the nature of the contacts and charge transport mechanism does not change after annealing, Though this can only be concluded for the region near zero bias.

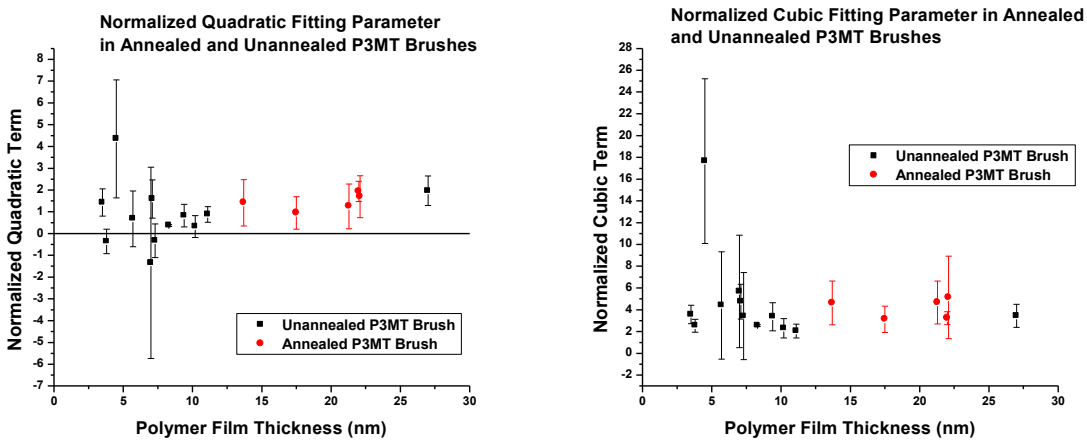

Figure 4-14: Normalized Quadratic and Cubic Fitting Parameters in Annealed P3MT Brushes

Normalized Quadratic and Cubic fitting parameters fit do not change after annealing. This implies that the charge transport mode does not change, either.

4.3.3.3 Power Law of Charge Transport and SCLC Mobility in Annealed P3MT Thin Films

The log-log IV curve plot reveals behavior that is not observed by comparing the fitting parameters (Figure 4-15). The slope of the power law at low bias is less than one at biases below 100 mV, indicating that there is a different mode of transport at low bias. Since the cubic fitting term is not as sensitive to behavior at lower biases as higher biases, this change would not show up using cubic fitting.

The charge carrier mobility increases after annealing in every case tested (Figure 4-15). The greatest increase was seen in the initially thinnest film and the smallest increase in the initially thickest film, though there is no systematic dependence on initial film thickness or change in film thickness on the change in mobility. The mobility values are still within reason for good P3AT films and are within one order of magnitude of reports of films with oriented P3AT chains.[32]

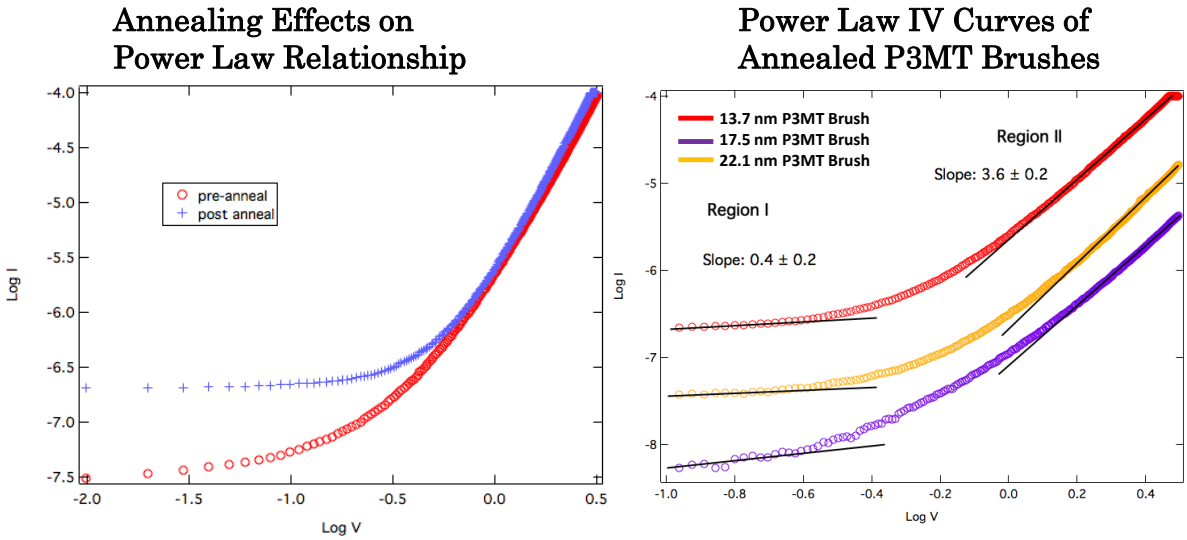

Figure 4-16: Power Law IV Curves for Annealed P3MT Brushes

(Left) For a single sample, the power law behavior before and after annealing is significantly different at low bias, but the same behavior is retained at high bias. This implies that transport is changing at low bias but remains the same at higher biases.
(Right) All annealed samples show similar behavior to the annealed power law curve on the left. This implies that there is some universal change in charge transport after annealing.

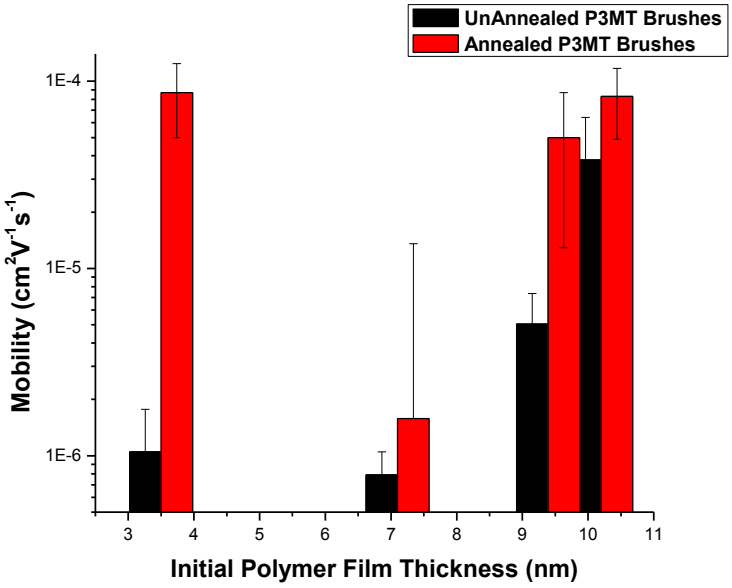

Figure 4-15: Charge Carrier Mobility in Annealed P3MT Films

After annealing, mobility universally increases. The largest and smallest increase in mobility are for the shortest and longest initial polymer length respectively. In the extreme case, a 100x increase in mobility is observed.

4.4 Modelling the Junction with Measured HOMO Levels and Bandgaps

The relevant energy levels of the P3MT brush junction are diagrammed in Figure 4-17. The HOMO level of P3MT is nearly aligned with both the ITO electrode and Au electrode. This corresponds to a very low barrier of injection for holes into P3MT brushes, but a high barrier for electron injection. This means that charge carriers in these systems are most likely holes.

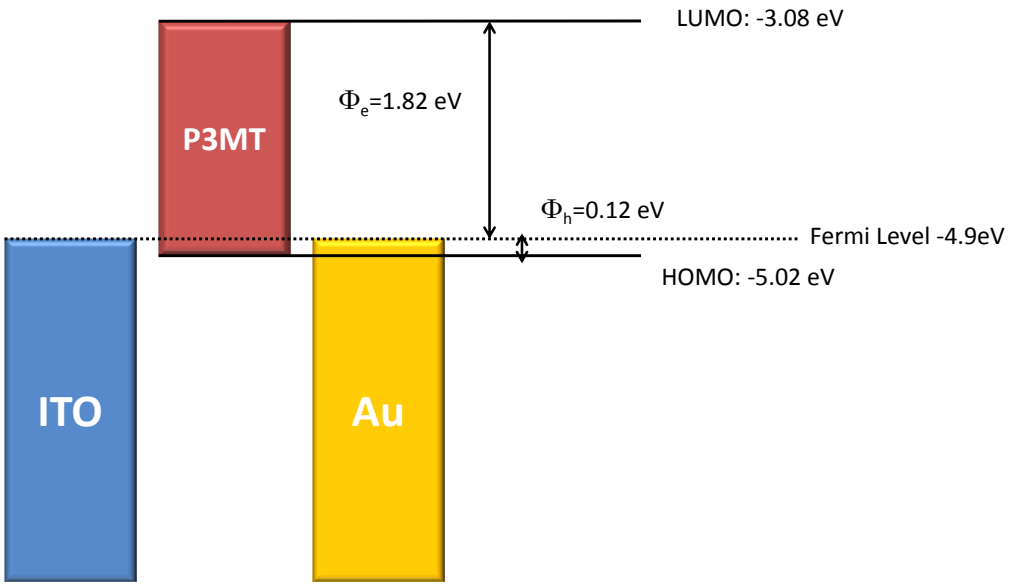

Figure 4-17: Band Level Diagram of P3MT Charge Transport Junction
The Fermi level is taken to be the work function of the ITO measured by UPS (-4.9 eV). The literature work function for Au approximately -5.1 eV, but the Fermi level is likely to change somewhat based on interaction with the P3MT and ITO. The injection barrier for holes is much smaller than that of electrons. It is likely that the primary charge carrier in these devices is holes rather than electrons.

4.5 Discussion

A novel method for creating molecular electronic devices utilizing KTP was developed to test charge transport properties through P3MT polymer brushes. Out of all device types attempted, KTP was the only one that could be used to test devices in high volume to create data sets that can be statistically analyzed to characterize charge transport through P3MT brushes.

High quality P3MT brush films exhibit very low ß values when put into devices, indicating that charges transport very efficiently through the conjugated polymer. The ß values for P3MT brushes is among the lowest ever reported, similar to other conjugated molecular systems.[78c] The low ß values of the as grown films could be due to several factors. First, the barrier to inject holes into the HOMO from either direction is quite low. The difference in energy is approximately 0.1 eV in either case. In tunneling devices, small tunneling barriers are associated with low ß values. The mechanism of transport here is likely not tunneling due to the thickness of the P3MT films, but the barrier could still play an important role in transporting charges. Furthermore, the normalized cubic and quadratic terms are constant with regard to polymer film thickness. The quadratic term implies that transport is nearly symmetric at low bias, and that it is consistently, slightly favored in the forward bias direction as evidenced by the positive sign of the fitting parameter. The cubic term is more difficult to interpret. This term also does not change, implying charges transport the same way no matter the thickness of the P3MT layer, but no physical meaning can be extracted.

More evidence regarding how charges are transported is taken from the log-log plot. At every tested length, the power law between current and voltage is the same in unannealed films. This is better evidence that the transport is not changing because the log-log plot is sensitive to the whole IV curve, not just a portion near zero. The SCLC charge carrier mobility is calculated using the Mott-Gurney law in P3MT films as grown by modelling portions of the IV curve where the power law is two, and values are similar to those reported in literature for other P3MT films.[81] Mobility and resistance are the only terms to depend explicitly on device area. Resistance is assumed to decrease with larger top electrode size (assuming constant current density, increasing the electrode size should increase the current), but mobility is calculated from the current density. Since it is known that the effective device area is much less than the printed device in many cases, the actual mobility is likely much higher than that which is calculated by as much as a factor of 3 based on the effective area.

As discussed in chapter 3, P3MT brush films can be annealed to enhance chain conformation and film morphology towards a more ideal system. Charge transport properties also seemed to change in some ways after annealing. Unannealed films used to calculate the ß value were carefully chosen so only the highest quality films were included in the study, but to study annealing four films were chosen without prejudice. Before annealing, the films' resistance did not exhibit any systematic dependence on length, but after annealing the behavior observed in good films was recovered. The unannealed ß value of 0.14 nm^{-1} for short

chains was reproduced in annealed films exhibiting a ß value of 0.15 nm^{-1}. Though these numbers are nearly the same magnitude, the P3MT film thickness used to calculate the ß value for annealed films are much longer than those in unannealed films. The same film thicknesses for unannealed films yield a ß value of 0.034 nm^{-1}. In literature reports, this has been attributed to a change in the charge transport mechanism from tunneling to charge hopping.[40,44] The charge transport mechanism here is likely not tunneling due to the low ß value of 0.14 nm^{-1} corresponding to a marginal resistance that is very weakly exponential. This ß value is also reproduced in annealed films with charge transport distances too long for tunneling to make physical sense. Furthermore, all attempts at modelling the IV-curves with tunneling models failed.

There is another possible explanation for this occurrence. Though ß is directly physically interpreted as a current decay or marginal resistance, even if the charge transport mechanism is not tunneling, the physical mechanism giving rise to different ß values can be interpreted in many ways. If the charge transport mechanism is tunneling, ß directly corresponds to the exponential term in the Simmons equation (2). For charge hopping, which is a series of activated tunneling events,[86] the ß value can be related to the number of "hops" through a junction. For a single hop which is identical to tunneling, the effective decay would be ß. As the number of hops increases, the length of each hop decreases, and the expression for resistance needs (5) to be adjusted accordingly. For an *n* step hopping process, the expression for resistance would be:

$$R = nR_0 e^{\frac{\beta l}{n}} \quad (13)$$

The new effective decay factor is ß/n. For n=1, the original behavior in equation (5) is recovered. Using charge hopping as the mechanism to interpret the ß values observed in unannealed films suggests that after a certain point (approximately 10 nm) the number of hops must increase for charges to transport across the film. The transition in ß is not observed at this transport length for annealed films, though a similar transition could be present at greater thicknesses. Interpreting ß as an effective value based on the number of hops an electron must make, it follows that fewer hopping events must occur for charge carriers to transfer across a film. This interpretation is consistent with the model for polymer morphology described in chapter 3, which stated after annealing, the vertical orientation of polymer chains and average spacing between monomers in adjacent chains increases. The larger distance between monomers on adjacent chains decreases the probability that charge carriers will transport between chains.

The log-log current-voltage relationship also suggests changes in charge transport after annealing films, but only at low bias (e.g less than 100 mV). At high bias, the power laws in annealed and unannealed films are identical, but at low bias annealed films behave significantly differently. For annealed films, the power law decreases, suggesting that at low bias there is a difference in the charge transport in thin films. Current-Voltage dependences less than one are sometimes associated with diffusion currents in organic semiconductors.[87] In order to determine if this is indeed the case, more experiments must be conducted to determine the nature of

the device contacts (ohmic vs nonohmic) and more fitting must be done to verify this model makes physical sense.

Using the morphological model of P3MT films from chapter 3, the effects being measured due to annealing are from increasing orientation of polymer chains with lower chances of charges hopping between polymer chains. The conditions used to model the change in film morphology and chain conformation necessitate chains elongate, orient vertically, and occupy more volume. As a result, charges that transfer along the backbone of two identical chains will travel different distances for the same number of hops, with charges in annealed films traversing a larger distance. Furthermore, since the chains are farther apart after annealing, the

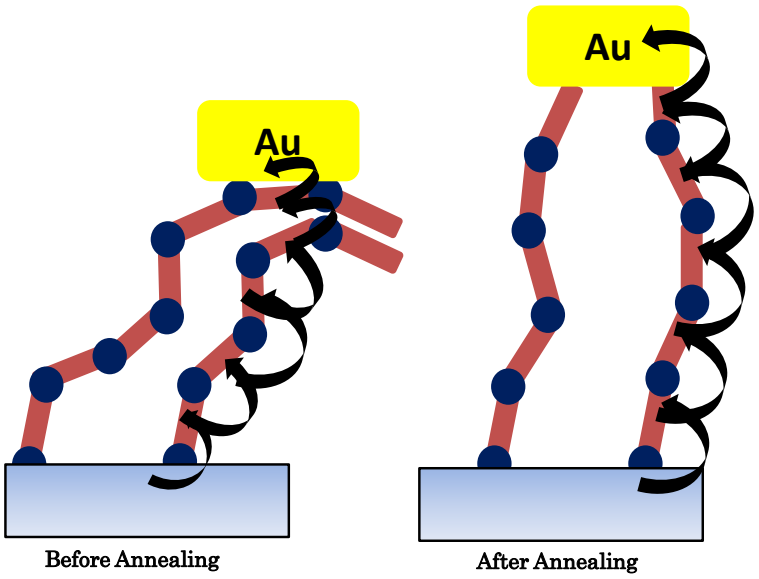

Figure 4-18: Possible Charge Transport Pathways in P3MT Brush Films

In the model developed in chapter 3, the annealed films are comparatively more uncoiled, further apart, and vertically oriented. These are all important features of the model when describing the possible difference between charges transporting through the films. When chains orient vertically and become uncoiled, the charges that transport exclusively along the backbone will travel a longer distance in few hops. Furthermore, when chains are further apart, the likelihood of interchain hopping is reduced.

likelihood of charges transferring between chains is larger, as well. In Figure 4-18, this is represented diagrammatically. In reality, the situation is likely much more complicated, but using the model made in chapter 3, it is reasonable to conclude that the enhancement in mobility and recovery of good charge transport properties after annealing is due to charges transferring primarily along the backbones of P3MT chains.

4.6 Experimental Procedures

Kinetically Controlled Transfer Printing

Silicon Oxide wafers are cut to size and cleaned in RCA solution (1:2:2 Water: H_2O_2: Ammonium Hydroxide) for 30 minutes, washed with copious water and ethanol, then cleaned with ozone for 30 minutes, then the surface is modified with HMDS. In a cleanroom, the following steps are taken: substrates are spuncast with JSR-NFR negative resist at 3000RPM for 30 s and prebaked at 95 °C for 90s on a hotplate, exposed for 10s, postbaked at 95 °C for 90 s, then developed for 3 minutes. Slides are rinsed with water and dried with nitrogen. A thin film of Au (200nm) is sputtered at 2Å/s using a KJL PVD 75. Outside the cleanroom, the photoresist is lifted by washing with acetone, sonicating to help if necessary. Inside the cleanroom, substrates are etched with 5% HF for 5s, washed with copious amounts of water, and dried. (Warning: HF is a major health hazard. Do not use this unless you are wearing the proper PPE, taking proper precautions, and using the proper procedures.) Outside the cleanroom, thick (1 cm) PDMS stamps are prepared by mixing 1:3.5 crosslinker:polymer (Sylgard), removing bubbles by vacuum, and curing at 70 °C overnight. Stamps are cut to size, mounted glass slides with double sided tape, brought into contact with etched surfaces, and ripped off quickly by flipping the glass slide. The metallated stamp is removed from the slide, and brought into contact with a cleaned (MeOH wash, dried with nitrogen) P3MT brush film and the stamp is left to wet the surface for ~1-2 minutes. After the stamp has

thoroughly wet the surface, it is slowly peeled back to transfer the metal to the P3MT surface.

SEM and AFM Micrographs of Au films transferred via KTP Indicating No Micro/Nanocracking and High Volume Transfer

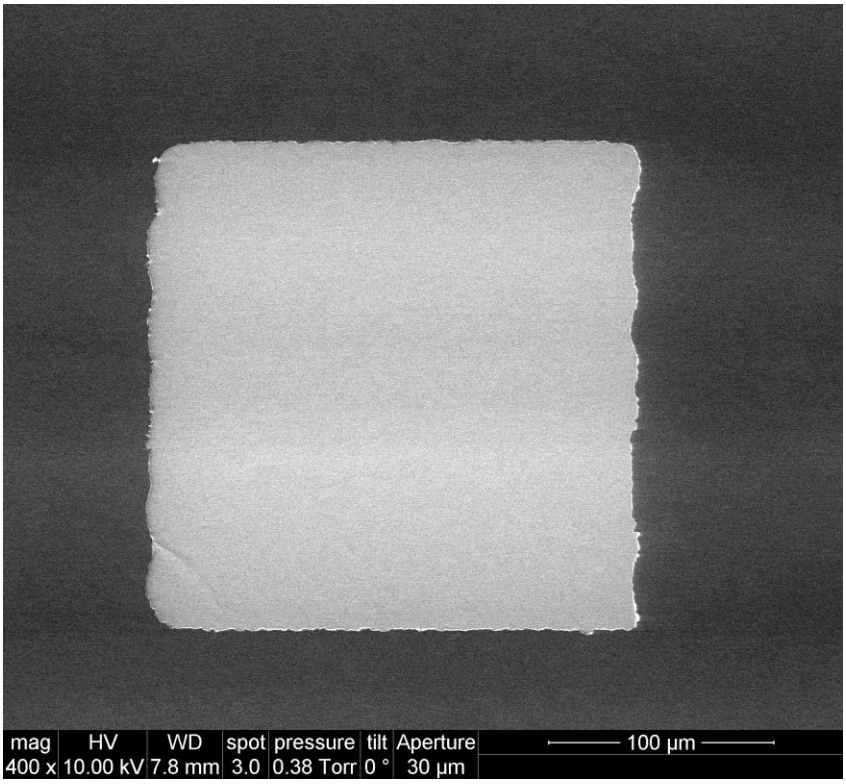

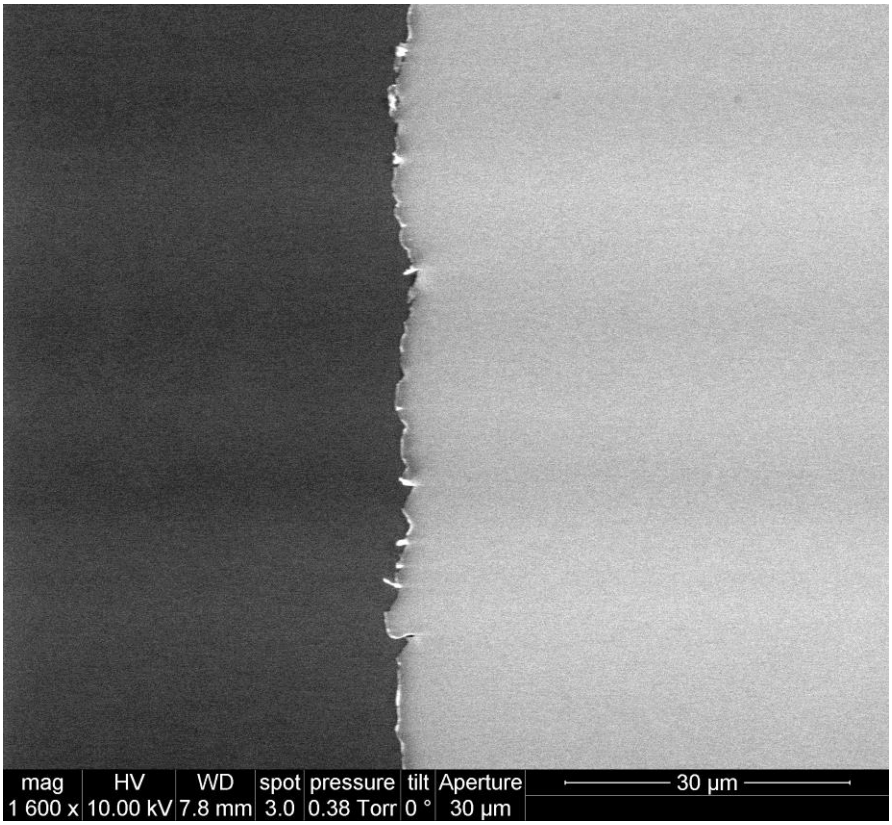
mag
1 600 x
HV
10.00 kV
WD
7.8 mm
spot
3.0
pressure
0.38 Torr
tilt
0 °
Aperture
30 µm
30 µm

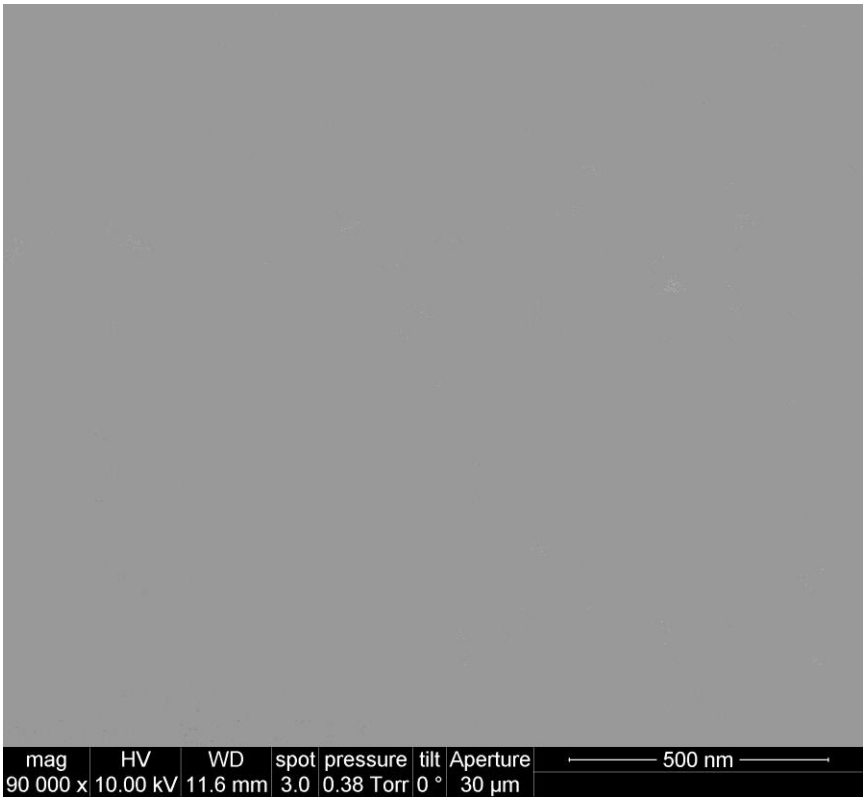
mag
90 000 x
HV
10.00 kV
WD
11.6 mm
spot
3.0
pressure
0.38 Torr
tilt
0 °
Aperture
30 µm
500 nm

7 μm Au electrode transferred by nTP

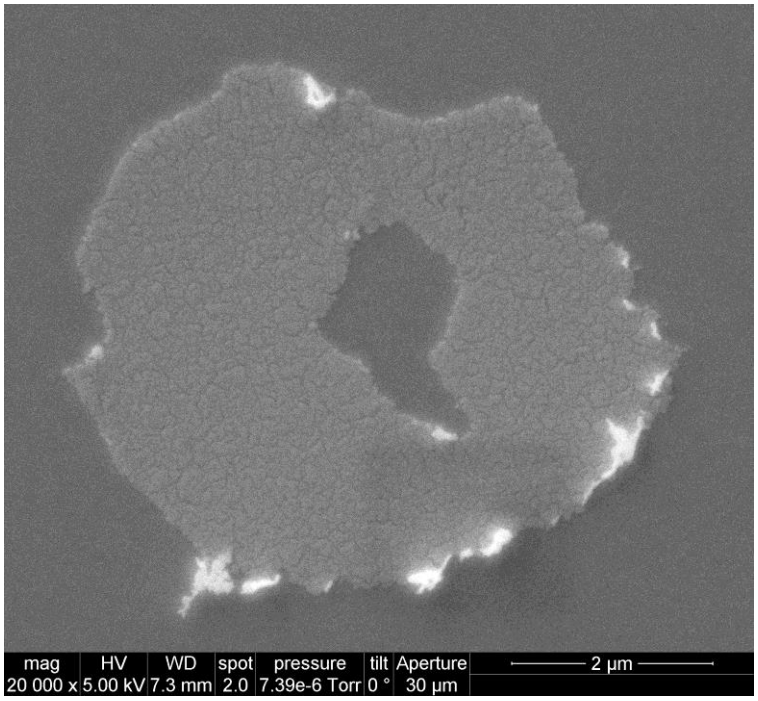

7 μm Au electrode transferred by KTP

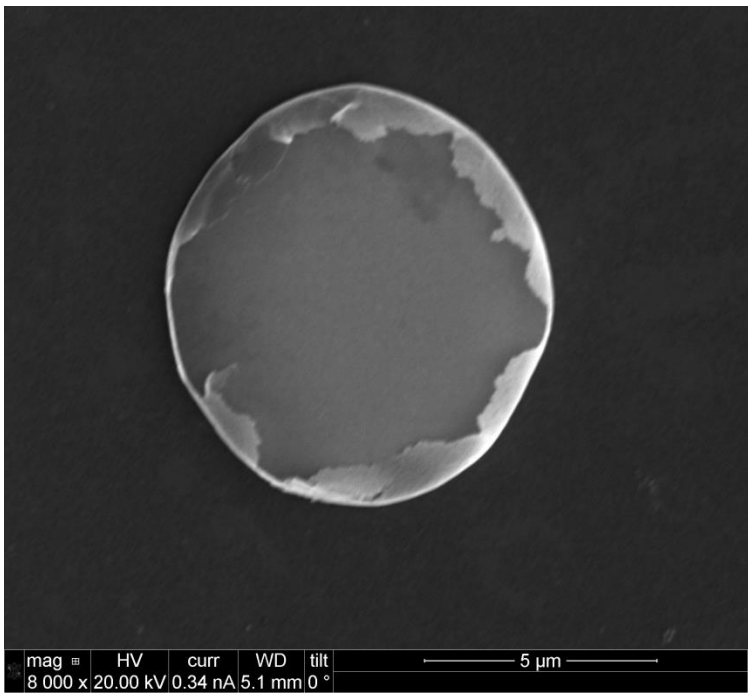

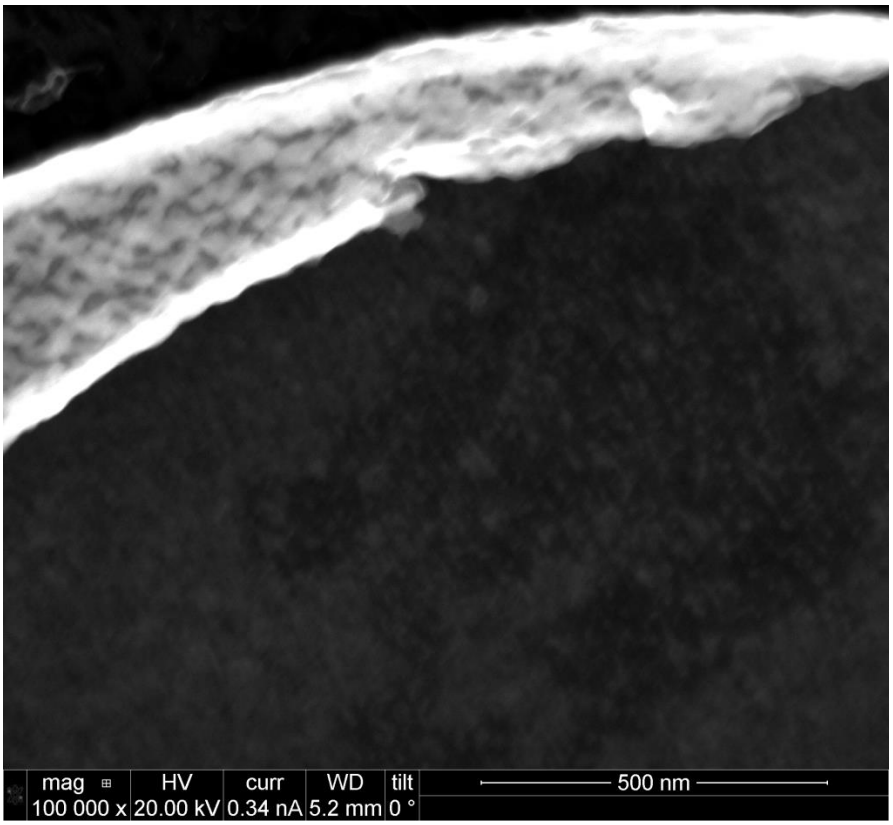
mag
HV
curr
WD
tilt
100 000 x
20.00 kV
0.34 nA
5.2 mm
0 °
500 nm

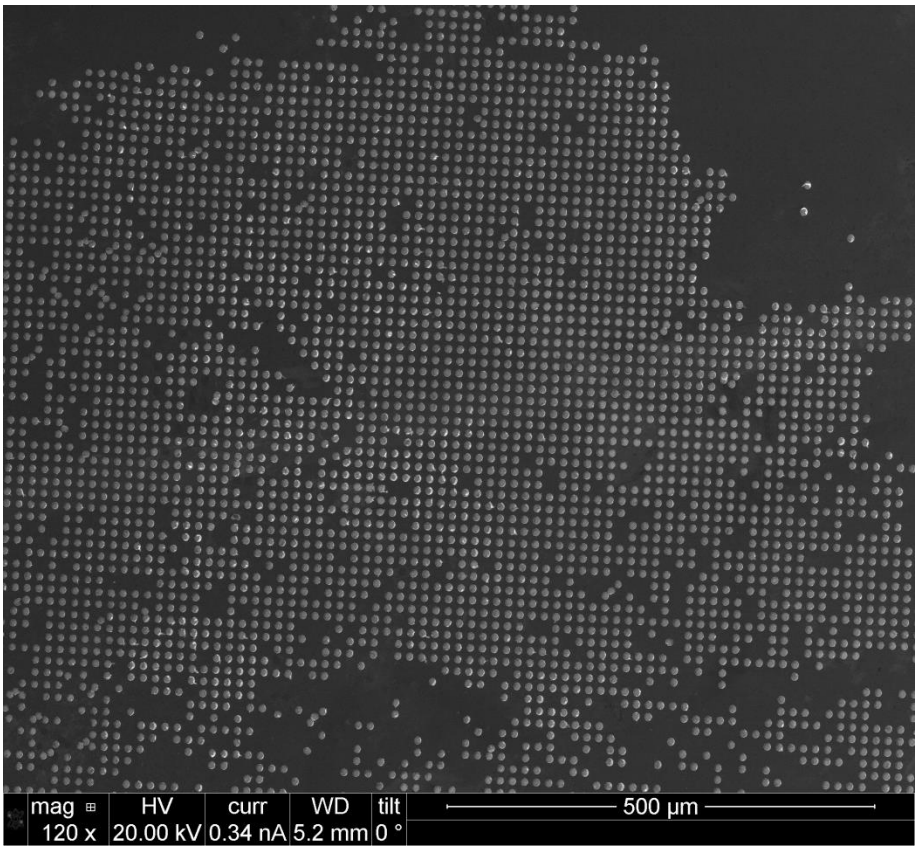
mag
HV
curr
WD
tilt
120 x
20.00 kV
0.34 nA
5.2 mm
0 °
500 µm

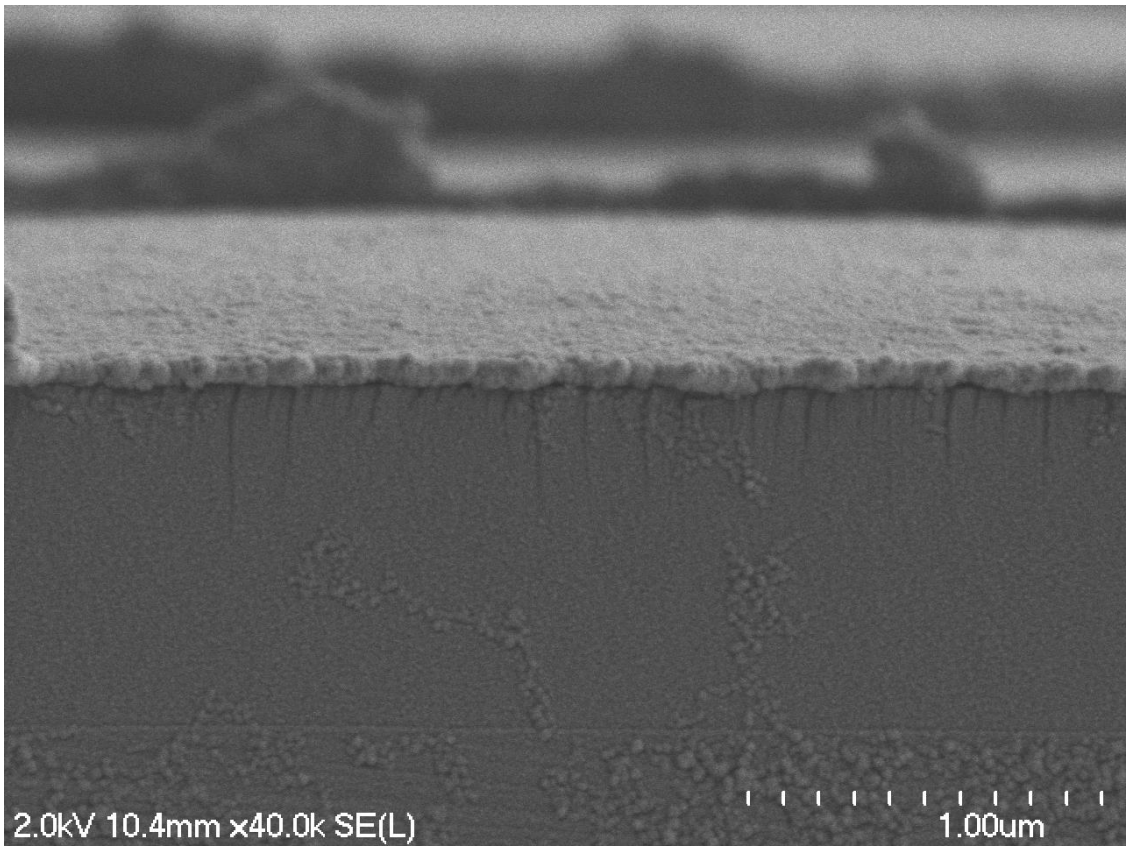
2.0kV 10.4mm x40.0k SE(L)
1.00um

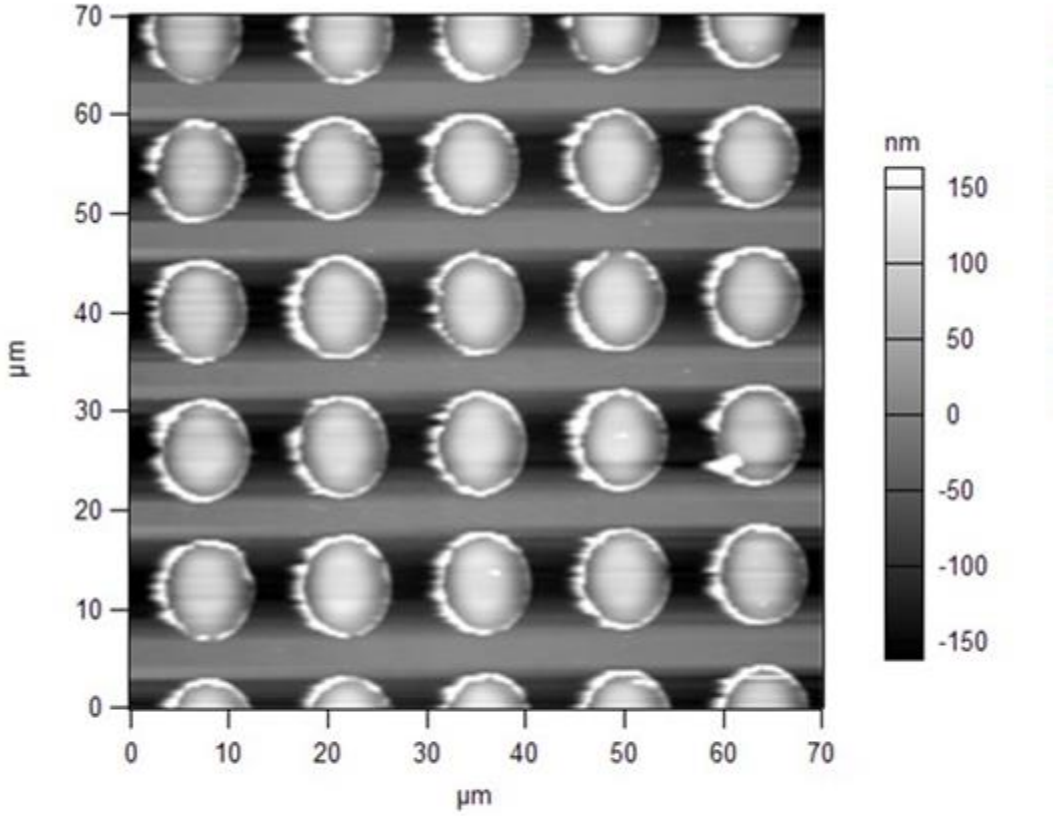
70
60
50
40
30
20
10
0
µm
0
10
20
30
40
50
60
70
µm
nm
150
100
50
0
-50
-100
-150

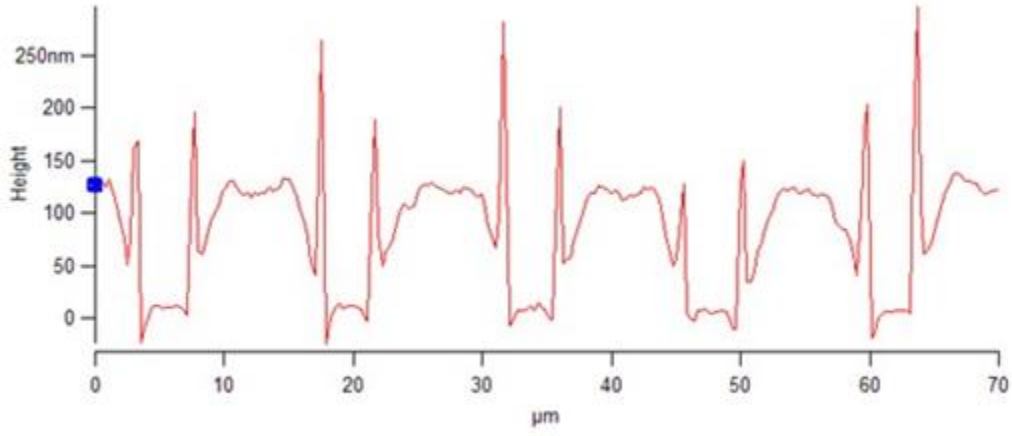
250nm
200
150
100
50
0
Height
0
10
20
30
40
50
60
70
µm

Measuring IV-Curves with cAFM

A wire is attached between the ITO surface and the electronics inside of an Asylum MFP3D AFM. A large area (90μm) tapping mode surface scan is taken of a region of the polymer brush thin film to find the printed features using a gold plated AFM probe. The AFM is then turned to contact mode and the probe is located over the features and feedback is turned on. The set point is increased from 0.2 V to make contact between the tip and the printed electrode at lowest set point potential. The tip is then biased to drive current through the device and the IV curve is measured in WaveMetrics IGOR software provided by Asylum.

4.7 Supporting IV-Curves and Distributions

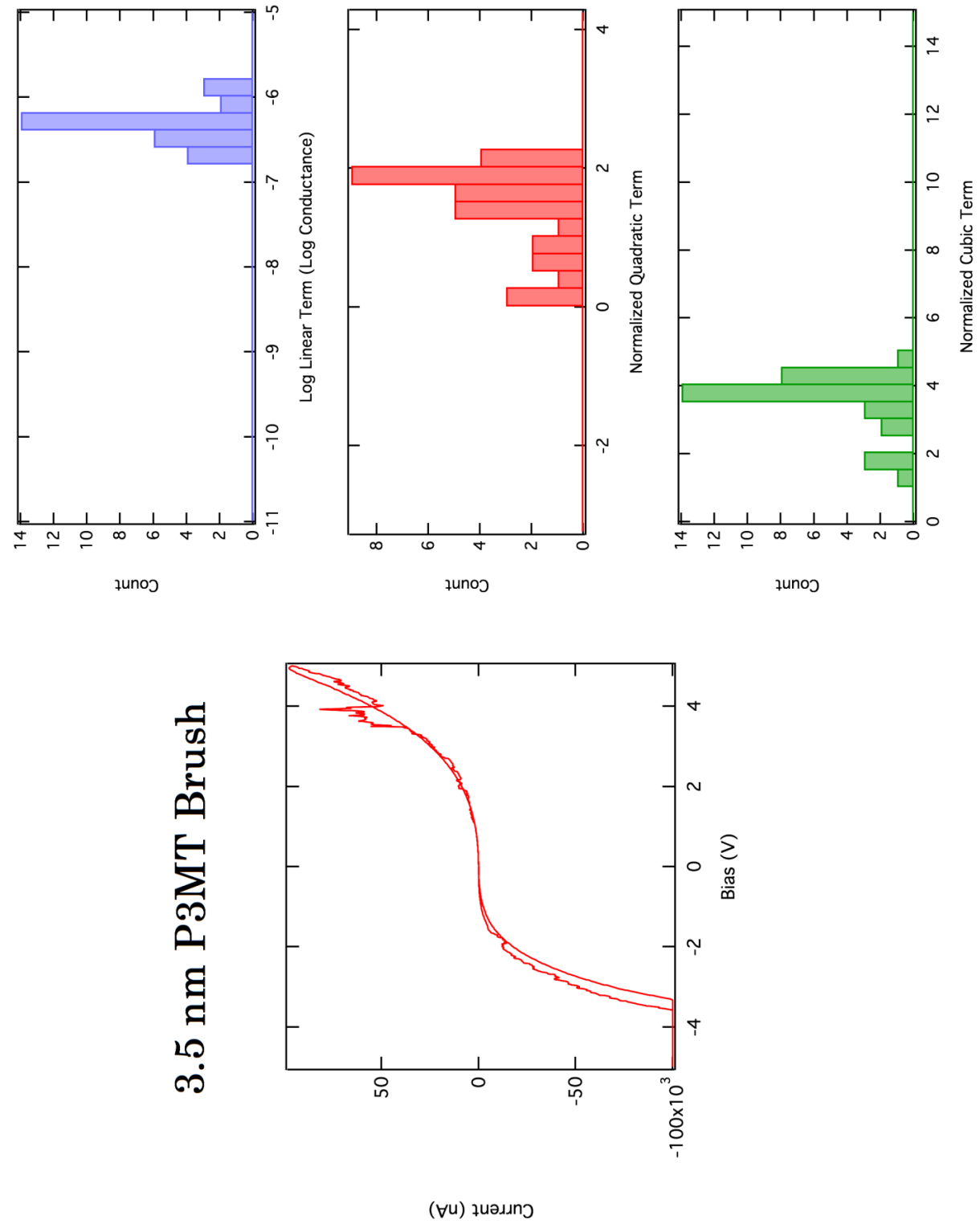

3.8 nm P3MT Brush

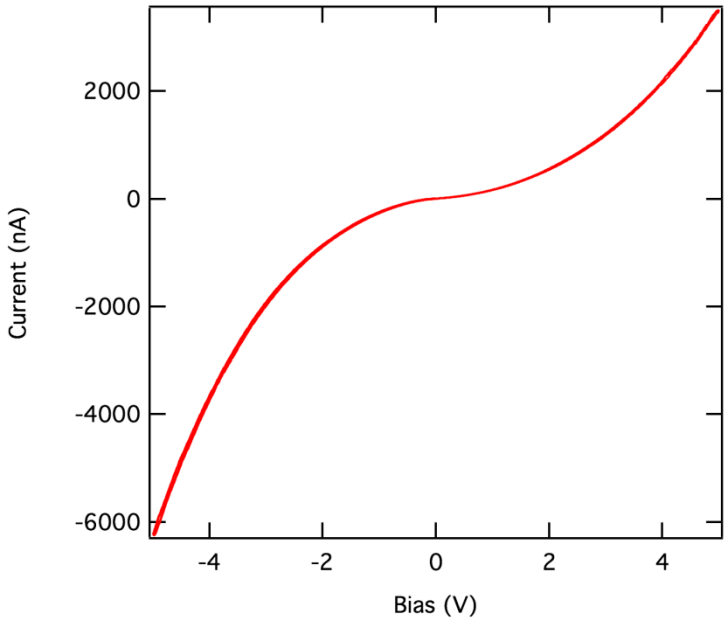

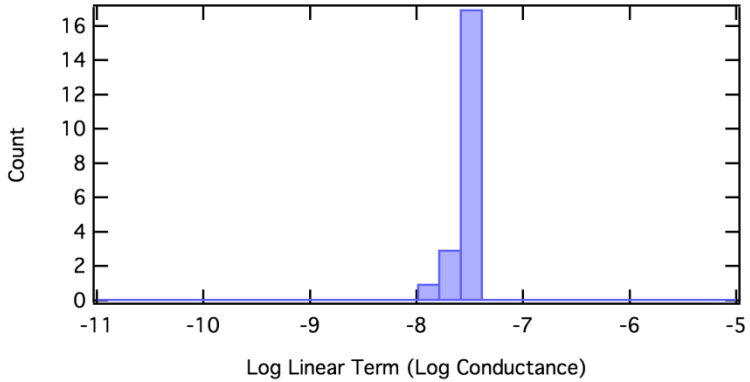

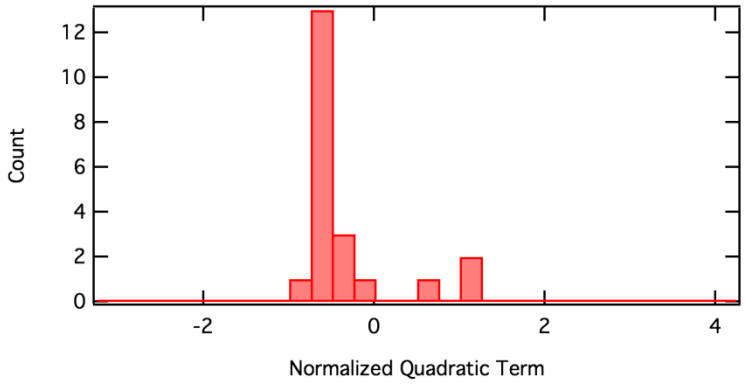

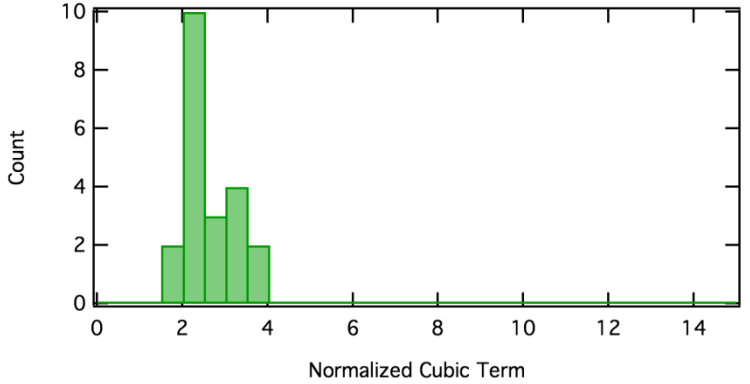

6 nm P3MT Brush

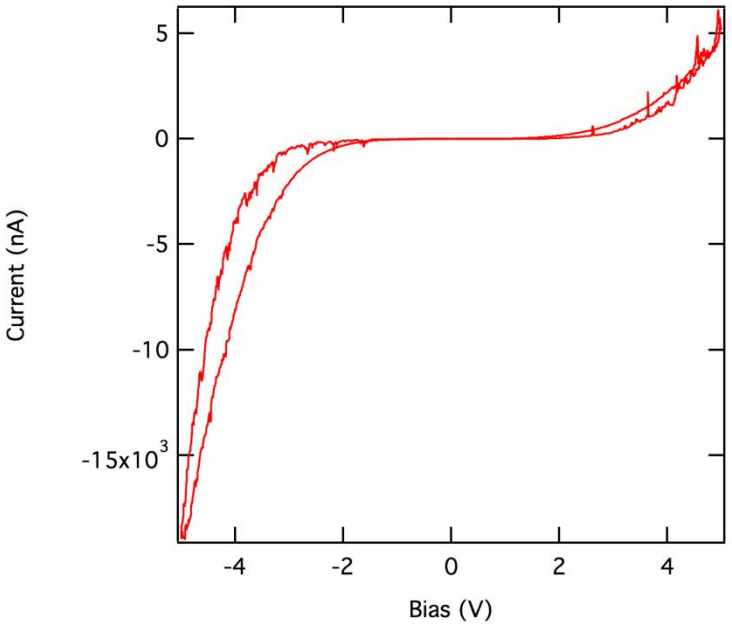

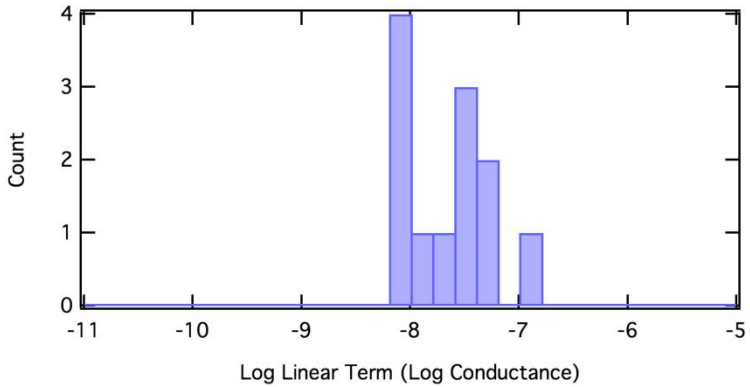

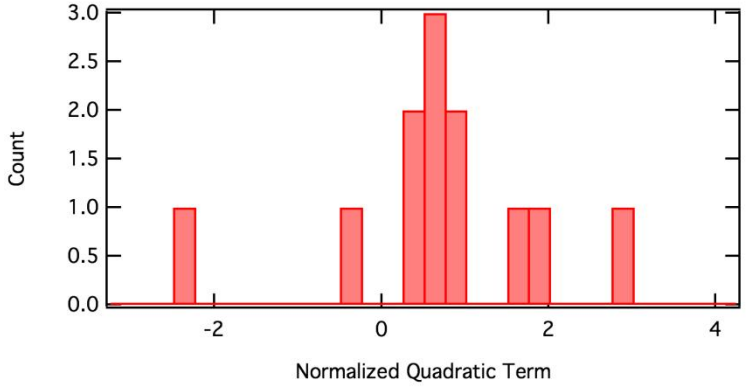

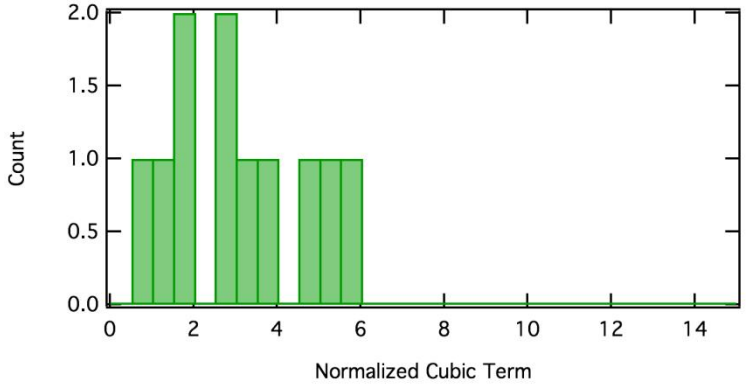

7 nm P3MT Brush

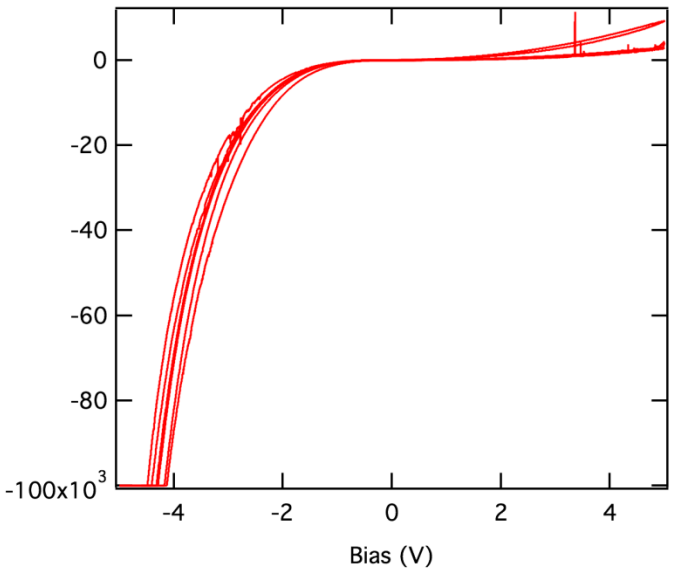

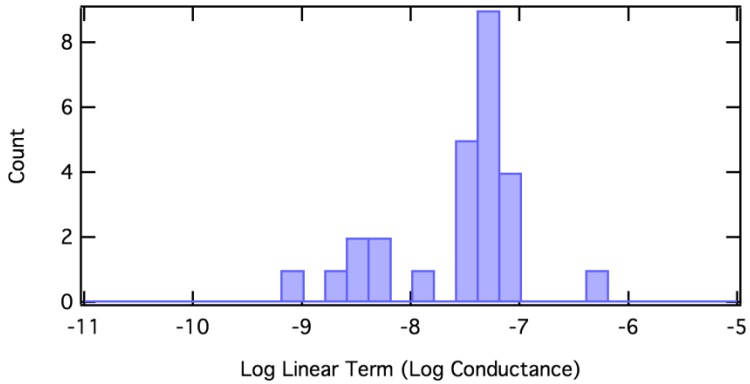

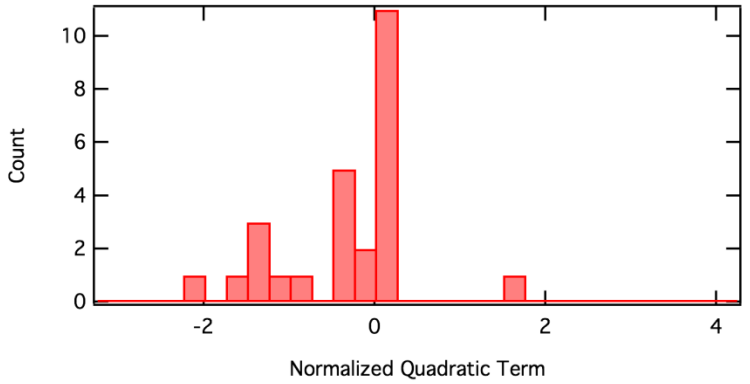

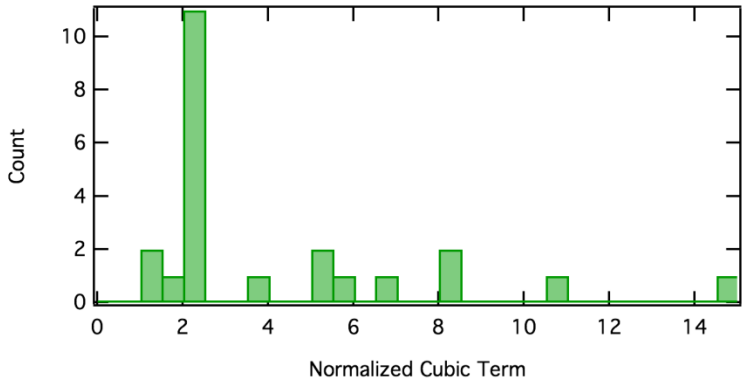

7.5 nm P3MT Brush

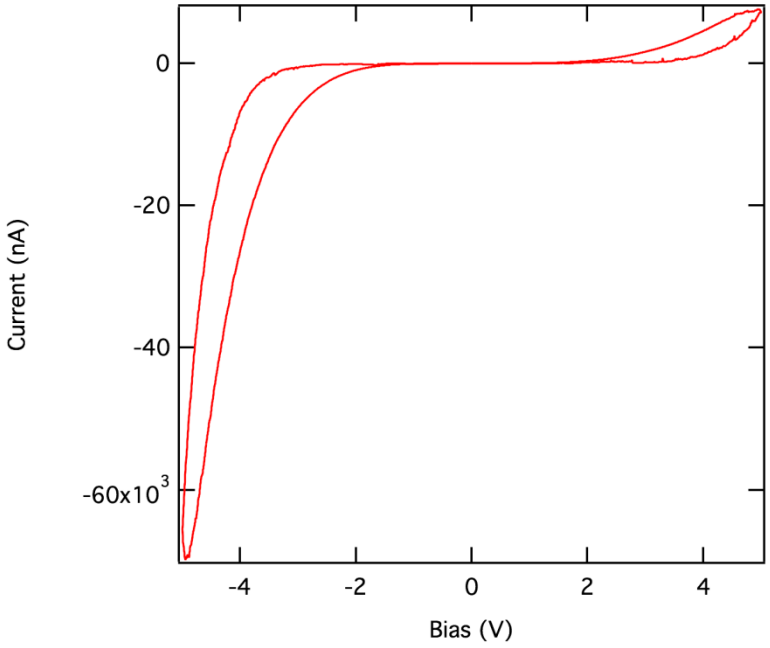

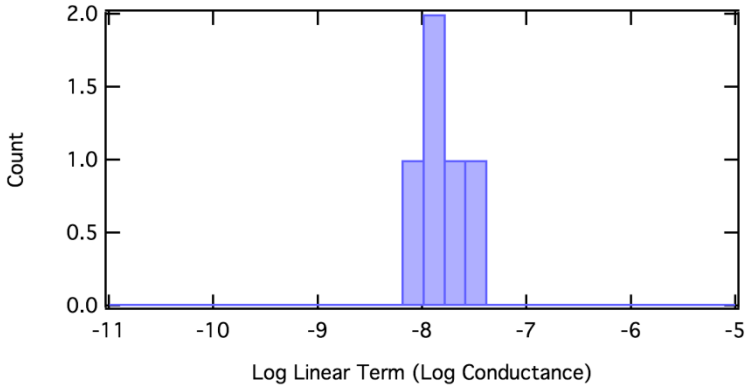

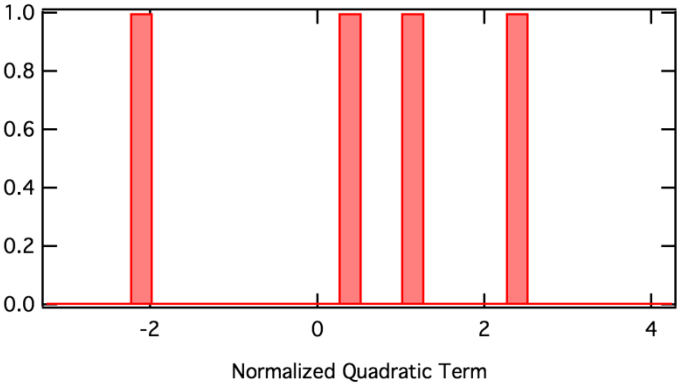

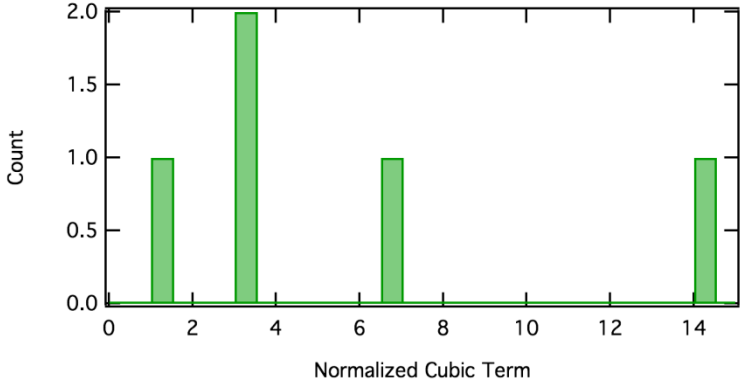

9.5nm P3MT Brush

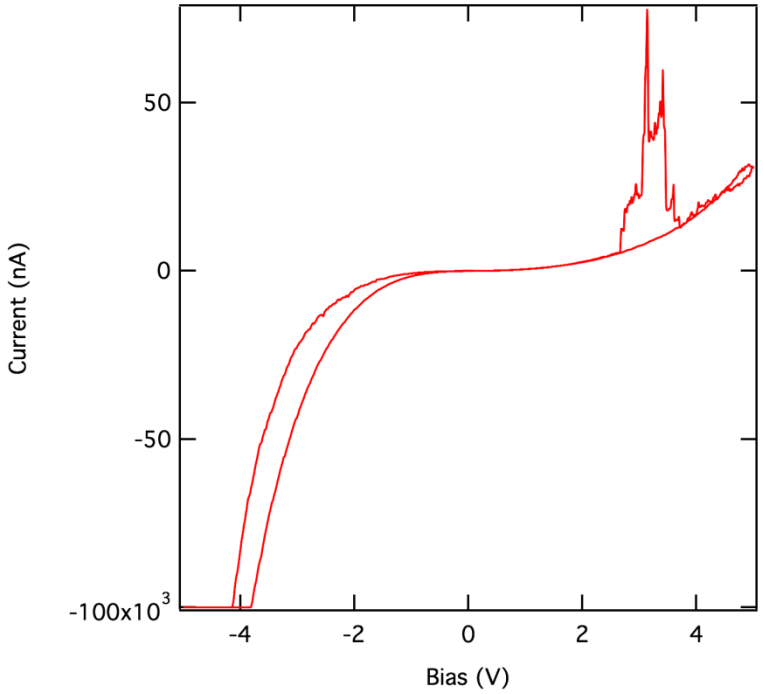

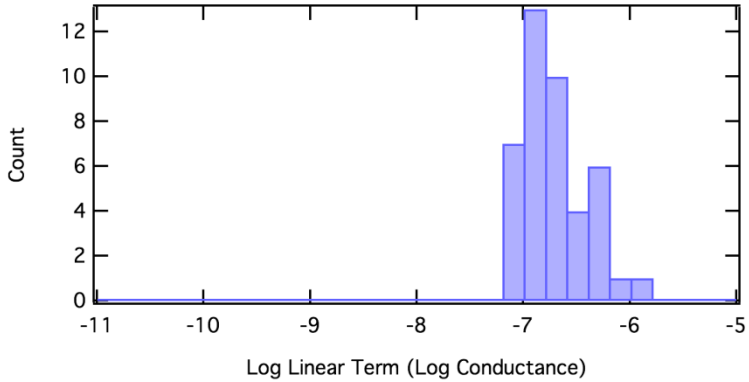

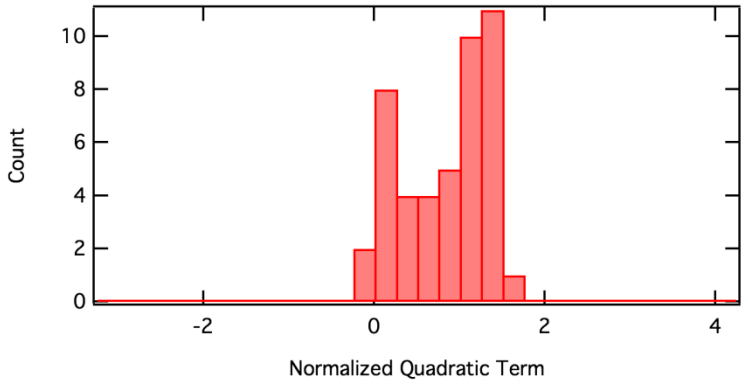

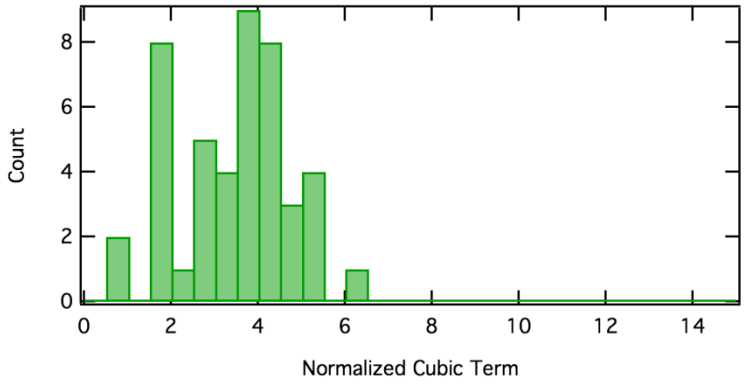

10.2 nm P3MT Brush

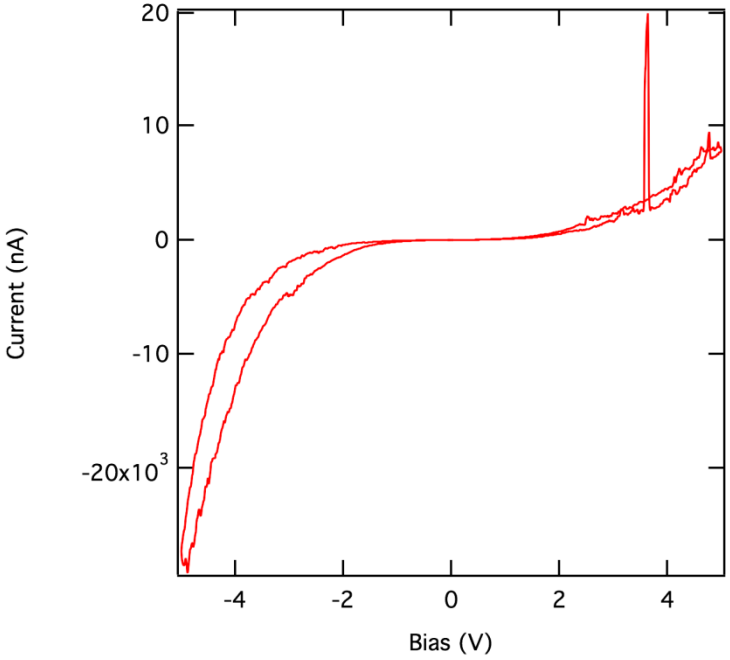

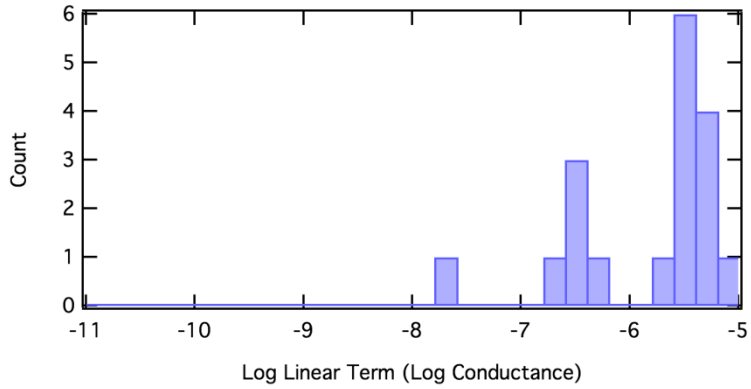

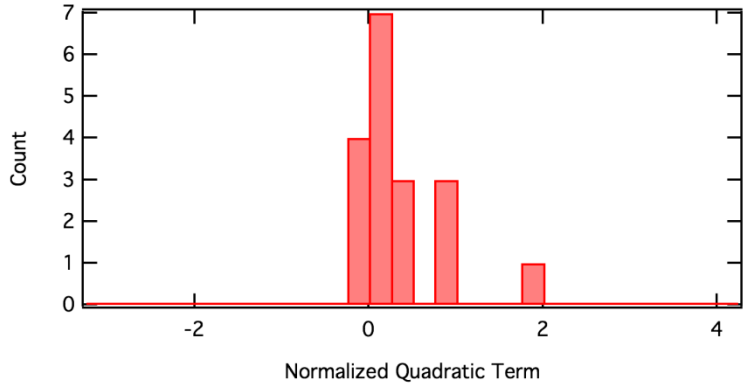

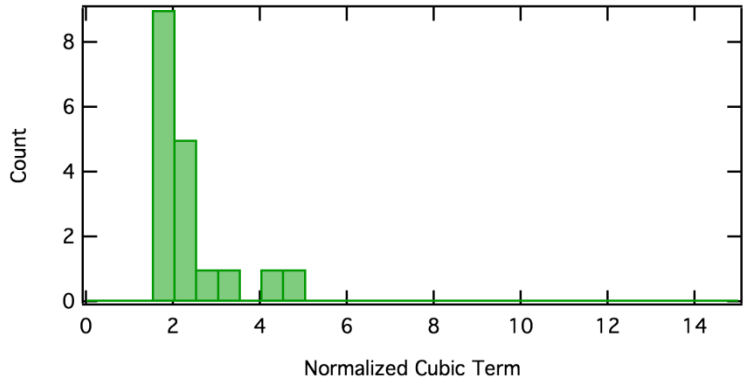

10.9nm P3MT Brush

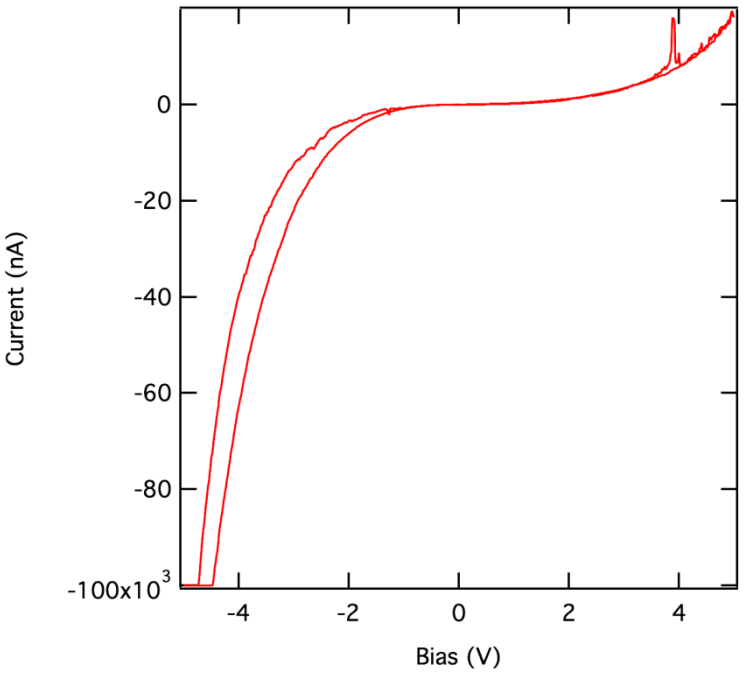

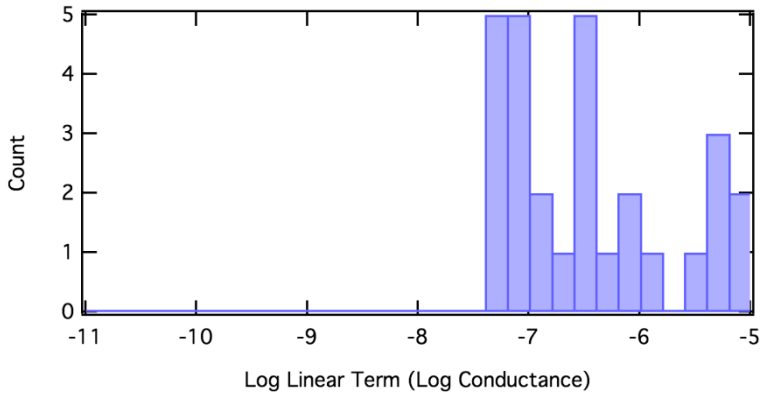

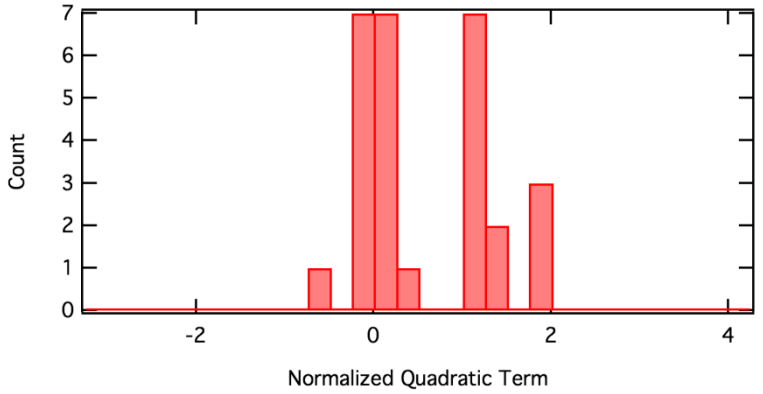

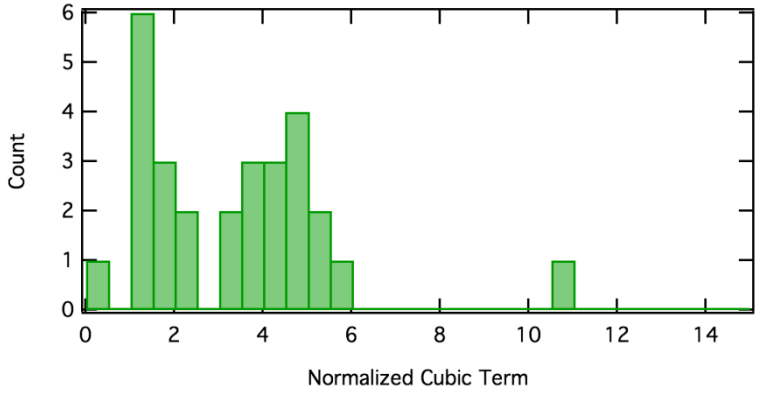

11nm P3MT Brush

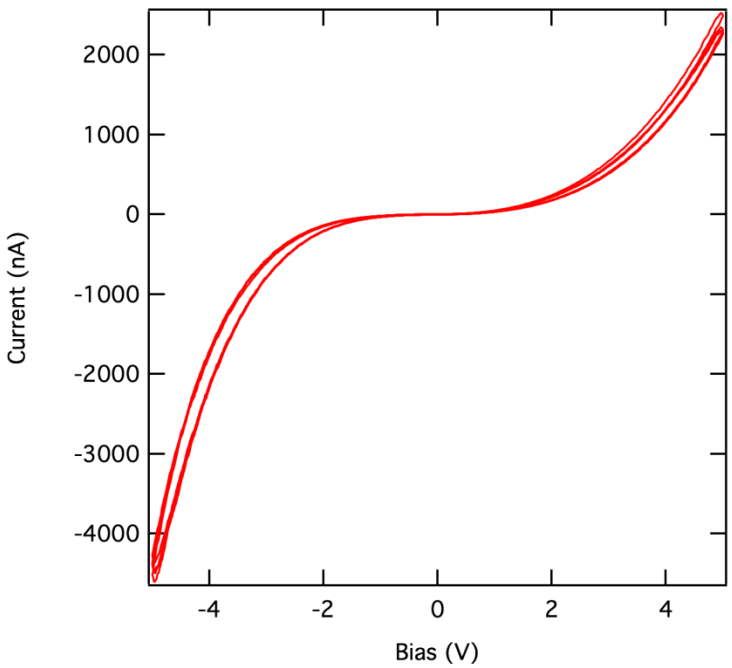

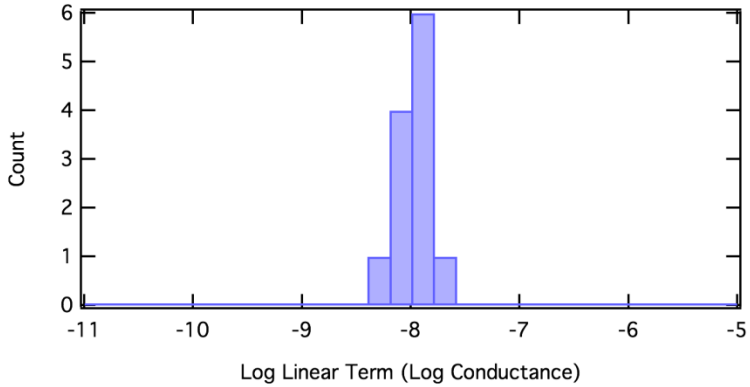

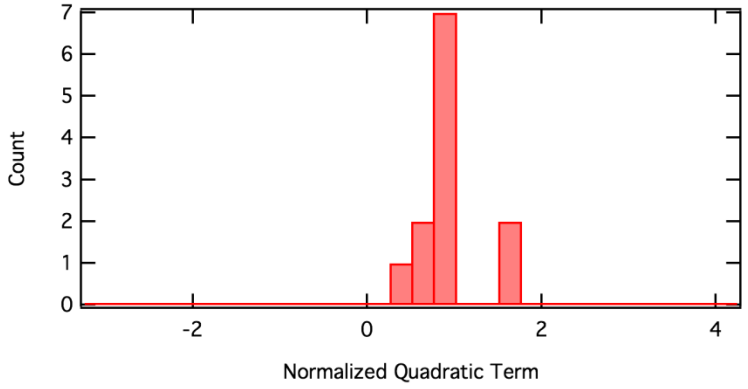

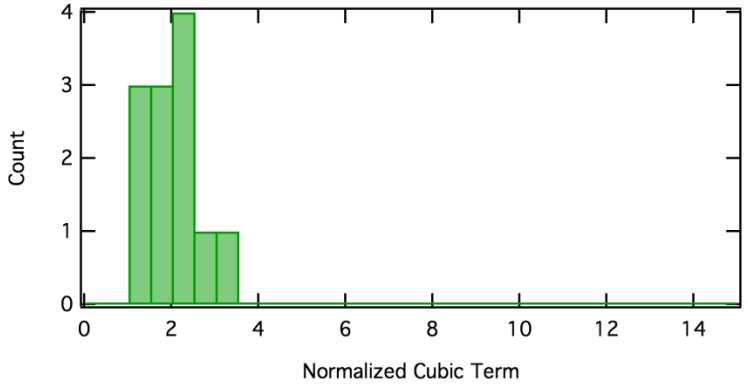

11.5 nm P3MT Brush

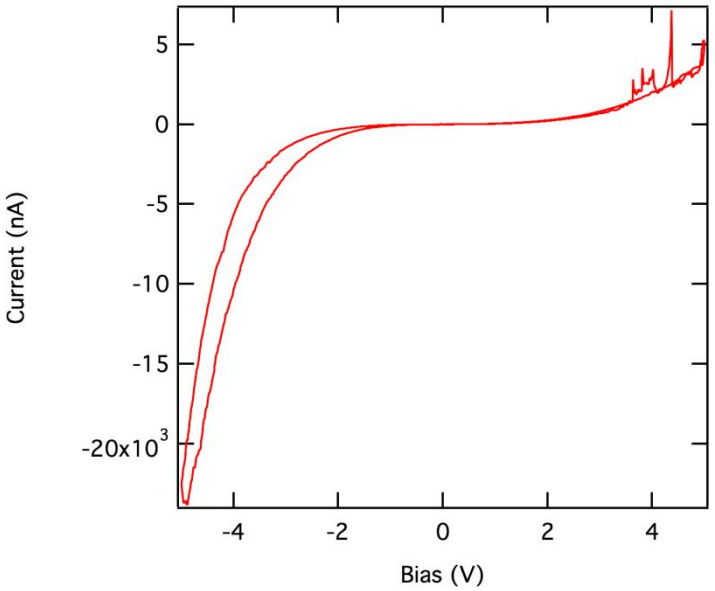

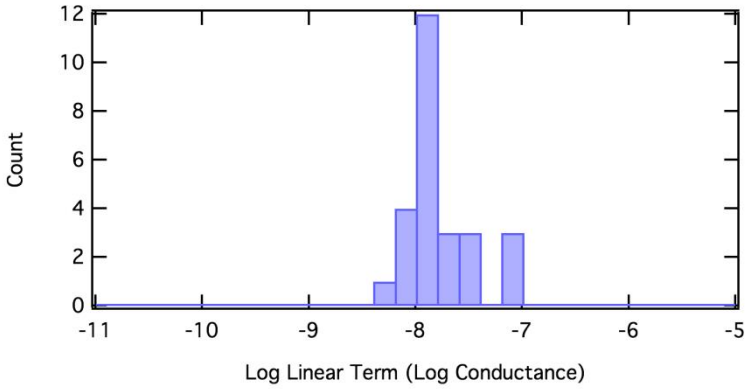

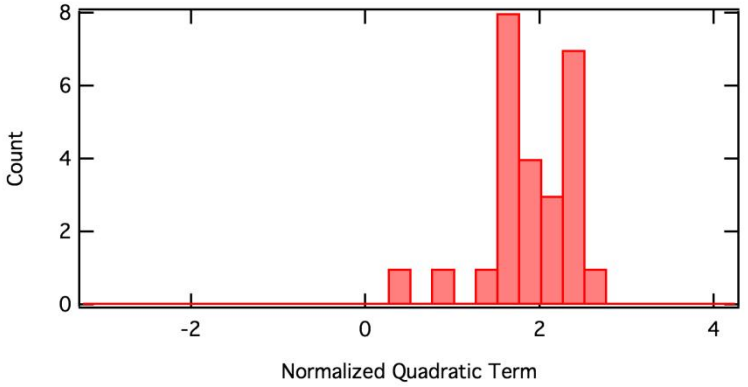

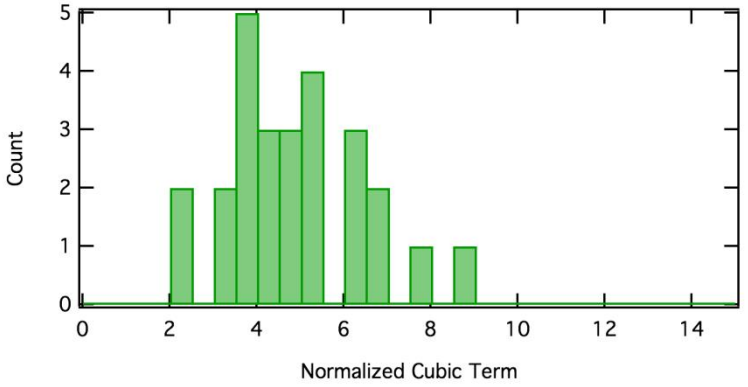

Annealed
13.5 nm P3MT Brush

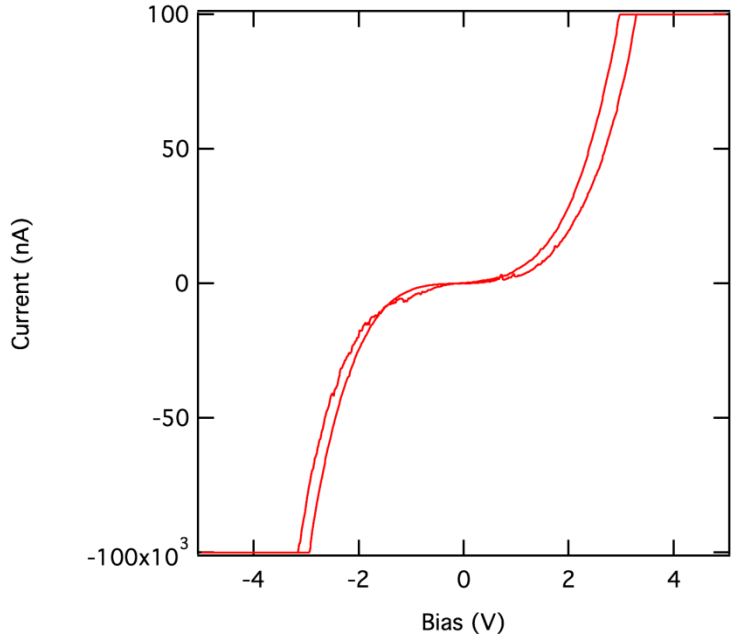

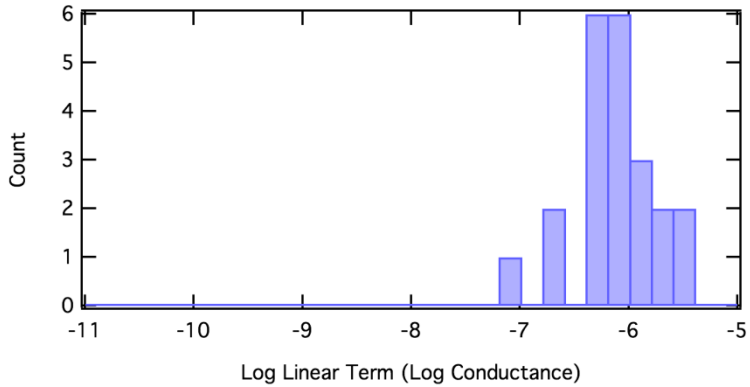

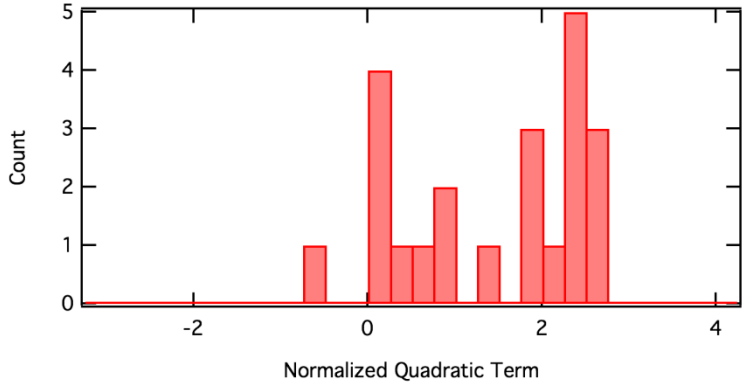

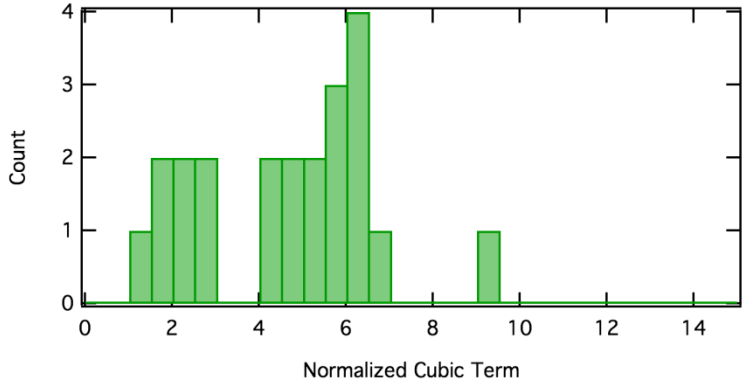

Annealed
17.5 nm P3MT Brush

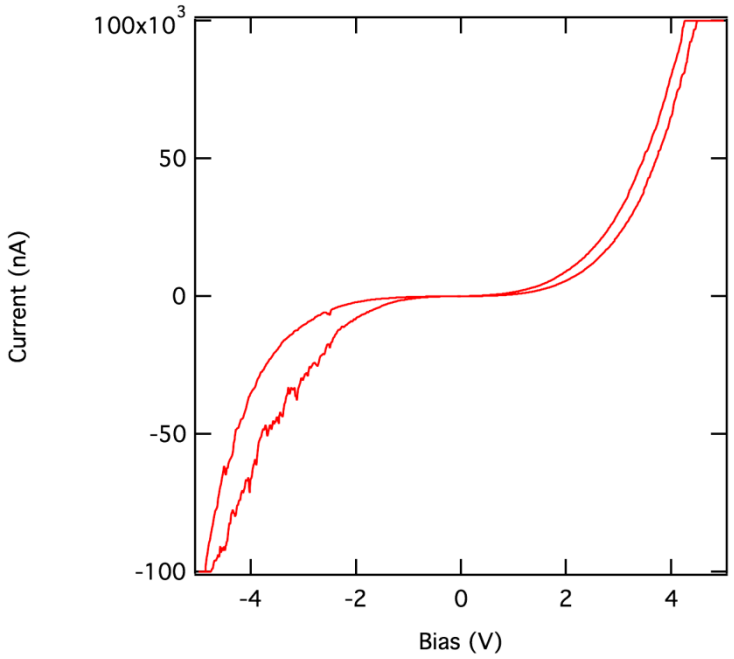

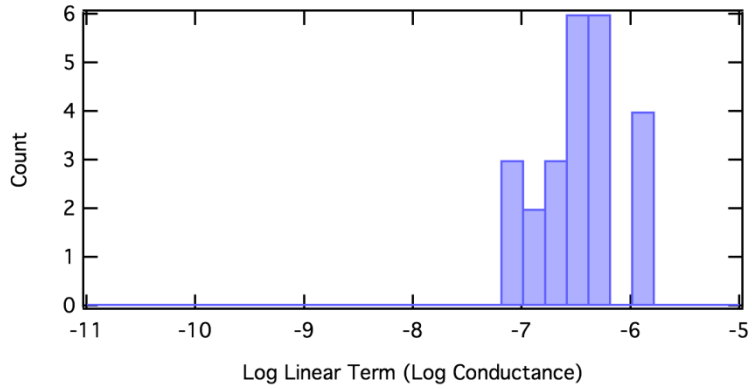

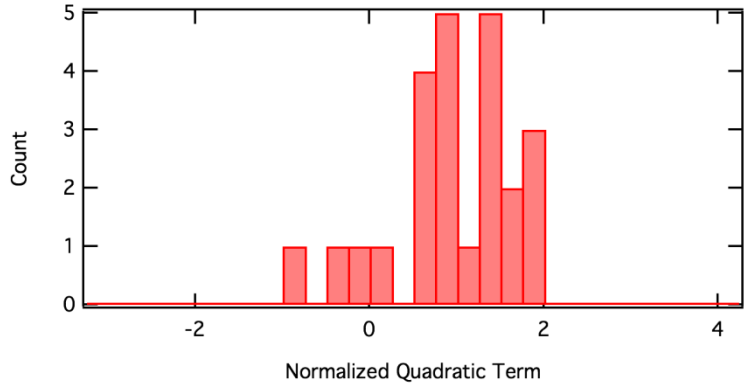

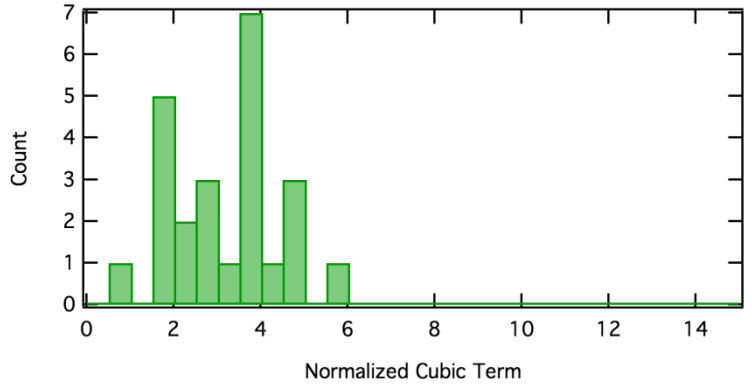

Annealed
21.3 nm P3MT Brush

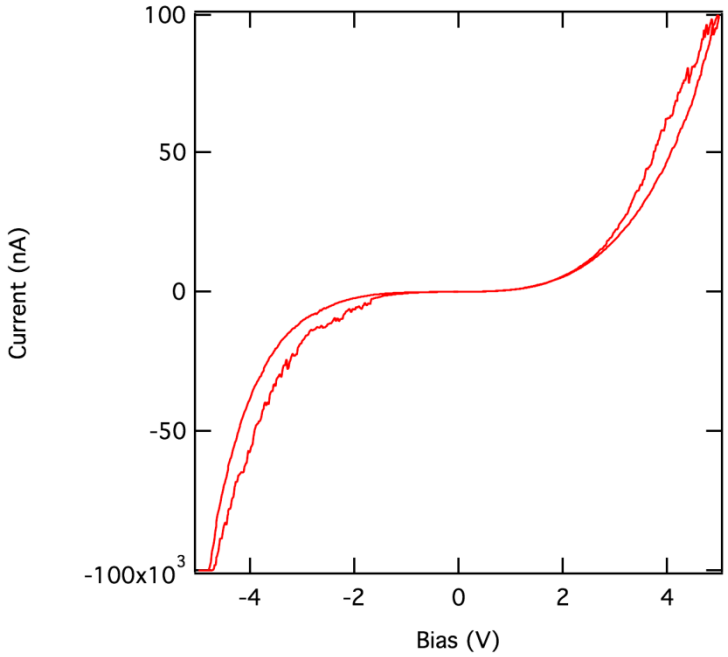

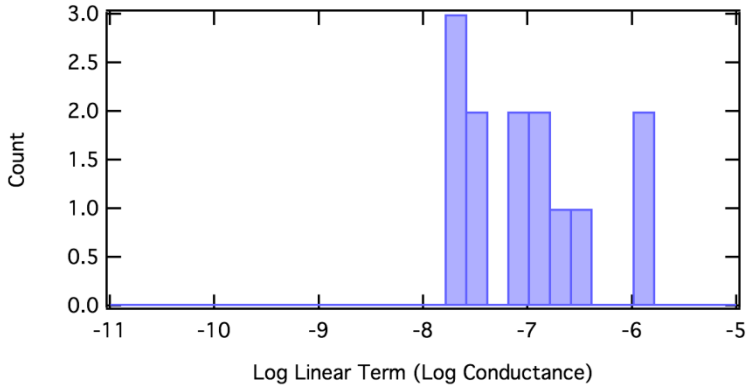

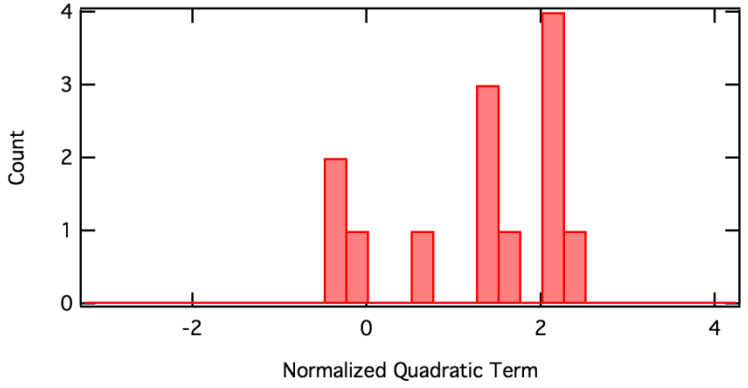

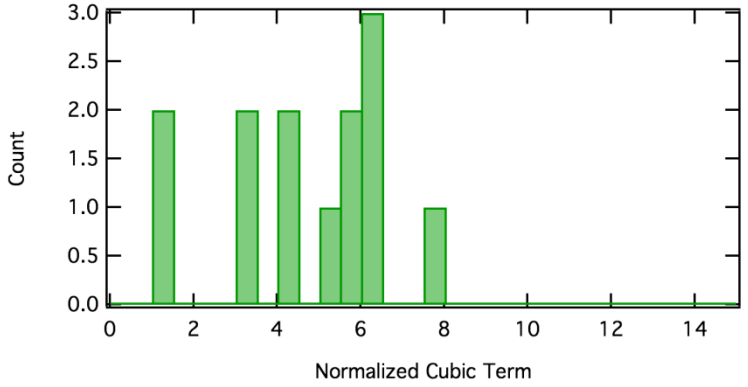

Annealed
22 nm P3MT Brush

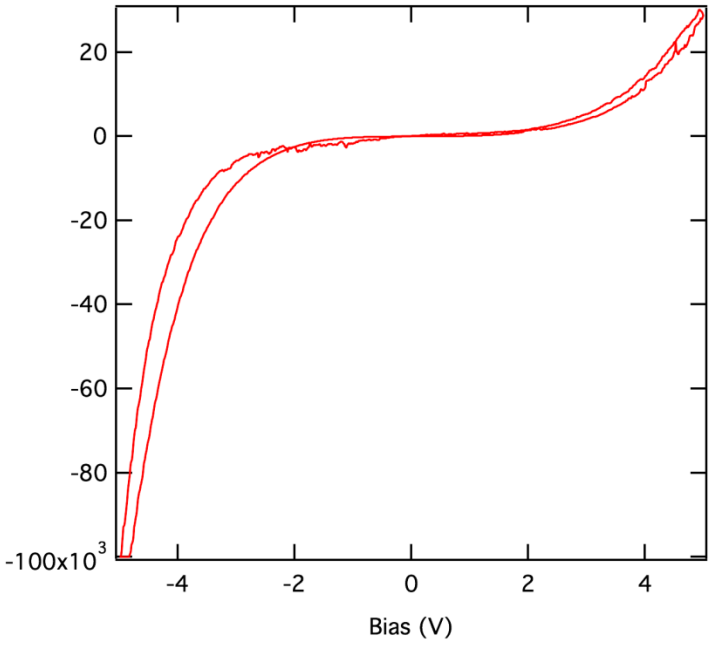

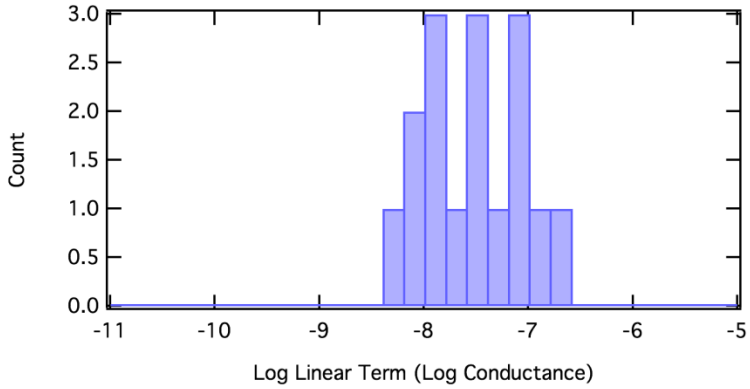

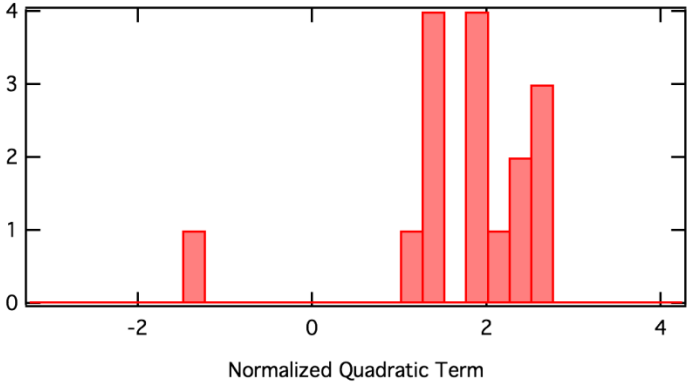

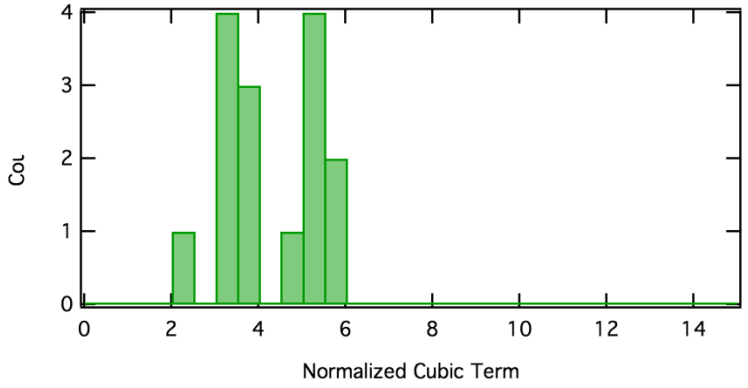

CHAPTER 5 CONCLUSION AND FUTURE DIRECTION

5.1 Summary and Conclusions

5.1.1 Summary of Work

As more new organic semiconducting materials and organic electronic devices are made in laboratories, conjugated semiconductors get closer to widespread application in commercial OLEDs, OPVs, and OFETs.[4-5, 19] Even with current technology, utilization of organic materials is projected to increase by a factor of 10 within the next five years.[8] Typical conjugated polymer devices form active layers by spincasting, bladecoating, or printing films on a bottom electrode with the top electrode being deposited by thermal evaporation. Unlike device active layers made from inorganic wafers which are highly crystalline, polymer materials are at best semicrystalline and have little to no long range order. Device properties are determined by charge transport through active layers, which is one of the reasons inorganic materials outperform organic materials in many applications.

For a charge carrier to transport through a polymer thin film, it must transport between chains, across grain boundaries, and inject through barriers at each electrode.[28-29] Theoretical studies predict that the best way for charge carriers to transport in conjugated polymers is through the backbone along short distances so it does not hop between polymer chains or chain segments.[17] Though local charge

transport along backbones of conjugated polymers has been measured using analytic techniques, devices that specifically exploit this one-dimensional aspect of charge transport in conjugated polymers transport are few, and in every case the active layer in such devices feature a large component of unoriented polymer necessitating that charges transfer through a typical polymer film at some point in the device.[31-32, 45] This work endeavored and succeeded in creating P3MT brush films of controllable length consisting of a single layer of polymer chains oriented vertically from the growth substrate. These films are ideal for measuring intramolecular, or along the backbone, charge transport in polymer chains. Polymer brush thin films are integrated into devices, and the charge transport properties are measured through vertically oriented conjugated polymers.

5.1.2 Controlled Growth of Conjugated Polymer Brushes

Though controlled synthesis of P3MT brushes has been reported in literature,[57, 67] the polymerization parameter space has not been explored to the extent that films of controllable thickness can be made repeatedly from different surface attachment groups. Film growth in literature is linear with respect to time, which is expected for first order polymerization kinetics with constant monomer concentration. However, fine control over film thickness was not reported, only an increase in absorption of films with respect to time. Also missing from literature reports is a thorough report of the effects of temperature and concentration on polymer film growth. Furthermore, only the relatively poorly conducting phosphonic acid anchoring group has been used to graft chains from surfaces. For electronic

devices, fine control must be exercised over film thickness to make films of desired length. Also, the anchoring group should be tunable to optimize charge injection into polymer films.

Carboxylic acid anchoring groups were investigated as a new candidate for grafting polymer brushes from ITO surfaces. The model compound, 5-bromo-4-methylthiophene-2-carboxylic acid was synthesized to test the efficacy of carboxylic acids for SI-KCTP. Contact angle and XPS measurements suggest that the carboxylic acid functionalized molecules form monolayers of slightly lower quality than phosphonic acids. Measuring the electrochemical oxidation from a ferrocene labelled molecule attached to surface bound molecules by Kumada coupling indicated that the active catalyst coverage on the surface is also lower than that of phosphonic acids. Despite performing lower in all tested metrics, polymer brush films were attempted to be grafted from carboxylic acid monolayers. Under no growth conditions were P3MT brushes able to be grown from carboxylic acid anchored molecules using SI-KCTP.

Polymerization reaction conditions are also investigated in order to grow high quality films. In literature, only a single temperature and monomer concentration are reported to describe Pd catalyzed SI-KCTP, though these conditions yield a linear increase in grown polymer film with respect to reaction time as evidenced by increase in absorbance. Here, the actual polymer thickness is measured as a function of reaction time, and optimal monomer concentrations and reaction temperatures are determined by systematically varying parameters. Polymer film

thickness, just like absorption, was shown to increases linearly with reaction time, providing further evidence that the polymerization is first order in monomer concentration.

Additionally, polymer growth temperature is varied between 30-50 °C to test the temperature dependence of polymer growth rate. The previously reported temperature of 40 °C is the optimum temperature for Pd catalyzed SI-KCTP,[27] with different behavior observed above and below this temperature. Above the optimum temperature, catalyst detaches from the growing polymer chain and causes solution polymerization, with only thin films growing on the surface. Grown films show UV/Vis absorption spectra without signatures of H-aggregation, giving evidence of having lower surface density than optimized films. Below the optimum temperature, films grow slowly, with little solution polymerization observed. Films do have signatures of H-aggregation, suggesting that the surface density is still quite high.

Using the optimum growth temperature, and knowing that polymer films grow linearly with respect to time, the monomer concentration was varied and the rate of polymer film growth with respect to monomer concentration gives further evidence of first order kinetics. At every concentration, linear growth in polymer film thickness with respect to time was observed. At low concentrations, the change in reaction rate (measured by increase in film thickness per hour) increases linearly with monomer concentration, but above 0.1 M, increasing the monomer concentration becomes self-limiting, with the increase in reaction rate diminishing.

This is most likely due to the harsh polymerization conditions from KCTP Grignard monomers etching phosphonic acids off the surface. Nonetheless, a linear region in the plot of reaction rate vs. concentration suggests that film thicknesses should be controllable and reproducible in that range of concentrations. Despite the control that can be exercised over film growth under ideal conditions, films often do not grow or deviate greatly from this behavior. This is a sign that the SI-KCTP reaction is extremely sensitive to some uncontrolled conditions.

5.1.3 Characterizing and Controlling Morphology of Conjugated Polymer Brushes

Several characterization techniques were applied to P3MT films to characterize the morphological and electronic properties of P3MT brush thin films before and after annealing.

Absorption spectra of films (as grown) indicate that polymer chains strongly associate with each and form H-aggregates in the plane of the substrate, but after annealing the planar structure largely disappears from absorption spectra. Furthermore, after annealing, the wavelength of maximum absorbance red shifts by nearly 100 nm and the integrated absorbance more than doubles, but the onset of absorption does not change. The shift in absorption max is due to the signature of H-aggregates disappearing, and the increase in absorbance is attributed to better interaction between chains. The unchanging onset of absorption is a sign that the conjugation length of the P3MT brush does not change after annealing, meaning that the conjugation length is achieved early in the reaction. Polarized variable

angle UV/Vis absorption spectra indicate that films have some vertical orientation as grown, but after annealing it significantly increases.

Surface characterization using AFM indicate that film roughness is in general less than 50% of the film thickness, which is quite high, but smaller than roughnesses reported in literature P3MT brushes.[57, 66-67] The P3MT surfaces are not as smooth as SAMs used in molecular electronics, though. Thicker P3MT films have higher surface roughness, but the roughness relative to the thickness decreases for thicker films. Annealing films does slightly increase surface roughness, but due to films increasing in length after annealing this causes the relative roughness to decrease.

The average transition dipole orientation is calculated from NEXAFS for P3MT brushes and physisorbed P3MT, but not annealed films. Analysis indicates that on average, grafted chains as grown are oriented 60° out of the plane of the substrate. This is in contrast for physisorbed P3MT chains which are shown to be laying on the surface. Combining this initial state with the increase in vertical orientation observed after annealing as measured by polarized UV/Vis suggests that annealed films are quite oriented.

Polymer film thicknesses are measured using three methods, all yielding similar results. Atomic force microscopy profilometry is the only direct method of measuring film thickness, but this is the most destructive, so it is not an ideal method. A calibration plot using polymer film absorbance and polymer film thickness was made as a countermeasure against the destructive AFM technique,

but small inconsistencies in the absorption spectra cast doubt on the validity of such a plot. Ellipsometry is the ideal technique used to measure film thickness. Though it does not directly measure film thickness like AFM, films are individually modelled and fit to ensure inconsistencies in films are accounted for. Nonetheless, films characterized by all techniques yield three film thicknesses that are similar to one another within the error of each measurement.

When the thickness of a film is measured before and after annealing, an unexpected but desirable trend appears. Polymer film thickness increases after annealing in all measured films. This result can be interpreted in many ways, but in the context of the results from the other characterization techniques, the increase in length is the key piece of evidence needed to affirm that annealed films are changing morphology such that chains adopt ideal conformation. Combining the interpretations and conditions that each characterization technique introduces for annealed films, the final model of polymer film morphology is approaching the ideal case for chain conformation and overall microstructure with chains becoming more vertically oriented and rigid. Simply stated, P3MT brushes become more brushlike after annealing.

5.1.4 Measuring Charge Transport through Conjugated Polymer Brushes

A new protocol for forming molecular electronic devices using KTP to transfer print small and large Au electrodes on top of molecular layers was developed to conduct this work.

Though the exact mechanism of charge transport through P3MT brush films was not able to be determined by experimental evidence, the mechanism is most likely charge hopping due to behavior observed in similar films.[40, 43] Charge carriers transport across the film by hopping between conjugated segments on the polymer backbones. Transport in annealed and unannealed films appears to be similar at intermediate biases as evidenced by similar ß values in annealed films and short, well made films. Similar normalized quadratic and cubic fitting terms also suggest that the mechanism for charge transport at high voltages is the same in all films. Furthermore, annealing has been shown to recover "good" ß values in poorly made films and correct abnormalities in the relationship between resistance and polymer film thickness. For unannealed films, a change in the ß value for thick films suggested that charges must hope more in order to cross the junction.

Power law plots show that at low biases less than 100 mV, annealed films and unannealed films have different IV behavior. This could possibly be due to diffusion current at low biases.[87]

The SCLC mobility of charge carriers through P3MT films was universally enhanced after annealing, in many cases by several orders of magnitude. The increase in mobility is attributed to structural changes in the P3MT brush film towards more ideal morphologies for transporting charges through the polymer backbone. Due to effective device areas being lower than total area of the electrode, the magnitude of the mobility may be more than three times greater than what is measured.

Based on electrochemical measurements of the HOMO level of P3MT and UPS measurements of the work function of functionalized ITO, a band structure of a P3MT device was constructed. The small difference between the measured HOMO and work function for P3MT and ITO, respectively, and the literature value of the work function of Au,[85] suggests that holes are most likely the primary charge carrier in these devices. The injection barrier for holes is approximately 0.1 eV, but that of electrons is approximately 1.8 eV.

Though the actual charge transport pathway may be impossible to measure, P3MT brushes made for this work approach ideal morphologies for transporting primarily along polymer backbones. Increases in vertical orientation, planarity of polymer chains, and distance between polymer chains accompanied by systematic increases in charge carrier mobility by up to three orders of magnitude provide evidence that intramolecular transport pathways play a significant role in charge transport in these devices.

5.2 Suggested Future Work

5.2.1 Determining The Charge Transport Mechanism in P3MT Films

Determining the charge transport mechanism should be a top priority in future studies involving P3MT Brush films. In similar studies, the charge transport mechanism was determined by measuring IV-curves at reduced temperature.[44] Large area contacts should be printed on to P3MT brush films, and devices should be cooled down. The temperature dependence of the IV measurements will give

more evidence of how charges transport through the films. Further evidence should also be gathered to determine if annealed films have diffusion limited current.[87]

5.2.2 New Surface Chemistry

Several preexisting solution based chemistries can be applied to the surface to make new active layers for implementation in devices. Some of these ideas have been tried to some extent, but none of them significantly impacted the course of this work.

5.2.2.1 New Polymer Backbones

This work focused solely on P3MT to study intramolecular charge transport. The choice of using P3MT was wise due to the fact that P3ATs are one of the best studied classes of conjugated polymers in literature. Using P3MT was more out of

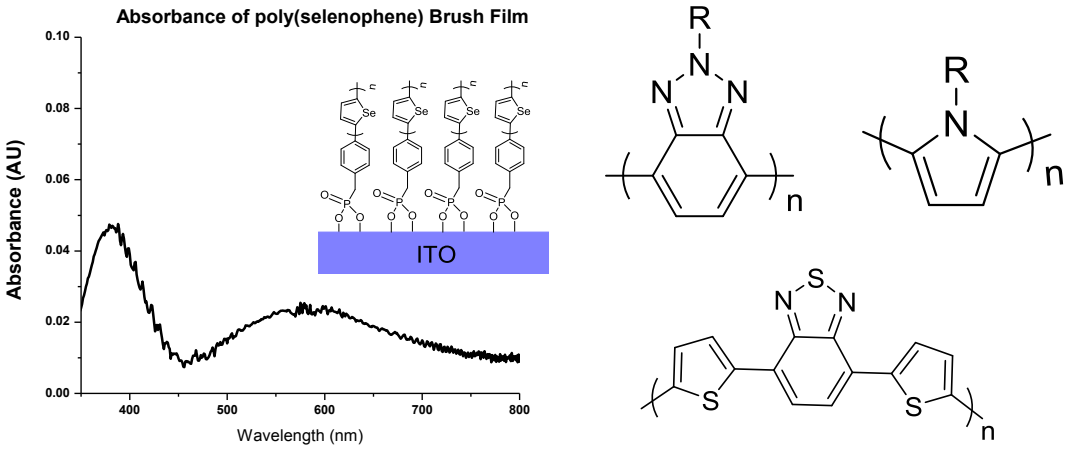

Figure 5-1: Future SI-KCTP Polymer Backbones

Poly(selenophene) has been made using SI-KCTP as diagrammed above. Other possible monomers for SI-KCTP are triazole, pyrrole, and dithienylbenzothiadiazole, (DTBT). DTBT is of particular interest because it is a donor-acceptor polymer which are useful in OPV applications.

necessity than wisdom because the best reports of conjugated polymer brushes use P3MT. Several molecules are compatible with solution based KCTP, though the only other polymer backbone besides poly(thiophene) to be reported in literature using SI-KCTP is poly(*p*-phenylene).[56] Besides 3-methylthiophene, two other molecules were attempted to be polymerized: 3-hexylthiophene and selenophene. Out of these two molecules, only selenophene was successfully polymerized, but due to the lack of alkyl group, polymer films were of low quality (Figure 5-1). It is documented in literature that an alkyl chain on the 3 position is important to direct SI-KCTP and KCTP. The likely reason 3-hexylthiophene did not polymerize is due to the relatively bulky hexyl sidechain. Out of other non-questionable reports of SI-KCTP, only short sidechains of methyl or ethyl are reported.

With this information in mind, 3-methylselenophene is an ideal candidate for SI-KCTP. Other ideal candidates are listed in (Figure 5-1).[88,63, 89]

5.2.2.2 Different Polymerization Chemistry

One of the major drawbacks of SI-KCTP is the harsh reaction conditions created by the Grignard monomer. The phosphonic acid anchor group is not completely stable in these conditions and can etch off of the surface and monomers susceptible to nucleophilic attack are not stable either, severely limiting the scope of the reaction. Surface initiated Stille coupling was briefly investigate using the same Pd catalyst as used in SI-KCTP, but this approach was summarily abandoned after initial success was unable to be reproduced (Figure 5-2). Several P3MT films were created using Stille coupling without any trace of solution polymerization. Recent

literature reports of successful Stille catalyst-transfer polycondensations using a different catalyst may have promise for a surface initiated polymerization.[77]

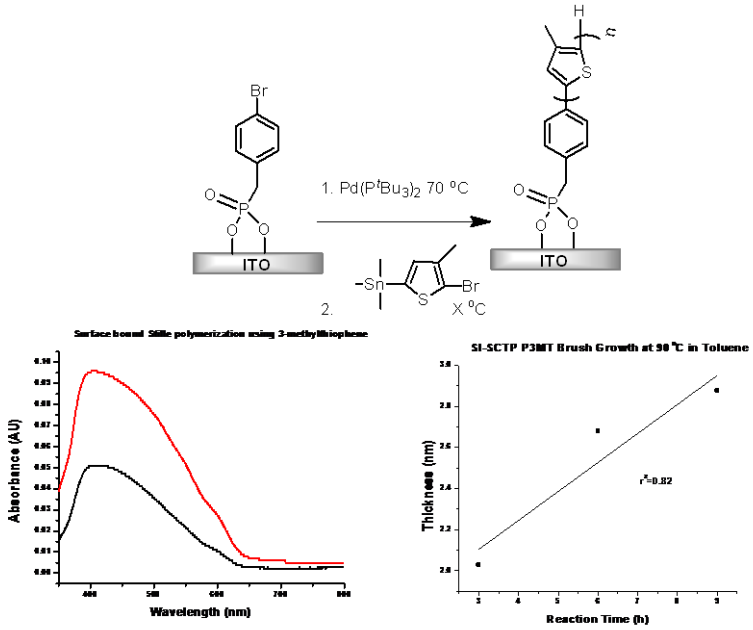

Figure 5-2: Surface Initiated Stille Catalyst-Transfer Polycondensation

(Top) This is a representative schematic of a surface initiated Stille polymerization. Stille coupling is less harsh than Kumada coupling, and a great variety of functional groups are compatible with the Stille reaction.
(Left) Two absorption spectra from films grown with SI-SCTP show significant H-aggregation, similar to SI-KCTP.
(Right) This is a single experiment on a time study to understand the rate of Stille coupling on the surface. Reactions were completed at 70 °C and 90 °C in toluene, but the reaction is quite slow, and systematic data were only collected for this experiment.

5.2.2.3 New Attachment Chemistry

If Stille coupling can be used to grow conjugated polymer brushes from surfaces, then it is possible to use weaker attachment chemistry to anchor initiators on surfaces. Carboxylic acids on oxides such as ITO as described in chapter 2.

5.2.2.4 End Group Modification

Briefly, end group modification was used to attempt to support electrodes transferred by nTP, but ultimately it was left out of the discussion because this reaction was done using P3MT brushes made with Ni catalysts which were not characterized to the same extent as current brushes. Protected thiols were introduced at the end of reactions, and deprotected after end capping was complete (Figure 5-3). Though there is evidence that the reaction works, and does enhance

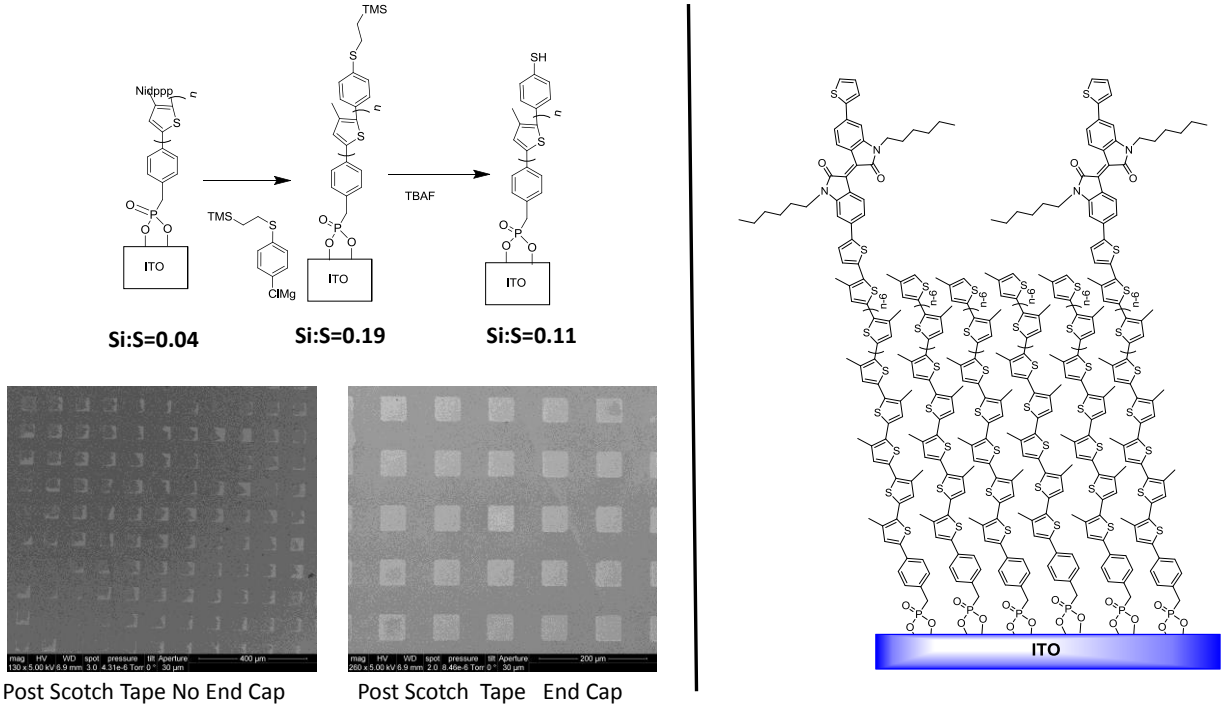

Figure 5-3: End Group Modification of P3MT Brushes

(Left) In P3MT films grown with Ni catalyzed SI-KCTP, end capping films with a protective thiol and subsequent deprotection (See atomic ratios from XPS located below chemical structures) enable ntP of large Au squares. After attempted removal with Scotch tape, features came off only on samples with no thiol on the surface.
(Right) Attempts at putting electron acceptors on P3MT surfaces have so far been fruitless, but this planned structure is currently being investigated.

nTP, the reaction is not reproducible yielding inconsistent results. Perhaps other end groups, such as electron acceptors (Figure 5-3) can be used to measure other properties of these brushes.

5.2.3 New Device Types

Only charge transport devices were fabricated and tested in this work. Polymer brushes can be integrated into many other kinds of devices

5.2.3.1 Thermoelectric Devices

One exciting application of molecular electronics is in thermoelectrics.[90,91] Thermoelectrics is the production of electricity from a heat gradient, or creating a heat gradient from electric power. For molecular junctions, it has been measured in short molecules, and predicted in longer molecules, that long aromatic chains will

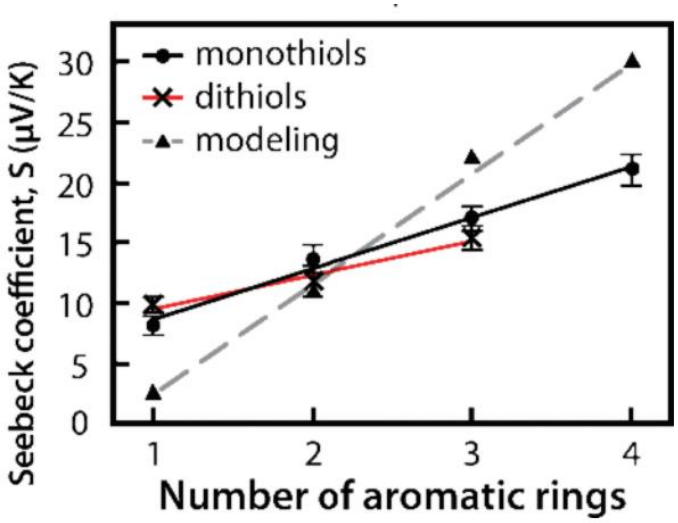

Figure 5-4: Extended Aromatic Molecules Show Great Promise for Molecular Thermoelectrics

An experimental and theoretical literature report of oligophenyl molecules suggests that the Seebeck effect will increase greatly as the number of aromatic rings increase in a molecular junction. Conjugated polymer brushes can be used to test this prediction. Image copyright is respective owner.

have high thermoelectric responses as evidenced by measured Seebeck coefficients (Figure 5-4) and calculated thermopowers.[91, 92] Conjugated polymer brushes are a perfect candidate to use as a vehicle to explore this untapped area of thermoelectrics. Conjugated polymers consisting of 10s of aromatic rings could have very high thermoelectric response in this regime.

5.2.3.2 Spintronic Devices

Another exciting application for conjugated polymer brushes is in molecular spintronics. To date, large area molecular spintronic devices have proven elusive and difficult to make, but two recent papers documenting the formation of SAMs on $La_{0.7}Sr_{0.3}MnO_4$ (LSMO) and put into spin architecture revitalized the conversation on molecular electronics.[93,94] Furthermore, spintronic properties of P3ATs have been studied in traditional organic semiconductor devices consisting of LSMO bottom contacts with spuncast P3HT films and evaporated Co top contacts.[95] Spin valve devices with P3HT interlayers that are strongly chemically associated with the bottom LSMO electrode have enhanced magnetoresistance. Association between covalent grafts and conjugated polymers is quite high, so the conjugated polymer brush (molecular) approach is a very attractive platform to study charge injection from a ferromagnetic material into an organic semiconductor. To this end, P3MT brushes have been grown from LSMO surfaces using the same procedures described in chapter 2 (Figure 5-5), and preliminary devices have been made and tested. Films grown on patterned LSMO substrates exhibit magnetoresistance at low temperature. The magnetoresistance, defined as:

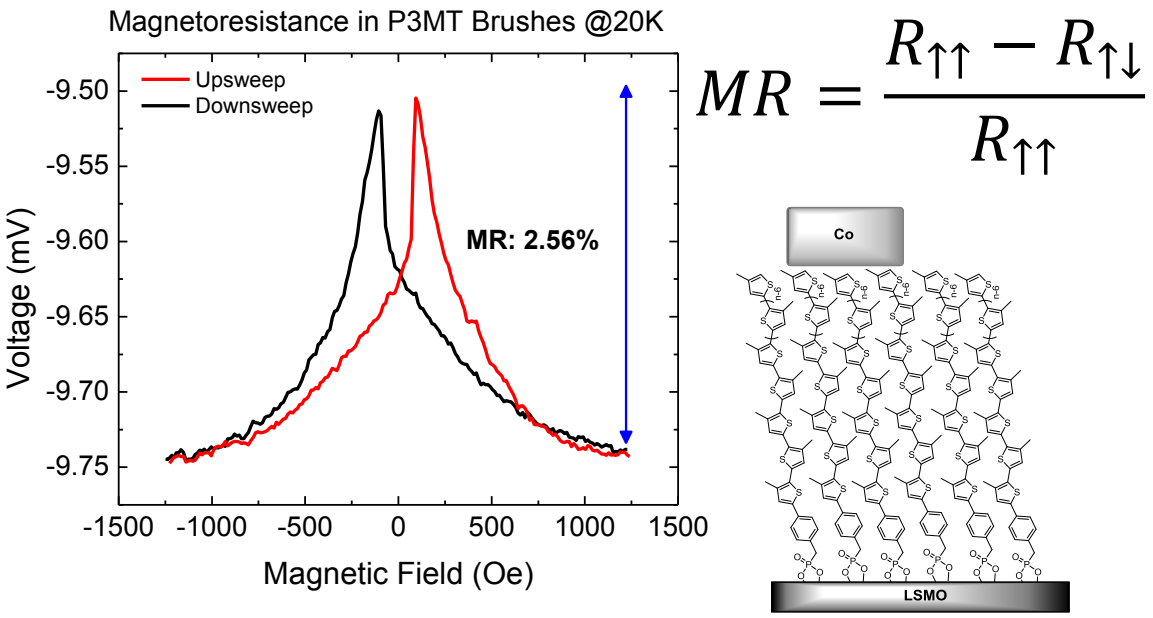

Figure 5-5: P3MT Films Grown on LSMO in Spin Valve Devices

Magnetoresistance is observed in spin valve devices made with P3MT brushes as an organic spacing layer. Magnetoresistance is defined as the difference between the resistance of the device when the electrodes are aligned and antiligned divided by the resistance when the electrodes are aligned. Devices are made by evaporating narrow bands of Co on top of thin films of P3MT. In this device, a 15nm P3MT film acts as a spin transport layer.

$$\boldsymbol{MR = \frac{R_{\uparrow\uparrow} - R_{\uparrow\downarrow}}{R_{\uparrow\uparrow}}} \tag{14}$$

is determined by the ability for a current of spin polarized electrons from one ferromagnetic electrode to be detected by a separate ferromagnetic electrode. The polarizations of the electrodes are controlled by an external magnetic field and can be switched at fields stronger than the coercive field of the electrode. Though this is a promising initial result, a thorough investigation of this phenomenon including investigating length dependent effects, must be conducted to better understand the transport of spin through polymer backbones. At first approximation, film surfaces

appear high quality when measured with AFM. Surfaces are relatively smooth and there are no defects over short ranges. Unlike ITO, LSMO substrates are not transparent, so characterization will be much more difficult.

5.3 Broad Scientific Impact

It is impossible to know what a work's impact, if any, will have on a larger field of science. Few device level studies have come close to achieving the goal achieved in here of transporting charges across single layers of vertically oriented polymers. Though the active layers in made in this work are among the best suited for this application, the high difficulty in synthesizing the polymer brush makes them unideal for use in commercial devices. Nonetheless, many theoretical studies have predicted that properties such as magnetoresistance, thermopower, and mobility increase to unprecedented levels when charges can be primarily transported through polymer backbones. Already mobility has been shown to increase by several orders of magnitude in this work by just surveying charge transport properties. Though the actual magnitude of mobility is quite low compared to the highest performing polymers, device engineering will likely increase the mobility another several orders of magnitude to amplify the affect already observed.[96] This effect will hopefully spur interest in measuring magnetoresistance and thermopower to verify theoretical predictions, generate interest in creating devices to test one dimensional transport in next generation polymers, and develop new syntheses that create similar structures with higher degrees of reproducibility.

REFERENCES

1. eMarketer Smartphone Users Worldwide Will Total 1.75 Billion in 2014. http://www.emarketer.com/Article/Smartphone-Users-Worldwide-Will-Total-175-Billion-2014/1010536 (accessed April 15).

2. Chiang, C. K.; Fincher, C. R.; Park, Y. W.; Heeger, A. J.; Shirakawa, H.; Louis, E. J.; Gau, S. C.; MacDiarmid, A. G., Electrical Conductivity in Doped Polyacetylene. *Phys Rev Lett* **1977,** *39* (17), 1098-1101.

3. Shirakawa, H.; MacDiarmid, A. G.; Chiang, C. K.; Heeger, A. J., <Shirakawa Heeger McDiarmid.pdf>. *J.C.S. Chem Comm* **1977**, 3.

4. Facchetti, A., π-Conjugated Polymers for Organic Electronics and Photovoltaic Cell Applications†. *Chem Mater* **2011,** *23* (3), 733-758.

5. Geffroy, B.; le Roy, P.; Prat, C., Organic light-emitting diode (OLED) technology: materials, devices and display technologies. *Polym Int* **2006,** *55* (6), 572-582.

6. Braga, D.; Horowitz, G., High-Performance Organic Field-Effect Transistors. *Adv Mater* **2009,** *21* (14-15), 1473-1486.

7. Korzhov, M.; Andelman, D.; Shikler, R., Dreaming in Plastic. *Physic World* 2008.

8. Chansin, G.; Ghaffarzadeh, K.; Zervos, H., *OLED Display Forecast 2015-2025: the Rise of Plastic and Flexible Displays*. IDTechEX: 2015; p 253.

9. Das, C. Samsung New Smartphone News, Rumors: Tech Titan to Launch Foldable/Bendable Devices Next Year? http://www.breathecast.com/articles/samsung-new-smartphone-news-rumors-tech-titan-to-launch-foldable-bendable-devices-next-year-26229/ (accessed April 15).

10. Zhang, X.; Bronstein, H.; Kronemeijer, A. J.; Smith, J.; Kim, Y.; Kline, R. J.; Richter, L. J.; Anthopoulos, T. D.; Sirringhaus, H.; Song, K.; Heeney, M.; Zhang, W.; McCulloch, I.; DeLongchamp, D. M., Molecular origin of high field-effect mobility in an indacenodithiophene-benzothiadiazole copolymer. *Nat Commun* **2013,** *4*, 2238.

11. Letheby, H., On the Production of a Blue Substance by the Electrolysis of Sulphate of Aniline. *J Chem Soc* **1862,** *15*, 3.

12. Stuadineger, H., Uber Polymerization. *Chemische Berichte* **1920**, 13.

13. Kearns, D.; Calvin, M., Photovoltaic Effect and Photoconductivity in Laminated Organic Systems. *J Chem Phys* **1958,** *29* (4), 950.

14. Koezuka, H.; Tsumura, A.; Ando, T., Field-Effect Transistor with Polythiophene Thin Film. *Synthetic Met* **1987,** *28*, 6.

15. Tang, C. W.; VanSlyke, S. A., Organic electroluminescent diodes. *Appl. Phys. Lett.* **1987,** *51* (12), 913.

16. Yu, G.; Gao, J.; Hummelen, J. C.; Wudl, F.; Heeger, A. J., Polymer Photovoltaic Cells: Enhanced Efficiencies via a Network of Internal Donor-Acceptor Heterojunctions. *Science* **1995,** *270*, 3.

17. Yu, G.; Heeger, A. J., Charge separation and photovoltaic conversion in polymer composites with internal donor/acceptor heterojunctions. *J Appl Phys* **1995,** *78* (7), 4510.

18. Hummelen, J. C.; Knight, B. W.; Lepeq, F.; Wudl, F., Preparation and Characterization of Fullerioid and Methanofullerene Derivatives. *J. Org. Chem.* **1995,** *60*, 7.

19. Heeger, A. J., 25th anniversary article: Bulk heterojunction solar cells: understanding the mechanism of operation. *Adv Mater* **2014,** *26* (1), 10-27.

20. NREL Best Research-Cell Efficiencies. http://www.nrel.gov/ncpv/ (accessed February 23).

21. (a) DUPONT, Teflon PTFE fluoropolymer resin. In *DUPONT*, DUPONT, Ed. DUPONT: Wilmington 1996; (b) Saini, P.; Aror, M., Microwave Absorption and EMI Shielding Behavior of Nanocomposites Based on Intrinsically Conducting Polymers, Graphene and Carbon Nanotubes. **2012**; (c) Serway, R. A., *Principles of Physics (2nd ed.)*. Saunders College: Fort Woth, Texas, 1998.

22. Norden, B.; Krutmeiher, E., The Nobel Prize in Chemistry, 200: Conductive Polymers. Sciences, T. R. S. A. o., Ed. The Royal Swedish Academy of Sciences: Stockholm, 2000; p 16.

23. Xie, W.; McGarry, K. A.; Liu, F.; Wu, Y.; Ruden, P. P.; Douglas, C. J.; Frisbie, C. D., High-Mobility Transistors Based on Single Crystals of Isotopically Substituted Rubrene-d28. *J Phys Chem C* **2013,** *117* (22), 11522-11529.

24. Tseng, H. R.; Phan, H.; Luo, C.; Wang, M.; Perez, L. A.; Patel, S. N.; Ying, L.; Kramer, E. J.; Nguyen, T. Q.; Bazan, G. C.; Heeger, A. J., High-mobility field-effect transistors fabricated with macroscopic aligned semiconducting polymers. *Adv Mater* **2014,** *26* (19), 2993-8.

25. Yuan, Y.; Giri, G.; Ayzner, A. L.; Zoombelt, A. P.; Mannsfeld, S. C.; Chen, J.; Nordlund, D.; Toney, M. F.; Huang, J.; Bao, Z., Ultra-high mobility transparent organic thin film transistors grown by an off-centre spin-coating method. *Nat Commun* **2014,** *5*, 3005.

26. (a) O'Connor, B. T.; Reid, O. G.; Zhang, X.; Kline, R. J.; Richter, L. J.; Gundlach, D. J.; DeLongchamp, D. M.; Toney, M. F.; Kopidakis, N.; Rumbles, G., Morphological Origin of Charge Transport Anisotropy in Aligned Polythiophene Thin Films. *Adv. Func. Mater.* **2014,** *24* (22), 3422-3431; (b) Twente, U. o. Organic single-crystal devices with inorganic dielectrics. http://www.utwente.nl/tnw/ims/pictures/Research/devices/research_deveen/ (accessed Apr 15).

27. Prins, P.; Grozema, F. C.; Schins, J. M.; Patil, S.; Scherf, U.; Siebbeles, L. D. A., High Intrachain Hole Mobility on Molecular Wires of Ladder-Type Poly(p-Phenylenes). *Phys Rev Lett* **2006,** *96* (14).

28. Kline, R. J.; McGehee, M. D., Morphology and Charge Transport in Conjugated Polymers. *J Macromol Sci C* **2006,** *46* (1), 27-45.

29. Himmelberger, S.; Vandewal, K.; Fei, Z.; Heeney, M.; Salleo, A., Role of Molecular Weight Distribution on Charge Transport in Semiconducting Polymers. *Macromolecules* **2014,** *47* (20), 7151-7157.

30. Noriega, R.; Salleo, A.; Spakowitz, A. J., Chain conformations dictate multiscale charge transport phenomena in disordered semiconducting polymers. *Proc Natl Acad Sci U S A* **2013,** *110* (41), 16315-20.

31. Ma, J.; Hashimoto, K.; Koganezawa, T.; Tajima, K., Enhanced vertical carrier mobility in poly(3-alkylthiophene) thin films sandwiched between self-assembled monolayers and surface-segregated layers. *Chem Commun (Camb)* **2014,** *50* (27), 3627-30.

32. Ma, J.; Hashimoto, K.; Koganezawa, T.; Tajima, K., End-on orientation of semiconducting polymers in thin films induced by surface segregation of fluoroalkyl chains. *J Am Chem Soc* **2013,** *135* (26), 9644-7.

33. Aviram, A.; Ratner, M., Molecular Rectifiers. *Chemical Physical Letters* **1974,** *29* (2), 7.

34. Mann, B., Tunneling through Fatty Acid Salt Monolayers. *J Appl Phys* **1971,** *42* (11), 4398.

35. Ratner, M., A brief history of molecular electronics. *Nat Nanotechnol* **2013,** *8* (6), 378-81.

36. Capozzi, B.; Dell, E. J.; Berkelbach, T. C.; Reichman, D. R.; Venkataraman, L.; Campos, L. M., Length-dependent conductance of oligothiophenes. *J Am Chem Soc* **2014,** *136* (29), 10486-92.

37. Reed, M. A.; Zhou, C.; Muller, C. J.; Burgin, T. P.; Tour, J. M., Conductance of a Molecular Junction. *Science* **1997,** *278*, 4.

38. Reed, M. A.; Zhou, C.; Muller, C. J.; Burgin, T. P.; Tour, J. M., Conductance of a Molecular Junction. *Science* **1997,** *278*, 3.

39. Beebe, J. M.; Kim, B.; Gadzuk, J. W.; Daniel Frisbie, C.; Kushmerick, J. G., Transition from Direct Tunneling to Field Emission in Metal-Molecule-Metal Junctions. *Phys Rev Lett* **2006,** *97* (2).

40. Ho Choi, S.; Kim, B.; Frisbie, C. D., Electrical resistance of long conjugated molecular wires. *Science* **2008,** *320* (5882), 1482-6.

41. Kim, B.; Choi, S. H.; Zhu, X. Y.; Frisbie, C. D., Molecular tunnel junctions based on pi-conjugated oligoacene thiols and dithiols between Ag, Au, and Pt contacts: effect of surface linking group and metal work function. *J Am Chem Soc* **2011,** *133* (49), 19864-77.

42. Luo, L.; Benameur, A.; Brignou, P.; Choi, S. H.; Rigaut, S.; Frisbie, C. D., Length and Temperature Dependent Conduction of Ruthenium-Containing Redox-Active Molecular Wires. *J Phys Chem C* **2011,** *115* (40), 19955-19961.

43. Luo, L.; Balhorn, L.; Vlaisavljevich, B.; Ma, D.; Gagliardi, L.; Frisbie, C. D., Hopping Transport and Rectifying Behavior in Long Donor–Acceptor Molecular Wires. *J Phys Chem C* **2014,** *118* (46), 26485-26497.

44. Luo, L.; Frisbie, C. D., Length-Dependent Conductance of Conjugated Wires synthesized by Click Chemistry. *J Am Chem Soc* **2010,** *132*, 2.

45. Wang, G.; Yoo, H.; Na, S.-I.; Kim, T.-W.; Cho, B.; Kim, D.-Y.; Lee, T., Electrical conduction through self-assembled monolayers in molecular junctions: Au/molecules/Au versus Au/molecule/PEDOT:PSS/Au. *Thin Solid Films* **2009,** *518* (2), 824-828.

46. Akkerman, H. B.; Blom, P. W.; de Leeuw, D. M.; de Boer, B., Towards molecular electronics with large-area molecular junctions. *Nature* **2006,** *441* (7089), 69-72.

47. Akkerman, H. B.; Naber, R. C.; Jongbloed, B.; van Hal, P. A.; Blom, P. W.; de Leeuw, D. M.; de Boer, B., Electron tunneling through alkanedithiol self-assembled monolayers in large-area molecular junctions. *Proc Natl Acad Sci U S A* **2007,** *104* (27), 11161-6.

48. Seo, S.; Min, M.; Lee, J.; Lee, T.; Choi, S. Y.; Lee, H., Solution-processed reduced graphene oxide films as electronic contacts for molecular monolayer junctions. *Angew Chem Int Ed Engl* **2012,** *51* (1), 108-12.

49. Niskala, J. R.; You, W., Metal-molecule-metal junctions via PFPE assisted nanotransfer printing (nTP) onto self-assembled monolayers. *J Am Chem Soc* **2009,** *131* (37), 13202-3.

50. Niskala, J. R.; Rice, W. C.; Bruce, R. C.; Merkel, T. J.; Tsui, F.; You, W., Tunneling characteristics of Au-alkanedithiol-Au junctions formed via nanotransfer printing (nTP). *J Am Chem Soc* **2012,** *134* (29), 12072-82.

51. (a) Beebe, J. M.; Engelkes, V. B.; Miller, L. L.; Frisbie, C. D., Contact Resistance in Metal-Molecule-Metal Junctions Based on Aliphatic
SAMs: Effects of Surface Linker and Metal Work Function. *J Am Chem Soc* **2002,** *124* (38), 2; (b) Van Hal, P. A.; Smits, E. C.; Geuns, T. C.; Akkerman, H. B.; De Brito, B. C.; Perissinotto, S.; Lanzani, G.; Kronemeijer, A. J.; Geskin, V.; Cornil, J.; Blom, P. W.; De Boer, B.; De Leeuw, D. M., Upscaling, integration and electrical characterization of molecular junctions. *Nat Nanotechnol* **2008,** *3* (12), 749-54.

52. Simmons, J. G., Generalized Formula for the Electric Tunnel Effect between Similar Electrodes Separated by a Thin Insulating Film. *J Appl Phys* **1963,** *34* (6), 1793.

53. Huang, M. J.; Hsu, L. Y.; Fu, M. D.; Chuang, S. T.; Tien, F. W.; Chen, C. H., Conductance of tailored molecular segments: a rudimentary assessment by Landauer formulation. *J Am Chem Soc* **2014,** *136* (5), 1832-41.

54. Halperin, A.; Tirrel, M.; Lodge, T. P., *Macromolecules: Synthesis, Order and Advanced Properties*. Springer-Verlage Berlin Heidelberg: Minneapolis, 1992; Vol. 100, p 41.

55. Rubinstein, M.; Colby, R. H., *Polymer Physics*. Oxford University Press: New York, 2003.

56. Marshall, N.; Sontag, S. K.; Locklin, J., Surface-initiated polymerization of conjugated polymers. *Chem Commun (Camb)* **2011,** *47* (20), 5681-9.

57. Huddleston, N. E.; Sontag, S. K.; Bilbrey, J. A.; Sheppard, G. R.; Locklin, J., Palladium-Mediated Surface-Initiated Kumada Catalyst Polycondensation: A Facile Route Towards Oriented Conjugated Polymers. *Macromol Rapid Commun* **2012**.

58. Xu, S.; Kim, E. H.; Wei, A.; Negishi, E.-i., Pd- and Ni-catalyzed cross-coupling reactions in the synthesis of organic electronic materials. *Sci Technol Adv Mat* **2014,** *15* (4), 044201.

59. Odian, G., *Principles of Polymerization*. 4th Edition ed.; John Wiley & Sons Inc.: Hoboken, 2004.

60. figure, p. g.

61. Loewe, R. S.; Ewbank, P. C.; Liu, J.; Zhai, L.; McCullough, R. D., Regioregular, Head-to-Tail Coupled Poly(3-alkylthiophenes) Made Easy by the GRIM Method: Investigation of the Reaction and the Origin of Regioselectivity. *Macromolecules* **2001,** *34*, 10.

62. Osaka, I.; McCullough, R. D., Advances in Molecular Design and Synthesis of Regioregular Polythiophenes. *Accounts Chem. Res.* **2008,** *41* (9), 13.

63. Komber, H.; Senkovskyy, V.; Tkachov, R.; Johnson, K.; Kiriy, A.; Huck, W. T. S.; Sommer, M., Ring Walking versus Trapping of Nickel(0) during Kumada Catalyst Transfer Polycondensation Using Externally Initiated Electron-Accepting Thiophene–Benzothiadiazole–Thiophene Precursors. *Macromolecules* **2011,** *44* (23), 9164-9172.

64. Bryan, Z. J.; McNeil, A. J., Conjugated Polymer Synthesis via Catalyst-Transfer Polycondensation (CTP): Mechanism, Scope, and Applications. *Macromolecules* **2013,** *46* (21), 8395-8405.

65. Orski, S. V.; Fries, K. H.; Sontag, S. K.; Locklin, J., Fabrication of nanostructures using polymer brushes. *J Mater Chem* **2011,** *21* (37), 14135.

66. Sontag, S. K.; Sheppard, G. R.; Usselman, N. M.; Marshall, N.; Locklin, J., Surface-confined nickel mediated cross-coupling reactions: characterization of initiator environment in Kumada catalyst-transfer polycondensation. *Langmuir* **2011,** *27* (19), 12033-41.

67. Doubina, N.; Jenkins, J. L.; Paniagua, S. A.; Mazzio, K. A.; MacDonald, G. A.; Jen, A. K. Y.; Armstrong, N. R.; Marder, S. R.; Luscombe, C. K., Surface-Initiated Synthesis of Poly(3-methylthiophene) from Indium Tin Oxide and its Electrochemical Properties. *Langmuir* **2012,** *28* (3), 1900-1908.

68. (a) Clark, J.; Silva, C.; Friend, R. H.; Spano, F. C., The Role of Intermolecular coupling in the Photophysics of Disordered Organic Semiconductors: Aggregate emission in Regioregular Polythiophene. *Phys Rev Lett* **2007,** *98* (206406), 10; (b) Gierschner, J.; Cornil, J.; Egelhaaf, H. J., Optical Bandgaps of π-Conjugated Organic Materials at the Polymer Limit: Experiment and Theory. *Adv Mater* **2007,** *19* (2), 173-191.

69. Spano, F. C.; Silva, C., H- and J-aggregate behavior in polymeric semiconductors. *Annu Rev Phys Chem* **2014,** *65*, 477-500.

70. Gurau, M. C.; DeLongchamp, D. M.; Vogel, B. M.; Lin, E. K.; Fischer, D. A.; Sambasivan, S.; Richter, L. J., Measuring Molecular Order in Poly(3-alkylthiophene) Think Films with Polarizing Spectroscopies. *Langmuir* **2007,** *23*, 9.

71. Spearman, P.; Borghesi, A.; Campione, M.; Laicini, M.; Moret, M.; Tavazzi, S., Directional dispersion in absorbance spectra of oligothiophene crystals. *J Chem Phys* **2005,** *122* (1), 14706.

72. Spano, F. C., The Spectral Signatures of Frenkel Polarons in H- and J-Aggregates. *Accounts Chem. Res.* **2010,** *43* (3), 11.

73. Eisfeld, A.; Briggs, J. S., The J- and H-bands of organic dye aggregates. *Chem Phys* **2006,** *324* (2-3), 376-384.

74. Yoneyama, M.; Sugi, M.; Saito, M.; Ikegami, K.; Kuroda, S.; Iizima, S., Photoelectric Properties of Coper Pthalocyanine Langmuir-Blodgett Film. *JPN J Appl Phys* **1986,** *25* (7), 6.

75. DeLongchamp, D. M.; Sambasivan, S.; Fischer, D. A.; Lin, E. L.; Chang, P.; Murphy, A. R.; Frechet, J. M. J.; Subramanian, N., Direct Correlation of Organic Semiconductor Film Structure to Field-Effect Mobility. *Adv Mater* **2005,** *17*, 5.

76. Co, J. W., JA Woollam Variable angle Spectroscopic Ellipsometer.

77. Qiu, Y.; Mohin, J.; Tsai, C. H.; Tristram-Nagle, S.; Gil, R. R.; Kowalewski, T.; Noonan, K. J., Stille Catalyst-Transfer Polycondensation Using Pd-PEPPSI-IPr for High-Molecular-Weight Regioregular Poly(3-hexylthiophene). *Macromol Rapid Commun* **2015**.

78. (a) Krabbenborg, S. O.; Wilbers, J. G. E.; Huskens, J.; van der Wiel, W. G., Symmetric Large-Area Metal-Molecular Monolayer-Metal Junctions by Wedging Transfer. *Adv. Func. Mater.* **2013,** *23* (6), 770-776; (b) McCreery, R. L., Molecular Electronic Junctions. *Chem. Mater.* **2004,** *16*, 20; (c) Tuccito, N.; Ferri, V.; Cavazzini, M.; Quici, S.; Zhavernerko, G.; Licciardello, A.; Rampi, M. A., Highly Conductive ~40-nm-long Molecular Wires Assembled by Stepwise Incorporation of Metal Centres. *Nat Mater* **2008,** *8*, 7.

79. McCreery, R. L., Molecular Electronic Junctions. *Chem. Mater.* **2004,** *16* (4496), 20.

80. Brinkman, W. F.; Dynes, R. C.; Rowell, J. M., Tunneling Conductance of Asymmetrical Barriers. *J Appl Phys* **1969,** *41* (5), 7.

81. Valaski, R.; Bozza, A. F.; Micaroni, L.; Hummelgen, I. A., Electrical Characterization of poly(3-methylthiophene) electrosynthesized onto a tin-oxide substrate. *J Solid State Electrochem* **2000,** *4*, 4.

82. (a) Kokil, A.; Yang, K.; Kumar, J., Techniques for characterization of charge carrier mobility in organic semiconductors. *J Polym Sci B Polym Phys* **2012,** *50* (15), 1130-1144; (b) Tiwari, S.; Greenham, N. C., Charge mobility measurement techniques in organic semiconductors. *Optical and Quantum Electronics* **2009,** *41* (2), 69-89.

83. Meitl, M. A.; Zhu, Z.-T.; Kumar, V.; Lee, K. J.; Feng, X.; Huang, Y. Y.; Adesida, I.; Nuzzo, R. G.; Rogers, J. A., Transfer printing by kinetic control of adhesion to an elastomeric stamp. *Nat Mater* **2005,** *5* (1), 33-38.

84. Brown, H. R., The Adhesion Between Polymers. *Annu. Rev. Mater. Sci.* **1991,** *21*, 29.

85. Haynes, W. M., *CRC Handbook of Chemistry and Physics*. 95 ed.; Taylor and Francis Group LLC: Boca Raton, 2014; p 2704.

86. Vissenbery, M. C. M. J.; Matters, M., Theory of the field-effect mobility in amorphous organic transistors. *Phys Rev B* **1998,** *57* (20), 4.

87. Wetzelaer, G.-J. A. H.; Blom, P. W. M., Diffusion-driven currents in organic-semiconductor diodes. *NPG Asia Materials* **2014,** *6* (7), e110.

88. Bridges, C. R.; McCormick, T. M.; Gibson, G. L.; Hollinger, J.; Seferos, D. S., Designing and refining Ni(II)diimine catalysts toward the controlled synthesis of electron-deficient conjugated polymers. *J Am Chem Soc* **2013,** *135* (35), 13212-9.

89. Nanashima, Y.; Yokoyama, A.; Yokozawa, T., Synthesis of Well-Defined Poly(2-alkoxypyridine-3,5-diyl) via Ni-Catalyst-Transfer Condensation Polymerization. *Macromolecules* **2012,** *45* (5), 2609-2613.

90. Reddy, P.; Jang, S. Y.; Segalman, R. A.; Majumdar, A., Thermoelectricity in Molecular Junctions. *Science* **2007,** *315*, 5.

91. Tan, A.; Balachandran, J.; Sadat, S.; Gavini, V.; Dunietz, B. D.; Jang, S. Y.; Reddy, P., Effect of length and contact chemistry on the electronic structure and thermoelectric properties of molecular junctions. *J Am Chem Soc* **2011,** *133* (23), 8838-41.

92. Bergfeld, J. P.; Solis, M. A.; Stafford, C. A., Giant Thermoelectric Effect from Transmission Supernodes. *ACS Nano 4* (9), 7.

93. Galbiati, M.; Barraud, C.; Tatay, S.; Bouzehouane, K.; Deranlot, C.; Jacquet, E.; Fert, A.; Seneor, P.; Mattana, R.; Petroff, F., Unveiling self-assembled monolayers' potential for molecular spintronics: spin transport at high voltage. *Adv Mater* **2012,** *24* (48), 6429-32.

94. Tatay, S.; Barraud, C.; Galbiati, M.; Seneor, P.; Mattana, R.; Bouzehouane, K.; Deranlot, C.; Jacquet, E.; Forment-Aliaga, A.; Jegou, P.; Fert, A.; Petroff, F., Self-Assembled Monolayer-Functionalized Half-Metallic Manganite for Molecular Spintronics. *ACS Nano* **2012,** *6* (10), 5.

95. Majumdar, S.; Laiho, R.; Laukkanen, P.; Vaÿrynen, I. J.; Majumdar, H. S.; Österbacka, R., Application of regioregular polythiophene in spintronic devices: Effect of interface. *Appl. Phys. Lett.* **2006,** *89* (12), 122114.

96. Blakesley, J. C.; Castro, F. A.; Kylberg, W.; Dibb, G. F. A.; Arantes, C.; Valaski, R.; Cremona, M.; Kim, J. S.; Kim, J.-S., Towards reliable charge-mobility benchmark measurements for organic semiconductors. *Org Electron* **2014,** *15* (6), 1263-1272.